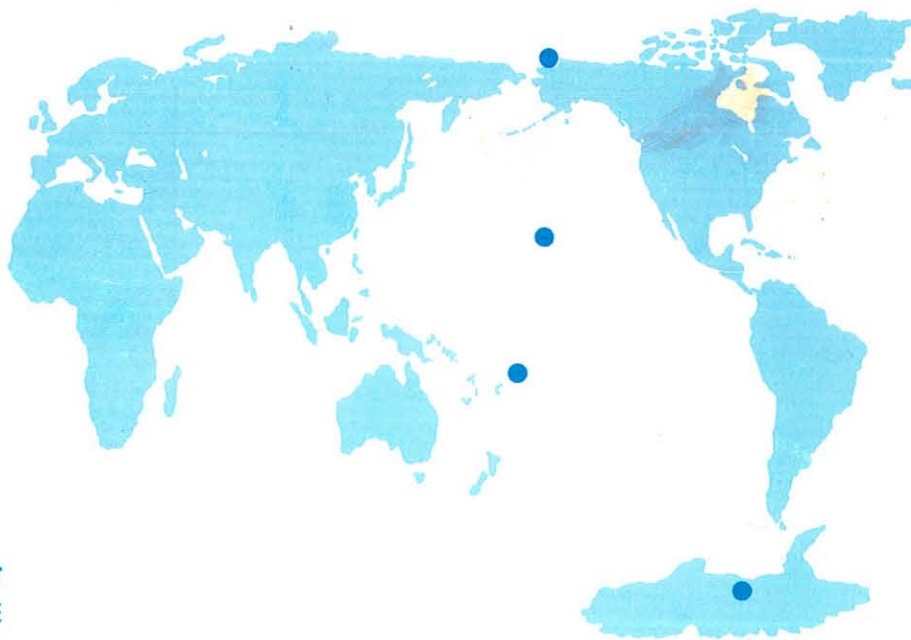# *Geophysical Monitoring for Climatic Change*

No. 11

Summary Report 1982

**U.S. DEPARTMENT
OF COMMERCE**

**NATIONAL
OCEANIC AND
ATMOSPHERIC
ADMINISTRATION**

**ENVIRONMENTAL
RESEARCH
LABORATORIES**

Geophysical Monitoring for Climatic Change No. 11

Summary Report 1982

Joyce M. Harris and Barry A. Bodhaine, Editors
Air Resources Laboratory
Geophysical Monitoring for Climatic Change

Boulder, Colorado

December 1983

NOTICE

Mention of a commercial company or product does not constitute
an endorsement by NOAA Environmental Research Laboratories.
Use for publicity or advertising purposes of information from
this publication concerning proprietary products or the tests
of such products is not authorized.

CONTENTS

FOREWORD

When I was invited to prepare this foreword to Number 11 of the Geophysical Monitoring for Climatic Change Summary Report series, the first and obvious thought was of the opportunity for a retrospective, comparative analysis of this vital program as it moved from a single site to multiple sites; survived the teething pangs of difficult logistics (and bureaucratic impedimenta), staffing, and instrumentation development; and is now involved in data analysis and interpretation, a massive (and almost real-time) archiving effort, and impressive activities in data precision and quality control. However, I think that this program, opening its second decade, is better viewed as the maturing of the concept of chemical climatology of the atmosphere and its role in the conventional idea of climate in terms of temperature and precipitation. The next 10 years will be a decade of challenges to determine the inventories and biogeochemical cycling of a host of trace gases; the role of particulate materials in the transformation chemistry of gases; and the quantitative influences of submicron particles on cloud formation/persistence, precipitation, and solar and IR radiation fluxes.

The unique CO_2 time series at Mauna Loa Observatory, now covering 25 years, stimulated the inclusion of changing gas concentrations in global climate models. Now we find, apparently, that tropospheric methane is on the increase. Also, the chlorofluorocarbons continue to increase as does trichloroethane. One could add to the list many other compounds whose concentrations and trends appear to be changing. Many of these compounds absorb IR radiation and add to the potential CO_2 "greenhouse" effect, but their concentration histories are much less known. As the understanding of atmospheric chemistry has advanced, radical compounds (e.g., OH, H_2O_2) in the atmosphere have assumed a central role in the transformation and, often, the accelerated removal of many compounds. The role of aqueous chemistry in cloud water is also being recognized. When one thinks that about one-half of the globe is always cloud covered, the necessity of understanding these processes is obvious.

This list of unknown areas is woefully incomplete, but we do see chemical gradients over local, regional, continental, and interhemispheric scales. The transport of aerosols over distances of more than 10,000 km and the ubiquitous presence of organic and sulfur compounds in even the cleanest of rains at remote sites are now documented. The intellectual challenges to an adequate understanding of atmospheric chemistry, and of sources and sinks for both natural and anthropogenic materials, are stunning.

To date, our documentation of clean-air tropospheric chemistry is from only a handful of permanent observatories, less than 10 globally. Fortunately, research expeditions using ships and aircraft have provided much new information. A major new development is the use of indirect sensing techniques to extend the vertical dimension of the measurements. Such sensors (notably for ozone), mounted on satellite platforms, are providing almost-synoptic data.

Yet it is primarily from the fixed sites that we find diurnal, seasonal, and interannual variability of concentration. The year-to-year variability in the CO_2 airborne fraction is an important case in point for which there is, as yet, no adequate explanation.

Thus, a second series of challenges for the next decade is to coordinate and correlate the new techniques and platforms to obtain the most informative data series. Determining the role of fixed, ground-based sites in providing satellite ground truth is an obvious need. However, there are other issues: What are the optimum sampling schedules for the many gaseous compounds that must be measured, and for near-surface aerosols and aerosol profiles? What are the chemical profiles of various size fractions of the aerosols at various locations?--The recent multiagency study of Arctic haze provided not only important scientific information but also a model of coordinated observations. Can automation and modern data processors make continuous monitoring more cost-effective than periodic grab sampling is? What new instruments are required? Can accurate multicompound nitrogenous species and continuous OH measurement methods be developed? Are such data required?

Answers to these challenges and these questions (and many others not stated here or not yet known) will alter the GMCC program by 1992. What will not change is the continuing need for precise and accurate gas and aerosol measurements from which radiation and cloud behavior can be derived. By 1992 it is expected that temperature effects from the increase in CO_2 concentration will be detectable in relatively conventional measurements. Quantitative separation of this influence from effects of changes in other trace gases and from aerosol influences will require the continued dedication to excellence that has characterized the GMCC staff.

A new generation of observers and scientists will enter the program in the next decade. They too must carry on this tradition and meet these challenges.

<div style="text-align: right">

Donald H. Pack
Consulting Meteorologist

</div>

PREFACE

This document presents a summary of the research operations and accomplishments by the Geophysical Monitoring for Climatic Change (GMCC) program and by outside investigators working cooperatively with GMCC in 1982. It includes descriptions of management and operations at GMCC's four baseline sites, scientific data from the measurement projects, conclusions from analyses of data, and recent basic research achievements.

The GMCC program, established in 1971, is one of several research programs within the Air Resources Laboratory under the directorship of Lester Machta. Its four observatories are located at Barrow, Alaska (in service since 1973); Mauna Loa, Hawaii (in service since 1956); American Samoa (in service since 1973); and South Pole (in service since 1957). Background measurements of aerosols, gases, and solar radiation that are important to the climate of the Earth are made at the observatories. The primary groups within GMCC are Monitoring Trace Gases, Aerosols and Radiation Monitoring, Acquisition and Data Management, and Analysis and Interpretation. Specific names of individuals in GMCC are not given in the main text of the report; however, the membership of each GMCC group is given in sec. 9. Publications and presentations by GMCC staff are given in sec. 7.

ACRONYMS AND ABBREVIATIONS

A&DM	Acquisition and Data Management (GMCC)
AES	Atmospheric Environment Service, Canada
AGASP	Arctic Gas and Aerosol Sampling Program
ARL	Air Resources Laboratory, Rockville, Md. (ERL)
ARM	Aerosols and Radiation Monitoring (GMCC)
ASCS	Alaska Soil Conservation Service
ASRC	Atmospheric Sciences Research Center, SUNYA, Albany, N.Y.
BDL	Below detection level
BLM	Bureau of Land Management (USGS)
BRW	Barrow Observatory, Barrow, Alaska (GMCC)
CAF	Clean Air Facility
CDC	Control Data Corporation
CIRES	Cooperative Institute for Research in Environmental Sciences
CMA	Chemical Manufacturers Association
CN	Condensation nuclei
CNC	Condensation nucleus counter
CPU	Central processing unit
CSIRO	Commonwealth Scientific and Industrial Research Organization, Australia
CSU	Colorado State University, Ft. Collins, Colo.
DOE	Department of Energy
DOY	Day of year, Julian
EC	Elemental carbon
ECC	Electrochemical concentration cell
EML	Environmental Measurements Laboratory (DOE)
ENSO	El Niño - Southern Oscillation
EPA	Environmental Protection Agency
ERL	Environmental Research Laboratories, Boulder, Colo. (NOAA)
FID	Flame ionization detector
FPD	Flame photometric detector
GC	Gas chromatograph
G.E.	General Electric
GEOSECS	Geochemical Ocean Section Study
GHA	Greenwich hour angle
GHOST	Global Horizontal Sounding Technique
GMCC	Geophysical Monitoring for Climatic Change, Boulder, Colo. (ARL)
GSA	General Services Administration
HASL	Health and Safety Laboratory (EPA)
HASP	High Altitude Sampling Program
HP	Hewlett-Packard
HVO	Hawaiian Volcano Observatory
IAEA	International Atomic Energy Agency, Vienna, Austria
ICDAS	Instrumentation Control and Data Acquisition System
IGY	International Geophysical Year
IICAMS	Interactive Instrumentation Control and Monitoring System
IR	Infrared
ITCZ	Intertropical Convergence Zone
IT&T	International Telephone and Telegraph
KEY	Key Biscayne, Fla.
KUM	Cape Kumukahi, Hawaii
LBL	Lawrence Berkeley Laboratory (DOE)
LLL	Lawrence Livermore Laboratory (DOE)
MLO	Mauna Loa Observatory, Hawaii (GMCC)

MSL	Mean sea level
MTG	Monitoring Trace Gases (GMCC)
NADP	National Atmospheric Deposition Program
NARL	Naval Arctic Research Laboratory, Barrow, Alaska
NASA	National Aeronautics and Space Administration
NBS	National Bureau of Standards
NCAR	National Center for Atmospheric Research, Boulder, Colo.
NCC	National Climatic Center, Asheville, N.C.
NDIR	Nondispersive infrared
NIAR	Norwegian Institute for Arctic Research
NIP	Normal incidence pyrheliometer
NMC	National Meteorological Center, Suitland, Md.
NOAA	National Oceanic and Atmospheric Administation
NRL	Naval Research Laboratory, Washington, D.C.
NSF	National Science Foundation, Washington, D.C.
NWR	Niwot Ridge, Colo.
NWS	National Weather Service
OGC	Oregon Graduate Center, Beaverton, Oreg.
ONR	Office of Naval Research
OPC	Optical particle counter
OPEC	Organization of Petroleum Exporting Countries
OWRM	Office of Weather Research and Modification, Boulder, Colo. (ERL)
PISSA	Particulate integrating sampling sector analyzer
PIXE	Particle induced X-ray emission
PMEL	Pacific Marine Environmental Laboratory, Seattle, Wash. (ERL)
PMT	Photomultiplier tube
PROM	Programmable read-only memory
PV	Photovoltaic
P^3	Portable pressurizing pack
RDOS	Real-time Disk Operating System (Data General)
RMS	Root mean square
R/V	Research Vessel
SCM	Standard cubic meters
SIO	Scripps Institution of Oceanography, La Jolla, Calif.
SMO	Samoa Observatory, American Samoa (GMCC)
SPO	South Pole Observatory, Antarctica (GMCC)
SUNYA	State University of New York at Albany
Tg	10^{12} grams
TOMS	Total Ozone Mapping Spectrometer
UPS	Universal Power Supply
URI	University of Rhode Island, Kingston, R.I.
USCG	United States Coast Guard
USGS	United States Geological Survey
UV	Ultraviolet
WDC-A	World Data Center-A, Asheville, N.C.
WFM	Whiteface Mountain Observatory, N.Y. (ASRC)
WMO	World Meteorological Organization, Geneva, Switzerland
WPL	Wave Propagation Laboratory, Boulder, Colo. (ERL)
WSU	Washington State University, Pullman, Wash.

EL CHICHON SUNRISE AT MAUNA LOA
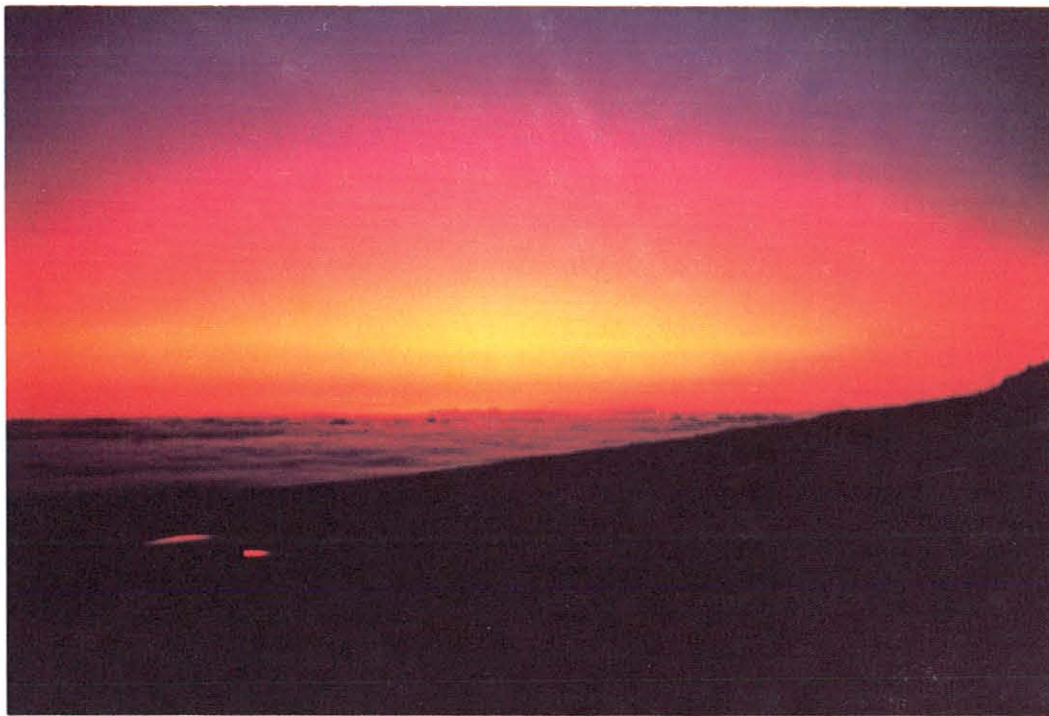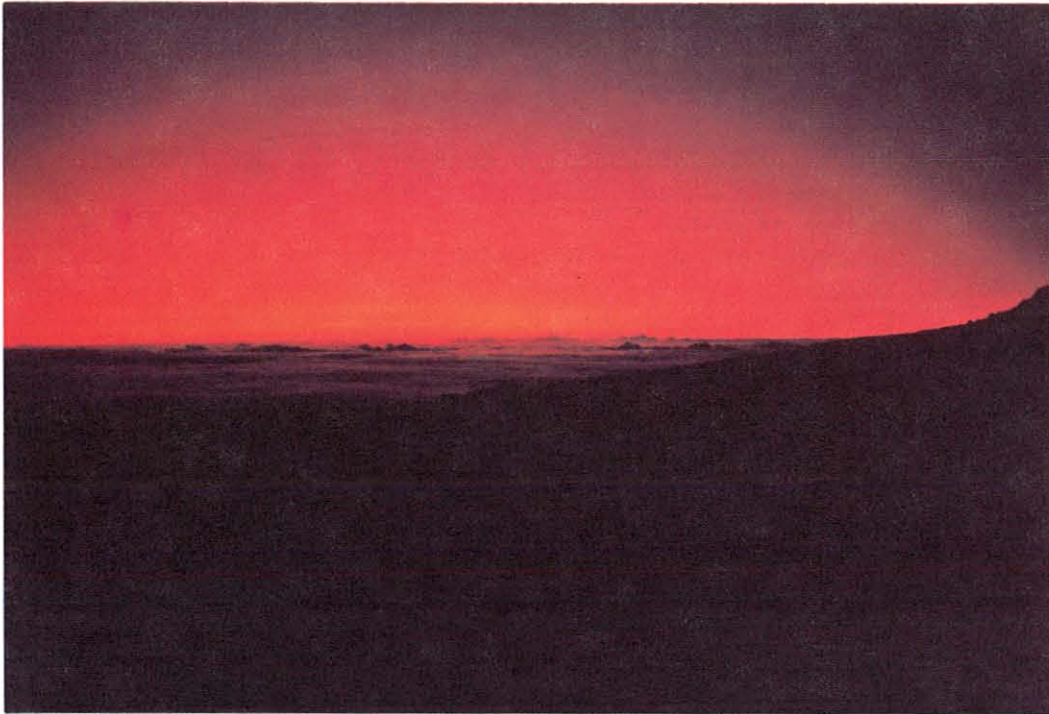
Photographs of the horizon taken by K. Coulson from Mauna Loa Observatory
during the presunrise period on 14 May 1982, showing the dramatic color in-
duced by the El Chichon volcanic cloud. On this day the cloud over MLO was at
its most strongly developed phase, as shown by lidar measurements. The top of
the cloud was at about 30-km altitude MSL. Local times and solar depression
angles, respectively, for these pictures were 0500, -10.0° (upper left);
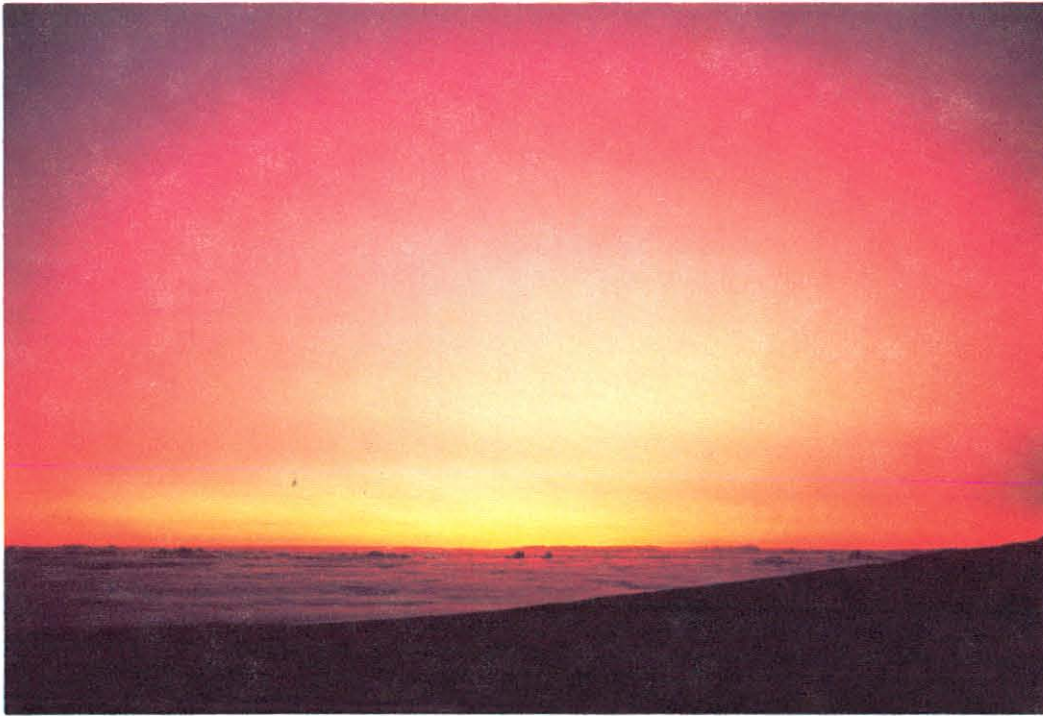
0512, -7.5° (lower left); 0522, -5.3° (upper right); and 0540, -1.6° (lower right). Local sunrise time was 0548. In the first picture of this series (not shown), taken at 0439 (-14.4° solar depression angle), a very faint red glow appeared on the horizon. This evidence of sky color at such a large solar depression conforms with observations from various locations following the eruption of Krakatoa in 1883.

GEOPHYSICAL MONITORING FOR CLIMATIC CHANGE

NO. 11

Summary Report 1982

1. SUMMARY

At MLO, a new steel building was constructed to house the lidar and po-larimeter systems. The existing lidar dome was required for a new solar tracker on which a pyrheliometer, seven-wavelength radiometer, and an IR hy-grometer are mounted. Two volcanic clouds appeared over Hawaii during 1982, the Mystery Cloud of unknown origin detected on 27 January and the El Chichon cloud detected on 9 April. Modifications of and additions to the regular observational program were made to provide a complete record of these impor-tant historical events. The Mystery Cloud was centered at about 18-km alti-tude and had a maximum total-to-Rayleigh backscatter ratio of approximately 2.5. The El Chichon cloud was centered at about 25-26 km and had a maximum backscatter ratio of about 220.

At BRW, NARL remains in a caretaker status and BRW continues to receive power from NARL. However, scientific research at NARL has been discontinued. GMCC has requested that 100 acres of land surrounding the observatory be transferred from ONR to NOAA. This land is temporarily under the custodial care of BLM.

At SMO, the central air conditioner was replaced and new ducting was designed to accommodate the PV system controller installed in the instrumen-tation room. Major repairs were performed on the roofs of the GMCC housing units and both units were completely repainted.

At SPO, the ^{14}C sampler was moved from the skylab to the high-volume pump room in CAF. At the same time, the decking beneath the pumps was replaced and pump-room wiring was reconfigured. The entire CAF wiring plan was reviewed and some changes to power distribution were made in the circuit breaker box. A new survey of the entire SPO complex, including CAF, was performed.

The measurement programs continued at the four GMCC observatories. These programs include CO_2, total columnar ozone, ozone vertical distribution, sur-face ozone, stratospheric water vapor, CFC-11 and -12, N_2O, stratospheric aerosols, volumetric aerosol scattering coefficient, CN concentration, solar radiation, meteorological variables, and precipitation chemistry.

The continuous CO_2 measurement program continued at all four stations. The entire record of CO_2 data at each station has been edited, corrected, and converted to the X81 mole fraction scale. The four stations yield a mean global CO_2 growth rate of about 1.50 ppm yr^{-1}. A total airborne fraction of about 0.54 still seems appropriate for a total industrial production of about 36 Gt of carbon during 1976-1982. The latitude gradient of CO_2 from BRW to SPO has remained fairly constant at about 3.5 ppm during the last decade, although variations of up to 0.5 ppm related to ENSO events occurred during 1976, 1979, and 1982. The CO_2 annual cycle at BRW and MLO has increased in amplitude by ~0.6%-0.8% yr^{-1} over the last two decades and the MLO annual cycle may have increased by as much as 2% yr^{-1} since 1975.

The CO_2 flask sampling sites remained nearly the same as in 1981, although sampling at Falkland Islands and Point Six Mountain, Mont., was discontinued and new cooperative stations were initiated near Christchurch, New Zealand; Halley Bay, Antarctica; Cape Meares, Oreg.; and Kitt Peak, Ariz. The entire flask data set since 1968 has been edited, corrected, and converted to the X81 mole fraction scale. An important result from the flask network is the fine definition of the latitudinal gradient and annual cycle, particularly in the equatorial regions where the atmospheric concentration is sensitive to ENSO events and oceanic upwelling. The flask CO_2 data also show a gradient of about 3.5 ppm between BRW and SPO.

Total ozone observations with Dobson spectrophotometers continued at the four GMCC observatories and seven contiguous U.S. stations. Observations were discontinued at White Sands, N. Mex., and BRW, but a new station was established in Fresno, Calif. Work continued with the WMO Global Ozone Research and Monitoring Project to upgrade foreign Dobson spectrophotometers. Special calibration lamps, which were calibrated using World Standard Dobson Instrument no. 83, have been supplied for all Dobson spectrophotometers around the world to maintain calibration on an absolute scale. Ozone vertical profiles were obtained in Boulder using an automated Dobson ozone spectrophotometer for Umkehr observations. This automated instrument was also used to perform standard total ozone observations. Monthly ozonesonde flights were made in Boulder, Colo., and Hilo, Hawaii, using balloon-borne ECC instruments for comparison with ozone profiles obtained using the Umkehr technique. The Hilo flights were initiated in September to study the impact of El Chichon and will be continued for about a year. Surface ozone measurements continued at the four GMCC observatories. Least-squares trend analyses for the surface ozone record show no significant trends; however, large annual cycles are evident at all four observatories.

The stratospheric water vapor measurement program was continued in Boulder, Colo. However, because of problems with neoprene balloons, only six successful monthly flights were possible.

The halocarbon and N_2O measurement program continued at the four GMCC observatories and at NWR. Installation of an air conditioner in the Boulder analysis laboratory produced more consistent results from the flask analyses. Calibration gas standards were found to be stable since 1977. CFC-11 and -12 data show mean mixing ratios in the ranges 202-215 and 345-365 pptv, respectively, and growth rates in the ranges of 10-14 and 9-16 pptv yr^{-1}, respectively. N_2O data show mean mixing ratios in the range 302-310 ppbv and growth rates in the range 0.6-1.6 ppbv yr^{-1}.

Lidar measurements of stratospheric aerosol profiles continued at MLO. Increased numbers of observations were made to provide more detailed descriptions of the Mystery Cloud and the El Chichon cloud.

Continuous measurements of volumetric aerosol light scattering and CN concentration continued at the four GMCC observatories. The entire data set has been edited and corrected and a new least-squares trend analysis showed no significant long-term trend at any station.

The solar radiation measurements continued at the four GMCC observatories. Photometers operating at the 778- and 862-nm wavelengths were added to the program at all four stations. An IR hygrometer was installed at SPO.

2

Development of the GMCC atmospheric trajectory program continued with two new versions in addition to the original program that produces backward isobaric trajectories for the Northern Hemisphere. One new version uses gridded data for every 2.5° of latitude and longitude and can produce backward isobaric trajectories anywhere on the globe, including trajectories that cross the Equator. The newest version produces backward isentropic trajectories that trace paths determined by the wind field on surfaces of constant potential temperature.

GMCC personnel conducted numerous research projects and data analyses, many of which are summarized in sec. 4. Several of these studies used the CO_2 record. A two-dimensional model was developed that simulates vertical and latitudinal CO_2 transport in the atmosphere; CO_2 flux into, out of, and within the ocean; and CO_2 flux into and out of the biosphere. Comparison of the model results with the CO_2 measurement record shows that the model can explain a large proportion of the variability of CO_2 during the year. A study was performed correlating the variability of BRW CO_2 concentration with atmospheric flow regimes, meteorological variables, pollution aerosol measurements, and air mass origin. It was concluded that much of the Arctic is not a CO_2 source and that the Arctic is most strongly influenced by direct transport from mid-latitude industrial source regions.

In May-June, GMCC participated in a cruise aboard the R/V DISCOVERER in the equatorial and northern Pacific Ocean. Thirty-six pairs of flask samples were collected for subsequent analysis by the MTG group. These shipboard data are valuable for determining atmospheric CO_2 gradients over this region of the Pacific and identifying possible marine sources and sinks of CO_2.

Special skylight polarization measurements were made at MLO to detect the effect of the El Chichon stratospheric dust cloud. The dust cloud caused a reconfiguration of the polarization field compared with that for a clear atmosphere.

Aerosol and solar radiation experiments continued at WFM during the summer of 1982. Preliminary results indicate that the most hazy conditions at WFM were when trajectories arrived from the west after passing over the Great Lakes region. Trajectories from the east, having a maritime origin, gave the clearest conditions, and trajectories from the north or south were representative of continental background conditions. A trajectory study at MLO showed that the springtime Asian dust event at MLO was significantly greater in 1979 than in subsequent years because of a more direct transport route from the Asian deserts in 1979. Subsequent years show trajectories with less curvature and origins to the south of the Asian deserts.

Work continued on the development of the Umkehr method for determining the ozone profile in the stratosphere. The appearance of the El Chichon dust cloud provided an opportunity to investigate possible errors in the Umkehr measurement caused by stratospheric dust.

The GMCC ARM group participated in three NASA flights designed to establish the latitudinal extent and variability of the El Chichon dust cloud. The flights were near the tropopause so that the optical depth of the stratosphere could be measured as a function of latitude from BRW to New Zealand. Significant latitudinal variations existed at least 8 months after the eruption. Normal incidence irradiance at MLO analyzed by the apparent transmission

method was compared with actual solar irradiances obtained by the Robinson method. Previous to the El Chichon eruption a linear relationship existed between the results of the two methods. The eruption of El Chichon resulted in the largest decrease in normal incidence flux measured at MLO since measurements began in 1958, and the linear relationship between apparent transmission and absolute flux no longer existed.

In 1982, GMCC supported a substantial number of cooperative research projects. Fourteen summary reports resulting from these projects are presented in sec. 5. They cover such topics as atmospheric benzene and toluene; aerosol absorption, composition, and size distribution measured at MLO during Asian dust episodes; solar radiation at BRW; CO_2 and other gases measured at Palmer station; Raman study of graphitic carbon in the Arctic; a global network of sunburning UV solar radiation meters; a sampling strategy to avoid the problem of aliasing at MLO; a model study of atmospheric electrical properties above a mountain such as Mauna Loa; a comprehensive study of atmospheric bromine in the Arctic; a spectral analysis of meteorological and aerosol chemistry data at BRW; and a study of the long-term change in the amplitude of the seasonal cycle in CO_2 at MLO.

2. OBSERVATORY REPORTS

2.1 Mauna Loa

2.1.1 Facilities

A new 14- × 20-ft steel building was constructed at the observatory site to house the lidar and polarimeter systems that were moved from the Ash Dome. The dome was required for installation of a new solar tracker. A special requirement for the steel building was a port in the roof that could be opened for taking lidar and skylight observations. The building was purchased from Porta House of Oakland, Calif., and erected on the site by a local contractor. Although the building was completed in early May, the instrumentation was not moved until 24 August.

The tracker was delivered from Boulder to MLO in September, and its installation in the dome was completed by Boulder personnel in early October. The instruments mounted on it are an Eppley pyrheliometer, a seven-wavelength radiometer, and an IR hygrometer. Operation of the instruments was generally satisfactory once a problem with the data-logging system was resolved.

The four-wavelength nephelometer, which had been in Boulder for repairs during the last 6 months of 1981, was returned to MLO and put back in service during May. It operated well for the remainder of the year.

The microammeter associated with the Dobson spectrophotometer sustained water damage during a severe storm on 11 February. No ozone measurements were made until the device was replaced about 2 weeks later.

Sunphotometer SN D1015 was taken out of service during January and replaced by a new model, SN J202. Unfortunately, this latter instrument had no reliable calibration when it was delivered to MLO, and it was not until 26 February that a moderately precise calibration was obtained. Another sunphotometer, SN J314, which operates in two near-IR spectral regions, was put into serivce at MLO on 30 June. Both instruments were used for turbidity measurements during the remainder of the year.

An Optronics spectrometer was borrowed from the University of California, Davis, and used for solar spectral measurements at MLO at various times during October and November. The Eppley precision spectral pyranometers fitted with GG22 and OG1 cutoff filters were reinstalled on 18 August to obtain more data on the effects of the El Chichon volcanic cloud. They had not been in operation for several months prior to reinstallation.

One of the observatory automobiles, the Ford station wagon, was involved in a serious accident on the saddle road on 17 September as the observers were returning to Hilo. After considerable delay, the car was replaced by a 1983 Plymouth station wagon.

During 1982, operation of ICDAS improved greatly. It was offline for various reasons for a total of only about 265 hours, or about 3% of the time.

The walls and door of the precipitation chemistry laboratory were modified during August to bring them up to GSA fire-proofing standards. The modification was effected without major disruption of the program.

5

2.1.2 Programs

Two volcanic clouds appeared over Hawaii during the year, and several of the programs were adapted to maximize the amount of information obtained under such anomalous conditions. The first cloud was originally detected by the MLO lidar on 27 January. The source of the cloud is not specifically known, hence the term "Mystery Cloud" generated by the news media. When it first appeared over Hawaii, the Mystery Cloud was centered at about 18-km altitude and had a maximum total-to-Rayleigh backscatter ratio of approximately 2.5. The Mystery Cloud had not completely disappeared from the stratosphere when it was over-shadowed by the so-called "Monster Cloud" from the 4-5 April eruption of El Chichon in Mexico. The Monster Cloud was first detected at MLO on the evening of 9 April, although there is some evidence of its existence a day or two prior to that date. It was indeed a monster in comparison with previous vol-canic clouds observed at MLO, and it persisted over Hawaii, with only a slow degradation, throughout the remainder of the year. When first observed, the Monster Cloud had a peak lidar backscatter ratio of about 220, and was cen-tered at 25-26 km. As the cloud matured there was a temporary but very sig-nificant buildup of material above 25 km, probably generated by gas-to-particle conversion. By year's end, the upper region of the cloud had de-creased in density, and the peak backscatter ratio of approximately 10 was located in the 21- to 22-km altitude region.

These major geophysical events were, and still remain, of great interest to the MLO program. As a result, the frequency of many of the regular meas-urements was increased, and additional observations were added. The net re-sult is that MLO has what is probably the best set of observations of volcanic effects ever assembled by a single observatory. Modifications to some of the measurement programs made in response to the volcanic episodes were appro-priate to enable collection of the complete data set.

The principal programs carried out at MLO during 1982 are summarized in table 1 and further described below.

Carbon Dioxide

The concentration of atmospheric CO_2 was continuously monitored by the URAS-2 NDIR gas analyzer during 1982. The instrument performed satisfactorily without major problems. The aluminum intake line on the high tower was re-placed with new tubing on 29 September. Preliminary results indicate that the rate of increase of atmospheric CO_2 concentration had decreased to approxi-mately 1.0 ppm yr^{-1} for 1982.

The GMCC weekly CO_2 flask sampling programs at MLO and KUM continued during the year. Flasks were lost or broken during shipment on only two occasions.

The study of possible vertical CO_2 gradients in the atmospheric boundary layer at MLO was completed successfully, with the result that the magnitude of any persistent gradient was below the level of detection.

Outgassing from the volcanic caldera at the summit of Mauna Loa caused disruptions of some CO_2 records in every month of the year. It occurred main-ly between midnight and 0800 LST during the downslope wind flow regime. The monthly occurrences of outgassing are listed in table 2.

Table 1.--Summary of sampling programs at MLO in 1982

Program	Instrument	Sampling frequency	Remarks
Gases			
Carbon dioxide	URAS-2 infrared analyzer	Continuous	
	0.5-ℓ glass flasks, P^3	1 pair wk^{-1}	
	0.5-ℓ glass flasks, through analyzer	1 pair wk^{-1}	Mountain and seacoast
	5-ℓ evacuated glass flasks	1 pair wk^{-1}	Mountain and seacoast
Surface ozone	Dasibi ozone meter	Continuous	
Total ozone	Dobson spectrophotometers nos. 63, 65	3 day^{-1}	No. 63, Jan-May; no. 65, Jun-Dec
Ozone profile	Dobson spectrophotometer no. 65	5 obs. wk^{-1}	Umkehr, Nov-Dec
	Balloon-borne ECC	1 wk^{-1}	From Hilo Airport
CFC-11, CFC-12, and N_2O	300-mℓ stainless steel flasks	1 pair wk^{-1}	
Aerosols			
Condensation nuclei	Pollak CNC	Discrete	4 meas., weekdays; 0, weekends
	G.E. CNC	Continuous	
Optical properties	Four-wavelength nephelometer	Continuous	450, 550, 700, 850 nm
Stratospheric aerosols	Lidar	Discrete	694.3 nm, 2 J
Skylight polarization	Polarizing radiometer	Discrete	8 wavelengths
Solar Radiation			
Global irradiance	Eppley pyranometers with Q, GG22, OG1, and RG8 filters	Continuous	
Direct irradiance	Eppley pyrheliometers (2) with Q filters	Continuous	
	Eppley pyrheliometer with Q, OG1, RG2, and RG8 filters	Discrete	
	Eppley pyrheliometer with 13 filters	Continuous	
	Seven-wavelength radiometer	Continuous	
Diffuse irradiance	Eppley pyranometer with shading disk and Q filter	Continuous	
Turbidity	Sunphotometers with 380-, 500-, 778-, and 862-nm narrowband filters	Discrete	
Meteorology			
Air temperature	Thermistor	Continuous	
	Max.-min. thermometers	1 day^{-1}	
	Hygrothermograph	Continuous	MLO and Kulani Mauka
Soil temperature	Thermistor	Continuous	
Dewpoint temperature	Dewpoint hygrometer	Continuous	
Relative humidity	Hygrothermograph	Continuous	MLO and Kulani Mauka
	Sling psychrometer	Discrete	
Pressure	Capacitance transducer	Continuous	
	Microbarograph	Continuous	
	Mercurial barometer	Discrete	
Wind (speed and direction)	Bendix Aerovane	Continuous	
Precipitation	Rain gage, 8-in	1 day^{-1}	
	Rain gage, 8-in	Twice wk^{-1}	Kulani Mauka
	Rain gage, tipping bucket	Continuous	
Total precipitable water	Foskett infrared hygrometer	Continuous	
	Spectral infrared hygrometer	Continuous	
Precipitation Chemistry			
pH	pH meter	Discrete	Rainwater collections, 6 sites
Conductivity	Conductivity bridge	Discrete	
Chemical components	Ion chromatograph	Discrete	
Cooperative Programs			
Carbon dioxide (SIO)	Infrared analyzer (Applied Physics)	Continuous	
	5-ℓ evacuated glass flasks	1 pair wk^{-1}	Mountain and seacoast
Surface SO_2 (EPA)	Chemical bubbler system	Every 12 days	
Total surface particulates (DOE)	High-volume sampler	Continuous	Dependent on wind direction; 1 filter wk^{-1}
Total surface particulates (EPA)	High-volume sampler	Every 12 days	
Atmospheric electricity (Univ. of Minnesota)	Field mill, air conductivity meter, surface antenna	Continuous	
Ultraviolet radiation (Temple Univ.)	Ultraviolet radiometer	Continuous	Radiation responsible for sunburning of skin
Precipitation collection (DOE)	HASL wet-dry collector	Continuous	
Precipitation collection (EPA)	Misco model 93	Continuous	
Precipitation collection (Univ. of Paris)	Likens funnel collector	Twice wk^{-1}	
Precipitation collection (IAEA)	Likens funnel collector	Twice wk^{-1}	
Wet-dry deposition (Univ. of Illinois)	Exposed collection pails	Continuous	NADP
Aerosol chemistry (Univ. of Maryland)	Nuclepore filters	Continuous	Day-night discrimination
Aerosol chemistry (Univ. of Arizona)	Quartz filters	Continuous	Day-night discrimination
^{13}C (USGS, Denver)	10-ℓ stainless steel flasks	2 wk^{-1}	
Radiocarbons (USGS, Menlo Park)	NaOH collector	Discrete	

7

Table 2.--Monthly occurrences of outgassing from the
volcanic caldera on Mauna Loa during 1982

	Jan	Feb	Mar	Apr	May	Jun	Jul	Aug	Sep	Oct	Nov	Dec
No. of days	10	5	10	5	8	10	3	3	9	17	5	13
Percent of days	32	18	32	17	26	33	10	10	30	55	17	42

Ozone

Surface ozone was measured continuously with a Dasibi ozone meter. Total ozone in the atmospheric column was measured on about 230 days during 1982 using a Dobson spectrophotometer. In addition, this instrument was used for measuring the ozone profile by the Umkehr technique 5 days per week from 10 May to the end of the year in an effort to determine the effects of the El Chichon cloud on atmospheric ozone.

A special series of ozonesonde observations was started during a visit of Boulder personnel to MLO in the last half of September, and was continued as an MLO program through the remainder of the year. This program was also started in response to the volcanic cloud. Ten flights were made over the 3.5-mo period.

Surface Aerosols

Both the G.E. and Pollak CNC's operated normally throughout the year. The four-wavelength nephelometer was returned to operation in May and yielded good data for the remainder of the year.

Stratospheric Aerosols--Lidar

The MLO lidar observations of the two volcanic clouds over Hawaii during 1982 are the most complete taken and constitute an excellent data set for characterizing the stratospheric clouds. MLO was in a very advantageous location for the observations, because the cloud was initially confined to the low-latitude regions of the Earth and was thus not observed at the numerous lidar stations at more northerly latitudes. Therefore, the rapid changes of the cloud during its first several weeks of existence were observed only at MLO.

The lidar equipment operated quite well throughout the year considering the age and complexity of the system. Seventy observations were made in 1982, each observation consisting of 60-150 laser shots. Observations of the El Chichon cloud taxed the capability of the system because of the high altitudes reached by the volcanic material and the limited dynamic range of the 8-bit analog-to-digital converter. In many cases, multiple profiles were taken with different settings of signal delay and photomultiplier voltage to extend the range of the system. In addition, it was necessary to obtain profiles in the lower altitude range to determine the most appropriate altitude for normalization of the lidar response.

Solar Radiation

A great deal of emphasis was put on solar radiation observations at MLO during 1982 to characterize the effects of volcanic clouds on the solar radiation regime. The frequency of sunphotometer and filter-wheel pyrheliometer measurements was increased; a second sunphotometer operating at near-IR wavelengths was put into use; and two spectral pyranometers that had previously been removed were put back online.

Solar-tracking capability was improved by the installation of a sophisticated active tracker. The multiwavelength filter radiometer mounted on the tracker greatly extended the spectral measurements being made. As a result of these improvements, the solar radiation observations at MLO are some of the best and most complete available for assessing the radiative effects of volcanic clouds.

The intensity and polarization of skylight were measured frequently during the year to determine the light-scattering effects of the volcanic cloud. It was found that the cloud had particularly pronounced effects on the polarization field, although the skylight intensity also changed significantly. The maximum polarization at near-IR wavelengths was decreased by a factor of 2 by the cloud, and the distribution over the sky was modified significantly. The results have been described by Coulson (1983a, 1983b), and further work is in progress.

Meteorology

Meteorological measurements continued without major problems throughout the year.

Precipitation Chemistry

Precipitation chemistry continued without problems at about the same level of activity as in prior years.

Cooperative Programs

The relatively large number of cooperative programs continued normally through 1982; some new projects were added; and some special projects were pursued by visiting scientists. A brief summary of cooperative efforts follows.

Aerosols continued to be collected on Nuclepore filters for the University of Maryland and on quartz filters for the University of Arizona. An electronic controller operated the pumps on the basis of wind speed and direction, particulate content of the ambient air, and time of day. Both projects were continued throughout the year, and filters were changed on a weekly schedule. A daily schedule was used in changing filters for an aerosol absorption study by the University of Washington. The aerosol collection equipment of the University of California, Davis, was taken offline and returned to that institution on 23 February. Special aerosol studies were made by W. Zoller and three students from the University of Maryland over a 10-day period in May. A. Clarke of the University of Washington spent the period 20 April-31 May making different types of aerosol measurements at MLO, and left his collectors for MLO personnel to operate when he returned to Washington.

J. Gras from CSIRO, Melbourne, Australia, spent 2 weeks in April at MLO collecting and analyzing aerosols. E. Butler from URI visited MLO for 3 weeks in September and October to collect methyl iodide and selenium aerosols. Aerosols continued to be collected by high-volume samplers for DOE and EPA.

J. DeLuisi and E. Dutton of GMCC in Boulder made special solar radiation observations in September and October to characterize the radiative effects of the El Chichon volcanic cloud. They also installed the solar tracker and radiometers in the solar dome, and trained MLO personnel on their operation. In November, W. Egan from Adelphi University spent a few days at MLO measuring the intensity and polarization of skylight in an effort to validate the aerosol models he developed for the El Chichon cloud. Erythema radiation measurements for Temple University continued throughout the year.

Three new cooperative projects for studies of atmospheric gases were started at MLO during 1982. A project for supplying flask samples of air from the observatory on a weekly basis for OGC was started in January and continued for the remainder of the year. The air samples are for measurements of the concentrations of six radiatively important trace gases in the atmosphere. A Brewer spectrophotometer was brought to MLO by AES of Canada on 25 April and put into operation for measurements of the total ozone and SO_2 content of the atmospheric column. The instrument was operated daily by MLO personnel during the last 8 months of the year. Samples of CO_2 collected by relatively long-term exposure of vats of NaOH solution at MLO were analyzed for their radio-carbon content by the USGS, Menlo Park.

In addition to these new cooperative projects, MLO continued to operate SIO's CO_2 analyzer, and flask samples of air from MLO continued to be supplied to SIO and to USGS, Denver. SO_2 samples were taken weekly for EPA.

MLO continued to participate in NADP by sending wet and dry samples of atmospheric deposition to the Illinois State Water Survey. Bulk collections of atmospheric deposition were supplied all year to DOE. In addition, precipitation samples were supplied on a routine basis to the University of Paris and IAEA. In a short-term project, six rainwater samples were sent to the Argonne National Laboratory for special analysis.

Two sets of equipment operated at MLO throughout 1982 for measurement of atmospheric electrical parameters. The equipment installed many years ago by W. Cobb, and now under the nominal direction of NCAR, operated well. Continuous records of potential gradient, air-Earth current, and positive and negative conductivity of the air were obtained. The instruments of D. Olson of the University of Minnesota for measuring potential gradient and air-Earth current also continued in operation, and the records were sent to him regularly.

2.1.3 MLO Meteorological Museum

The following items were added to the museum collection: (1) an ozonesonde developed in Germany by H. Paetzold and F. Piscaller for the 1957-1958 IGY, (2) samples of volcanic ash from the eruption of El Chichon, (3) a Boller and Chivens anemometer, and (4) miscellaneous books and publications on meteorology and related fields.

2.2 Barrow

2.2.1 Facilities

NARL, overseen by IT&T and Calista Corporation (a southern Alaskan native corporation), is still furnishing power to BRW. Scientific research at NARL has been discontinued, and the complex is being maintained on a caretaker status.

NWS is planning to build a new station and housing complex east of the town airport runway. GMCC has requested two living quarters there for future station personnel.

GMCC is officially requesting transfer, from ONR to NOAA, of the title to 100 acres of land surrounding the observatory. This land, along with much of the land northeast of the town of Barrow, is temporarily under the custodial care of BLM.

A new Motocross 300 snowmobile was purchased for transportation on the open tundra when the access road becomes heavily snow covered in the winter. The Bombi all-terrain vehicle was back in operation after a series of repairs. The 1969 Chevrolet pickup truck was excessed.

2.2.2 Programs

Programs carried out during 1982 at BRW are listed in table 3. Comments on some selected programs follow.

Carbon Dioxide

Because of a broken glass rod in the reference cell chamber, the URAS-2T analyzer was down for a few weeks in January. In addition, errors in the data linearity known as closure occurred early in the year and were corrected after an optical alignment. A new single-source reference cell was installed in June. The special ground-line sampling project designed to measure CO_2 flux near the surface continued with increasingly good results.

Ozone

The Dasibi surface ozone meter performed well throughout the year. In December, Dobson spectrophotometer no. 76 was returned to Boulder for calibration.

Halocarbons and Nitrous Oxide

Weekly flask sampling went smoothly for the year.

Surface Aerosols

Performance of the G.E. CNC was erratic. Absorption problems with the humidifier wick occurred, and the vacuum pump was repaired. The Pollak CNC and the four-wavelength nephelometer generally performed well throughout the year.

11

Table 3.--Summary of sampling programs at BRW in 1982

Program	Instrument	Sampling frequency
Gases		
Carbon dioxide	URAS-2T infrared analyzer	Continuous
	0.5-ℓ glass flasks, P^3	1 pair wk^{-1}
	0.5-ℓ glass flasks, through analyzer	1 pair wk^{-1}
	5-ℓ evacuated glass flasks	1 pair wk^{-1}
Surface ozone	Dasibi ozone meter	Continuous
Total ozone	Dobson spectrophotometer no. 76	3 day^{-1}
CFC-11, CFC-12, and N_2O	300-mℓ stainless steel flasks	1 pair wk^{-1}
Aerosols		
Condensation nuclei	Pollak CNC	Discrete
	G.E. CNC	Continuous
Optical properties	Four-wavelength nephelometer	Continuous
Aerosol chemistry	Streaker, Cascade impactor	Discrete (Mar-May)
Solar Radiation		
Global irradiance	Eppley pyranometers with Q and RG8 filters	Continuous
Direct irradiance	Eppley pyrheliometer with Q, OG1, RG2, and RG8 filters	Discrete
Turbidity	Sunphotometers with 380-, 500-, 778-, and 862-nm narrowband filters	Discrete
Meteorology		
Air temperature	Thermistor	Continuous
	Max.-min. thermometers	1 day^{-1}
	Hygrothermograph	Continuous
Soil temperature	Thermistor	Continuous
Temperature gradient	2 vertically separated thermistors	Continuous
Dewpoint temperature	Dewpoint hygrometer	Continuous
Relative humidity	Hygrothermograph	Continuous
Pressure	Capacitance transducer	Continuous
	Microbarograph	Continuous
	Mercurial barometer	Discrete
Wind (speed and direction)	Bendix Aerovane	Continuous
Wind (turbulence)	2 vertically separated anemometers	Continuous (Jul-Dec)
Precipitation Chemistry		
pH	pH meter (samples analyzed at MLO)	Discrete
Conductivity	Conductivity bridge (samples analyzed at MLO)	2 mo^{-1}
Cooperative Programs		
Total surface particulates (DOE)	High-volume sampler	Continuous (1 filter wk^{-1})
Aerosol chemistry (URI)	High-volume samplers	Continuous (one, 1 filter day^{-1}; the other, on an episodic basis)
Particulates (Carnegie-Mellon Univ.)	High-volume sampler	Continuous (Feb-May)
Global radiation (SRL)	6 Eppley pyranometers	Continuous
Ultraviolet radiation (Temple Univ.)	Ultraviolet radiometer	Continuous
Carbon dioxide (SIO)	5-ℓ evacuated glass flasks	1 pair wk^{-1}
Precipitation gage (ASCS)	Wyoming shielded precipitation gage	2 mo^{-1}
Carbonaceous particles (LBL)	Dichotomous sampler (quartz and Millipore filters)	Continuous (1 set of filters wk^{-1})
	High-volume filter	Continuous (1 filter day^{-1})
Halocarbons (OGC)	5-ℓ stainless steel flasks	1 wk^{-1} (3 flasks sample^{-1})
Incident and reflected radiation (Univ. of Alaska)	Up-down pyranometers	Continuous (program ended in Nov)
Magnetic fields (USGS)	Magnetometer	1 station check wk^{-1}
^{13}C (USGS)	10-ℓ stainless steel flasks	1 pair mo^{-1}

Solar Radiation

A new Leeds and Northrup chart recorder was installed at BRW to record pyranometer data.

Meteorology

New electronic boards to interface the meteorological sensors with ICDAS were installed in November. During the Arctic summer, two turbulence anemometers were installed on the meteorological tower, with approximately a 6-m vertical separation. The turbulence-parameter data will be used in a CO_2 flux model. CO_2 fluxes near BRW are thought to be caused primarily by photosynthesis, respiration, and decay of tundra vegetation.

Precipitation Chemistry

Rain samples were taken on an episodic basis. However, during the summer, samples were often difficult to obtain because of low rainfall rates.

ICDAS

Because of problems in alignment and data sensing, the tape drive system was replaced twice. ICDAS was down most of November and December as a result of a faulty multiplexer that interfaces the sensors with the NOVA computer.

Cooperative Programs

BRW cooperated with several groups on programs listed in table 3. The following occurred during 1982: (1) the outside sampling platform, which houses several cooperative filter sampling programs and is located approximately 30 m south of the main observatory building, was rewired; (2) an additional high-volume impactor was added to the LBL aerosol sampling program; (3) during February, filters were exposed on a second sampling system for URI; (4) a new pump was installed for the DOE high-volume filter system; (5) flask samples were taken during three aircraft flights (two in May and one in August), and surface air samples were also taken, supporting the OGC project to determine the vertical distribution of halocarbons in the lower Arctic troposphere; and (6) the University of Alaska solar radiation program was reinstated in June.

2.2.3 Arctic Haze Project

From approximately mid-March through mid-May, a special intensive data gathering project was undertaken to measure basic characteristics of the Arctic haze. During the project, some existing programs were expanded and new ones were initiated. Additional solar radiation measurements were taken using photometers and modified normal incidence pyrheliometers (GMCC and University of Alaska). Aerosol chemistry filter samples were obtained using a cascade impactor and a streaker for subsequent PIXE analysis. Halocarbon air samples were taken with increased frequency for OGC. An atmospheric bromine sampling program was initiated by NCAR.

13

2.3 Samoa

2.3.1 Facilities

No major changes in SMO facilities were made in 1982. Preliminary plans for installation of the PV system were made, however. These plans involved ordering a replacement central air conditioner and designing duct modifications for the ICDAS room where the PV system controller, inverter, and battery bank will be located. Structural timbers for the PV array supports were delivered in early December, and air-conditioning work will be completed early in 1983. In addition, the PV system batteries and scaffolding for use in erecting the PV array supports and the PV array modules were delivered in December. Construction of the PV supports is scheduled to begin in early 1983.

No changes were made in the GMCC remote sampling buildings at the point or on the ridge during 1982. A contract was let to repair and paint the two GMCC housing units. The most serious phase involved replacement of shake shingles rotted by chronic shading from vegetation adjacent to the house roofs. Several trees were removed and over 1500 ft^2 of shingles were replaced. In addition, on one unit, rotted 2×6 tongue and groove planking was replaced under the shingles. The shade from a large tree kept the area moist, and rot had penetrated deeply into the roof below the shingle layer. The units were also completely painted, resulting in considerable improvement in their appearance.

2.3.2 Programs

All 1982 programs are summarized in table 4. No additions to SMO GMCC programs were made during 1982, however major disruption of all programs occurred on 28 March when lightning struck the top level of the remote sampling tower located on the ridge, approximately 100 m east of the main building. Downtime for damaged equipment ranged from a few days to a few months, but eventually everything was put back online after much help from Boulder GMCC and considerable effort by R. Williams, the SMO electronic technician.

Carbon Dioxide

A URAS-2T analyzer (SN 0016), in continuous operation since February 1978, was upgraded in September by installation of a single IR source assembly. A set of GMCC CO_2-in-air traveling standards arrived onsite in October and will remain while the regular GMCC standards are returned to Boulder for recalibration. The regular standards should return to SMO by mid-1983. Periodic use of a GMCC CO_2-in-air surveillance tank was also implemented during October. It was substituted for a working-gas tank during the regular weekly calibration. The GMCC/SIO joint flask intercomparison continued all year.

Ozone

The SMO Dasibi ozone meter was damaged by the lightning strike, and was returned to Boulder along with its recorder in late March. An interim instrument sent from Boulder was used until October when the SMO unit was returned after repair. Dobson operation using instrument no. 42 was uninterrupted all year.

14

Table 4.--Summary of sampling programs at SMO in 1982

Program	Instrument	Sampling frequency
Gases		
Carbon dioxide	URAS-2T infrared analyzer	Continuous
	0.5-ℓ glass flasks, P^3	1 pair wk^{-1}
	0.5-ℓ glass flasks, through analyzer	1 pair wk^{-1}
	5-ℓ evacuated glass flasks	1 pair wk^{-1}
Surface ozone	Dasibi ozone meter	Continuous
	ECC meter (terminated Sep 81)	Continuous
Total ozone	Dobson spectrophotometer no. 42	3 day^{-1}
CFC-11, CFC-12, and N_2O	300-mℓ stainless steel flasks	1 pair wk^{-1}
Aerosols		
Condensation nuclei	Pollak CNC	Discrete
	G.E. CNC	Continuous
Optical proporties	Four-wavelength nephelometer	Continuous
Solar Radiation		
Global irradiance	Eppley pyranometers with Q and RG8 filters	Continuous
	Eppley pyranometers (2) with Q filters on tilted mounts	Continuous
Direct irradiance	Eppley pyrheliometer with Q filter	Continuous
	Eppley pyrheliometer with Q, OG1, RG2, and RG8 filters	Discrete
Turbidity	Sunphotometers with 380-, 500-, 778-, and 862-nm narrowband filters	Discrete
Meteorology		
Air temperature	Thermistor	Continuous
	Max.-min. thermometers	1 day^{-1}
	Hygrothermograph	Continuous
Soil temperature	Thermistor	Continuous
Dewpoint temperature	Dewpoint hygrometer	Continuous
Relative humidity	Hygrothermograph	Continuous
	Sling psychrometer	Discrete
Pressure	Capacitance transducer	Continuous
	Microbarograph	Continuous
	Mercurial barometer	Discrete
Wind (speed and direction)	Bendix Aerovane	Continuous
Precipitation	Polyethylene funnel, bottle	1 day^{-1}
Precipitation chemistry		
pH	Corning model 125 meter with semimicro combination electrode	1 day^{-1} (GMCC); 1 wk^{-1} (NADP)
Conductivity	Beckman model RC-16C meter	1 day^{-1} (GMCC); 1 wk^{-1} (NADP)
Cooperative Programs		
Carbon dioxide (SIO)	5-ℓ evacuated glass flasks	1 pair wk^{-1}
ALE project: CFC-11, CFC-12, N_2O, $CHCl_3$, CCl_4 (OGC)	HP5840A gas chromatograph	1 h^{-1}
CH_4, CO, CO_2 (OGC)	Carle gas chromatograph	3 h^{-1}
CH_3I, CH_3Cl, CH_4, CO (OGC)	Stainless steel flasks, 3 set^{-1}	1 wk^{-1}
^{13}C (USGS)	10-ℓ stainless steel flasks	2 pair mo^{-1}
Wet-dry deposition (NADP)	HASL wet-dry collector (new Chemetrics, Dec 81)	1 wk^{-1}, wet; 2 mo^{-1}, dry
Wet-dry deposition (EML)	HASL wet-dry collector (terminated May 81)	1 mo^{-1}
Bulk deposition (EML)	Plastic bucket	1 mo^{-1}

15

Surface Aerosols

The G.E. CNC was operational all year except for a few days after the lightning strike. As a result of the lightning damage, nephelometer operation was interrupted from late March to early June, Pollak CNC operation was interrupted for a few days while a replacement power supply was sent from Boulder, and the aerosol program chart recorder, which was also damaged, was returned to Boulder for repairs.

Solar Radiation

Quartz and RG8 pyranometers plus a tracking NIP and filter-wheel NIP were operational all year except for a period subsequent to the lightning strike. All the preamps were replaced and the damaged NIP was exchanged.

Meteorology

Normal operations prevailed until late March when all sensors suffered lightning damage. The Aerovane system, temperature sensors, pressure transducer, and all meteorology rack cards were damaged. Fortunately, a complete spare Aerovane system, scheduled for installation at the point, was on hand and was used as a replacement. The dewpoint hygrometer and the pressure transducer were both returned to Boulder, and remained offline for the rest of the year. Temperature sensors were in operation again by mid-April.

Precipitation Chemistry

Collection protocols remained unchanged from 1981. A GMCC daily bulk sample, an NADP weekly wet-deposition sample, and a monthly DOE bulk sample program were maintained. Onsite pH and conductivity measurements were performed on NADP and GMCC samples.

ICDAS

ICDAS operated normally all year except for a few days subsequent to the March lightning strike. The NOVA computer suffered minor damage, requiring exchange of only one board. The multiplexer-digitizer was finally returned to normal operation in mid-May, after major problems were solved.

2.4 South Pole

2.4.1 Facilities

The GMCC CAF at SPO underwent several changes during the 1982 season. The high-pressure compressor used for ^{14}C sampling was moved from its skylab location to the CAF pump room and connected to an unused sampling stack through the ceiling. An automatic pressure shutoff valve was connected into the system. While this move was under way, the high-volume pumps located in the cabinet in that room were removed, and the decaying decking was replaced with 1/2-in plywood covered with rubber matting. During reinstallation of the pumps, the wiring was replaced and the PISSA wind controller was brought back on line. Figures 1 and 2 illustrate current CAF internal and roof arrangements.
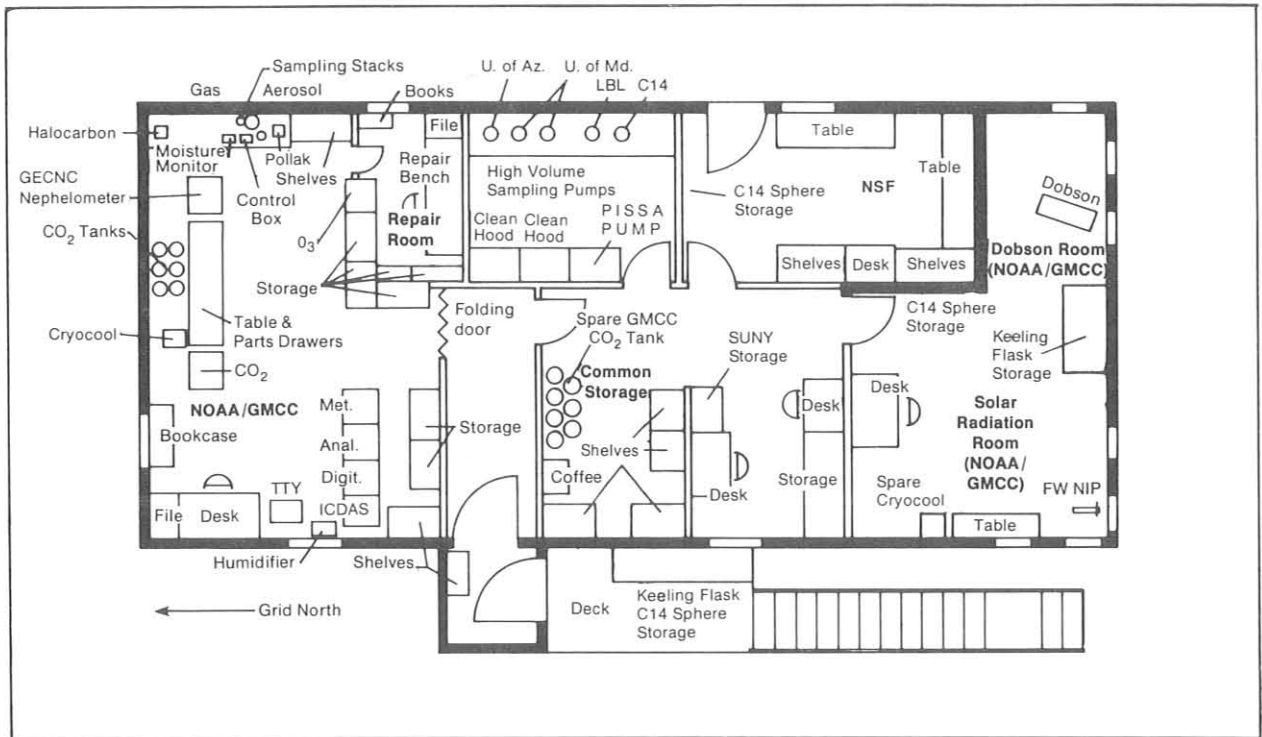
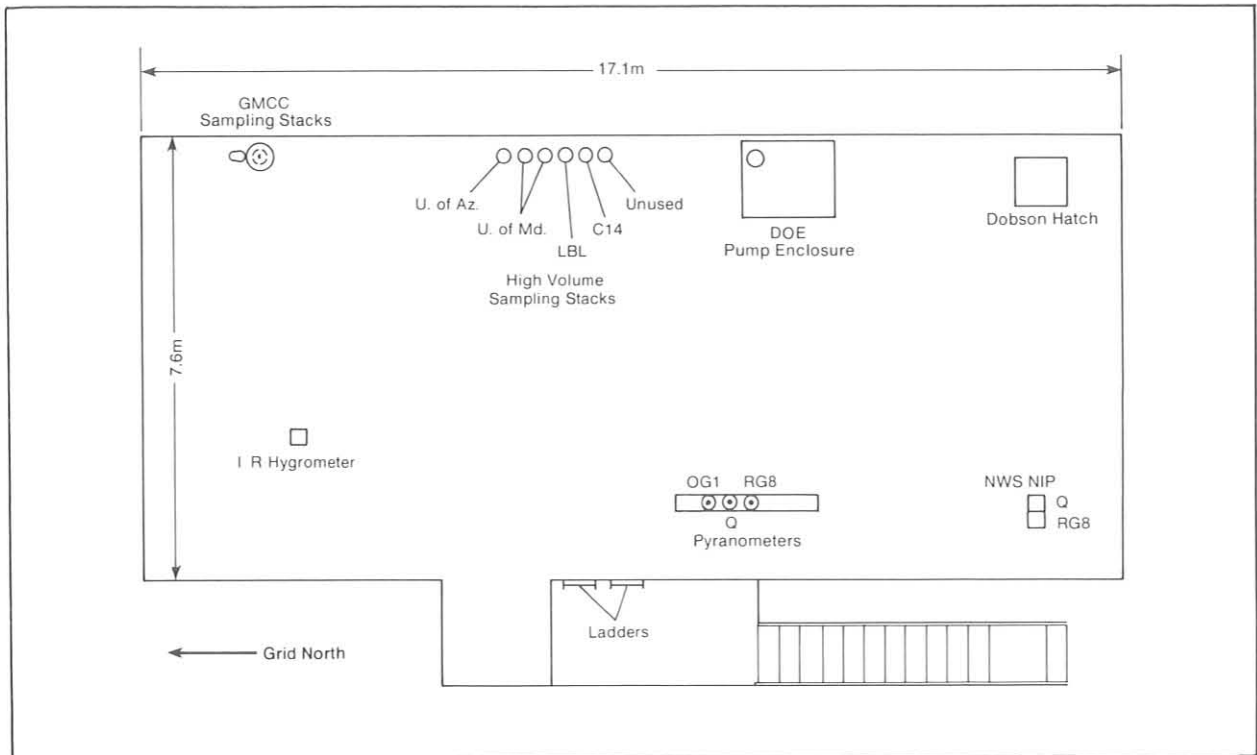Figure 1.--CAF floor plan at SPO, 1982.

Figure 2.--CAF roof plan at SPO, 1982.

CAF wiring was reviewed and two remote outlets, one plugged into a wall outlet and the other plugged into ICDAS regulated power, were rewired through the circuit breaker box. CAF power distribution is illustrated in figs. 3 and 4. The intake stacks for the various sampling programs were heat-taped and insulated to prevent continuous buildup of ice on them. A complete inventory of CAF equipment and spare parts was made. This inventory was entered into the station computer and organized so that printouts are available by equipment, part, and location. A procedure was also established for keeping the inventory current.

CAF is plagued by large temperature fluctuations during the summer, apparently due to solar heating. A thermostatically controlled fan was installed to help control these fluctuations. Another heat-related problem was water leaking into the building from the roof. This probably originated with spindrift that worked its way into the roof insulation during the winter. A special effort was made to keep the roof clear of snow to reduce this problem for the following summer. The heater located behind the CO_2 analyzer caused problems for previous crews. It was moved to a location near the humidifier.

During the summer, several researchers occupied CAF. Their relationship with GMCC personnel was remarkable for its spirit of cooperation. Their projects were S255B, S275A, and S279; detailed descriptions are contained in the NSF listing of Antarctic projects for 1981-1982. During winter, Y. Latov from the Soviet Union maintained part of his magnetic field project in CAF.

In the past, problems have been reported concerning human intrusion into the Clean Air Quadrant. This year, both the NSF representative and Station Manager worked closely with the GMCC Station Chief. Each arriving scientist was briefed by the NSF representative and each arriving support person was briefed by the Station Manager, resulting in very few unauthorized intrusions into the area.

During the first 2 months of 1982, several station power outages interrupted work at CAF. With normalization of the power plant, these interruptions ceased. The main station experienced three fires, one in the fuel arch in the primary fuel supply and two in the power plant. There were no serious consequences for CAF, however, as a result of these events. During the winter, a new survey of the entire SPO complex including CAF was conducted. Figure 5 is derived from this new survey, representing the most recent available information. Also, the second SPO winter airdrop, which occurred 21 June, was on the coldest day on record with a minimum temperature of -83.2°C.

2.4.2 Programs

SPO programs are listed in table 5 and are briefly described below.

Carbon Dioxide

The CO_2 system experienced a major breakdown. E. Green traveled to SPO in January to install a new URAS-2T analyzer. Near season's end, the gas distribution piping became partially clogged, causing erratic readings for several days. With the relocation of the heater, which was formerly behind the analyzer, the zero-drift problem of previous years was solved.
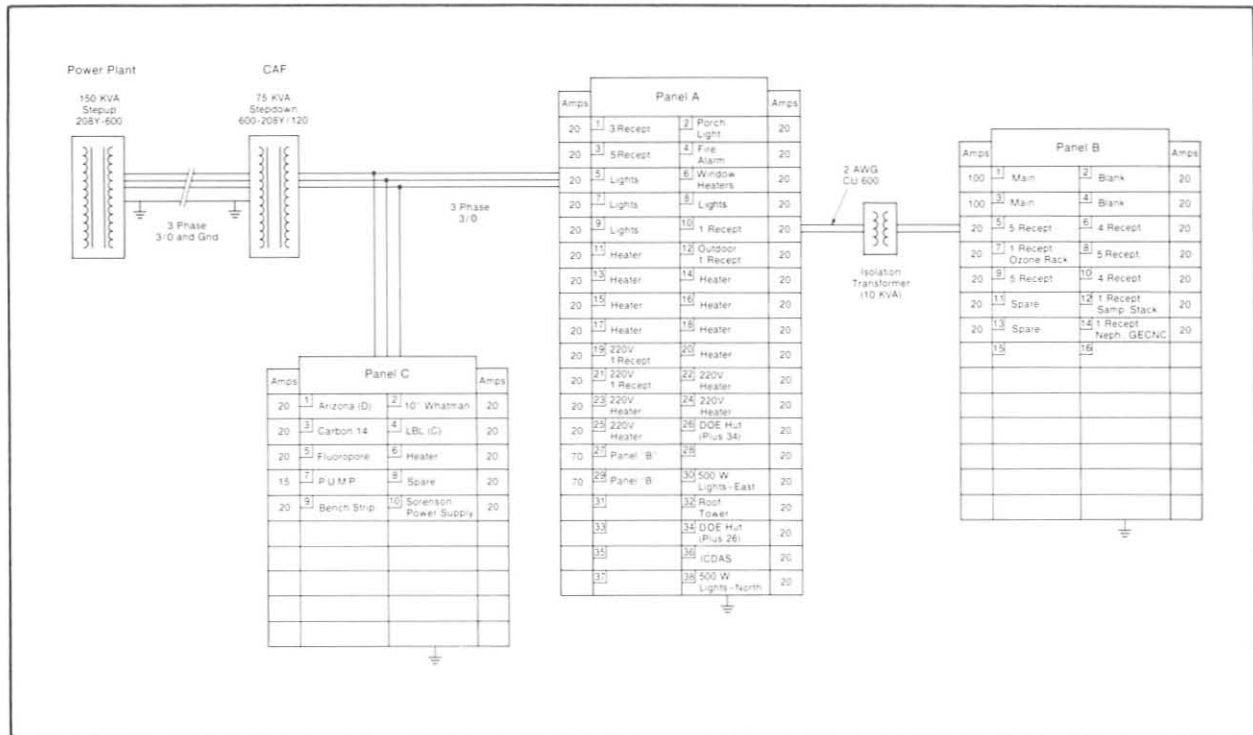
18

Power Plant
150 KVA Stepup 208Y-600

CAF
75 KVA Stepdown 600-208Y/120

3 Phase 3/0 and Gnd

3 Phase 3/0

2 AWG CU 600

Isolation Transformer (10 KVA)

Panel A

Amps	#		#		Amps
20	1	3 Recept	2	Porch Light	20
20	3	5 Recept	4	Fire Alarm	20
20	5	Lights	6	Window Heaters	20
20	7	Lights	8	Lights	20
20	9	Lights	10	1 Recept	20
20	11	Heater	12	Outdoor 1 Recept	20
20	13	Heater	14	Heater	20
20	15	Heater	16	Heater	20
20	17	Heater	18	Heater	20
20	19	220V 1 Recept	20	Heater	20
20	21	220V 1 Recept	22	220V	20
20	23	220V Heater	24	220V Heater	20
20	25	220V Heater	26	DOE Hut (Plus 34)	20
70	27	Panel 'B'	28		
70	29	Panel 'B'	30	500 W Lights - East	20
	31		32	Roof Tower	20
	33		34	DOE Hut (Plus 26)	20
	35		36	ICDAS	20
	37		38	500 W Lights - North	20

Panel B

Amps	#		#		Amps
100	1	Main	2	Blank	20
100	3	Main	4	Blank	20
20	5	5 Recept	6	4 Recept	20
20	7	1 Recept Ozone Rack	8	5 Recept	20
20	9	5 Recept	10	4 Recept	20
20	11	Spare	12	1 Recept Samp Stack	20
20	13	Spare	14	1 Recept Neph. GECNC	20
	15		16		

Panel C

Amps	#		#		Amps
20	1	Arizona (D)	2	10" Whatman	20
20	3	Carbon 14	4	LBL (C)	20
20	5	Fluoropore	6	Heater	20
15	7	P U M P	8	Spare	20
20	9	Bench Strip	10	Sorenson Power Supply	20

Figure 3.--CAF electrical power circuit diagram, 1982.

C9

A19, A21 220V

B9 B12 B12 B7 A11 (0000) C9 C9 A3 A17 A15 A3 B5 B5

C6 A13

B7 220V Room No. 2 A1 A1 Room No. 3 A3 A23, A25 220V

ET Shop A10 Room No. 4

A8 B9 A3 A3 B5

B14 B9 A8 B7 B7 B7 B5

Room No. 1 B6 B10 B8 B8 Room No. 5 A16

Hall Room No. 7 Room No. 6 B8

B6 B10

B9 B6 B10 B10 B8 B8 A14 B5 B8

A22, A24 220V B6 A18 B10 A20 B8

Vest. Deck

A12

A32 Roof and Tower Outlets
A26, A43 DoE Shack Heater (220V)

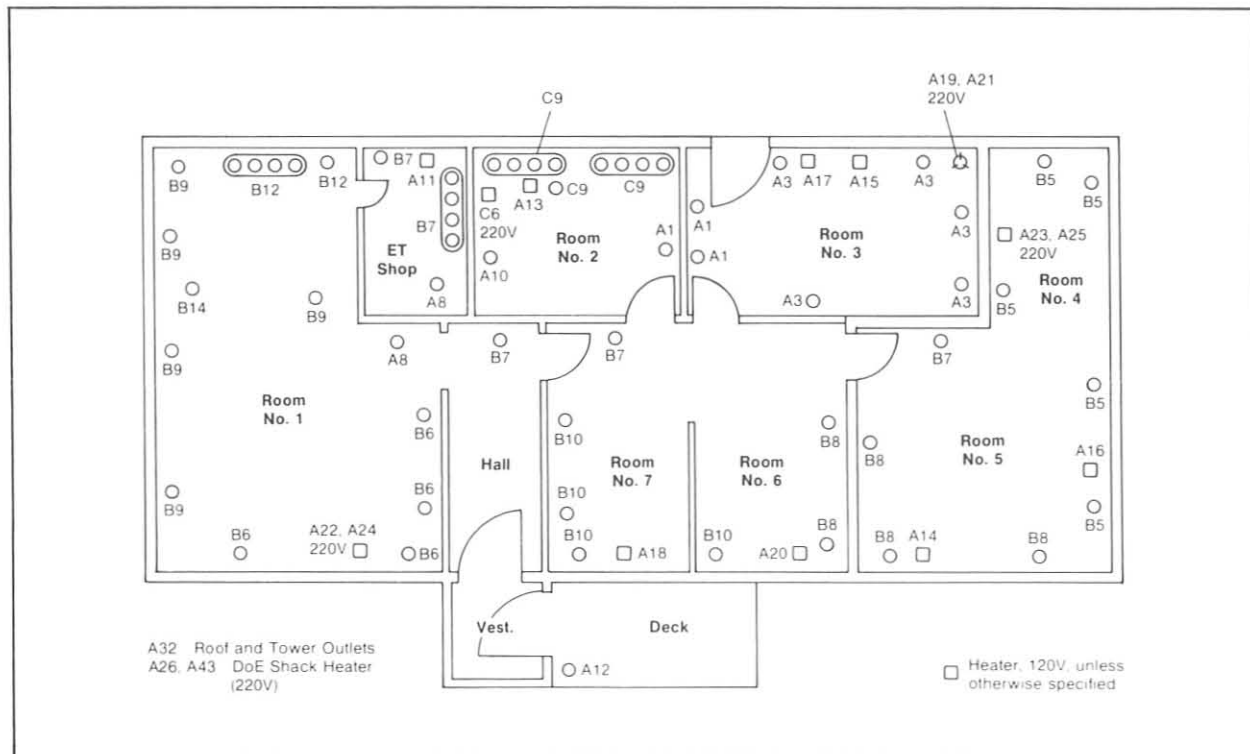Heater, 120V, unless otherwise specified

Figure 4.--CAF electrical power distribution, 1982.

Figure 5.--SPO survey, 1981-1982.

Table 5.--Summary of sampling programs at SPO in 1982

Program	Instrument	Sampling frequency	Remarks
Gases			
Carbon dioxide	URAS-2T infrared analyzer	Continuous	Jan 74-present (excl. Nov 78-Nov 79)
	0.5-ℓ glass flasks, P[3]	1 pair wk^{-1}	Jun 81-present
	0.5-ℓ glass flasks, through analyzer	1 pair wk^{-1}	Nov 79-present
Surface ozone	Dasibi ozone meter	Continuous	Jan 76-present
Total ozone	Dobson spectrophotometer no. 80	3 day^{-1}	Dec 63-present
CFC-11, CFC-12, and N_2O	300-mℓ stainless steel flasks	1 pair wk^{-1}	Jan 77-Dec 79
		1 pair wk^{-1}, austral summer	Jan 80-present
Aerosols			
Condensation nuclei	Pollak CNC	Discrete	Jan 74-present
	G.E. CNC	Continuous	Jan 74-present
Optical properties	Four-wavelength nephelometer	Continuous	Jan 79-Dec 79; Jan 81-present
Aerosol chemistry	Streaker, Cascade impactor	Discrete	Jan-Dec 82
Solar radiation			
Global irradiance	Eppley pyranometers with Q, OG1, and RG8 filters	Continuous	Feb 74-present
Direct irradiance	Eppley pyrheliometers with Q and RG8 filters	Continuous	Oct 75-present
	Eppley pyrheliometer with Q, OG1, RG2, and RG8 filters	Discrete	Jan 77-present
Turbidity	Sunphotometers with 380-, 500-, 778-, and 862-nm narrowband filters	Discrete	Jan 74-present
Albedo	Eppley pyranometers with Q, OG1, and RG8 filters	Continuous	Jan 82-present
Meteorology			
Air temperature	Thermistor	Continuous	Mar 77-present
Snow temperature	Thermistor	Continuous	Mar 77-present
Room temperature	Thermistor	Continuous	Jul 78-present
Water vapor density	Du Pont 303 moisture monitor	Continuous	Mar 77-present
Pressure	Capacitance transducer	Continuous	Dec 75-present
	Microbarograph	Continuous	Feb 80-present
	Mercurial barometer	Discrete	Jan 80-present
Wind (speed and direction)	Bendix Aerovane	Continuous	Dec 75-present
Total precipitable water	Infrared hygrometer	Discrete	Dec 81-Jan 82
Cooperative Programs			
Carbon dioxide (SIO)	5-ℓ evacuated glass flasks	2 mo^{-1} (3 flasks sample^{-1})	1957-present
Total surface particulates (DOE)	High-volume sampler	Continuous (1 filter wk^{-1})	May 70-present
Total surface particulates (EPA)	High-volume sampler	Continuous (1 filter wk^{-1})	May 70-present
Aerosol chemistry (Univ. of Maryland)	High-volume samplers	Continuous	Jan 79-present
Aerosol chemistry (Univ. of Arizona	High-volume samplers	Continuous	Jan 82-present
Aerosol physical properties (SUNYA)	Pollak CNC with diffusion battery	Discrete	Jan 74-present
Carbon aerosol (LBL)	High-volume sampler	Continuous	Jan 82-present
Halocarbons (OGC)	5-ℓ stainless steel flasks	Twice mo^{-1} (3 flasks sample^{-1})	1980-present
[13]C (USGS)	10-ℓ stainless steel cylinder	1 mo^{-1} (2 cylinders sample^{-1})	Jan 81-present
[14]C (NOAA/ARL)	3,000 psi spheres	500 psi day^{-1}, austral summer	1972-present
Drifting snow (Univ. of Alaska)	Snow crystal counter	Continuous	Jan 82-present

The P^3 sampler was difficult to operate during the cold winter months. Two heat guns were pointed continuously at the flask valves to facilitate closing them when the temperature was lower than -50°C.

Ozone

The surface ozone program continued through the year with no major problems.

Halocarbons

Halocarbon collection presented no problems this year.

Surface Aerosols

The main sources of trouble in the aerosol program were the G.E. CNC and the Pollak CNC microammeter. The optical chamber of the G.E. CNC flooded shortly after reinstallation following its return to SPO. During the year this instrument drifted more than expected probably because of a leak in the air intake path. The microammeter used for Pollak counter readings failed in April, and a substitute was used until the midwinter airdrop in June.

Solar Radiation

Solar radiation was monitored without major problems. During the summer an IR hygrometer measured discrete total-column water-vapor levels several times a day. A new discrete and continuous albedo measuring system was installed this year.

Meteorology

The only major problem in the meteorology program was the failure of the Du Pont moisture monitor, which prevented collection of further moisture data.

ICDAS

ICDAS failed 24 times during 1982. Four failures were related to the station power-plant fires; one was because of operator error; one occurred for no known reason; and the remaining were caused by erratic station-generator governors. A tape-transport problem delayed data collection for several days.

This year, all returned data tapes were sealed in metalized plastic Polyseal.

Cooperative Programs

No problems occurred with the SIO CO_2 flask sampling program. The DOE aerosol sampling system lost only a few hours of data from a mechanical and an electrical failure during the year. No problems occurred with the OGC halocarbon flask sampling program or the USGS ^{13}C program.

The University of Maryland and University of Arizona aerosol chemistry systems were not fully operational when the station opened in November 1981. The installation was electrically makeshift and physically deteriorated. The wind-sector controller was nonfunctional except as an on/off switch for each

unit. The system was physically and electrically upgraded and the controller was repaired. The downpipes were heat-taped to prevent icing. During the winter, there were several pump failures. The University of Arizona system suffers from a design defect that allows the filter to be sucked up the intake pipe when the holder is opened for filter removal.

The newly installed LBL carbon aerosol system consists of a roof intake, flexible downpipe, filter holder (10-cm diameter), and another downpipe connected to a pump. The pump exhaust flows through a continuously registering, accumulating flow meter. The hard pipe between the filter and the pump broke as a result of vibration, and was replaced with a flexible tube. The pump motor developed problems with the centrifugal switch, which eventually was bypassed with a toggle switch.

The newly installed snow crystal counting system turned out to be temperature sensitive and would not function properly below -50°C. An electromagnetic interference problem with one of the other SPO projects also affected the results of the system.

3. CONTINUING GMCC PROGRAMS

3.1 Carbon Dioxide

3.1.1 Continuous CO_2 Measurements

Continuous measurement of atmospheric CO_2 by NDIR analysis continued in 1982 at the four GMCC stations. Data acquisition and preliminary processing procedures remained as described in previous GMCC Summary Reports (Peterson, 1978, pp. 20-25; Mendonca, 1979, pp. 16-23). The entire record of continuous CO_2 measurements at each station has been recently corrected, converted to the X81 mole fraction scale, and edited. The selection of these finalized sets for background conditions is now under way and should be completed by the end of 1983, in time for archival with WMO and with the DOE Carbon Dioxide Information Center in Oak Ridge, Tenn. Provisional monthly mean values of background CO_2 concentration at the four observatories are presented in table 6, and plotted in fig. 6. In this form, the values reported are much closer to final than those given in previous GMCC Summary Reports, but must still be considered provisional. The major episodes of line contamination and instrument malfunction have been excluded from these records, and the previous problem of drifting CO_2 calibration standards (~ 0.1 ppm yr^{-1}) with respect to the WMO standards maintained by C. Keeling at SIO has now been resolved.

Table 6.--Provisional selected monthly mean CO_2 concentrations (ppm relative to dry air--X81 mole fraction scale) for continuous measurements at BRW, MLO, SMO, and SPO

Year	Jan	Feb	Mar	Apr	May	Jun	Jul	Aug	Sep	Oct	Nov	Dec
BRW												
1973	--	--	--	--	--	--	--	322.1	325.1	329.4	333.0	333.8
1974	(336.2)*	(337.2)*	336.7	337.2	336.9	335.9	330.1	324.7	325.8	329.1	332.2	335.3
1975	336.9	337.0	337.2	337.8	338.3	335.3	328.6	324.1	325.2	329.4	334.8	336.5
1976	337.3	337.3	337.8	338.1	337.8	336.8	330.7	324.0	325.6	330.3	334.2	336.7
1977	336.9	336.9	338.3	339.2	339.4	337.9	330.1	326.6	328.2	332.3	335.0	338.8
1978	339.3	340.3	341.6	341.0	340.8	339.4	332.0	328.2	328.7	332.9	338.9	339.5
1979	340.2	341.4	342.5	342.4	342.9	342.0	333.2	328.5	330.4	333.2	338.4	341.6
1980	342.0	342.5	343.4	343.3	343.3	342.7	336.7	331.9	331.6	338.5	340.7	342.9
1981	344.4	345.6	344.6	345.8	346.9	344.1	336.8	331.8	333.7	339.0	342.4	344.8
1982	345.8	347.5	348.2	348.4	348.0	345.8	339.1	332.8	334.2	338.5	342.1	344.7
MLO												
1974	--	--	--	--	333.0	332.1	331.0	329.1	327.4	327.3	328.3	329.5
1975	330.7	331.5	332.1	333.3	333.8	333.9	331.8	330.0	328.5	328.3	329.3	330.5
1976	331.7	332.8	333.5	334.9	334.8	334.5	333.0	330.7	329.3	320.7	330.2	331.4
1977	332.0	332.3	334.9	336.2	336.9	336.1	335.0	332.6	331.3	331.3	332.3	333.6
1978	335.1	335.4	336.8	337.8	338.1	338.0	336.5	334.5	332.4	332.4	333.8	334.9
1979	336.3	336.8	338.3	338.9	339.3	339.1	337.6	335.5	333.8	334.2	335.3	336.8
1980	337.8	338.4	340.0	340.9	341.4	341.3	339.5	337.3	336.0	336.1	337.3	338.4
1981	339.2	340.0	341.7	342.4	343.1	342.5	340.7	338.5	337.1	337.3	338.7	339.9
1982	341.2	341.7	342.7	343.8	344.3	343.3	341.8	340.2	337.7	337.9	339.1	340.7
SMO												
1976	(330.7)†	(330.6)†	331.3	331.2	330.6	331.3	331.1	331.1	331.3	331.5	331.9	331.8
1977	331.7	332.0	332.2	332.2	332.8	333.7	333.2	333.1	332.8	(332.9)†	(333.4)†	(333.7)†
1978	--	--	--	--	--	--	--	--	--	--	--	--
1979	(334.6)†	(335.3)†	(336.0)†	335.6	335.9	336.0	336.4	336.3	336.3	336.6	336.6	336.9
1980	337.5	337.6	337.9	337.3	337.7	338.0	338.3	338.3	338.2	338.1	338.5	339.3
1981	339.0	339.3	338.8	339.6	338.9	339.1	339.0	339.2	339.2	338.9	339.5	339.8
1982	340.4	340.4	340.4	341.2	339.9	340.0	340.5	340.4	340.1	340.0	340.2	340.3
SPO												
1975	328.2	328.3	328.5	328.3	328.1	328.6	329.4	330.2	330.8	331.0	330.6	330.3
1976	330.1	329.8	329.6	329.6	329.7	329.9	330.3	330.7	331.0	331.1	331.1	331.1
1977	330.9	330.3	330.3	330.6	331.0	331.4	331.8	332.2	332.7	333.0	333.0	332.7
1978	332.6	332.4	332.3	332.5	333.0	333.3	333.8	334.4	334.9	335.0	334.9	(334.6)†
1979	--	--	--	--	--	--	--	--	--	--	--	--
1980	336.1	336.0	336.0	336.2	336.6	336.9	337.4	337.7	337.9	338.1	338.0	338.0
1981	337.8	337.8	337.9	337.9	338.1	338.3	338.7	339.0	339.2	339.1	338.9	338.2
1982	338.5	(338.6)†	338.4	338.6	338.9	338.9	339.2	339.6	339.9	339.8	339.5	339.2

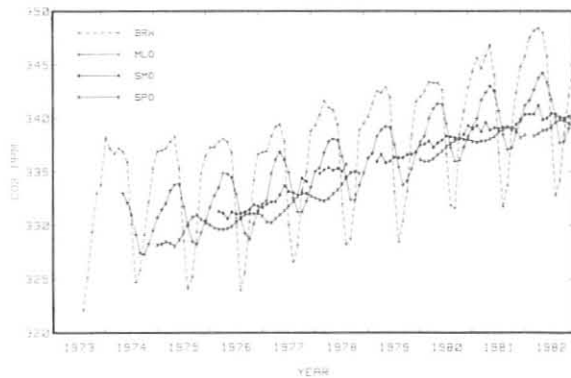*Less reliable data.
†Substituted flask data.

Figure 6.--Provisional selected monthly mean CO_2 concentrations from continuous measurements at BRW, MLO, SMO, and SPO. Values are in ppm with respect to dry air (X81 mole fraction scale).

Detailed reports on the continuous CO_2 record at each station are forthcoming, but some preliminary interpretations are already possible. Each of the four stations shows a CO_2 increase of nearly 9.0 ppm for 1976-1982, yielding a mean global growth rate for atmospheric CO_2 of 1.50 ± 0.02 ppm yr^{-1}. From the data of Rotty (1983), the total industrial CO_2 production from fossil fuel combustion and cement manufacture for this same interval may be estimated as ~35.8 Gt of carbon or 16.8 ppm atmospheric CO_2 equivalent. The implied global average airborne fraction $\eta \simeq 0.54$ for this period is virtually identical to the average ($\eta = 0.53$) of the airborne fractions from the CO_2 observations by C. Keeling at MLO ($\eta = 0.55$) and SPO ($\eta = 0.51$) during the period 1959-1978 (Bacastow and Keeling, 1981). Although there is some indication that the latitude dependence of the airborne fraction has weakened in the last decade of slower fossil fuel CO_2 release, a mean value of $\eta \simeq 0.54 \pm 0.02$ still seems appropriate for model projections of future atmospheric increases.

A second conclusion based upon the data of table 6 is that the latitude gradient of CO_2 concentration from BRW to SPO has remained near 3.5 ppm during the last decade. Interannual variations of ±0.5 ppm are probably related to the ENSO events of 1976, 1979, and 1982 (Bacastow et al., 1980). The magnitude of this gradient is directly related to the rate of release of fossil fuel CO_2 to the atmosphere at northern midlatitudes. That this gradient, which increased rapidly from ~1 ppm in 1960 to ~3 ppm in the mid-1970's (Keeling, 1983) is now nearly steady, is a direct consequence of the dramatic slowing in the rate of global production and consumption of fossil fuels since the OPEC price increases of 1973. Fossil fuel growth rates have been less than 2% yr^{-1} since 1974, with zero or negative growth rates in 1980-1982, as compared with the mean growth rate of 4.6% yr^{-1} in 1950-1973 (Rotty, 1983).

A final comment on the continuous data concerns the stability of the CO_2 seasonal amplitude over the last decade. Several recent studies of the SIO long time series CO_2 records from MLO, BRW, and SPO, as well as the shorter series from Station P, all suggest that the seasonal amplitude at the northern midlatitude stations has increased by 0.6%-0.8% yr^{-1} during the last two decades, with a less certain indication of an even more rapid increase of ~2%-3% yr^{-1} at SPO (Bacastow et al., 1983; Cleveland et al., 1983; Keeling, 1983; Pearman and Hyson, 1980, 1981). Future studies of this type will more carefully define the changing seasonal amplitude in the GMCC flask and continuous data. See sec. 5.14 for a first, careful look at the MLO continuous record. However, even the simplest approach (i.e., examining the values in table 6 for the annual CO_2 growth rate on a month-by-month basis) suggests that the seasonal amplitudes at both MLO and BRW have been increasing rapidly (1.5%-2% yr^{-1}) since 1975. These results are consistent with previous studies of

25

the SIO data, which found that most of the increase in seasonal amplitude has occurred since the mid-1970's.

The same method applied to the GMCC flask and continuous CO_2 records at SPO does not show a pronounced increase in seasonal amplitude with time, but in fact suggests the reverse. The gradual growth in Northern Hemisphere seasonality is most logically explained as a biospheric response to the enhanced atmospheric CO_2 levels, although the rapid rate of increase is difficult to interpret in terms of known plant physiology. A second contribution is expected from increased heterotrophic respiration, or rotting of soil organic matter under warm, wet weather conditions, probably more important at BRW than at MLO. Possible changes in the seasonality of the anthropogenic CO_2 release are probably not responsible for the observed increase, but deserve further study.

3.1.2 Flask Sample CO_2 Measurements

The number of cooperating sites from which air samples were returned to GMCC for CO_2 analysis in 1982 remained nearly unchanged from the 20 sites reporting in 1981. A complete list of flask stations in operation by the end of 1982 is given in table 7, and their locations around the globe are shown in fig. 7. Detailed station information for most of these locations has been reported in the GMCC Summary Reports for 1979 and 1980 (Herbert, 1980; DeLuisi, 1981). A complete description of the GMCC flask network will appear in a forthcoming WMO special report.

Table 7.--GMCC CO_2 flask network as of December 1982

Code	Station	Latitude (deg)	Longitude (deg)	Elevation (m)
AMS	Amsterdam I.	37.95S	77.53E	150
ASC	Ascension I.	7.92S	14.42W	54
AVI	St. Croix, V.I.	17.75N	64.75W	3
AZR	Terceira I., Azores	38.75N	27.08W	30
BRW	Barrow, Alaska	71.32N	156.60W	11
CBA	Cold Bay, Alaska	55.20N	162.72N	25
CMO	Cape Meares, Oreg.	45.00N	124.00N	30
COS	Cosmos, Peru	12.12S	75.33W	4600
FLK	Falkland Is.	51.75S	57.83W	51
GMI	Guam, Mariana Is.	13.43N	144.78E	2
HBA	Halley Bay, Ant.	75.00S	27.00W	0
KEY	Key Biscayne, Fla.	25.67N	80.17W	3
KPA	Kitt Peak, Ariz.	32.00N	112.00W	2095
KUM	Cape Kumukahi, Hawaii	19.52N	154.82W	3
MBC	Mould Bay, Canada	76.23N	119.33W	15
MLO	Mauna Loa, Hawaii	19.53N	155.58W	3397
NWR	Niwot Ridge, Colo.	40.05N	105.63W	3749
NZL	New Zealand	43.83S	172.63E	3
PSA	Palmer Station, Ant.	64.92S	64.00W	10
SEY	Mahe' I., Seychelles	5.33S	55.17E	3
SMO	Cape Matatula, Am. Samoa	14.25S	170.57W	30
SPO	South Pole, Ant.	89.98S	24.80W	2810
STM	Station M	66.00N	2.00E	0

Figure 7.--Locations of the cooper-
ating flask sampling sites of the
GMCC global CO_2 network.

The hostilities between the British and Argentinians in the Falkland Islands (Code: FLK) terminated the CO_2 record there in February 1982 after barely 1 year of measurements, and all sampling equipment was lost or destroyed during the war. The reopening of this station is still under discussion, although the resupply logistics are now considerably more difficult and circuitous. To fill the gap in latitude coverage created by the loss of FLK (51.75°S, 57.83°W), a cooperative sampling program was initiated with L. Heidt of NCAR at the project GHOST station near Christchurch, New Zealand. The CO_2 record at this site (designated NZL, located on Kiatorete Spit, 43.83°S, 172.63°E) begins December 1982. A second new station was established in 1982 in cooperation with the British Antarctic Survey at their site at Halley Bay, Antarctica (75°S, 27°W). The first year of flask samples (December 1982-December 1983) will arrive in Boulder for CO_2 analysis in April 1984.

Finally, to fill the gap between MLO (19.53°N) and Cold Bay, Alaska (55.20°N), a cooperative arrangement was reached with OGC to have CO_2 samples collected at their clean-air site at Cape Meares (45°N, 124°W) on the Oregon coast.

The CO_2 sampling site at Point Six Mountain, Mont., was discontinued in 1982, and replaced by a new sampling program at Kitt Peak National Observatory (32°N, 112°W), near Tucson, Ariz. The Kitt Peak program, in cooperation with Battelle Laboratories, will relate the GMCC continuous CO_2 measurements at ground level to the total-column CO_2 values obtained simultaneously by the Battelle-Kitt Peak group using high-resolution Fourier transform spectroscopy on the McMath solar telescope.

In 1982, 3167 0.5-ℓ flasks and 322 5-ℓ flasks were received and analyzed using the semiautomatic CO_2 analysis system described by Komhyr et al. (1983). The only major changes in the analytical procedure for CO_2 flask analysis made in 1982 were the cleaning of the flask pump-down vacuum rack and the conversion from dry ice to liquid N_2 in the cold trap of the vacuum line. Tank calibration and flask analysis are now under the control of an HP-85 computer and an HP-6940B multiprogrammer. The conversion from silicone to Apiezon grease in the flask stopcocks and the special cleaning of all silicone residue from the full flask inventory was completed in 1982.

The provisionally edited flask data for 1979-1981 were reported in the GMCC Summary Report for 1981 (Bodhaine and Harris, 1982, pp. 21-29). Since that time the entire flask data set since 1968 has been corrected, converted

27

to the WMO X81 mole fraction scale, and edited for background conditions. Details of this process, the final flask data set, and data analysis results are presented by Komhyr et al. (1984). The annual means are reported here in table 8. The background CO_2 values from the flask program have been archived with the DOE Carbon Dioxide Information Center in Oak Ridge, Tenn., with WMO, and with WDC-A.

The 10,000 CO_2 flask measurements of the 20-site network from 1979-1982 have been used to create the zonally averaged global CO_2 distribution and its variation in space and time (fig. 8). This surface is smoother than the 1981 surface presented in last year's GMCC Summary Report (Bodhaine and Harris, 1982, p. 28) because of more careful editing of the data for background conditions and a revised procedure of first fitting spline functions to the time series at each station and then using the smoother spline values in synthesizing the interpolated global concentration surface. Note the great repeatability in regular breathing of the global biosphere, dominated by the land plants of the Northern Hemisphere.

The finer details of the interannual variations in the CO_2 seasonality and increase are better seen in a flat, two-dimensional projection of this concentration surface onto the time-latitude plane (fig. 9). These concentration contours represent the zonally averaged, mean CO_2 concentration at sea level with a resolution of 20 days and 10° latitude, so that particular features on smaller time and space scales (e.g., equatorial upwelling or the steep gradient at the ITCZ) will not be well represented. In generating the surface, only those sites of the network in remote marine locations (fig. 7) have been used, so that the inferred seasonal amplitudes are certainly minimum values that underestimate the much larger CO_2 seasonality expected for midcontinental locations.

An important result of the flask network is the fine definition of the latitude dependence of the atmospheric CO_2 concentration on an annual basis since 1979 (fig. 10). The equatorial local maximum is maintained primarily by the upwelling and outgassing to the atmosphere of CO_2-supersaturated deep water in equatorial oceanic regions. The mean BRW to SPO difference of ~3.5 ppm is a result of fossil fuel combustion in the Northern Hemisphere. The nearly complete failure of the normal upwelling during the trade wind anomalies of the extreme ENSO event of 1982-1983 produced a marked reduction in this equatorial feature in the 1982 latitude gradient, as shown in fig. 10 and discussed by Gammon and Komhyr (1983). The perturbation of the global carbon cycle by the 1982-1983 ENSO was sufficient to halt the atmospheric increase due to fossil fuel combustion for several months in the fall of 1982, which implies short-term changes in the natural CO_2 sources and sinks of 1 Gt (10^{15} g) of carbon or more.

A comparison of the flask and continuous CO_2 annual means for BRW, MLO, SMO, and SPO is presented in fig. 10. The mean difference between the flask and continuous values at each station over the period 1979-1982 is typically 0.1 ppm (0.2 ppm for the mean of the absolute values of the differences).

A second check on the reliability of the flask CO_2 measurements is the ongoing program of flask comparisons with Keeling's laboratory at SIO, described in the GMCC Summary Report for 1981 (Bodhaine and Harris, 1982, p. 27).

28

Table 8.--Annual mean CO_2 atmospheric concentrations (ppm CO_2 in air-- X81 mole fraction scale) for the cooperating sites of the flask network

Sta.	1968	1969	1970	1971	1972	1973	1974	1975	1976	1977	1978	1979	1980	1981	1982
AMS	--	--	--	--	--	--	--	--	--	--	--	335.9*	337.8	339.3	339.4
ASC	--	--	--	--	--	--	--	--	--	--	--	337.3†	338.8	339.7	340.7
AVI	--	--	--	--	--	--	--	--	--	--	--	337.1	339.6	340.4	340.9
AZR	--	--	--	--	--	--	--	--	--	--	--	--	338.4	339.6	341.2
BRW	--	--	--	327.4	330.2	332.0	333.4	333.0	333.9	335.0	336.6	337.7	340.2	341.5	342.7
CBA	--	--	--	--	--	--	--	--	--	--	--	337.8	339.8	341.3	341.9
CMO	--	--	--	--	--	--	--	--	--	--	--	--	--	--	341.2
FLK	--	--	--	--	--	--	--	--	--	--	--	--	--	339.7	--
GMI	--	--	--	--	--	--	--	--	--	--	--	337.7	340.0	341.2	341.0
KEY	--	--	--	--	--	330.7	333.4†	--	332.7	335.2	336.7	338.8	340.2*	342.0	341.6
KUM	--	--	--	--	--	--	--	--	332.3	334.4	335.7	337.4	339.3	340.4	341.1
MBC	--	--	--	--	--	--	--	--	--	--	--	--	340.3	341.9	342.5
MKO	--	--	--	--	--	--	--	--	--	--	--	337.3	--	--	--
MLO	--	322.8†	325.2	--	--	--	--	--	332.1	333.6	335.2	336.7	338.9	340.4	341.0
NWR	323.1	324.1	325.6	325.2	326.3	330.2	334.0†	--	332.1	334.8	335.7	337.0	338.1	339.9	340.9
PSA	--	--	--	--	--	--	--	--	--	--	333.9	335.2	337.5*	340.0	339.8
SEY	--	--	--	--	--	--	--	--	--	--	--	--	339.3	340.1	340.5
SMO	--	--	--	--	--	330.2†	330.8	330.7	331.5	332.8	334.3	336.0	338.1	339.3	340.4
SPO	--	--	--	--	--	--	--	329.4	330.2	331.5	333.7	335.5	336.7	338.5	339.3
STC	--	324.0	326.4	326.9	327.6	--	--	--	--	--	--	--	--	--	--
STM	--	--	--	--	--	--	--	--	--	--	--	--	--	341.9	341.7

*Number of interpolated points $\geq$ 1/2 of total number of points.
†Incomplete year.
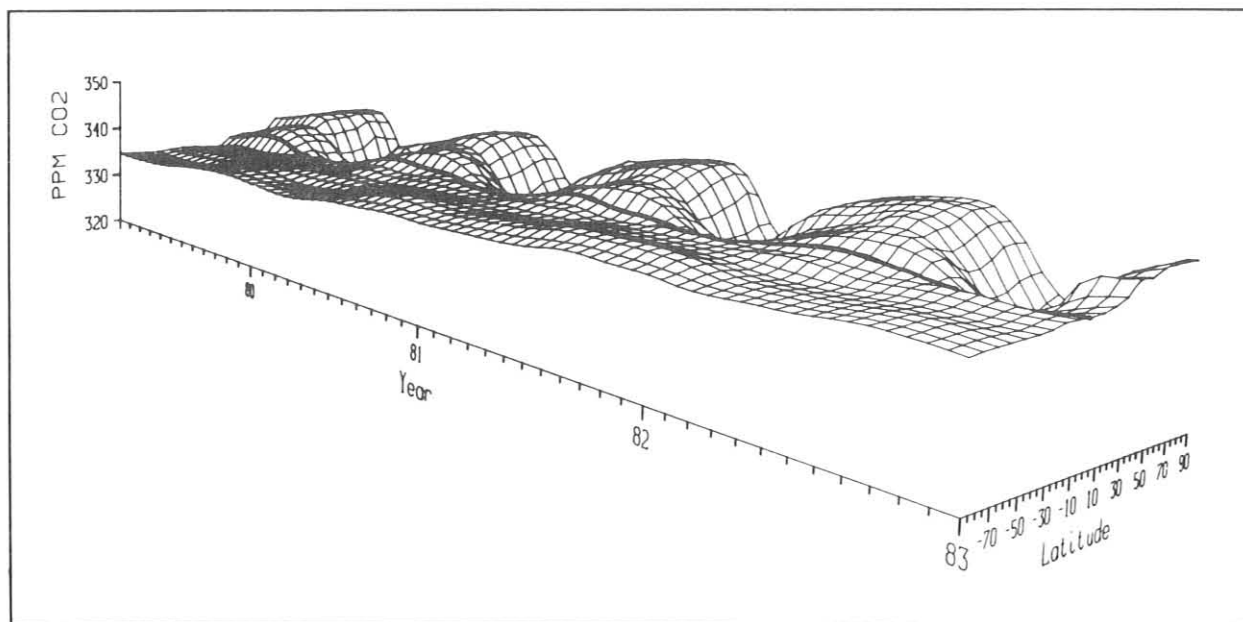
Figure 8.--A three-dimensional perspective of the "pulse-of-the-planet," the variation of the global atmospheric CO_2 concentration in latitude and time based on flask measurements for 1979-1982. This zonally averaged surface has a resolution of 20 days and 10° in latitude and was synthesized from results of ~10,000 individual flask samples returned from the 15 remote sea-level sites shown in fig. 7. On 31 December 1982 the CO_2 concentration is 339.5 ppm.
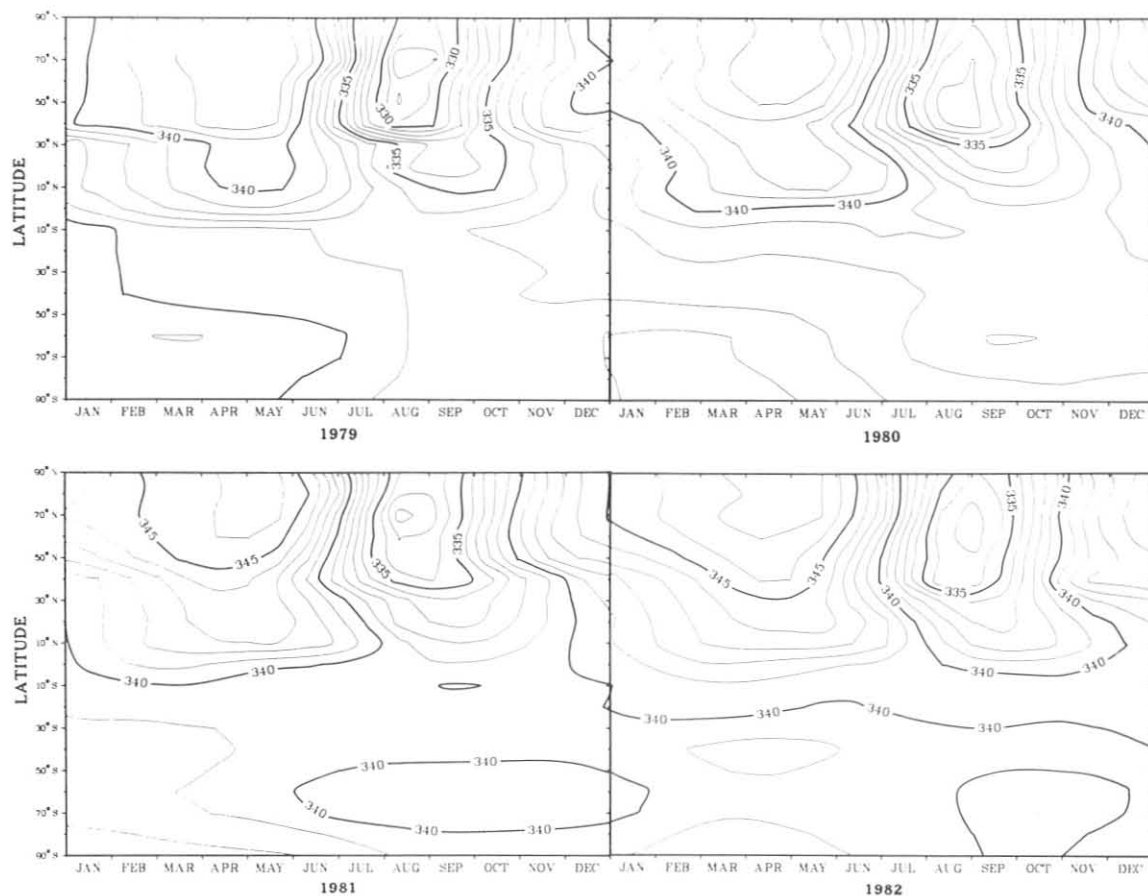
Figure 9.--A two-dimensional contour diagram, the projection of fig. 8 onto the latitude-time plane. The concentrations are zonally averaged, and strongly weighted toward remote, marine locations. The surface trends upward by 1.3-1.5 ppm yr^{-1} at all latitudes because of fossil fuel CO_2 emissions (~5 Gt of carbon yr^{-1}).

Figure 11 shows the GMCC-SIO flask CO_2 concentration differences since the comparison began in mid-1981. With the exception of SMO, the scatter has been decreasing and the agreement improving, so that as of December 1982, the two programs have converged to the limiting error of sampling and analysis (~±0.1-0.2 ppm).

Although the detailed description of the flask data and initial interpretations will appear in a future report, some of the longer time series of flask measurements finalized in 1982 are presented here. Figure 12 shows the selected flask data and fitted spline curves for BRW (1971-1982), NWR (1968-1982), KEY (1973-1982), KUM (1976-1982), MLO (1975-1982), SMO (1973-1982), and SPO (1974-1982).

In 1982, GMCC began CO_2 sampling on ships of opportunity, to assess the representativeness of our flask network and interpolated global distribution, and to observe finer features of the global distribution (e.g., ITCZ, equatorial upwelling, and longitudinal gradients). See sec. 4.12 for a report on the R/V DISCOVERER 1982 expedition in the North Pacific.

CO2 LATITUDINAL GRADIENT
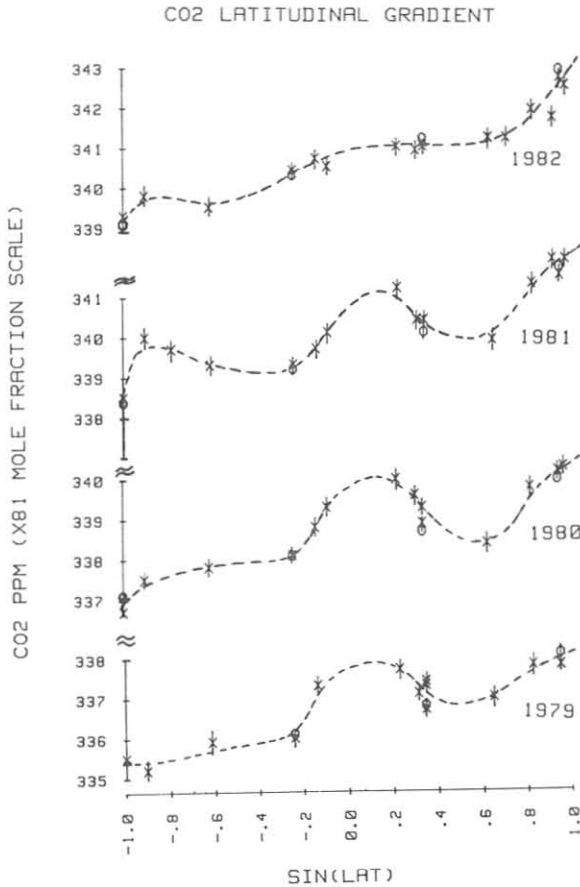
Figure 10.--Latitude gradients of annual mean atmospheric CO_2 concentrations at the flask network sites for 1979-1982 (*). The corresponding annual mean values from the continuous CO_2 measurements at the four baseline stations are also shown for comparison (O).
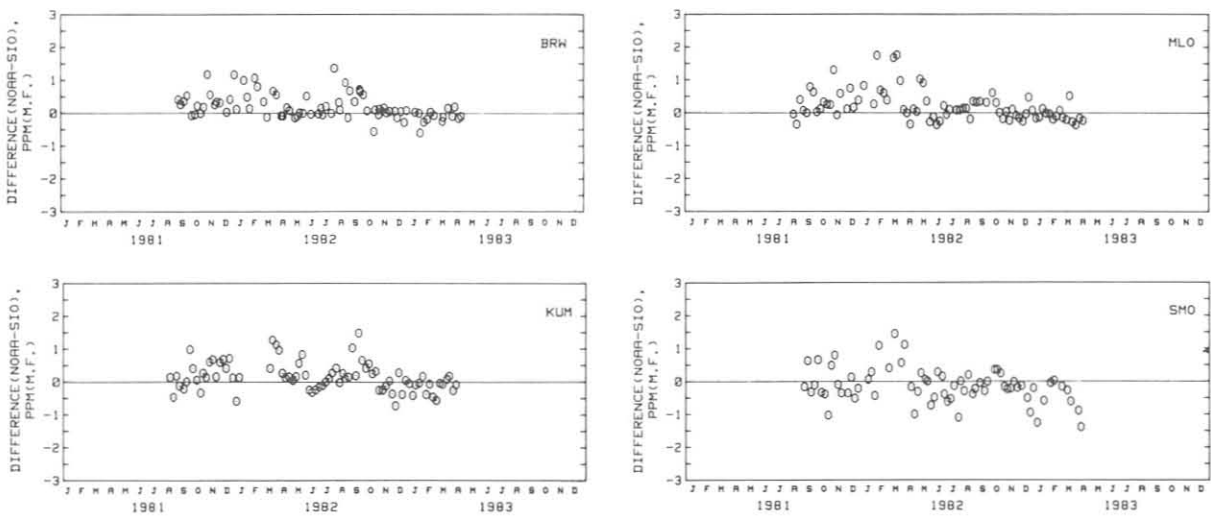
Figure 11.--The differences between the measured atmospheric CO_2 concentrations in nearly simultaneous flask samples, as measured by GMCC (0.5 ℓ) and SIO (5.0 ℓ) since mid-1981 for BRW, MLO, KUM, and SMO.

31
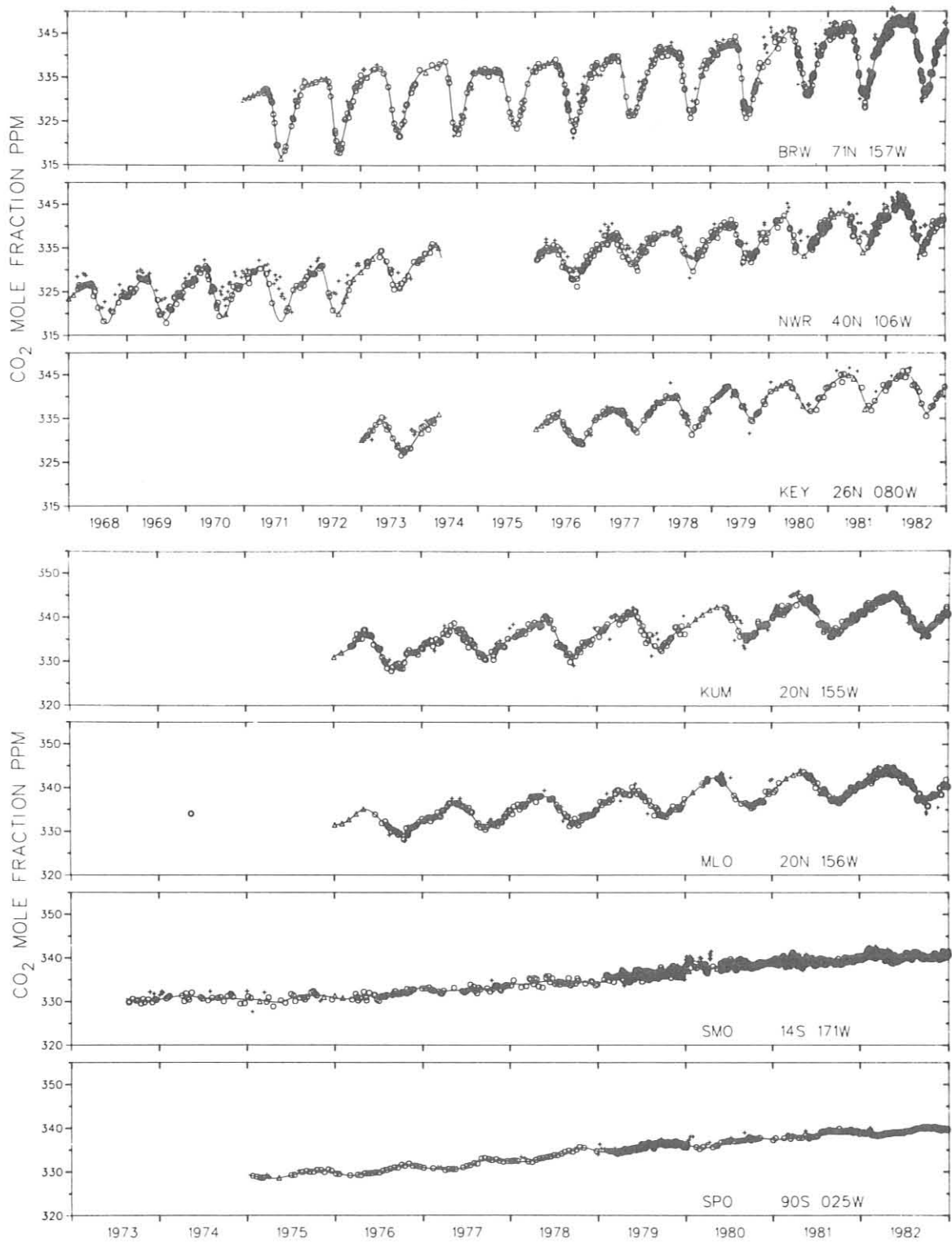
Figure 12.--Final flask data for BRW (1971-1982), NWR (1968-1982), KEY (1973-1982), KUM (1976-1982), MLO (1975-1982), SMO (1973-1982), and SPO (1974-1982). These records have been corrected, converted to X81 mole fraction scale, and edited for background conditions. The solid curve represents a spline fit to the background data O. Valid atmospheric samples not representing background conditions are denoted +. Data synthesized to constrain the spline are denoted Δ.

32

With proper latitude weighting, the estimated global annual CO_2 flask concentrations from the 20 cooperating sites are 337.2, 338.9, 340.2, and 341.0 ppm for 1979, 1980, 1981, and 1982 respectively. These global means may be compared with the MLO annual means from the GMCC continuous CO_2 program because MLO has often been considered to be globally representative. Tables 6 and 8 show that, in general, MLO data lie 0.2-0.4 ppm below the global annual mean derived from the flask program.

3.2 Total Ozone

3.2.1 Observations

Total ozone observations with Dobson spectrophotometers continued during 1982 at 11 stations that constitute the U.S. total-ozone network (table 9). On 29 January 1982 the U.S. Army terminated operation of the Dobson station at White Sands, N. Mex., and Dobson spectrophotometer no. 86, which was operated there, was transferred to GMCC. Plans are to relocate the instrument in the south central part of the United States. On 8 October 1982, Dobson measurements were terminated at BRW. The BRW instrument was returned to Boulder to be modified, recalibrated, and automated for Umkehr and total ozone observations planned for Poker Flat, Alaska (see sec. 4.3). In November 1982 Dobson spectrophotometer no. 94 was used to establish a west coast station at Fresno, Calif., but because of a shortage of personnel at the station, no observations were made during 1982.

Table 9.--U.S. Dobson ozone spectrophotometer station network for 1982

Station	Period of record	Instrument no.*	Agency
Wallops I., Va.	1 Jul 1967-present	38	NOAA-NASA
SMO	19 Dec 1975-present	42	NOAA
Tallahassee, Fla.	2 Jun 1973-present	58	NOAA
Boulder, Colo.	1 Sep 1966-present	61	NOAA
MLO	2 Jan 1964-present	63, 65†	NOAA
BRW	2 Aug 1973-8 Oct 1982	76	NOAA
Nashville, Tenn.	1 Jan 1963-present	79	NOAA
SPO	5 Dec 1963-present	80	NOAA-Army
Huancayo, Peru	14 Feb 1964-present	87	NOAA-Huancayo Obs.

*Instrument used throughout 1982.
†No. 63, Jan-May 1982; no. 65, Jun-Dec 1982.

3.2.2 Modernization and Calibration of Dobson Spectrophotometers

In 1982 GMCC continued the program that began in 1977 to upgrade foreign Dobson spectrophotometers under the auspices of the WMO Global Ozone Research and Monitoring Project. In May, Manila Dobson instrument no. 52 was shipped

to Boulder, Colo., for repair and recalibration. An initial calibration indicated that the instrument was -8.9% out of calibration. Major repairs were then made, including installation of an "air-space" optical wedge, and the instrument was optically aligned. Following calibration by direct comparison with World Standard Dobson Instrument no. 83, instrument no. 52 was returned to the Philippines.

3.2.3 Calibration Check of Dobson Spectrophotometers in the Global Network

During the international intercomparison of Dobson ozone spectrophotometers held in Boulder, Colo., in 1977, a technique was devised to check the calibration level of Dobson instruments by means of special, calibrated lamps. Two lamps, UQ1 and UQ2, were calibrated using World Standard Dobson Instrument no. 83. The calibration level of the World Standard was then transferred by means of lamp UQ1 to 14 instruments that had been calibrated previously by direct intercomparison with the World Standard. Results of this work indicated that Dobson instruments, whose optics are properly aligned and have accurate wavelength-setting and optical-wedge calibrations, can be calibrated on an absolute scale with calibrated lamps to within about ±1% (Komhyr et al., 1981). Conversely, such calibrated lamps can be used inexpensively to identify Dobson instruments requiring recalibration. Since the state of relative calibrations (wavelength setting and optical wedge) of such instruments is unknown, the results of the lamp tests should not be used to correct the calibration levels of these instruments. In August 1981 the world Dobson instrument network was divided into seven regions, and a special calibration lamp unit was built for each region. After calibration with Standard Instrument no. 83, the lamp units were sent to each region where calibration checks were made on instruments within the region.

Results of the calibration checks shown in table 10 indicate that a number of instruments in the global total ozone network require recalibration. The data have been provided to WMO as well as to the various institutions operating the instruments. The GMCC World Dobson Spectrophotometer Central Laboratory will continue to work with the WMO Global Ozone Research and Monitoring Project to upgrade the calibrations of these instruments.

3.2.4 Monthly Means

Daily 1982 total ozone amounts (applicable to local apparent noon at each station) for all stations in the U.S. network have been submitted for publication on behalf of WMO and are available in Ozone Data for the World, published by the World Ozone Data Center, Atmospheric Environment Service, 4905 Dufferin Street, Downsview, Ontario M3H5T4. Table 11 lists provisional monthly mean amounts of total ozone for 1982, for the GMCC observatories and cooperative stations.

Table 10.--Provisional calibration level of Dobson instruments
within the world Dobson network

Station	Dobson	Percent correction			Mean percent correction
		Lamp	Lamp	Lamp	
Region 1--North America		R11	R12	R13	
Toronto, Canada	77	+0.00	+0.29	--	+0.15
Resolute, Canada	59	+0.59	+0.88	--	+0.74
Churchill, Canada	60	-1.76	-1.47	--	-1.62
Goose Bay, Canada	62	-0.1	+0.15	--	±0.00
Edmonton, Canada	102	-0.44	+0.29	--	-0.08
Reykjavík, Iceland	50	-0.44	-0.15	--	-0.30
SPO	80	-1.61	-1.03	--	-1.32
Bismarck, N. Dak.	33	-1.47	--	-0.29	-0.88
Caribou, Maine	34	+1.03	+1.47	--	+1.25
Wallops I., Va.	38	+0.88	--	+1.03	+0.96
Tallahassee, Fla.	58	-0.88	--	-0.88	-0.88
Nashville, Tenn.	79	-1.32	--	-1.03	-1.18
MLO	63	+1.03	+1.47	--	+1.25
SMO	42	-0.73	--	-0.88	-0.81
BRW	76	-1.91	-1.32	--	-1.62
Boulder, Colo.	61	+0.29	+0.44	--	+0.37
Boulder, Colo.	82	-0.15	--	0.44	-0.30
Region 2--South America		R21	R22	--	
Mexico City, Mexico	98	-1.32	-1.32	--	-1.32
Huancayo, Peru	87	-4.69	-4.99	--	-4.84
Cachoeira Paulista, Brazil	114	+3.81	+3.52	--	+3.67
Natal, Brazil	93	+0.73	+0.73	--	+0.73
Buenos Aires, Argentina	97	+0.15	+0.00	--	+0.08
Buenos Aires, Argentina	99	+0.29	-0.15	--	+0.07
Region 3--Western Europe		R31	R32	--	
Bracknell, U.K.	41	+0.15	+0.15	--	+0.15
Bracknell, U.K.	2	+0.59	+0.59	--	+0.59
Halley Bay, U.K.	--	--	--	--	--
Argentine Is., U.K.	--	--	--	--	--
Seychelles, U.K.	--	--	--	--	--
St. Helena I., U.K.	--	--	--	--	--
King Edward VII Point, U.K.	--	--	--	--	--
Lerwick, U.K.	32	-2.20	-2.05	--	-2.13
Arosa, Switzerland	15	+1.03	+0.73	--	+0.88
Arosa, Switzerland	101	+0.15	+0.00	--	+0.08
Hohenpeissenberg, F.R.G.	104	+6.90	+6.17	--	+6.54
Cologne, F.R.G.	--	--	--	--	--
Oslo, Norway	56	-0.29	-0.15	--	-0.22
Oslo, Norway	8	+0.88	+0.73	--	+0.81
Tromsø, Norway	14	+1.17	+1.17	--	+1.17
Region 4--Western Europe		R41	R42	--	
Aarhus, Denmark	92	-0.59	-0.88	--	-0.74
Uccle, Belgium	40	-1.17	-1.32	--	-1.25
Biscarrosse, France	11	+2.49	+2.35	--	+2.42
Magney-Les-Hameaux	85	-1.91	-2.05	--	-1.98

Table 10.--Provisional calibration level of Dobson instruments
within the world Dobson network--Continued

Station	Dobson	Percent correction			Mean percent correction
		Lamp	Lamp	Lamp	
Region 4--Western Europe (Cont.)		R41	R42	--	
Lisbon, Portugal	13	+0.29	-0.15	--	+0.07
El Arenosillo, Spain	120	-0.44	-0.88	--	-0.66
Vigna Di Valle, Italy	47	-0.44	-0.44	--	-0.44
Brindisi, Italy	46	-3.23	-3.37	--	-3.30
Sestola, Italy	48	+0.15	+0.00	--	+0.08
Cagliari/Elmas, Italy	113	+1.32	+1.17	--	+1.25
Casablanca, Morocco	--	--	--	--	--
Cairo, Egypt	--	--	--	--	--
Region 5--Eastern Europe, U.S.S.R.		R51	R52	--	
Leningrad, U.S.S.R.	108	-0.29	-0.29	--	-0.29
Belsk Duży, Poland	84	-1.32	-1.32	--	-1.32
Hradec Kralové, Czechoslovakia	74	+3.23	+3.37	--	+3.30
Budapest-Lorinc, Hungary	110	+3.52	+3.52	--	+3.52
Bucharest, Romania	121	-3.37	-3.23	--	-3.30
Potsdam, G.D.R.	71	-0.59	-0.59	--	-0.59
Potsdam, G.D.R.	64	+0.44	+0.44	--	+0.44
Region 6--India		R61	R62	--	
New Delhi, India	36	-0.59	-0.29	--	-0.44
New Delhi, India	112	+1.61	+1.32	--	+1.47
Srinagar, India	10	-1.61	-1.91	--	-1.76
Varanasi, India	55	+1.76	+1.47	--	+1.62
Mt. Abu, India	54	-2.05	-2.49	--	-2.27
Poona, India	39	-0.29	-0.59	--	-0.44
Kodaikanal, India	45	-2.64	-2.49	--	-2.57
Quetta, Pakistan	43	--	--	--	--
Quetta, Pakistan	100	--	--	--	--
Bangkok, Thailand	90	-10.71	-10.86	--	-10.79
Singapore (U.K.)	7	--	--	--	--
Region 7--Australia and Japan		R71	R73	R74	
Sapporo, Japan	5702	+0.29	+0.59	--	+0.44
Sapporo, Japan	5706	-1.76	-1.76	--	-1.76
Kagoshima, Japan	5704	-4.40	-4.40	--	-4.40
Naha/Kagamizu, Japan	5705	+3.52	+3.52	--	+3.52
Tateno, Japan	116	-2.93	-3.23	--	-3.08
Tateno, Japan	122	-3.37	--	--	-3.37
Tateno, Japan	5703	+0.59	+0.15	--	+0.37
Srinagar, China	75	±0.00	-0.29	--	-0.15
K'un-ming, China	3	+1.32	+1.61	--	+1.47
Aspendale, Australia	105	-0.44	-0.73	--	-0.59
Aspendale, Australia	115	-0.15	-0.15	--	-0.15
Perth, Australia	111	+9.10	--	+8.80	+8.95
Cairns, Australia	81	-6.60	--	--	-6.60
Brisbane, Australia	6	+4.11	--	--	+4.11
Hobart, Australia	12	+8.80	--	--	+8.80
Macquarie I., Australia	78	+0.29	--	+0.29	+0.29
Invercargill, New Zealand	17	-0.15	--	-0.15	-0.15

36

Table 11.--Provisional 1982 monthly mean total ozone amounts (milli-atm-cm)

Station	Jan	Feb	Mar	Apr	May	Jun	Jul	Aug	Sep	Oct	Nov	Dec
Bismarck, N. Dak.	375	399	392	405	377	362	340	310	296	291	312	329
Caribou, Maine	399	420	420	427	386	376	359	376	334	323	326	338
Wallops I., Va.	345	332	364	380	377	340	337	328	310	287	272	283
SMO	257	258	259	257	253	251	251	252	259	258	265	271
Tallahassee, Fla.	292	300	333	325	--	326	334	315	307	--	263	268
Boulder, Colo.	341	368	375	383	366	341	312	308	294	272	286	321
MLO	256	252	285	290	288	281	272	267	256	247	238	236
BRW	--	--	464	487	427	360	323	301	300	293	--	--
Nashville, Tenn.	322	340	351	366	359	346	330	339	321	296	275	289
SPO	304	284	--	--	--	--	--	--	--	239	264	336
White Sands, N. Mex.	301	--	--	--	--	--	--	--	--	--	--	--
Huancayo, Peru	265	269	271	263	265	263	269	273	272	271	262	254

3.3 Ozone Vertical Distribution

3.3.1 Umkehr Observations

Umkehr observations continued in Boulder in 1982 with automated Dobson instrument no. 61. Use of that instrument (see sec. 4.3) significantly increased the number of observations made compared with previous years.

After the eruption of the El Chichon volcano in Mexico in April 1982, an intensive program of Umkehr observations was begun at MLO in May 1982. A classic set of data was obtained showing how volcanic stratospheric aerosols perturb ozone vertical distributions derived from Umkehr measurements. For conventional Umkehr observations, the effect is to diminish computed ozone amounts in the high stratosphere while simultaneously accentuating tropospheric ozone values. This is illustrated in fig. 13a, which shows a mean ozone profile derived from eight conventional Umkehr observations made in May 1982, about a month after the eruption of El Chichon. Note that the deduced ozone amount in Umkehr layer 9 is negative. By December 1982, the stratospheric aerosol layer over MLO was considerably diminished, at which time conventional Umkehr observations yielded more realistic ozone amounts in the troposphere and stratosphere (fig. 13b). Short Umkehr measurements (figs. 13c and 13d), on the other hand, appear to be less sensitive to stratospheric aerosols. However, compared with vertical ozone distributions derived from ECC ozone soundings, the altitude of maximum ozone concentration appears from the short Umkehr profiles to be about 4 km too low.

3.3.2 ECC Ozonesonde Observations

Monthly ozonesonde flights were made in Boulder throughout the year. All flights were made using type 4A ECC ozonesondes and 400-m^3 thin-film plastic balloons. Balloon performance was excellent, with 39-km altitudes attained regularly. The sondes appear to give reasonable ozone values to altitudes of ~38-39 km. Above these altitudes the ozone signals fall off abruptly, indicating some instrument problem. All flights during 1982 were made with hypsometer type radiosondes that give greater confidence in measured altitudes than

37
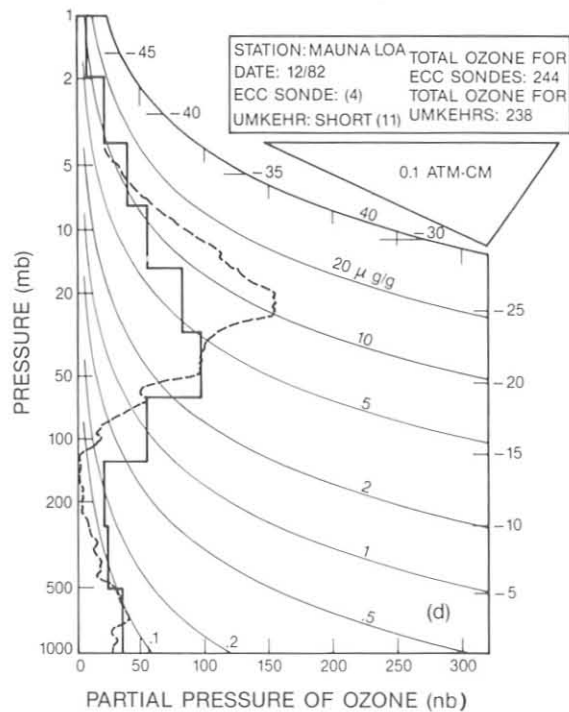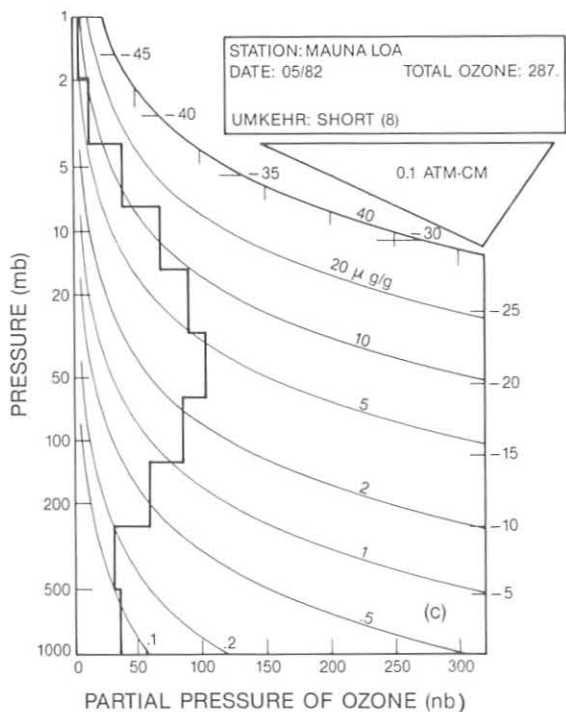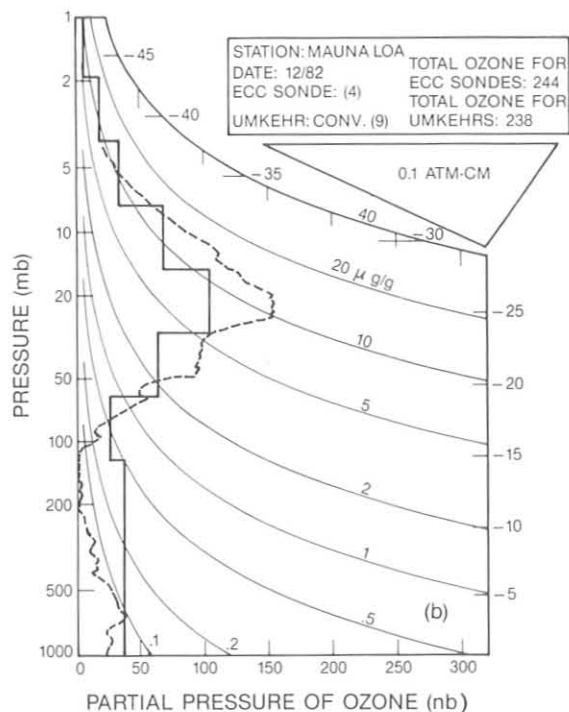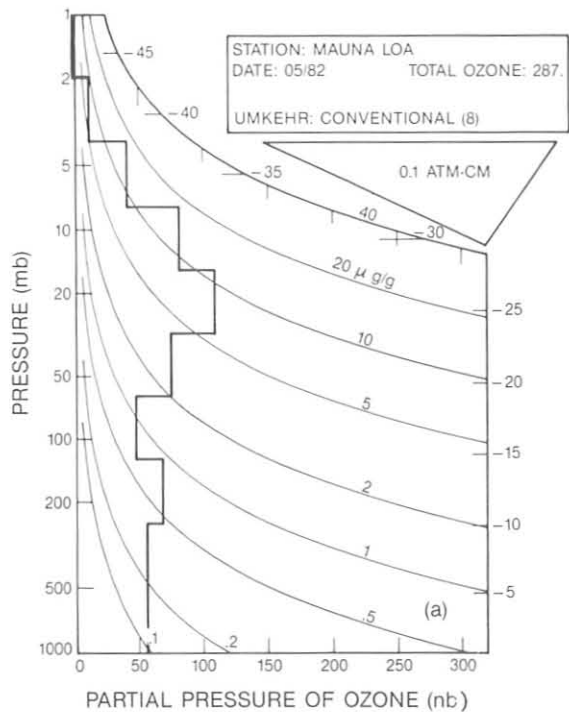
Figure 13.--(a), (b) Mean conventional and (c), (d) mean short Umkehr profiles obtained at MLO in May and December 1982. Dashed curves are ozone profiles derived from four ECC ozonesondes flown from Hilo, Hawaii, in December 1982.

38

do nonhypsometer radiosondes. A program of comparative measurements between the ECC ozonesondes and other high-altitude ozone-sounding instruments was carried out during the year. Results of these comparisons, made in Palestine, Tex., in June and October, are not available, pending completion of pump efficiency tests on the sondes.

In conjunction with the Umkehr sounding program established at MLO, a program of high-altitude ECC ozone soundings was initiated at Hilo, Hawaii, in September 1982. Because NWS modified its balloon inflation shelter and because the shelter was unavailable for our use, the desired frequency of soundings per month was not attained until December. Mean data for four soundings made at Hilo during December are shown in fig. 13b.

3.4 Surface Ozone

3.4.1 Operations

Surface ozone was measured continuously at the four GMCC observatories throughout the year with Dasibi ozone monitors. An attempt during 1981-1982 to use a second ozone monitor as a calibration standard at SPO does not appear to have improved significantly the certainty with which a calibration level can be assigned to the station monitor. Therefore, the previous practice of assigning a calibration level based on an annual comparison with the network standard instrument has been resumed. Because of the pressure of other projects, it was not possible to assign a second ozone monitor to MLO as a calibration instrument during 1982.

3.4.2 Data Analysis

The year 1982 marked the tenth year of surface ozone observations at BRW and MLO. Monthly mean surface ozone amounts for each of the four stations are shown in fig. 14. A linear least-squares trend line, which cannot be distinguished at SMO and SPO from the series mean (also plotted as a straight line), is shown with the monthly data. The trend was also computed for the monthly anomalies (monthly values from which the long-term monthly mean has been removed). Since each station has a prominent seasonal cycle, use of the anomalies considerably reduces the scatter about the trend line. It also eliminates the effect upon the trend computation of beginning the series at midyear as was done for BRW and MLO. This information is summarized in table 12. The

Table 12.--Linear least-squares trend analyses of the monthly means and anomalies of surface ozone partial pressure at BRW, MLO, SMO, and SPO

	Mean (nb)	Monthly mean		Monthly anomaly	
		Trend (% yr^{-1})	Std. error (% yr^{-1})	Trend (% yr^{-1})	Std. error (% yr^{-1})
BRW	25.8	1.58	2.36	1.23	1.16
MLO	25.1	0.50	1.99	0.59	1.11
SMO	13.8	0.26	4.37	-0.88	1.80
SPO	20.1	-0.08	2.11	-0.52	1.16
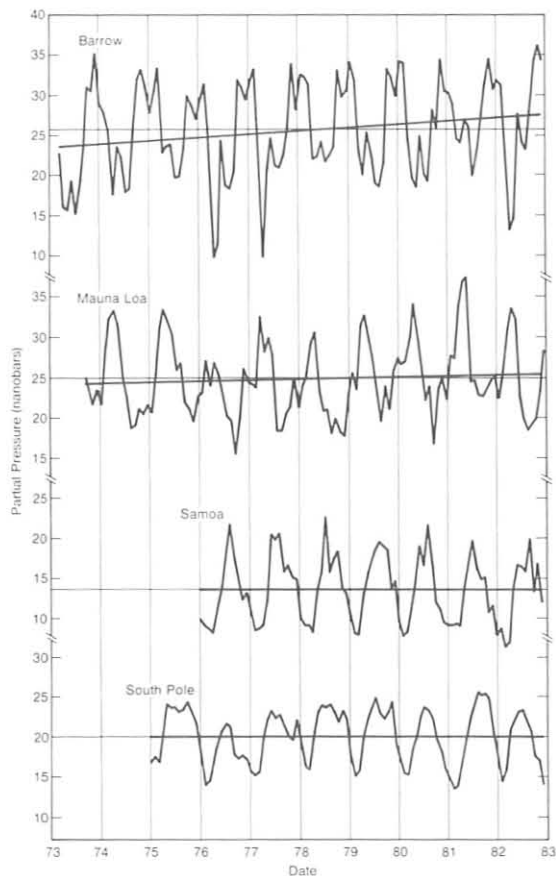
Figure 14.--Monthly mean surface
ozone amounts. A linear trend
(thick) line for the period of ob-
servation is also shown. At SMO
and SPO the trend line cannot be
distinguished from the mean of the
series also drawn as a straight
(thin) line.

trends are notable for their lack of significance, with none of the computed
trends approaching the two-standard-error criterion for significance at the
95% level.

Imposed on the annual cycle seen in fig. 14 at all of the GMCC locations
are large day-to-day variations in ozone. Daily surface ozone amounts for
1981 and 1982 are shown in fig. 15. At BRW, during March-May, large daily
excursions occur with both the highest and lowest daily values recorded during
this period. At MLO large day-to-day variations characterize the entire year.
At SMO large variations are spaced somewhat farther apart with high values
appearing on a 2- to 3-week time scale. The smallest day-to-day variability
is at SPO with the largest changes occurring during the austral summer.

3.5 Stratospheric Water Vapor

3.5.1 Operations

After 1981, a year generally free from balloon performance problems,
major difficulties with the balloons resurfaced in 1982. A new shipment of
4,000-g neoprene balloons proved to be totally unreliable. This type of bal-
loon was used successfully in 1981, but the manufacturer was apparently unable
to maintain the same standard of performance. A 3,000-g natural rubber bal-
loon was found that is capable of carrying the frost-point hygrometer to the
desired 30-km altitude. Problems arose however, in getting this balloon to
valve properly and to achieve an adequate descent profile required for the
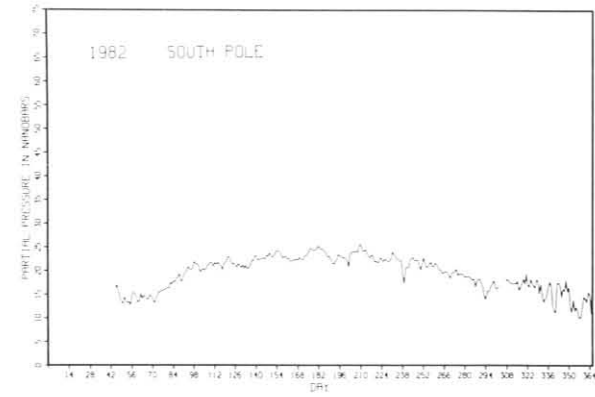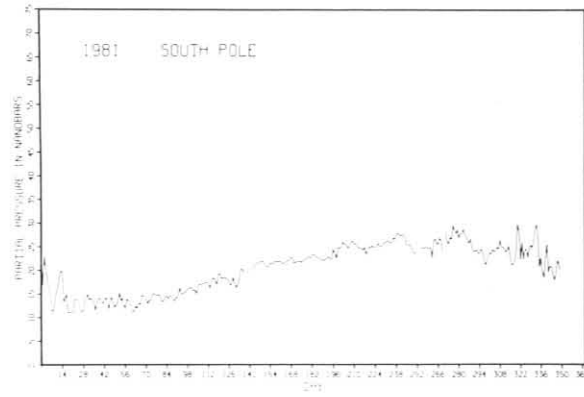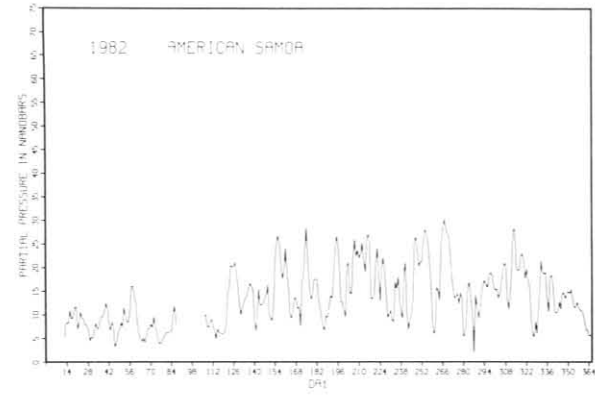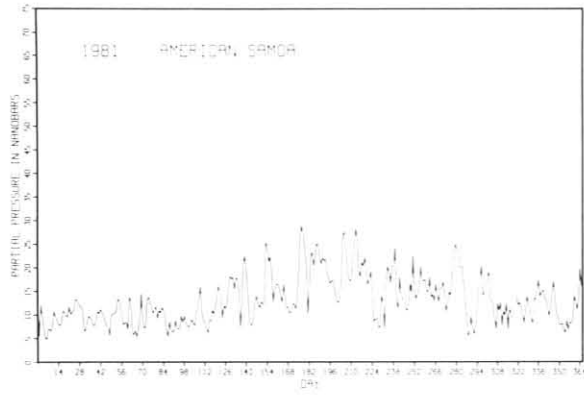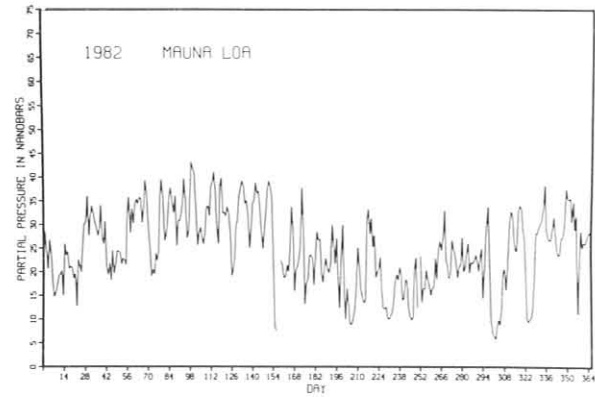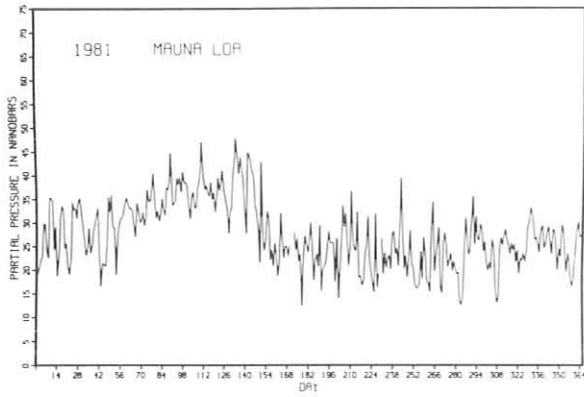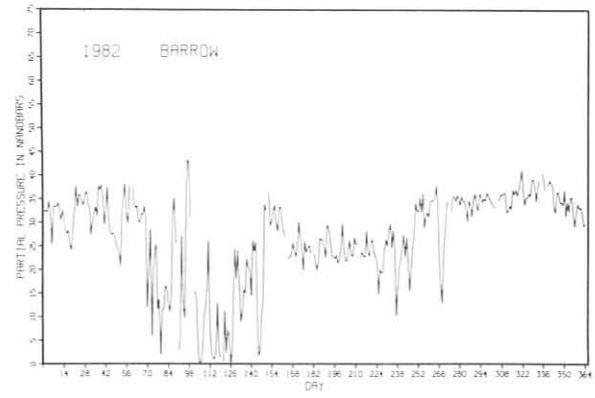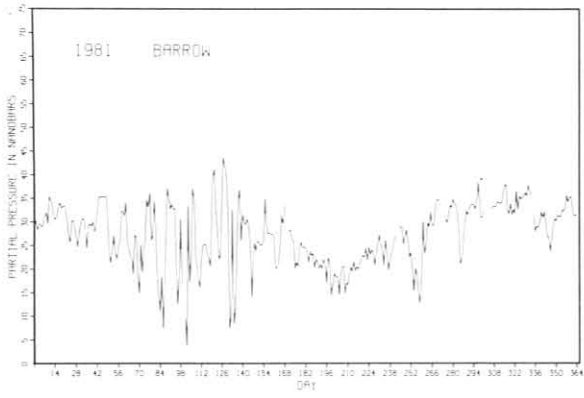
Figure 15.--Daily surface ozone amounts for 1981 and 1982 at the GMCC observatories.

41

highest quality data. Near the end of the year a technique was worked out
using two of the 3,000-g balloons. The instrument package ascends until one
of the balloons breaks and then descends in a controlled manner on the reduced
lift provided by the remaining balloon. This method proved to be reasonably
good, although efforts are continuing to refine the technique. In any case,
the rubber balloons have been much more reliable than the neoprene ones and
cost only about one-fourth as much. Although at least one sounding was at-
tempted each month, only six successful monthly flights were made in Boulder,
primarily because of the problems with the neoprene balloons.

3.5.2 Data Analysis

The stratospheric portions of the six soundings for Boulder are shown in
fig. 16. The November sounding exhibits a water vapor profile somewhat dif-
ferent from that normally seen in the 80- to 10-mb region, increasing steadily
from ~2 to 4 ppmm. This contrasts with the other flights in which the mixing
ratio is generally consistent or increasing slightly above about the 60-mb
level from 2.5 to 3 ppmm. A December balloon flight in Boulder and a Septem-
ber flight from Hilo, Hawaii (both flights not shown), exhibited even more
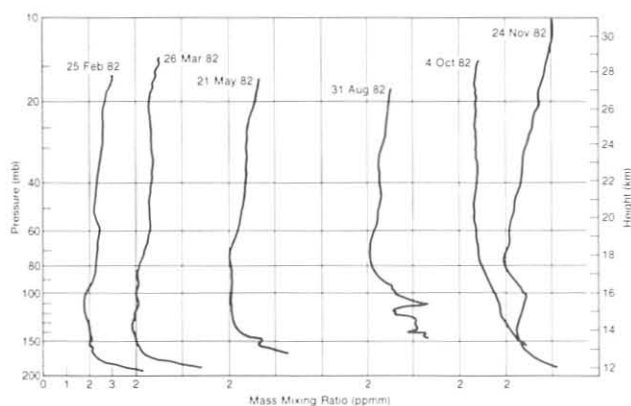
Figure 16.--Water vapor mass mixing
ratio profiles for soundings at
Boulder, Colo.

drastic increases. It is possible that all three of these flights were affec-
ted by sulfuric acid droplets in the stratosphere resulting from the El Chi-
chon eruption. Such droplets are thought to have been present in Hawaii and
to have moved over Boulder in October. It is possible that these droplets
were being deposited on the mirror of the frost-point hygrometer, thus indica-
ting elevated water vapor amounts. Because the September and December flights
gave erratic signals that did not meet the criteria for a properly performing
instrument, these flights have not been included in the set of representative
soundings. For the November flight, however, all of the in-flight checks
appeared normal and no objective criteria were met for rejecting it. The
possibility of contamination should be kept in mind, however, in interpreting
this flight.

A complete discussion of the water vapor time series at Boulder, Colo.,
and at Washington, D.C., was presented by Mastenbrook and Oltmans (1983).

3.6 Halocarbons and Nitrous Oxide

3.6.1 Operations

Air was collected weekly in paired stainless steel flasks at BRW, NWR, MLO, and SMO during 1982. Weekly flask pairs were collected only during January, November, and December at SPO. Flasks were shipped to and from the stations in small wooden boxes until April when the boxes were replaced by high-strength cardboard shipping containers. Also in April, an extra pair of flasks was shipped to BRW, MLO, and SMO to be added to the three pairs already being used at each station. This ensured that samples would be taken even if shipping time to and from Boulder increased.

When flask samples reached the Boulder chromatographic laboratory, they were analyzed for CFC-11 (CCl_3F), CFC-12 (CCl_2F_2), and nitrous oxide (N_2O). A new programmable integrating recorder that provides direct peak-height measurements and control of the analysis by a timetable was purchased in April. Computer programs were revised for speedy entry, reduction, and plotting of the data.

At the Boulder laboratory, room-temperature fluctuations had been large and had degraded chromatographic performance, until September when an air conditioner was installed. The stabilized room temperature has resulted in more consistent results from the gas chromatograph.

Only one change was made to equipment at the field stations: a PV array was installed at NWR to charge the batteries that run the sampling pump.

Sample flasks normally used at SPO during the February-October winter-over period were kept in Boulder for special tests in 1982. Fifty flasks were purged and pressurized with high-purity nitrogen. After a few weeks, the flasks were analyzed on the gas chromatograph for pressure loss and contamination. After the problem flasks were made free of leaks, all flasks were taken to NWR and filled with air over a 4-h period. Again, after sitting for a few weeks, the flasks were analyzed. Inconsistent and contaminated flasks were baked at 180°C while being evacuated. This procedure eliminated flask problems.

The sampling instructions and background articles given to new station personnel for use in training were revised and upgraded this year.

3.6.2 Calibration

The calibration gas standard, tank 3072, was taken to OGC in January for its routine stability check. CFC-11 and N_2O have not significantly changed since 1977 whereas CFC-12 has increased by 2.5 pptv yr^{-1}. However, continued quarterly comparisons of tank 3072 with two other gas standards, tanks 3079 and 3088, show no significant relative concentration changes in any of the three constituents.

Two absolute calibration systems, one for N_2O/CO_2 gas mixtures and the other for CFC-11/CFC-12/N_2O mixtures, were built in February. Calibration data confirmed previous results that the correct N_2O concentrations for tank 3072 are 10% less than OGC originally reported.

43

When attempts were made to prepare CFC-11 and CFC-12 calibration mixtures using N_2O as the internal standard, no GC response to N_2O was seen. The electron capture detector's response to N_2O increased as the CO_2 concentration increased. This anomalous behavior was confirmed by other laboratories. Tests are under way to ascertain the effect of CO_2 secular trends and annual cycles on the N_2O flask data.

3.6.3 Data Analyses

Halocarbon and N_2O selected data for 1982 have been combined with 5 years of previous data for statistical analyses and plotting. Figures 17, 18, and 19 are plots of CFC-11, CFC-12, and N_2O data respectively. BRW halocarbon data exhibit an annual cycle with highest concentrations during December and lowest values in June. No other station shows a statistically significant periodicity. SPO data continue to be the most variable. N_2O data at BRW also have an annual cycle, but this could be due to variations in CO_2 that affect the measurements and will be corrected later. SMO N_2O data show an unexplained increase in concentration all through 1982.

Tentative mean concentrations for 1982 and first- and second-order least-squares regression analyses on the 6-yr halocarbon and N_2O data sets are summarized in table 13. Only MLO continues to show a statistically significant

Table 13.--Mean mixing ratios for 1982, and results of first- and second-order regression analyses of CFC-11, CFC-12, and N_2O data for 1977-1982[*]

Station	No. of obs.	Mean mixing ratio for 1982	Mixing ratio on 1 Jan 1977[†]	Growth rate[†]	Growth rate change[†]
CFC-11		(pptv)	(pptv)	(pptv yr^{-1})	(pptv yr^{-2})
BRW	258	214.9	154.1 ± 0.40	11.12 ± 0.11	--
NWR	268	210.5	150.1 ± 0.43	10.93 ± 0.12	--
MLO	261	206.3	142.9 ± 0.68	13.38 ± 0.50	-0.32 ± 0.08
SMO	269	202.2	134.7 ± 0.37	12.10 ± 0.11	--
SPO	85	214.9	134.6 ± 1.96	12.70 ± 0.57	--
CFC-12		(pptv)	(pptv)	(pptv yr^{-1})	(pptv yr^{-2})
BRW	244	362.9	273.4 ± 1.89	14.15 ± 1.26	0.38 ± 0.18
NWR	228	356.8	280.7 ± 2.23	11.12 ± 1.44	0.45 ± 0.21
MLO	243	353.8	268.5 ± 1.03	15.67 ± 0.28	--
SMO	258	345.8	245.3 ± 1.28	15.30 ± 0.92	0.49 ± 0.14
SPO	83	364.5	242.8 ± 4.10	9.03 ± 2.70	2.09 ± 0.41
N_2O		(ppbv)	(ppbv)	(ppbv yr^{-1})	(ppbv yr^{-2})
BRW	250	303.8	300.1 ± 0.20	0.61 ± 0.05	--
NWR	243	304.8	299.1 ± 0.23	0.99 ± 0.06	--
MLO	250	304.0	298.3 ± 0.25	0.99 ± 0.07	--
SMO	239	309.3	299.1 ± 0.31	1.59 ± 0.09	--
SPO	105	302.2	297.5 ± 0.32	0.81 ± 0.09	--

[*]Coefficients are followed by their standard deviations. If a second-order coefficient was not significant, a first-order analysis was performed.
[†]95% confidence interval.
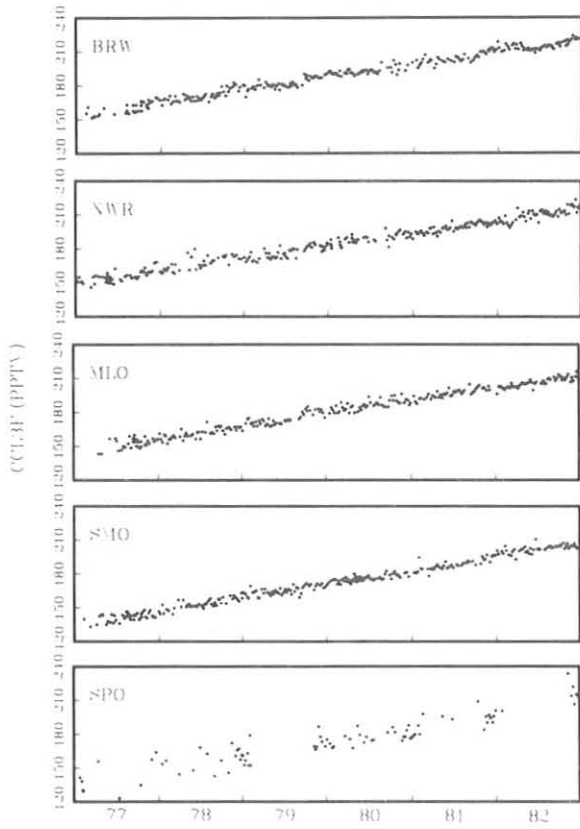
Figure 17.--CFC-11 data record.
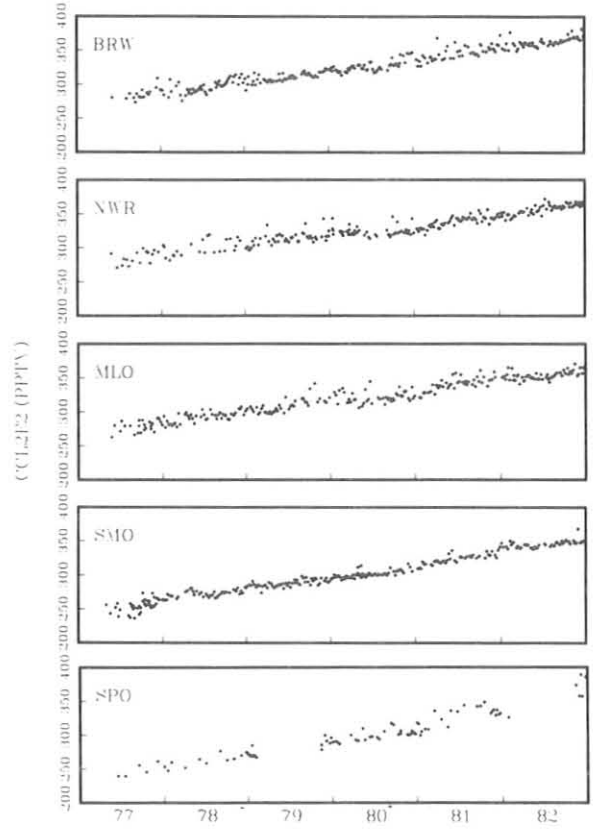
Figure 18.--CFC-12 data record.
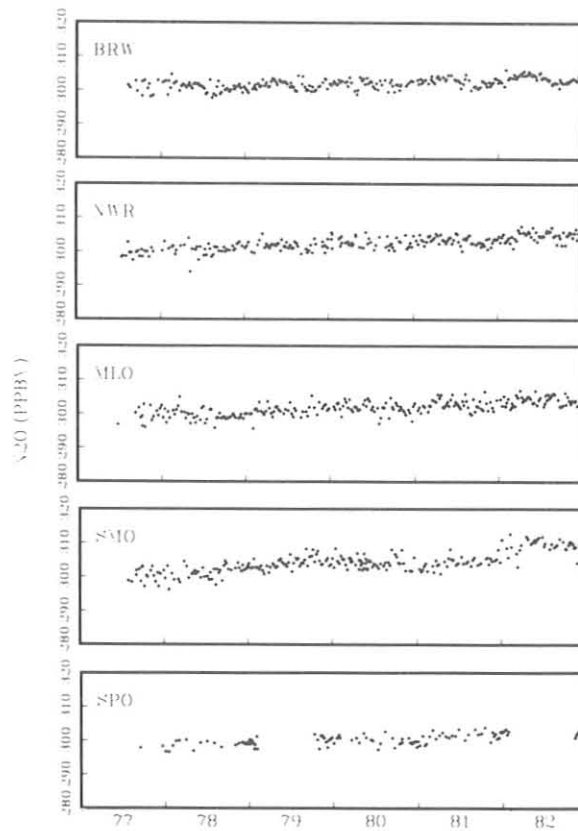
Figure 19.--N₂O data record.

45

decrease in CFC-11 growth rate, whereas it is the only station not showing an increasing growth rate in CFC-12.

3.7 Stratospheric Aerosols--Lidar

GMCC lidar activity at MLO came into national prominence on 28 January 1982 when the Mystery Cloud was first detected and reported by T. DeFoor and K. Coulson. The commercial news media publicized the discovery and some commotion was raised because of the unknown origin of the cloud. The cloud spread northward rapidly and was detected by lidars located at higher latitudes. Interest in the cloud faded rapidly, as did the cloud. However, at the end of March and in early April, Mexico's El Chichon volcano erupted and produced a tremendous stratospheric dust cloud that persisted the entire summer as an annulus in an equatorial band between about 10°S and 30°N.

Information on the El Chichon cloud was quickly relayed to the scientific community as a highly significant meteorological event. The El Chichon stratospheric cloud mass was about the same order of magnitude as the Agung stratospheric cloud in 1963. MLO lidar operators increased the observation rate from once to twice per week to obtain finer time resolution of changes in cloud-profile structure, and more than 50 observations were made. GMCC received numerous requests for MLO lidar data. Among applications of the data are investigations of satellite remote sensing errors, Umkehr remote-sensing errors, climate modeling, ozone photochemistry modeling, and stratospheric dynamics. In the annals of historical meteorology, the MLO lidar data will occupy an important position. A summary of the MLO lidar data is given in sec. 4.8.

3.8 Surface Aerosols

The GMCC surface aerosol monitoring program during 1982 included continuous measurement of CN concentration and integrated light scatterring at BRW, MLO, SMO, and SPO. All data were recorded as 1-min and 1-h means on magnetic tape and also on backup chart recorders. CN concentrations were measured using G.E. CNC's (catalog no. 112L428) with modifications suggested by N. Ahlquist of the University of Washington. Calibration points for the automatic CNC's were provided by daily Pollak CNC observations. Light scattering was measured using four-wavelength nephelometers that measure the scattering portion of aerosol extinction simultaneously at wavelengths of 450, 550, 700, and 850 nm. Calibrations of the nephelometers are performed at 2-mo intervals by filling them with CO_2 gas and adjusting the instrument outputs to the known scattering coefficients of CO_2.

3.8.1 Barrow

The BRW Pollak CNC operated properly throughout 1982 and provided daily observations for routine calibration checks of the G.E. automatic CNC. The G.E. CNC produced acceptable data for about 47% of the year. Other than downtime for routine maintenance and calibration, the major periods of downtime were DOY 1-12, 23-47, 49-53, 61-77, 124-140, 142-173, 251-265, 282-284, and 314-316.

The nephelometer produced acceptable data for about 76% of the year, with the only significant periods of downtime occurring during DOY 137-141, 219,

and 325-342. The 325-342 data will be recovered from the backup chart recorder.

3.8.2 Mauna Loa

The MLO Pollak CNC, which operated properly throughout 1982, provided daily observations for routine calibration checks of the G.E. automatic CNC. The G.E. CNC produced acceptable data for about 95% of the year. Other than downtime for routine maintenance and calibration, the major periods of downtime were DOY 1-4, 115-116, and 197-202.

The nephelometer produced acceptable data for about 49% of the year. The major period of downtime was DOY 1-119 when the instrument was at the University of Washington for repair. Although two problems were repaired (the white object solenoid and photomultiplier), the signal-to-noise ratios of the 700- and 850-nm channels have been excessive so that Angstrom exponents calculated from 550 and 700 nm and from 700 and 850 nm are not as reliable as in previous years. However, long-term averages of the data remain reliable.

3.8.3 Samoa

The SMO clean-air sampling building received a direct lightning strike at 1500 LST on 28 March (DOY 87). All aerosol instruments were damaged except the G.E. CNC. A new Pollak CNC power supply was mailed to SMO and was back online DOY 95. The Leeds and Northrup chart recorder was shipped to Boulder for repair and was returned to SMO and was back online DOY 148. The nephelometer was repaired at the SMO site and was back online DOY 155. Since ICDAS was also damaged by the lightning, data were not available on magnetic tape until DOY 141. The lightning strike accounted for the major periods of downtime for all aerosol instrumentation during 1982.

The SMO Pollak CNC (SN 20) was operated until 7 March when it was replaced with Pollak CNC SN 22 because of erratic operation. Pollak CNC SN 22 was operated throughout the remainder of 1982. Daily observations of the Pollak counters provided routine calibration checks for the G.E. CNC, which produced acceptable data for about 82% of the year. Although the instrument itself was operational, data were lost during DOY 87-141 because no recording equipment was available. Routine calibration and maintenance accounted for the remaining amount of downtime.

The SMO nephelometer produced acceptable data for about 68% of the year. Other than downtime for routine calibrations, the significant periods of downtime were DOY 50-68 for repair of the filter wheel motor, DOY 88-154 for repair of damage caused by the lightning strike, and DOY 160 for spare board repairs.

3.8.4 South Pole

The SPO Pollak CNC operated properly throughout 1982. Daily observations from it provided routine calibration checks for the G.E. automatic CNC. A new Rawson-Lush microammeter (0-10 μA) was included in the midwinter airdrop to replace a broken unit. The broken unit was sent for repair to Boulder on the opening flight. The G.E. CNC produced acceptable data for about 71% of the

year. Other than downtime for routine calibration and maintenance, the major periods of downtime were DOY 1-31 and 316-319. A complete spare G.E. CNC was mailed to SPO at the end of the year. When problems occur with the G.E. CNC in the future, it can be replaced with the spare unit, and the inoperative unit can be repaired in Boulder during the austral summer.

The SPO nephelometer operated properly throughout 1982 and produced acceptable data for about 69% of the year. Downtime was caused by slow recovery of the instrument after calibrations, power outages, and times of extremely low aerosol concentrations that caused the instrument to drift off scale.

3.8.5 Data Analysis

Data analysis proceeded as described in the previous GMCC Summary Reports. All observer notes and chart recorder data are examined upon receipt in Boulder to assure proper instrument performance. Aerosol data are stripped from the monthly tapes made available by the A&DM group, and files of hourly means and 10-min graphics are produced. Missing data are then filled in, and necessary editing and calibration are applied. All aerosol data are available from GMCC in printout, microfiche, magnetic tape, or graphic form.

3.8.6 Discussion of Selected Data

Light-scattering and CN data for the four stations are presented in tables 14-17 and fig. 20. All available data were used to calculate monthly

Table 14.--BRW monthly geometric means of CN concentration (cm^{-3}) and light scattering (m^{-1}) at 450, 550, 700, and 850 nm, where values appear in a compact exponential format ($5.68-6 = 5.68 \times 10^{-6}$)

	JAN	FEB	MAR	APR	MAY	JUN	JUL	AUG	SEP	OCT	NOV	DEC
1975 CN	87	210	285	252	123	47	325	232	174	45	160	224
1976 CN	177	327	579	172	175	109	179	351	111	182	252	201
b(450)	-	-	-	-	5.68-6	2.17-6	7.05-7	-	-	-	-	-
b(550)	-	-	-	-	4.16-6	1.47-6	4.71-7	-	-	-	-	-
b(700)	-	-	-	-	3.12-6	1.08-6	3.64-7	-	-	-	-	-
b(850)	-	-	-	-	2.09-6	7.11-7	2.44-7	-	-	-	-	-
1977 CN	184	150	363	299	106	41	61	156	86	61	65	147
b(450)	-	3.04-5	1.70-5	1.94-5	1.47-5	-	-	4.27-6	3.83-6	6.69-6	1.09-5	1.52-5
b(550)	-	2.84-5	1.49-5	1.65-5	1.15-5	-	-	3.12-6	3.02-6	4.94-6	7.61-6	1.13-5
b(700)	-	2.10-5	1.00-5	1.08-5	6.65-6	-	-	2.77-6	2.76-6	4.66-6	6.60-6	1.04-5
b(850)	-	1.68-5	7.45-6	7.90-6	4.46-6	-	-	2.69-6	2.80-6	4.62-6	6.13-6	9.92-6
1978 CN	181	152	252	138	-	107	147	363	122	112	168	97
b(450)	1.32-5	1.22-5	1.58-5	1.47-5	6.58-6	3.74-6	-	2.36-6	2.99-6	5.00-6	7.97-6	6.59-6
b(550)	9.83-6	1.07-5	1.33-5	1.22-5	5.24-6	2.67-6	-	2.34-6	2.92-6	4.25-6	7.35-6	6.15-6
b(700)	9.14-6	7.14-6	8.70-6	7.74-6	3.19-6	1.41-6	-	1.94-6	2.33-6	2.80-6	5.35-6	4.50-6
b(850)	8.85-6	5.25-6	6.23-6	5.39-6	2.19-6	8.41-7	-	1.71-6	1.94-6	2.02-6	4.12-6	3.44-6
1979 CN	317	482	366	272	111	180	594	199	91	95	125	227
b(450)	6.69-6	9.63-6	2.16-5	1.20-5	5.10-6	1.43-6	3.73-6	3.26-6	2.21-6	6.39-6	7.32-6	1.46-5
b(550)	6.15-6	8.81-6	2.01-5	1.09-5	4.26-6	1.13-6	3.14-6	-2.98-6	2.13-6	6.29-6	7.18-6	1.41-5
b(700)	4.42-6	6.19-6	1.42-5	7.46-6	2.66-6	6.77-7	2.05-6	2.23-6	1.73-6	5.02-6	5.57-6	1.05-5
b(850)	3.35-6	4.60-6	8.78-6	4.41-6	1.65-6	4.75-7	1.49-6	1.72-6	1.30-6	4.01-6	4.48-6	8.05-6
1980 CN	232	305	300	124	91	678	99	164	55	54	46	309
b(450)	1.05-5	5.46-6	7.33-6	8.99-6	3.10-6	1.26-6	1.18-6	2.54-6	2.55-6	2.07-6	5.50-6	1.32-5
b(550)	1.04-5	5.12-6	6.86-6	7.60-6	2.65-6	1.05-6	9.96-7	2.34-6	2.22-6	1.83-6	4.83-6	1.26-5
b(700)	7.83-6	3.57-6	4.48-6	4.96-6	1.71-6	6.28-7	6.45-7	1.72-6	1.59-6	1.20-6	3.19-6	8.78-6
b(850)	5.98-6	2.57-6	3.06-6	3.36-6	1.10-6	4.30-7	4.56-7	1.35-6	1.21-6	8.99-7	2.29-6	6.53-6
1981 CN	514	316	185	217	140	133	364	286	132	88	237	254
b(450)	1.29-5	1.22-5	1.07-5	1.04-5	4.75-6	1.78-6	2.41-6	1.26-6	2.63-6	5.05-6	1.50-5	2.85-5
b(550)	1.25-5	1.12-5	9.89-6	9.03-6	3.82-6	1.47-6	2.26-6	1.13-6	2.43-6	4.53-6	1.39-5	2.71-5
b(700)	8.93-6	7.58-6	6.73-6	5.49-6	2.18-6	8.39-7	1.71-6	8.69-7	1.86-6	3.16-6	1.06-5	2.01-5
b(850)	6.73-6	5.54-6	4.95-6	3.57-6	1.38-6	5.67-7	1.36-6	7.39-7	1.41-6	2.26-6	7.82-6	1.55-5
1982 CN	398	89	250	146	67	207	84	80	73	62	70	117
b(450)	1.31-5	1.89-5	2.63-5	2.18-5	9.22-6	2.24-6	2.82-6	4.67-6	2.79-6	3.36-6	7.64-6	1.74-5
b(550)	1.20-5	1.76-5	2.33-5	1.93-5	7.59-6	1.80-6	2.42-6	3.96-6	2.55-6	2.97-6	6.82-6	1.85-5
b(700)	8.42-6	1.26-5	1.50-5	1.24-5	4.57-6	1.13-6	1.69-6	2.66-6	1.91-6	2.06-6	4.70-6	1.62-5
b(850)	6.34-6	9.40-6	1.05-5	8.78-6	3.06-6	8.52-7	1.30-6	2.00-6	1.54-6	1.55-6	3.55-6	1.42-5

Table 15.--MLO monthly geometric means of CN concentration (cm^{-3}) and light scattering (m^{-1}) at 450, 550, 700, and 850 nm, where values appear in a compact exponential format ($5.68\text{-}6 = 5.68 \times 10^{-6}$)

		JAN	FEB	MAR	APR	MAY	JUN	JUL	AUG	SEP	OCT	NOV	DEC
1974	CN	-	-	-	-	-	270	232	271	232	228	154	166
	b(450)	1.35-6	1.64-6	2.86-6	8.05-7	1.46-6	7.89-7	5.37-7	5.18-7	7.34-7	3.28-7	3.76-7	2.91-7
	b(550)	8.69-7	1.27-6	1.88-6	5.83-7	1.24-6	6.27-7	3.89-7	3.65-7	5.23-7	2.46-7	2.63-7	2.03-7
	b(700)	6.19-7	1.04-6	1.24-6	4.28-7	1.04-6	4.64-7	2.72-7	2.49-7	3.50-7	1.70-7	1.86-7	1.45-7
	b(850)	3.82-7	7.47-7	7.90-7	2.95-7	7.71-7	3.40-7	1.64-7	1.54-7	2.11-7	1.07-7	1.19-7	9.84-8
1975	CN	193	208	268	205	190	217	326	262	280	334	256	275
	b(450)	3.39-7	9.23-7	8.12-7	2.04-6	2.31-6	7.92-7	7.08-7	5.40-7	3.07-7	2.41-7	2.41-7	2.71-7
	b(550)	2.37-7	6.82-7	5.95-7	1.64-6	2.10-6	6.23-7	5.32-7	3.99-7	2.01-7	1.51-7	1.38-7	1.62-7
	b(700)	1.66-7	5.04-7	4.38-7	1.23-6	1.84-6	4.53-7	3.46-7	2.48-7	1.18-7	8.33-8	7.90-8	9.68-8
	b(850)	1.00-7	3.29-7	2.54-7	8.67-7	1.61-6	2.73-7	1.94-7	1.32-7	7.27-8	6.05-8	5.80-8	6.30-8
1976	CN	209	225	216	230	283	245	218	232	303	298	200	181
	b(450)	3.98-7	6.94-7	8.68-7	1.64-6	1.82-6	9.23-7	4.88-7	6.27-7	8.14-7	3.11-7	3.36-7	3.16-7
	b(550)	2.54-7	5.01-7	·6.58-7	1.24-6	1.54-6	7.69-7	3.67-7	4.55-7	5.89-7	2.09-7	2.57-7	2.18-7
	b(700)	1.58-7	3.29-7	4.27-7	8.70-7	1.24-6	5.78-7	2.34-7	2.77-7	3.63-7	1.18-7	1.80-7	1.46-7
	b(850)	1.06-7	1.57-7	2.88-7	5.30-7	9.01-7	3.77-7	1.60-7	1.83-7	2.44-7	9.51-8	1.32-7	1.24-7
1977	CN	221	155	115	173	137	130	189	246	235	160	240	236
	b(450)	6.81-7	7.82-7	9.29-7	1.54-6	1.04-6	1.26-6	7.94-7	5.54-7	9.37-7	-	-	-
	b(550)	5.53-7	6.82-7	7.12-7	1.21-6	9.16-7	1.02-6	6.25-7	3.92-7	5.70-7	-	-	-
	b(700)	3.54-7	4.77-7	4.93-7	8.26-7	7.15-7	7.71-7	3.95-7	2.38-7	3.04-7	-	-	-
	b(850)	2.34-7	3.24-7	3.51-7	5.11-7	4.89-7	5.05-7	2.54-7	1.58-7	2.10-7	-	-	-
1978	CN	375	192	293	393	265	312	183	135	195	160	198	214
	b(450)	4.13-6	1.14-6	1.92-6	5.05-6	2.20-6	2.75-6	1.30-6	1.14-6	1.14-6	1.75-6	5.70-7	6.14-7
	b(550)	2.86-6	8.18-7	1.37-6	3.89-6	1.75-6	2.08-6	8.53-7	7.25-7	7.39-7	1.15-6	3.32-7	4.01-7
	b(700)	1.79-6	5.60-7	8.87-7	2.85-6	1.35-6	1.52-6	5.08-7	4.08-7	4.30-7	6.39-7	1.62-7	1.96-7
	b(850)	1.21-6	3.71-7	6.15-7	2.30-6	1.10-6	1.24-6	3.25-7	2.80-7	3.15-7	4.85-7	1.36-7	1.33-7
1979	CN	188	226	422	177	316	428	280	230	285	290	209	275
	b(450)	6.74-7	9.35-7	4.57-6	3.40-6	3.69-6	3.97-6	3.10-6	-	9.23-7	1.03-6	6.94-7	8.69-7
	b(550)	4.40-7	5.94-7	3.34-6	2.60-6	2.93-6	2.97-6	2.23-6	-	5.58-7	6.70-7	4.54-7	5.54-7
	b(700)	2.48-7	3.34-7	2.21-6	1.84-6	2.23-6	2.09-6	1.51-6	-	3.15-7	3.68-7	2.45-7	2.79-7
	b(850)	1.85-7	2.14-7	1.55-6	1.39-6	1.76-6	1.51-6	1.05-6	-	2.00-7	2.29-7	1.60-7	1.66-7
1980	CN	246	213	156	229	239	469	295	303	337	277	201	216
	b(450)	7.41-7	1.07-6	2.16-6	3.07-6	1.94-6	2.98-6	9.68-7	1.33-6	1.11-6	7.51-7	4.64-7	4.83-7
	b(550)	5.13-7	7.57-7	1.45-6	2.28-6	1.55-6	2.12-6	6.64-7	9.16-7	7.60-7	4.94-7	3.00-7	3.01-7
	b(700)	3.04-7	4.53-7	8.87-7	1.59-6	1.14-6	1.37-6	3.76-7	5.68-7	4.43-7	2.68-7	1.72-7	1.74-7
	b(850)	1.63-7	2.54-7	6.34-7	1.22-6	8.66-7	9.19-7	2.20-7	3.23-7	2.85-7	1.97-7	1.35-7	1.39-7
1981	CN	195	239	195	242	252	190	294	293	321	335	241	284
	b(450)	4.68-7	1.56-7	1.37-6	1.52-6	1.54-6	-	-	-	-	-	-	-
	b(550)	3.37-7	1.50-7	1.00-6	1.21-6	1.35-6	-	-	-	-	-	-	-
	b(700)	1.82-7	1.00-7	9.27-7	8.89-7	1.19-6	-	-	-	-	-	-	-
	b(850)	1.17-7	9.27-8	6.84-7	6.83-7	1.11-6	-	-	-	-	-	-	-
1982	CN	245	234	189	221	256	311	204	306	303	400	275	281
	b(450)	-	-	-	-	2.06-6	7.95-7	3.70-7	4.41-7	4.02-7	3.81-7	3.69-7	5.03-7
	b(550)	-	-	-	-	1.73-6	6.29-7	3.05-7	3.41-7	3.17-7	2.80-7	3.10-7	3.93-7
	b(700)	-	-	-	-	1.42-6	5.05-7	2.36-7	2.70-7	2.59-7	2.19-7	2.53-7	3.02-7
	b(850)	-	-	-	-	9.13-7	3.49-7	1.41-7	1.67-7	1.51-7	1.27-7	1.48-7	1.86-7

Table 16.--SMO monthly geometric means of CN concentration (cm^{-3}) and light scattering (m^{-1}) at 450, 550, 700, and 850 nm, where values appear in a compact exponential format ($5.68\text{-}6 = 5.68 \times 10^{-6}$)

		JAN	FEB	MAR	APR	MAY	JUN	JUL	AUG	SEP	OCT	NOV	DEC
1976	CN	314	332	299	248	240	205	180	221	198	218	193	195
1977	CN	231	217	229	237	225	257	259	241	272	255	226	226
	b(450)	-	-	-	-	-	-	1.35-5	3.01-5	2.30-5	3.02-5	2.61-5	3.42-5
	b(550)	-	-	-	-	-	-	1.12-5	2.71-5	1.97-5	2.64-5	2.36-5	3.11-5
	b(700)	-	-	-	-	-	-	1.14-5	2.97-5	1.97-5	2.73-5	2.50-5	3.31-5
	b(850)	-	-	-	-	-	-	1.24-5	3.33-5	2.09-5	2.95-5	2.76-5	3.64-5
1978	CN	289	414	248	265	265	335	296	286	302	280	285	360
	b(450)	2.04-5	3.12-5	1.94-5	1.28-5	2.35-5	2.13-5	1.99-5	1.98-5	2.29-5	1.88-5	-	-
	b(550)	1.81-5	2.77-5	1.71-5	1.08-5	2.04-5	1.93-5	1.89-5	1.80-5	2.09-5	1.72-5	-	-
	b(700)	1.88-5	2.83-5	1.74-5	1.07-5	2.12-5	1.98-5	2.00-5	1.86-5	2.16-5	1.79-5	-	-
	b(850)	2.04-5	3.02-5	1.88-5	1.14-5	2.28-5	2.11-5	2.16-5	1.99-5	2.31-5	1.92-5	-	-
1979	CN	327	328	293	382	284	262	269	304	265	327	303	305
	b(450)	-	-	1.57-5	1.55-5	1.25-5	1.91-5	2.66-5	-	-	-	-	-
	b(550)	-	-	1.42-5	1.42-5	1.20-5	1.81-5	2.12-5	-	-	-	-	-
	b(700)	-	-	1.43-5	1.44-5	1.28-5	1.94-5	2.55-5	-	-	-	-	-
	b(850)	-	-	1.60-5	1.58-5	1.46-5	2.21-5	3.27-5	-	-	-	-	-
1980	CN	309	303	271	282	211	232	261	291	275	279	357	411
1981	CN	321	445	437	305	268	303	393	365	362	323	378	440
	b(450)	-	-	1.28-5	1.35-5	1.22-5	2.13-5	1.34-5	1.04-5	1.49-5	1.69-5	9.55-6	1.10-5
	b(550)	-	-	1.40-5	1.28-5	1.15-5	1.95-5	1.32-5	9.76-6	1.36-5	1.59-5	8.96-6	1.05-5
	b(700)	-	-	1.50-5	1.32-5	1.26-5	2.15-5	1.45-5	1.02-5	1.38-5	1.65-5	9.46-6	1.11-5
	b(850)	-	-	1.65-5	1.44-5	1.30-5	2.75-5	1.65-5	1.12-5	1.49-5	1.79-5	1.05-5	1.24-5
1982	CN	462	483	339	270	226	250	234	195	338	193	186	233
	b(450)	1.42-5	1.56-5	1.48-5	-	-	1.23-5	1.30-5	1.37-5	1.44-5	1.27-5	1.90-5	1.23-5
	b(550)	1.29-5	1.43-5	1.32-5	-	-	1.17-5	1.24-5	1.37-5	1.42-5	1.25-5	1.93-5	1.21-5
	b(700)	1.29-5	1.41-5	1.29-5	-	-	1.21-5	1.27-5	1.46-5	1.50-5	1.31-5	2.09-5	1.26-5
	b(850)	1.38-5	1.51-5	1.38-5	-	-	1.31-5	1.38-5	1.63-5	1.66-5	1.45-5	2.34-5	1.40-5

Table 17.--SPO monthly geometric means of CN concentration (cm^{-3}) and light scattering (m^{-1}) at 450, 550, 700, and 850 nm, where values appear in a compact exponential format $(5.68\text{-}6 = 5.68 \times 10^{-6})$

	JAN	FEB	MAR	APR	MAY	JUN	JUL	AUG	SEP	OCT	NOV	DEC
1974 CN	–	97	178	52	31	23	20	18	41	95	153	–
1975 CN	99	106	113	41	21	10	11	15	31	79	173	114
1976 CN	125	132	125	62	21	13	11	14	32	98	166	115
1977 CN	123	136	105	37	28	15	13	13	32	107	133	132
1978 CN	103	168	91	31	18	7	8	7	21	77	152	113
1979 CN	111	185	143	50	19	15	14	19	28	90	144	118
b(450)	4.65-7	4.86-7	2.45-7	1.38-7	1.45-7	2.07-7	2.94-7	8.28-7	3.23-7	3.76-7	5.10-7	–
b(550)	2.72-7	3.14-7	1.95-7	1.24-7	1.41-7	2.16-7	2.93-7	7.94-7	3.14-7	3.74-7	4.66-7	–
b(700)	1.22-7	1.74-7	1.36-7	8.00-8	9.76-8	1.59-7	2.29-7	6.25-7	2.48-7	2.91-7	3.81-7	–
b(850)	5.52-8	9.17-8	8.86-8	4.93-8	6.40-8	1.15-7	1.72-7	4.97-7	1.84-7	2.22-7	3.08-7	–
1980 CN	131	207	96	46	21	17	11	22	38	103	179	133
1981 CN	139	144	98	35	27	13	17	17	29	62	145	137
b(450)	4.03-7	3.62-7	2.37-7	3.26-7	2.52-7	3.09-7	3.78-7	2.65-7	3.78-7	4.03-7	4.50-7	2.93-7
b(550)	2.78-7	2.08-7	1.34-7	2.20-7	1.84-7	2.49-7	3.43-7	2.08-7	2.97-7	3.23-7	3.97-7	1.85-7
b(700)	1.17-7	9.86-8	7.05-8	1.54-7	1.26-7	1.72-7	2.07-7	1.27-7	2.05-7	2.18-7	2.88-7	9.98-8
b(850)	5.65-8	6.18-8	4.73-8	1.23-7	1.02-7	1.41-7	1.50-7	9.62-8	1.58-7	1.78-7	2.36-7	6.54-8
1982 CN	–	144	84	41	12	12	12	20	27	73	113	73
b(450)	3.11-7	2.86-7	2.79-7	2.28-7	2.20-7	2.76-7	4.46-7	5.37-7	5.77-7	5.34-7	3.28-7	2.31-7
b(550)	2.08-7	1.82-7	2.10-7	1.71-7	1.83-7	2.09-7	3.82-7	4.48-7	5.17-7	4.85-7	2.47-7	1.61-7
b(700)	1.06-7	8.55-8	1.35-7	1.23-7	1.32-7	1.45-7	2.77-7	3.20-7	3.77-7	3.57-7	1.64-7	9.35-8
b(850)	6.37-8	5.69-8	1.19-7	9.31-8	1.07-7	1.19-7	2.27-7	2.80-7	3.32-7	3.07-7	1.25-7	7.06-8

geometric means, except for MLO, where only 0000-0800 LST data were used to avoid possible local contamination from the upslope wind. Linear least-squares trend analyses similar to those given in the last two GMCC Summary Reports (DeLuisi, 1981, p. 41; Bodhaine and Harris, 1982, p. 45) were applied to the data sets shown in tables 14-17 and fig. 20. The trend lines are super-imposed on the data in fig. 20 and the trend analyses are given in table 18. The trend lines for light scattering were calculated in all cases from the 550-nm data.

Table 18.--Least-squares trend analysis of the common logarithms of the data given in fig. 20*

	Slope	Intercept	S.E.†	Trend yr^{-1}
BRW				
$\overline{\sigma}_{sp}$	0.0003320	-5.293	0.3968	0.92%
N	-0.0008493	2.257	0.2783	-2.3%
MLO				
$\overline{\sigma}_{sp}$	0.001119	-6.236	0.3456	3.1%
N	0.0009124	2.325	0.1116	2.6%
SMO				
$\overline{\sigma}_{sp}$	-0.003490	-4.543	0.1057	-9.2%
N	0.001419	2.354	0.09268	4.0%
SPO				
$\overline{\sigma}_{sp}$	0.00004082	-6.591	0.1864	0.11%
N	-0.0004128	1.704	0.4270	-1.1%

*The scale of the abscissa in fig. 20 is such that January 1974 = 1 and December 1982 = 108.
†S.E. = standard error.
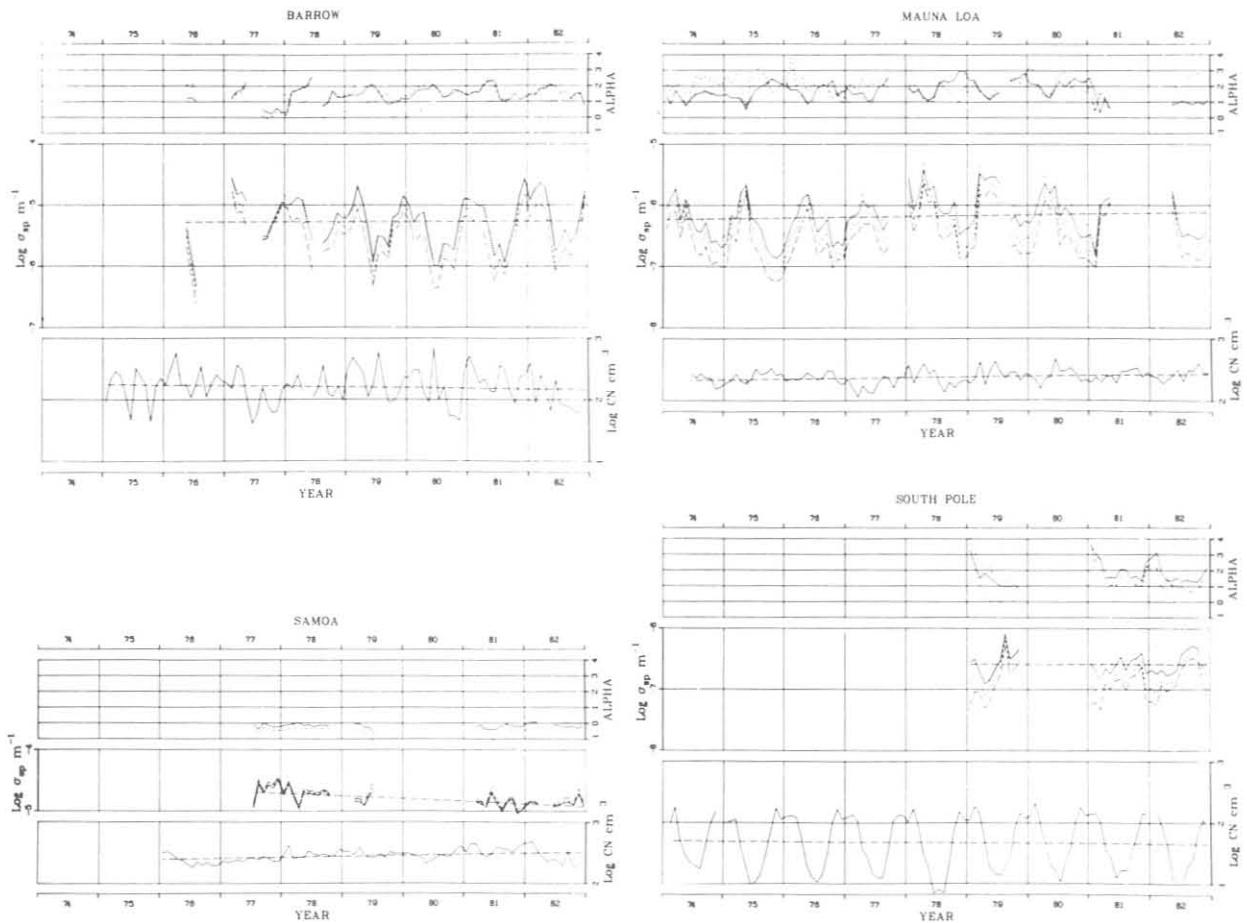
Figure 20.--Monthly geometric means of light-scattering and CN data at BRW, MLO, SMO, and SPO. Only 0000-0800 LST data were used for MLO. For each station, CN concentration (bottom) is shown as a solid line. Light-scattering data (middle) are shown for 450 nm (dotted), 550 nm (solid), 700 nm (dashed), and 850 nm (long-dashed). Angstrom exponents (top) were calculated from 450- and 550-nm (dotted), 550- and 700-nm (solid), and 700- and 850-nm (dashed) light-scattering data.

Long-term trends are generally less-pronounced in this year's analysis than in the previous analyses. For BRW light scattering in particular, the downward trend of previous years has reversed itself because of the high winter 1982 and spring 1983 monthly means. All other trends remain close to previously determined trends, and in each case the change from the beginning to the end of the data record is smaller than the standard error about the regression line. General discussions of the annual cycles and other features of the data shown in fig. 20 have appeared in the last several GMCC Summary Reports.

Figure 21 gives a more detailed presentation of light-scattering and CN data for the GMCC stations during 1982. For each station (except MLO) daily

51
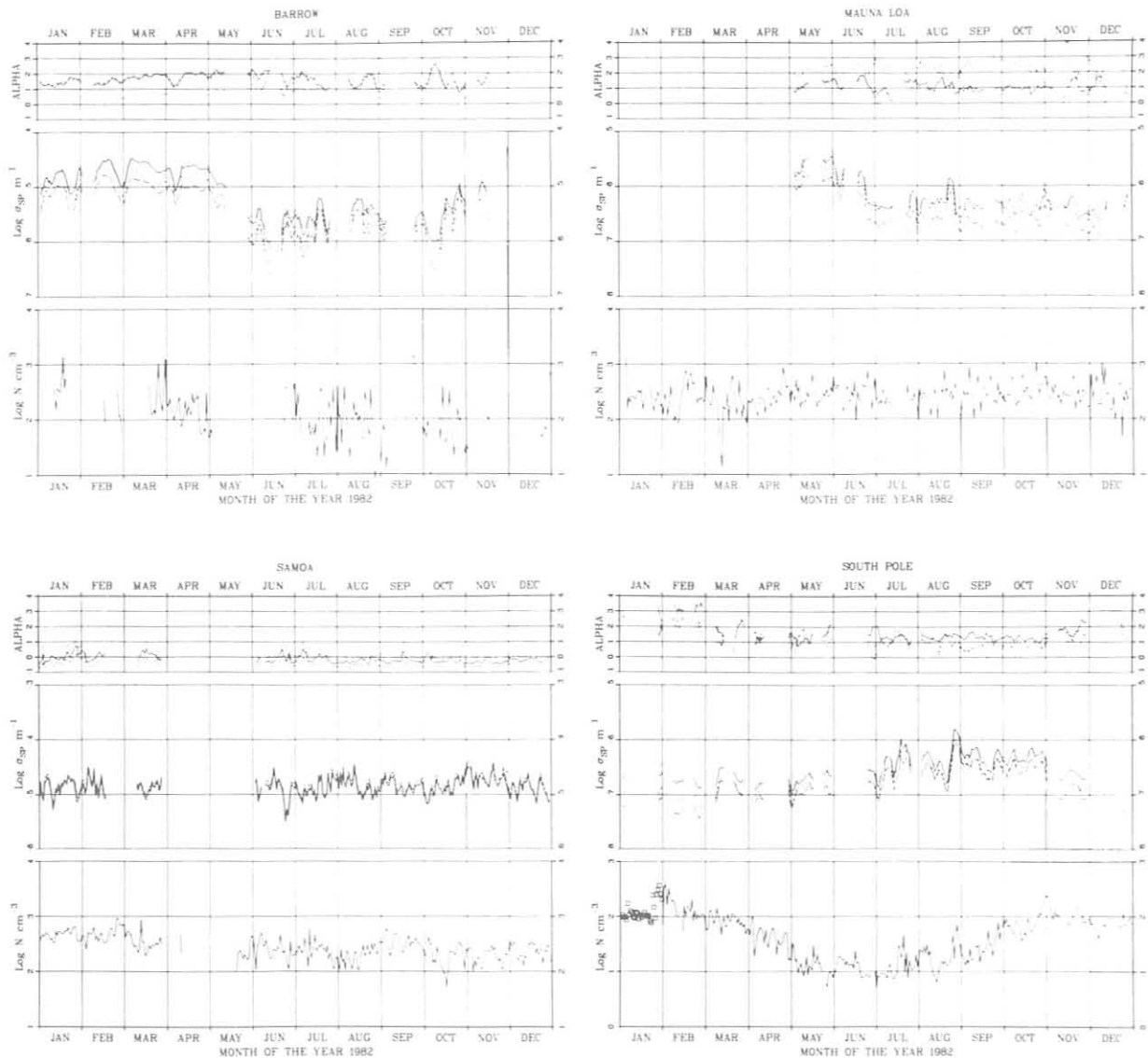
Figure 21.--Daily geometric means of light-scattering and CN data, as in fig. 20.

geometric means were calculated using all data. For MLO, only 0000-0800 LST data were again used to avoid contamination from the daytime upslope winds.

3.9 Solar Radiation

3.9.1 Introduction

The GMCC solar radiation program consists of many measurement and re-search efforts related to the interaction of solar radiation and climate. Long-term measurements of direct and global (direct plus diffuse) solar ra-diation are maintained to determine what effects the changing atmospheric composition may have on the Earth's shortwave energy balance. Short-term measurement programs are carried out in conjunction with particular events to

answer specific scientific questions and to supplement the monitoring data set. Some solar radiation measurements are used as tools to estimate the atmospheric quantity and radiative properties of certain constituents such as water vapor and aerosols.

3.9.2 Monitoring Instrumentation

Table 19 shows the monitoring instruments online at the four GMCC observatories at the end of 1982. The filter designations, Q, GG22, OG1, RG2, and RG8, are the standard WMO-recommended filters described in last year's GMCC Summary Report (Bodhaine and Harris, 1982, p. 50, table 14). Instruments first implemented during 1982 were the 778- and 862-nm sunphotometers and the SPO water vapor meter. The OG1 and GG22 pyranometers at MLO went back online

Table 19.--Solar radiation monitoring instruments, December 1982

Instrument	BRW	MLO	SMO	SPO	Comments
Eppley pyranometer					
Q	X	X	X	X	Continuous
RG8	X	X	X	X	Continuous
OG1	X	X	X	X	Continuous
Eppley pyrheliometer					
Q	X	X	X	X	Continuous
RG8				X	Continuous
Q	X	X	X	X	Discrete
OG1	X	X	X	X	Discrete
RG2	X	X	X	X	Discrete
RG8	X	X	X	X	Discrete
Sunphotometer					
380 nm, narrowband	X	X	X	X	Discrete
500 nm, narrowband	X	X	X	X	Discrete
778 nm, narrowband	X	X	X	X	Discrete
862 nm, narrowband	X	X	X	X	Discrete
Shaded pyranometer		X			Continuous
Solar IR hygrometer		X		X	Continuous

after being out of service for about 1 year. All pyranometers listed are operated in an upward-facing, level orientation. A complete history of the station instrument arrays is chronicled in the preceeding GMCC Summary Reports. The principal responsibility for maintaining the narrowband sunphotometers and handling the sunphotometer data has been returned to the NOAA Solar Radiation Facility in Boulder. Calibration and data acquisition details for most of the monitoring instruments were given in last year's GMCC Summary Report.

3.9.3 Instrument Intercomparison

The traveling-standard quartz pyranometer and pyrheliometer (Eppley SN 12617 and SN 13909) were sent to all four stations and the intercomparisons

with them and the station instruments were performed as in past years. Although a preliminary analysis of some of the results was completed, the final analysis is not ready for presentation at this time. The traveling-standard pyranometer was calibrated at the Solar Radiation Facility on several occasions during the past 2 years, and the most recent calibration indicated a change in its calibration beyond the acceptable limits of ±1.0%. Since the calibration standards of the Solar Radiation Facility were adjusted during the same time, we are investigating whether an actual change has occurred in our traveling standard.

3.9.4 Monitoring Data

Summaries of pyranometer and pyrheliometer data for several years were given in last year's GMCC Summary Report. No new data are ready for inclusion in this report.

3.9.5 Special Projects

Solar radiation measurement activities were dominated during 1982 by the presence of two large stratospheric dust clouds. One cloud, of unknown origin, was first detected in January 1982. The other, from the Mexican volcano El Chichon, was first detected in early April. Because of the global extent and large concentration of these clouds, especially El Chichon, all GMCC solar radiation measurements may be affected. The magnitude of the El Chichon cloud was so great and rare that it was considered by many as an event of the century. Certainly the impact on the MLO solar measurements was by far the largest in 25 years. It therefore seemed prudent to concentrate efforts on determining the radiative properties of the long-lived stratospheric component of the volcanic clouds. However, several ongoing special projects that were planned or were being implemented prior to the detection of the volcanic cloud were also carried to completion during 1982.

A major effort was the establishment of an automated solar observatory at MLO consisting of an active, precision, solar-tracking spar; a computer-operated Ash Dome; and automated data acquisition. Instruments on the spar are a solar IR hygrometer, an automated multiwavelength narrowband sunphotometer, and an Eppley NIP. The automated observatory was put into operation in the old lidar dome during September 1982. Dome operation for the day is initiated when an observer determines that weather conditions are suitable. The observer activates the dome and acquisition computer, and documents the daily log. The dome aperture and active tracking spar locate the Sun and follow it for the rest of the day. The dome automatically closes in the event of rain but otherwise must be closed by an observer at the end of the day. After closing, the dome and spar reset to the sunrise position. The most important time for the observatory to operate is in the early morning before upslope conditions begin. It is therefore necessary that an observer be at the site shortly after sunrise. This requirement was met during most of 1982 and into 1983, although it is not part of standard operating procedures at MLO. (The dome did not operate on weekends.) Further automation of the dome will allow it to sense weather conditions and to open and close for the day under computer control.

A principal objective of the MLO automated solar observatory is to provide spectral aerosol optical depth, which can best be derived from Langley
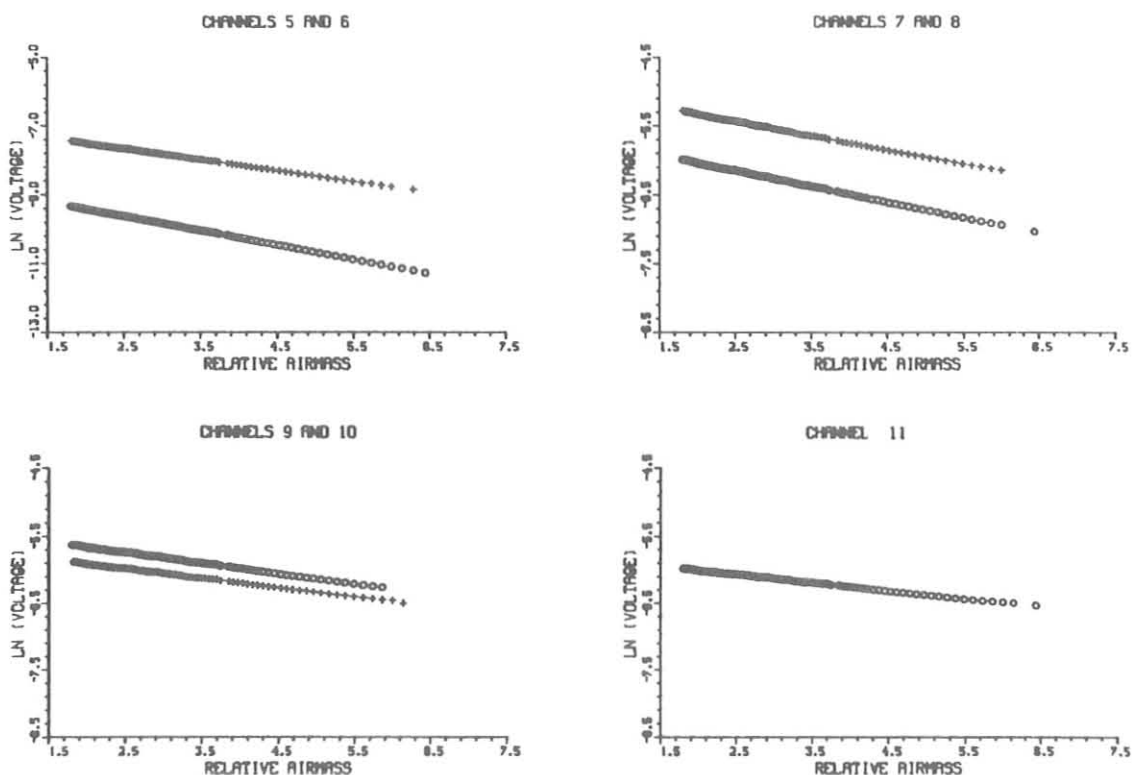
Figure 22.--Sample Langley plots from the seven-wavelength sunphotometer operating in the MLO automated solar dome, where the natural logarithm of the voltage is plotted against relative air mass.

plots. Since several hours of nearly continuous observations are required to obtain a single optical depth value from the Langley plot, an automated observing system has definite advantages. Figure 22 shows the results of Langley plots from 1 day, using the seven-wavelength sunphotometer mounted in the dome. The plotted data have been edited and restricted to the air mass range of 1.75-7.50. The Langley plots are of superior quality, with the correlation coefficient often exceeding 0.9990 for unedited data and 0.99990 for edited data.

A second sunphotometer intended for use at MLO has been designed and built. The new instrument, the PMOD triple sunphotometer, has three wavelengths, 380, 500, and 778 nm, and was designed to specifications and drawings supplied by WMO. The instrument will be calibrated frequently at MLO and will be used as a standard reference instrument for GMCC sunphotometer calibrations. The PMOD consists of three sunphotometers housed in a single unit that was precision machined to assure proper simultaneous alignment of all channels. The electronics, detectors, and filters are temperature controlled to within 0.1°C.

In the spring of 1982 and of 1983 GMCC made supplemental measurements at BRW designed to determine the optical properties of the Arctic haze aerosol. The measurements included spectral optical thickness, albedo, the ratio of spectral global diffuse to global total solar flux, and the ratio of zenith sky diffuse to direct solar flux. Since the derived quantities result from instantaneous measurements of solar radiation at the Earth's surface, the

aerosol optical properties are representative of the total vertically integrated aerosol. However, day-to-day and year-to-year changes in the measured quantities can be used to determine the optical properties of individual components of the aerosol overburden. Analysis of the 1982 and 1983 BRW data is ongoing.

Analysis results of some of the GMCC solar monitoring data relative to El Chichon, principally for MLO, have been given by DeLuisi et al. (1983), DeLuisi (1982), and Dutton and DeLuisi (1983a). These papers discuss the detection and the shortwave radiation effects of the debris cloud. In summary, the 500-nm optical depth of the cloud over MLO was initially near 0.7, but it varied greatly as the main original plume moved over the station. Four months after the eruption, the 500-nm optical depth stabilized at about 0.25. At the same time, the daily integrals of direct-solar and clear-sky-global solar flux were reduced by nearly 30% and 7% respectively, relative to several previous years. Although nonspectral global diffuse flux at MLO increased by almost 300%-400% in June and July 1982, this increase was not enough to be consistent with the large decrease in total flux, indicating unusually high backscattering and/or absorption by the volcanic cloud.

Information on the El Chichon cloud is less abundant from the other GMCC stations because of their locations relative to the volcano and also because of observing conditions. Preliminary examination of SPO filter wheel NIP and sunphotometer data for December 1982 indicate about 0.03 aerosol optical depth enhancement. However, a time series of the cloud evolution at SPO is not possible because of the 6-mo night. Normal optical depths at SMO are large compared with the expected El Chichon component. As a result, preliminary examination of the SMO optical data has not shown an obvious El Chichon signal, even though satellite measurements show the cloud over the station. Direct solar measurements required for optical depth determination are only possible in the spring at BRW.

3.10 Station Climatology

3.10.1 Instrumentation and Data Reporting

The interpretation of local measurements of trace gases, aerosols, and atmospheric turbidity requires accurate measurements of station pressure, air temperature, and moisture content. Surface winds must also be known to evaluate the potential influence of local pollution sources. Relatively standard off-the-shelf instrumentation was chosen for these measurements. Wherever possible, WMO-recommended standards for exposure were used.

A propeller-type anemometer is used (Aerovane, no. 141, Bendix Inc., Environmental Science Division, Baltimore, Md.) to measure the wind speed and direction. A synchro-to-DC converter is used to translate the phase representation of direction to a DC voltage. Orthogonal components are used to average the wind. Station pressure is measured with a capacitance-type transducer (no. 1201C, Rosemount, Inc., Minneapolis, Minn.). The voltage output of the transducer is recorded without further processing. At BRW, MLO, and SMO the air temperature is measured with linearized thermistors (no. 44212, Yellow Springs Instrument Co., Yellow Springs, Ohio). The thermistors are encapsulated in stainless steel shells that are exposed in aspirated sun shields (no. 43404, R. M. Young Co., Traverse City, Mich.). A resistance-type thermometer, with a minimum acceptable temperature of -85°C (no. 954PL, Stow

Labs., Hudson, Maine) is mounted in a naturally ventilated radiation shield (no. 43103-A, R. M. Young Co., Traverse City, Mich.) at SPO. Dewpoint hygrometers are used at all four stations (no. 911, EG&G Inc., Newton, Mass., at BRW and SMO; no. 1200ASP, General Eastern Instrument Co., Watertown, Mass., at MLO and SPO).

Hourly average values, scaled in metric units, are processed and reported for each measurement listed above. The data are stored on microfiche and magnetic tape. The microfiche listings are organized by station, date, time, and variable. The files are available 6 months after the end of the year.

3.10.2 Barrow

A description of the BRW site and its local climatology can be found in previous GMCC Summary Reports. Wind roses of the hourly average resultant wind speed, in three speed ranges, as a function of direction for 1977-1981 and for 1982, are in good agreement (fig. 23). For 1977-1981, wind from the easterly sector occurred 62% of the time, and in 1982 wind from this sector occurred 60% of the time. For wind speeds of 10 m s^{-1} or greater, the occurrence in 1982 was 80% compared with 85% over the past 5 years (Harris and Herbert, 1980). A major deviation from this pattern occurred in February when westerly winds prevailed for almost the entire month (easterlies occurred only 23% of the time). Colder-than-normal temperatures were also reported in February. Table 20 gives a monthly breakdown of average and extreme values of wind, air temperature, and station pressure. Recent comparisons with NWS data from Barrow indicate that the station pressures reported for BRW are low by about 2.5 mb. A study to be completed in 1983 will resolve this difference, and a correction will be applied.
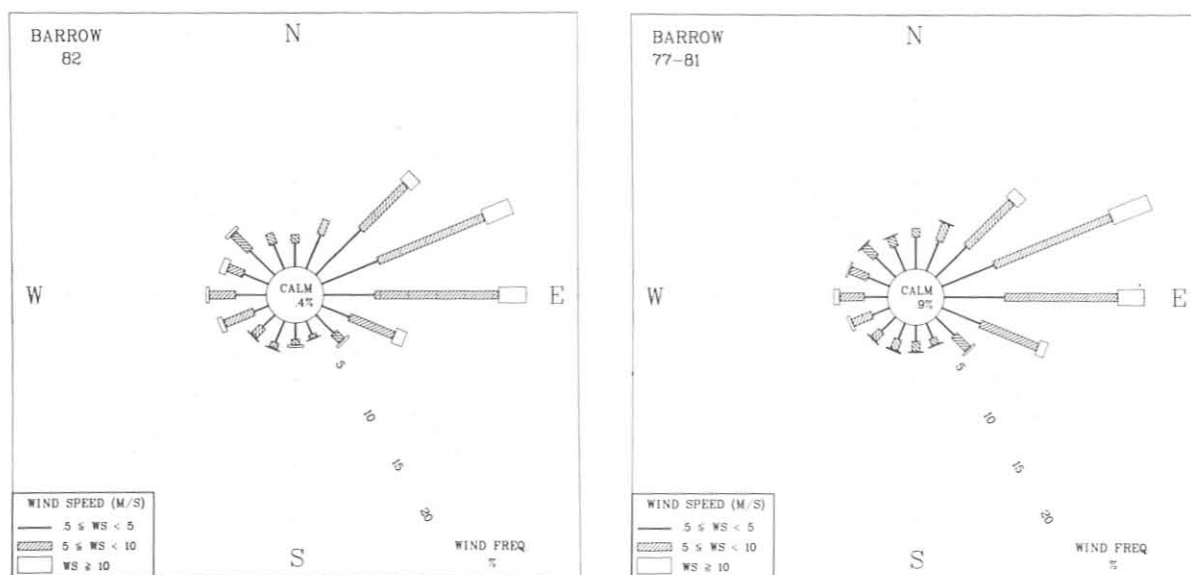
Figure 23.--Wind rose of surface winds for BRW for 1982 (left) and 1977-1981 (right). The distributions of the resultant wind direction and speed are in units of percent occurrence for the year and 5-yr period, respectively. Wind speed is shown as a function of direction in three speed classes.

Table 20.--BRW 1982 monthly climate summary*

	Jan	Feb	Mar	Apr	May	Jun	Jul	Aug	Sep	Oct	Nov	Dec
Prevailing wind direction	ENE	WNW	ENE	NE	E	E	E	WSW	ENE	NW	ENE	ENE
Average wind speed (m s^{-1})	6.6	6.1	5.8	4.6	5.0	5.7	5.2	5.1	4.5	5.5	4.9	8.4
Maximum wind speed† (m s^{-1})	16	19	12	12	11	14	11	10	14	14	16	16
Direction of max. wind† (deg.)	120	270	95	255	85	95	255	235	60	305	60	50
Average station pressure (mb)	1019.5	1021.3	1016.0	1012.8	1014.4	1011.7	1009.1	1011.1	1010.8	1009.5	1016.9	1016.3
Maximum pressure† (mb)	1038	1042	1027	1022	1025	1026	1019	1025	1026	1032	1027	1017
Minimum pressure† (mb)	998	1003	1001	994	1007	994	996	987	1001	982	1009	1015
Average air temperature (°C)	-24.7	-22.9	-25.3	-19.5	-8.6	0.7	3.0	3.0	-1.1	-13.8	-23.7	-23.2
Maximum temperature† (°C)	-7	1	-7	2	4	13	15	16	5	1	-17	-6
Minimum temperature† (°C)	-38	-45	-42	-33	-24	-4	-2	-3	-6	-25	-30	-34

*Instrument heights: wind, 16 m; pressure, 9.5 m (MSL); air and dewpoint temperature, 3 m. Wind and temperature instruments are on a tower located 25 m northeast of the main building.
†Maximum and minimum values are hourly averages.

3.10.3 Mauna Loa

A description of the MLO site and its local climatology can be found in previous GMCC Summary Reports. The combined wind distribution for 1977-1981 in fig. 24 shows a much higher occurrence of winds with a southerly component than does a large-scale trajectory analysis. Although the synoptic-scale flow pattern is more easterly or westerly, the effect of Mauna Loa Mountain is to redirect stronger winds from aloft down the slope, with a more southerly component. The departure from symmetry in the distribution of the southerly winds is to the south-southwest, the direction of the summit of Mauna Loa. Higher wind speeds ($\geq$10 m s^{-1}) occur most commonly (80% of the time) with
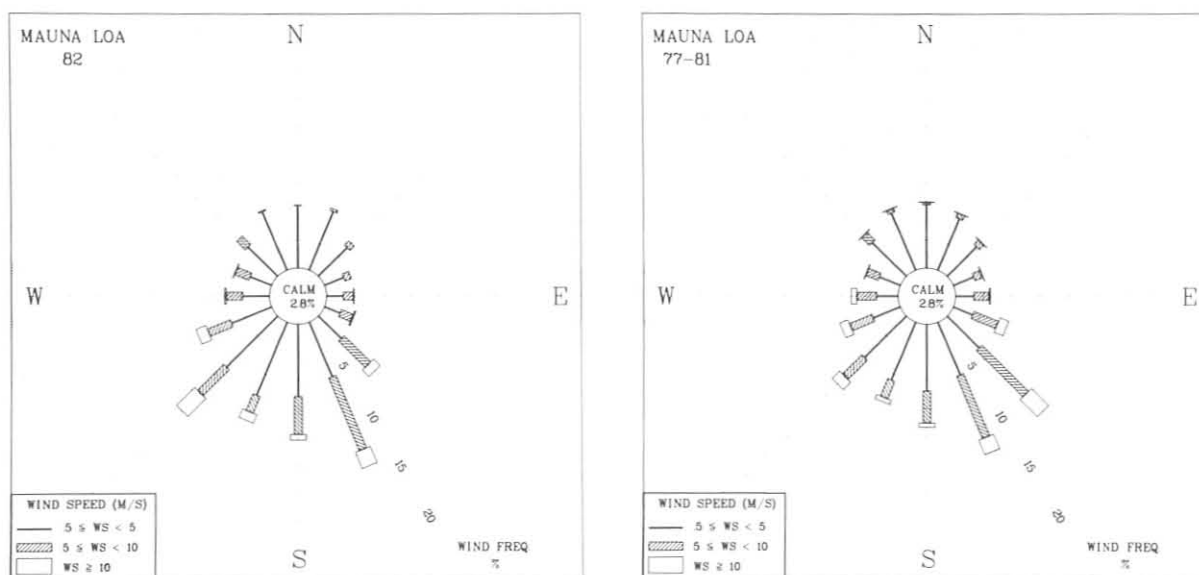
Figure 24.--Wind rose for MLO for 1982 (left) and 1977-1981 (right). See legend for fig. 23.

Table 21.--MLO 1982 monthly climate summary*

	Jan	Feb	Mar	Apr	May	Jun	Jul	Aug	Sep	Oct	Nov	Dec
Prevailing wind direction	SSW	SW	SW	WSW	SSE	SSE	SSE	SSE	SSE	S	SSE	SSE
Average wind speed (m s^{-1})	4.1	7.7	4.0	4.6	3.7	3.7	5.3	4.4	3.8	3.5	5.3	5.8
Maximum wind speed† (m s^{-1})	16	25	14	16	9	11	13	15	15	10	17	17
Direction of max. wind† (deg.)	235	220	185	240	30	200	210	165	155	165	205	215
Average station pressure (mb)	679.2	677.6	679.2	680.1	680.9	681.7	681.9	682.1	681.5	680.8	680.8	681.3
Maximum pressure† (mb)	683	685	683	684	683	684	685	685	685	683	684	685
Minimum pressure† (mb)	675	669	675	676	678	678	677	680	679	679	676	675
Average air temperature (°C)	4.7	4.1	4.0	5.8	7.5	9.1	9.1	7.8	7.8	8.2	8.3	6.6
Maximum temperature† (°C)	15	15	12	16	18	18	18	16	15	17	16	18
Minimum temperature† (°C)	-3	-3	-2	-1	1	1	3	3	0	1	2	0
Precipitation (mm)	198	257	317	56	16	16	120	141	35	9	43	34

*Instrument heights: wind, 10 m; pressure, 3399 m (MSL); air and dewpoint temperature, 2 m. Wind and temperature sensors are located approximately 15 m southwest of the main building on a tower. Pressure sensors are located in the observatory building.
†Maximum and minimum values are hourly averages.

stormy periods and are almost exclusively confined to the southerly directions. Of particular interest is the relatively large frequency of occurrence of winds greater than 10 m s^{-1} from the south-southeast. The upslope-downslope winds are generally represented by speeds of 5 m s^{-1} or less, conditions which occur approximately 62% of the time. Calm conditions (wind speed <0.5 m s^{-1}) occur 3% of the time on the basis of the 5-yr average. Monthly mean and extreme values for wind, pressure, and temperature are given in table 21. Precipitation amounts have been added this year.

The surface winds at MLO in February were considerably stronger than usual and relatively void of upslope-downslope influence for the entire month. Sixty-six percent of the time the wind blew from the southwesterly quadrant with speeds in excess of 5 m s^{-1}. For almost 42% of the month, the wind blew from the southwesterly direction alone. A peak wind speed of 25 m s^{-1} from 220° was reported. The lowest pressure in the last 5 years, 669 mb, was also reported. Northeasterly winds occurred less than 10% of the month.

3.10.4 Samoa

The exposure of the instrumentation at SMO is considerably different from that at the other GMCC stations. Since February 1977, the anemometer has been located at a height of 14 m on a sampling tower atop Lauagae Ridge. In this location there are no major obstacles to the wind flow from the westerly direction, but the shape of the bluff displaces the wind from easterly directions. Temperature is measured at a height of 7 m on the same tower. Dewpoint temperature is measured from air samples drawn from the sampling stack. Station pressure is measured in the main building located about 100 m west of the sampling tower. On 28 March 1982 lightning hit the sampling tower causing damage to most instruments located on top of the ridge as well as to some in the station building. Some sensors could be repaired, but the wind and pressure sensors required replacement. A significant part of the pressure and humidity record is missing as a result of this lightning strike.
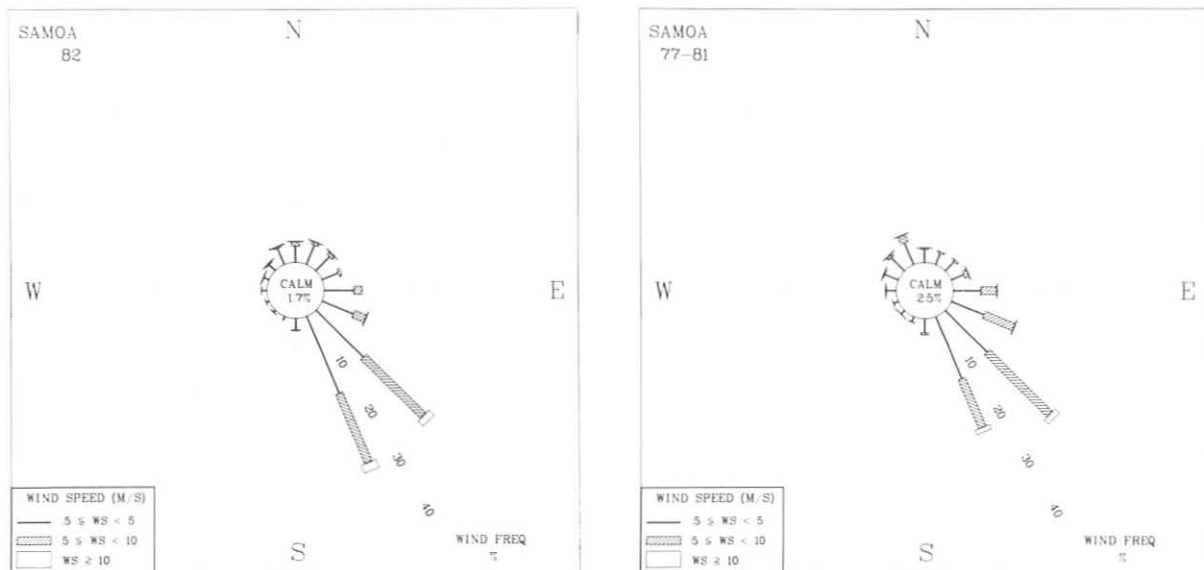
Figure 25.--Wind rose for SMO for 1982 (left) and 1977-1981 (right). See legend for fig. 23.

Southeasterly wind prevailed 66% of the time in 1982 as compared with 61% during the previous 5 years (fig. 25). No particularly strong evidence exists of a significant wind shift associated with the onset of the El Niño during the second half of the year. The only noticeable shift in the wind direction distribution is a slight increase in the percent occurrence of northeasterly winds at the expense of northwesterlies. Typically the northeasterlies occur about 8% of the time and northwesterlies 12%. In 1982 northeasterlies occurred 13% and northwesterlies 6%. Seasonal variations of all other meteorological

Table 22.--SMO 1982 monthly climate summary*

	Jan	Feb	Mar	Apr	May	Jun	Jul	Aug	Sep	Oct	Nov	Dec
Prevailing wind direction	NNE	SSE	SE	NNW	SE	SSE	SSE	SSE	SSE	SSE	SSE	SSE
Average wind speed (m s⁻¹)	3.5	4.8	4.5	3.2	3.9	4.4	4.6	5.3	5.8	5.3	7.9	4.4
Maximum wind speed† (m s⁻¹)	11	16	13	7	9	10	14	12	10	13	13	8
Direction of max. wind† (deg.)	355	350	345	350	100	110	150	165	170	170	170	165
Average station pressure (mb)	999.6	998.2	999.6	1000.5	1001.1	1001.6	--	--	--	--	--	--
Maximum pressure† (mb)	1005	1005	1005	1004	1005	1004	--	--	--	--	--	--
Minimum pressure† (mb)	996	990	991	997	996	997	--	--	--	--	--	--
Average air temperature (°C)	27.5	27.0	27.9	27.8	26.7	26.8	26.5	25.9	25.7	26.3	25.6	26.2
Maximum temperature† (°C)	31	31	32	34	31	31	31	29	30	31	28	30
Minimum temperature† (°C)	23	22	24	23	23	23	23	23	22	24	22	24
Precipitation (mm)	244	357	225	26	203	87	77	329	89	54	115	91

*Instrument heights: wind and dewpoint temperature, 14 m; pressure, 30 m (MSL); air temperature, 7 m. Wind and temperature sensors are located atop Lauagae Ridge, a distance 110 m northeast of the station. Pressure sensors are located in the station.
†Maximum and minimum values are hourly averages.

60

variables are small compared with other GMCC stations (table 22). Only slight-
ly higher winds and cooler temperatures occur in winter than in summer. The
monthly variation in precipitation was surprisingly large, with April the
driest month. The winds were unusual as well: the maximum speed was only
7 m s^{-1}, and winds greater than 5 m s^{-1} occurred only 5% of the time as com-
pared with an expected frequency of 40% based on the previous 5 years.

3.10.5 South Pole

Figure 26 displays, in polar coordinates, the distribution of the wind as
a function of speed and direction. The most prevalent direction on 1982 was
north-northeasterly as in previous years. For the second successive year, a
marked increase was observed in the percentage of stronger winds (≥10 m s^{-1})
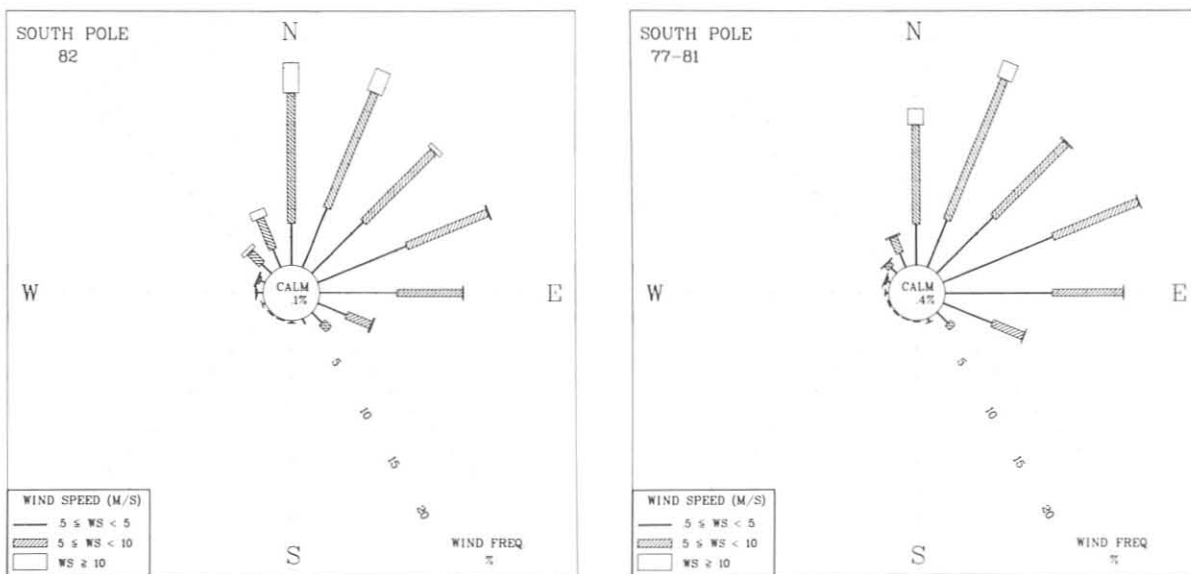
Figure 26.--Wind rose for SPO for 1982 (left) and 1977-1981 (right). See
legend for fig. 23.

that are predominantly from the north. During the previous 5 years, wind
speeds ≥10 m s^{-1} occurred 3% of the time. In 1982 wind speeds ≥10 m s^{-1} oc-
curred 7% of the time. Calm conditions (wind speeds <0.5 m s^{-1}) occurred
<0.1% of the time.

The full extent of the austral winter on the Antarctic plateau is shown
in the eight monthly average air temperatures that are below the annual aver-
age of -49.2°C (see table 23). The maximum hourly average temperature in 1982
was -18.3°C (DOY 001) and the minimum temperature was -82.5°C (DOY 173). This
was a new record low temperature for SPO.

Table 23.--SPO 1982 monthly climate summary*

	Jan	Feb	Mar	Apr	May	Jun	Jul	Aug	Sep	Oct	Nov	Dec
Prevailing wind direction	E	ENE	ENE	N	NE	N	NNE	NE	NNE	N	N	NNE
Average wind speed (m s^{-1})	4.2	4.6	5.2	6.2	6.1	6.0	7.5	6.5	6.0	8.3	6.9	4.5
Maximum wind speed† (m s^{-1})	10	7	9	10	13	12	16	12	12	17	17	9
Direction of max. wind† (deg.)	350	345	320	20	20	5	290	325	320	325	30	100
Average station pressure (mb)	686.5	680.4	670.5	672.6	672.6	668.5	674.7	669.2	667.0	673.1	683.8	690.7
Maximum pressure† (mb)	694	691	687	691	685	688	690	679	681	690	696	700
Minimum pressure† (mb)	673	672	655	651	655	645	658	651	655	655	668	677
Average air temperature (°C)	-26.8	-39.9	-54.0	-54.1	-56.4	-60.3	-57.9	-61.6	-61.4	-49.6	-37.6	-30.3
Maximum temperature† (°C)	-18	-22	-38	-34	-38	-39	-34	-38	-35	-30	-29	-20
Minimum temperature† (°C)	-33	-55	-68	-75	-77	-83	-73	-75	-77	-64	-46	-37

*Instrument heights: wind, 10 m; pressure, 2850 m (MSL); air temperature, 2 m. The anemometer and thermometer are located on a mast 30 m grid north of CAF. Pressure measurements are made inside CAF.
†Maximum and minimum values are hourly averages.

3.11 Precipitation Chemistry

The precipitation chemistry program continued with little change during 1982 at the 10 regional and 2 baseline NADP sites (see table 24). The sites located at Bishop, Calif., and Pendleton, Oreg., closed in July. Snow samples were analyzed for BRW and SPO, and special studies continued at MLO using the ion chromatograph. The Washington, D.C., network continued to operate with six observers.

3.11.1 Baseline Measurements

The five-site special network on the island of Hawaii and a sixth site on Kauai continued to operate on a daily or biweekly schedule. Site locations were discussed in previous GMCC Summary Reports. As seen in fig. 27, the

Table 24.--Annual weighted-average ion concentration (μeq ℓ^{-1}) at NADP regional and baseline sites from January to December 1982

WMO Site	H$^+$	SO$_4^=$	NO$_3^-$	Cl$^-$
Alamosa, Colo.	2.21	26.14	14.23	3.81
Bishop, Calif.*	2.36	12.79	6.53	1.77
Caribou, Maine	18.97	21.76	9.16	2.61
Huron, S. Dak.	3.25	27.64	21.89	2.94
Meridian, Miss.	20.78	36.94	12.93	10.43
Pendleton, Oreg.*	1.46	17.05	9.14	4.76
Washington Crossing, N.J.	42.11	53.43	22.21	7.75
Raleigh, N.C.	36.06	37.49	15.77	5.74
Salem, Ill.	36.57	47.03	17.27	4.50
Victoria, Tex.	8.59	21.84	8.51	19.30
MLO†	4.82	5.16	1.15	1.38
SMO†	3.27	27.30 (6.06)§	0.40	157.86 (3.20)§

*Closed July 1982; values based on January-June data.
†Baseline site.
§Values in parentheses represent the non-seasalt contribution.
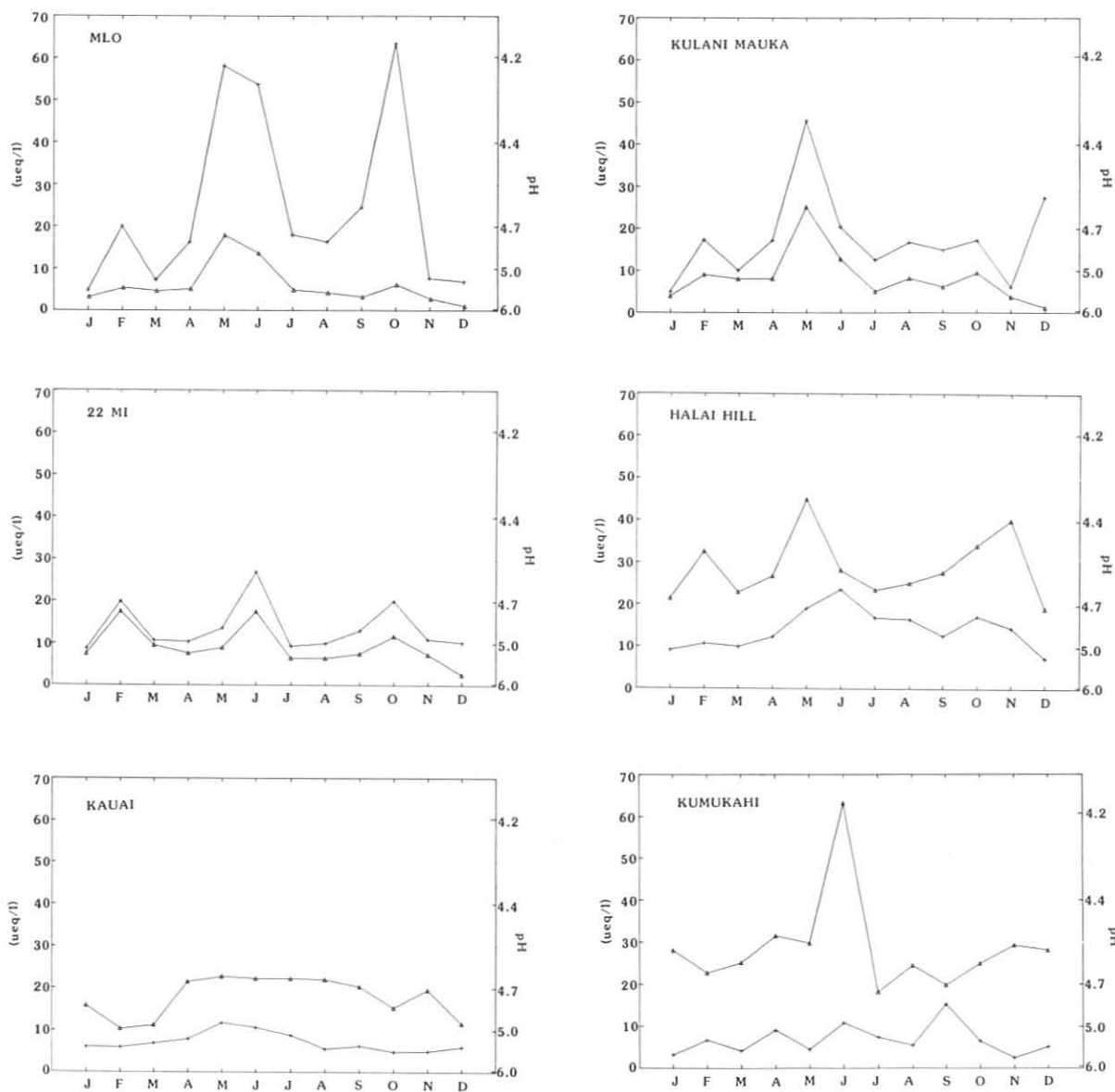
Figure 27.--Monthly precipitation weighted means for six sites on the islands of Hawaii and Kauai during 1982 (+ = H^+; Δ = $SO_4^=$). The sites in order of increasing elevation are Kumukahi, Kauai, Halai Hill, 22 Mi, Kulani Mauka, and MLO.

acidity increase with elevation is still quite evident, as in past years. An opposite trend, a decrease of sulfate with increasing elevation, is also evident. Removal of the seawater sulfate component (not shown), however, gives sulfate concentrations comparable with those observed at MLO. Agreement at Halai and Kauai, two sites with approximately the same elevation and orientation to the trade winds, is not as good as in past years.

Monthly weighted hydrogen ion and sulfate values for MLO and SMO NADP sites are shown in fig. 28. Annual weighted means are shown in table 24 where the values in parentheses for SMO were adjusted using Na to remove the seasalt contribution. Snow sample data for BRW and SPO are shown in fig. 29.
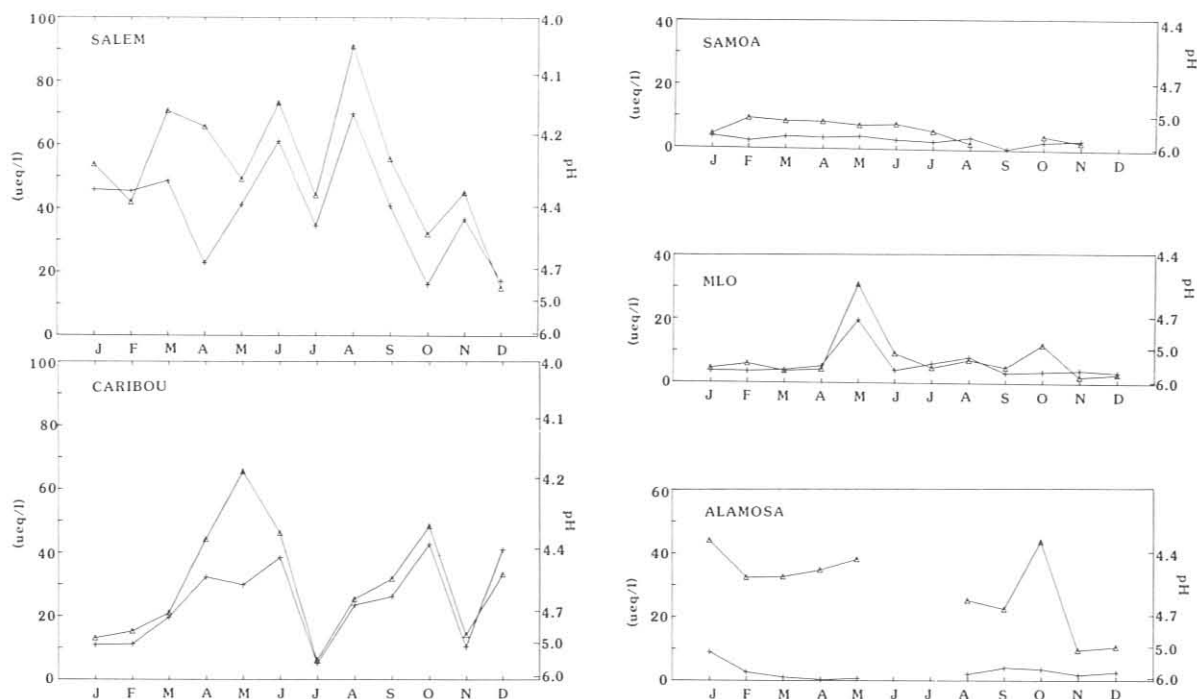
Figure 28.--Monthly precipitation weighted means for five regional and base-line NADP sites during 1982 ($+ = H^+$; $\Delta = SO_4^=$).

3.11.2 Regional Measurements

Annual weighted ion means for the 10 NADP regional sites are shown in table 24. Selected monthly weighted hydrogen ion and sulfate means are shown in fig. 28. A more extensive analysis has been completed for the Caribou, Maine, site; figs. 30 and 31 indicate the amount and quality of data available. Changes in quality assurance, quality control, and collection protocol since 1980 have increased the reproducibility of the data.

3.11.3 Washington, D.C., Network

The data for the Washington, D.C., network are shown in fig. 32.
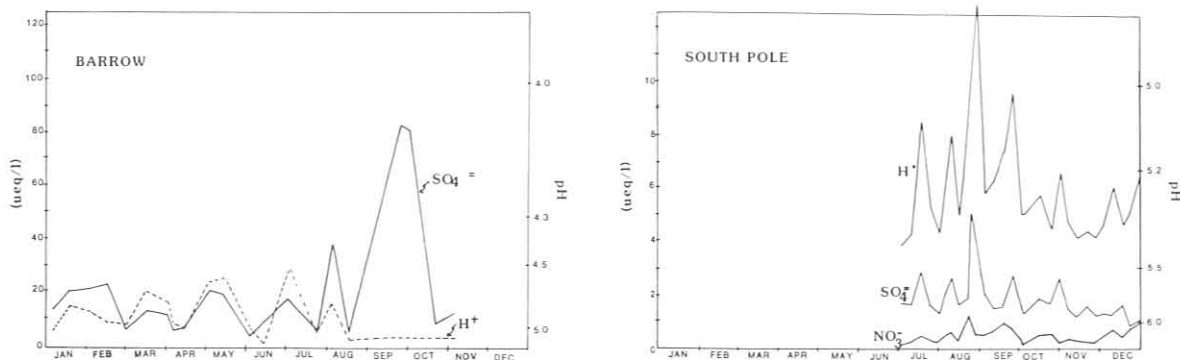
Figure 29.--Snow sample ion concentrations for BRW and SPO during 1982.
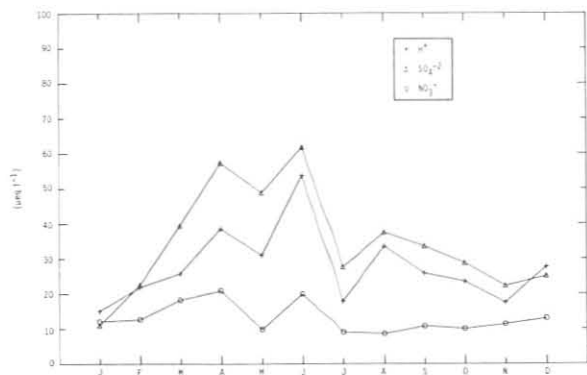
Figure 30.--Monthly precipitation weighted means for Caribou, Maine, for 1980-1982.
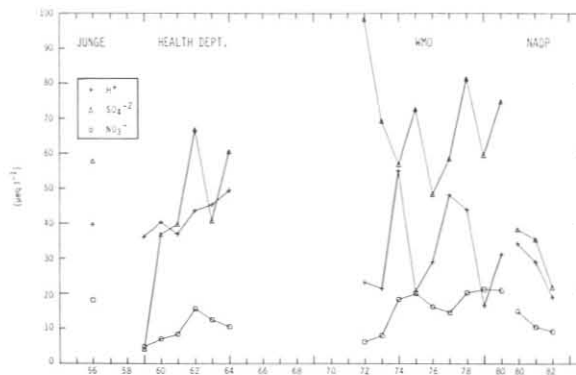
Figure 31.--Annual precipitation weighted means for Caribou, Maine, over the existing data record.
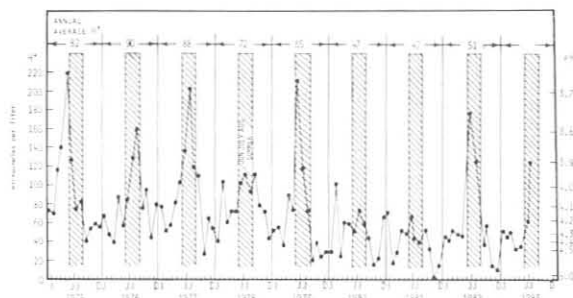
Figure 32.--Monthly precipitation weighted hydrogen ion concentration for the Washington, D.C., area. The center bars highlight the summer data. Each annual mean is noted at the top of its column.

3.12   Data Management

3.12.1   ICDAS

For over 6 years the A&DM group has overseen the automatic collection of continuous data by ICDAS at the four GMCC observatories. This minicomputer system records meteorological, aerosol, CO_2, O_3, and solar radiation data on magnetic tape in the form of minute voltages and hourly scaled values. The overall performance of ICDAS was good again this year with a 95% average data recovery for the four stations. The breakdown by station during 1982 is 99% at SPO, 97% at SMO, 96% at MLO, and 88% at BRW. ICDAS performance statistics by station and year for 1977-1982 are shown in fig. 33. If 1977 is discarded for MLO, when the station was rebuilt, ICDAS has operated over the entire period for 97% of the time at SPO, 95% at SMO, 97% at MLO, and 92% at BRW.

3.12.2   Reduction Facility

Successful data transfer from the GMCC stations to the CDC 750 computer in Boulder requires a complete rewriting of the data tapes. This is performed in the GMCC reduction laboratory. In 1981 both the hardware and software used for rewriting were upgraded. A faster NOVA 4 with a hardware multiply-divide function and a Winchester disk were installed. The larger disk allowed the use of the Data General RDOS. All software used for processing was converted to FORTRAN. This system operated without extensive downtime in 1982. By the end of the year 30% of the disk was used for permanent software files.
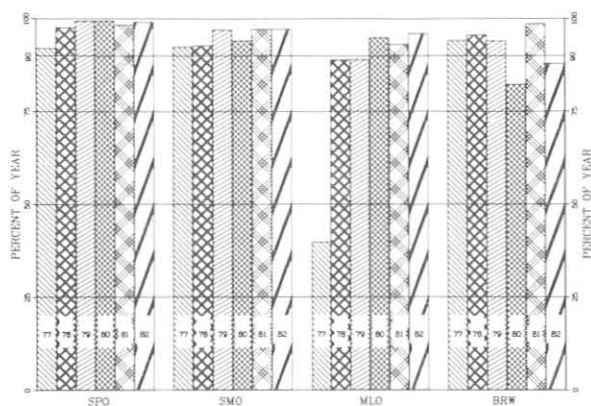
Figure 33.--ICDAS performance statistics by station and year for 1977-1982.

The DECtape II (TU-58) cartridge drive was used throughout the year to extract special solar radiation measurements recorded at MLO. Tape-reading problems occurred and in most cases were traced to faulty hardware. In only one case was a tape failure detected. This project will continue into 1983. All TU-58 cartridges recorded on IICAMS boxes will be processed through this system. Software is being prepared to print summary reports of the tapes and to make backup recordings of the contents on larger tape reels. This software will be completed well in advance of the deployment of IICAMS.

3.12.3 IICAMS Development and Testing

Significant advances were made in the development and testing of IICAMS, which will replace ICDAS in 1984. Component testing was given top priority, and for the most part the final complement of subcomponents was evaluated. A prototype data logger was constructed and installed at MLO to record signals from a set of solar radiation sensors. The performance of this system was satisfactory in most respects. Discussions with station staff and project leaders indicated that a printer would be a necessary part of each system. Thus, access to a common printer will be provided for each IICAMS data recorder.

The configuration of IICAMS includes a CPU (MDX-CPU1), programmable memory (MDX-UMC), battery-powered memory (MDX-BRAM), serial input-output boards (MDX-S102), a battery-powered clock (MDX-BCLK), and a digital input-output board (MDX-D10B1). The boards and the card cage in which they reside (MD-CC12) are manufactured by Mostek, Inc. Sensor voltages are acquired with an analog-to-digital converter (Data Translation DT 2742). The clock and random access memory are battery powered and are maintained for 5 days or more. The software resides in PROM so that the system will restart automatically after a power failure. Data are recorded on preformatted cartridge tapes (DEC, TU-58). Operation control is provided by a set of function switches and a numeric pad in a modular front panel terminal (Burr-Brown, TM-76). An Epson MX80FT printer will be used to print results. All components except the printer reside in an enclosure built in-house.

Specifications were prepared for the IICAMS CO_2 software after a series of meetings and discussions with the CO_2 staff. This is a complex package and a significant amount of testing will be necessary. Specifications for an IICAMS that will record the solar radiation, aerosol, surface ozone, and meteorological signals will be prepared early in 1983. Software will be written

in the summer of 1983, and testing will follow in the fall. Installation will be done station by station beginning in 1984. The plan calls for the construction of 24 IICAMS units to replace ICDAS at the four GMCC stations.

3.12.4 Archiving

The magnetic data tapes listed in table 25 were added to the inventory of GMCC data archived at WDC-A in Asheville, N.C. There are now 34 GMCC data tapes in the archive. A list of the data archived prior to 1982 can be found in the GMCC Summary Report, No. 10 (Bodhaine and Harris, 1982, p. 70).

Copies of the tapes can be obtained from User Services Branch, E/CC423, National Climatic Center, Asheville, NC 28801 (FTS 672-0682 or 704-258-2850, ext. 682). Planned new numbers are 672-6682 and 704-257-6682. GMCC archive tapes are located in tape deck no. 9708. GMCC also archived all available 1979 CO_2 flask data from stations in the CO_2 flask network (NESDIS, 1983).

Table 25.--GMCC data tapes sent to WDC-A in 1982

Tape name	Date of issue	Parameter	Station	Period of data
A82225	8/16/82	Solar irradiance (Research Cooperator format)	BRW	1981
A82226	8/16/82	Solar irradiance (Research Cooperator format)	MLO	1981
A82227	8/16/82	Solar irradiance (Research Cooperator format)	SMO	1981
A82228	8/16/82	Solar irradiance (Research Cooperator format)	SPO	1981

3.13 Atmospheric Trajectories

3.13.1 Introduction

Development of the GMCC atmospheric trajectory program continued in 1982. There are now three versions of the program. The first, called GAMBIT1, has been operational for well over a year. GAMBIT1, originally developed from the ARL trajectory model (Heffter and Taylor, 1975), produces backward isobaric trajectories for the Northern Hemisphere. Analyzed u and v winds for the Northern Hemisphere are the primary input. The wind data are produced by NMC's operational model and are supplied to GMCC by NCAR. A complete description of this version of the trajectory program as well as examples of output plots were presented by Harris (1982) and Bodhaine and Harris (1982, pp. 71-74).

The second version, GAMBIT2, is similar to the first, except it can produce trajectories for the entire globe. The input data are in the form of u

Table 26.--Description of NMC data purchased from NCAR

	Northern Hemisphere 65 × 65 grids	2.5° global grids
Dates	1975-Aug 1982	1977, 1979, 1980
Parameters	u, v, z, T	u, v, z, T
Levels	1000-100 mb (mandatory levels)	1000-100 mb (mandatory levels)
Program	GAMBIT1, GAMBIT3	GAMBIT2

and v analyzed winds for every 2.5° of latitude and longitude. The program can operate in three modes: (1) Northern Hemisphere only, (2) Southern Hemisphere only, or (3) both hemispheres. In the last mode, grids from the Northern Hemisphere and the Southern Hemisphere data tapes are spliced together allowing the computation of cross-equatorial trajectories. This program produced the SMO trajectories used in the case study in sec. 3.13.3. A disadvantage of GAMBIT2 is the added computer costs incurred when dealing with the larger global data set.

The third version of the trajectory program, GAMBIT3, produces isentropic trajectories that trace paths determined by the wind field on surfaces of constant potential temperature. Details of the computational method for GAMBIT3 and a case study are in sec. 3.13.4.

Table 26 gives a description of the NMC data, purchased from NCAR, that serve as input for the three versions of the trajectory program. The missing years have been ordered and should be obtained this year.

The quality of the 1982 data set decreased dramatically over previous years because of the amount of data missing. Following are the breaks in the 1982 data up to 31 August:

> 12-19 Jan
> 22-26 Feb
> 03-11 Jul
> 27-31 Jul
> 09-16 Aug

Breaks create a problem because trajectories cannot be computed for times when there are no data. Also, breaks prevent the program from being run in its most efficient mode; i.e., instead of computing trajectories for an entire month, the program must start or stop at breaks.

Next year the possibility of a more direct link to the data will be investigated. If found, this could prevent excessive loss of data and would give more rapid access to the data. When the data are obtained through NCAR there is at least a 6-mo delay.

3.13.2 GAMBIT1

Last year as part of the process of validating GAMBIT1, two special products were developed. An example of the first is given in fig. 34, which shows a plot of the gridded winds used as input to the trajectory program. Here the

NMC GRID WINDS FOR 700 MB 77 4 19 0Z
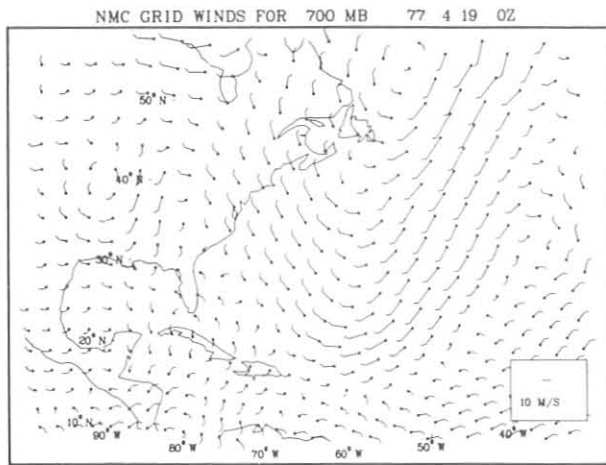
Figure 34.--NMC grid winds for
19 April 1977 at 0000 Z in the re-
gion around Bermuda. The direction
of the main vectors is the same as
wind direction (i.e., wind flowing
towards dots). Wind speed is pro-
portional to the length of the main
vectors.

winds are plotted on a map as vectors pointing in the direction of the wind
and proportional in length to the wind speed. Since these vectors show a
"snapshot" of the wind at one time (in this case for 19 April 1977 at 0000 Z)
and trajectories trace air flow over a finite period of time, the trajectories
were checked by examining wind speeds and directions from a series of wind
vector plots. This validation procedure, though somewhat inexact, gave fur-
ther evidence of the reliability of the GAMBIT1 program.

Figures 35 and 36 show trajectories arriving at nine destinations in the
MLO region. This second type of special plot shows how trajectories are af-
fected by a small change in destination. The nine destinations, spaced 3°
apart, form a cross with MLO in the center. Figure 35 shows remarkable agree-
ment among the nine independently computed trajectories, suggesting that the
wind field was fairly homogeneous at 500 mb on 1 May 1979. Several days ear-
lier on 25 April (fig. 36), a 3° difference in the destination made a signifi-
cant difference in the airflow pattern. The relationships among these tra-
jectories are consistent with a ridge being present to the north of Hawaii on
this day. The progression from south and west to north and east results in a
continuously larger deformation of the trajectories to the north.

500 MB TRAJECTORIES ARRIVING 79121 - 5 1 79 AT 0Z

500 MB TRAJECTORIES ARRIVING 79115 - 4 25 79 AT 0Z
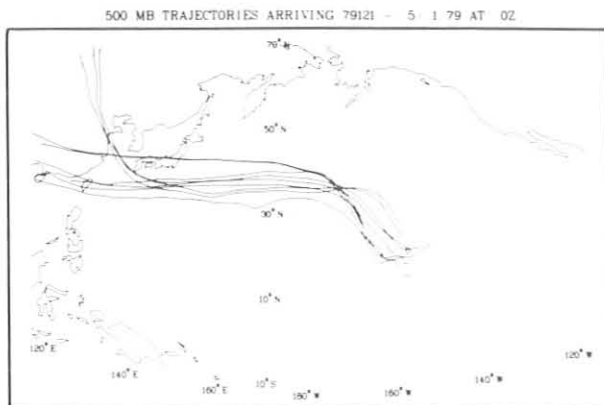
Figure 35.--Trajectories arriving
at nine destinations near Hawaii on
1 May 1979 at the 500-mb level.
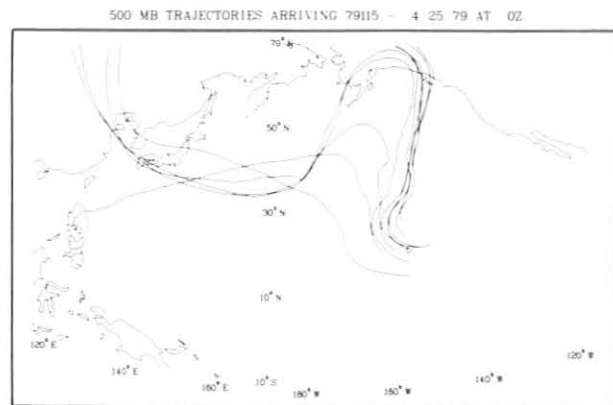
Figure 36.--Trajectories arriving
at nine destinations near Hawaii on
25 April 1979 at the 500-mb level.

3.13.3 GAMBIT2

This year the global trajectory model, GAMBIT2, produced GMCC's first trajectories for SMO. Trajectories for 1977 at the 1000- and 850-mb levels were computed in the dual-hemisphere mode so that airflow from SMO could be traced across the Equator from the Northern Hemisphere if necessary. The case study presented here is for March 1977. During the first part of the month, air flowed to SMO from the east (fig. 37). The predominant southeasterly trade winds at SMO result from counterclockwise flow around the South Pacific subtropical high. Figure 38 is an example of trajectories during the middle of March when a transition from easterly to westerly winds occurred. At this time some of the 10-day trajectories to SMO originated in the Northern Hemisphere. The NMC surface map for 17 March (fig. 39) shows tropical storm Norman to the west of SMO. During the last part of March westerly winds driven clockwise around this storm are seen in the trajectories in fig. 40.
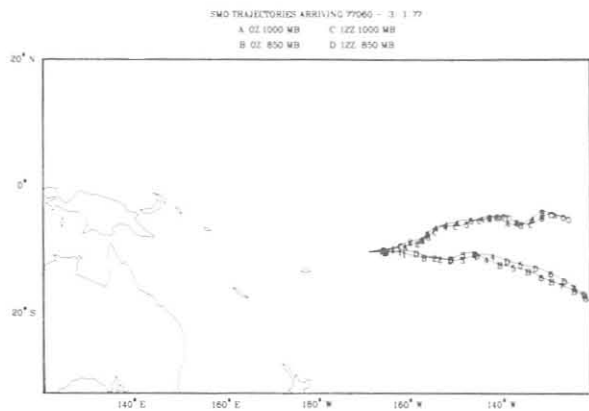
Figure 37.--SMO trajectories arriving on 1 March 1977 at the 1000- and 850-mb levels.
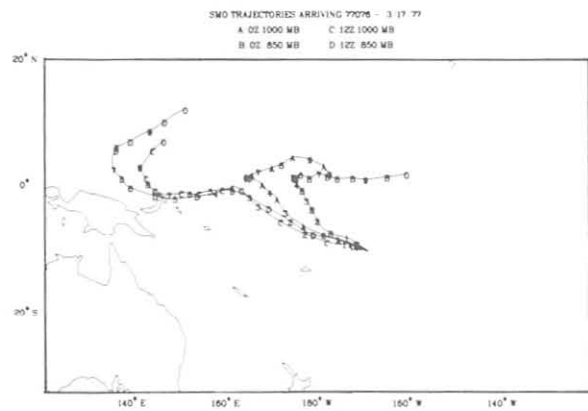
Figure 38.--SMO trajectories arriving on 17 March 1977 at the 1000- and 850-mb levels.

3.13.4 GAMBIT3

In an attempt to improve the accuracy of the trajectories, a procedure for computing kinematic trajectories on isentropic surfaces, GAMBIT3, was developed. Testing and comparison with the isobaric model continues. Because of its added complexity and cost of operation, GAMBIT3 is run on a case-study basis. Some preliminary results are presented below.

The computational method was determined in part by limitations on computer memory and costs. Rather than dynamic isentropic trajectories, the model produces simpler kinematic trajectories, but even these require a multi-step process involving more than a half dozen programs. The first step is to choose a potential temperature (θ) for the isentropic surface on which trajectories will be constructed. This is accomplished by computing θ from rawinsonde data at or near the desired trajectory destination, or from analyzed gridded data. Once the desired θ is determined, a series of θ surfaces are computed on an appropriate subgrid of the NMC 65 × 65 Northern Hemisphere grid. One such θ surface is shown in fig. 41 over the subgrid used for MLO. Note the characteristic rise of the isentropic surface toward the pole. Plots
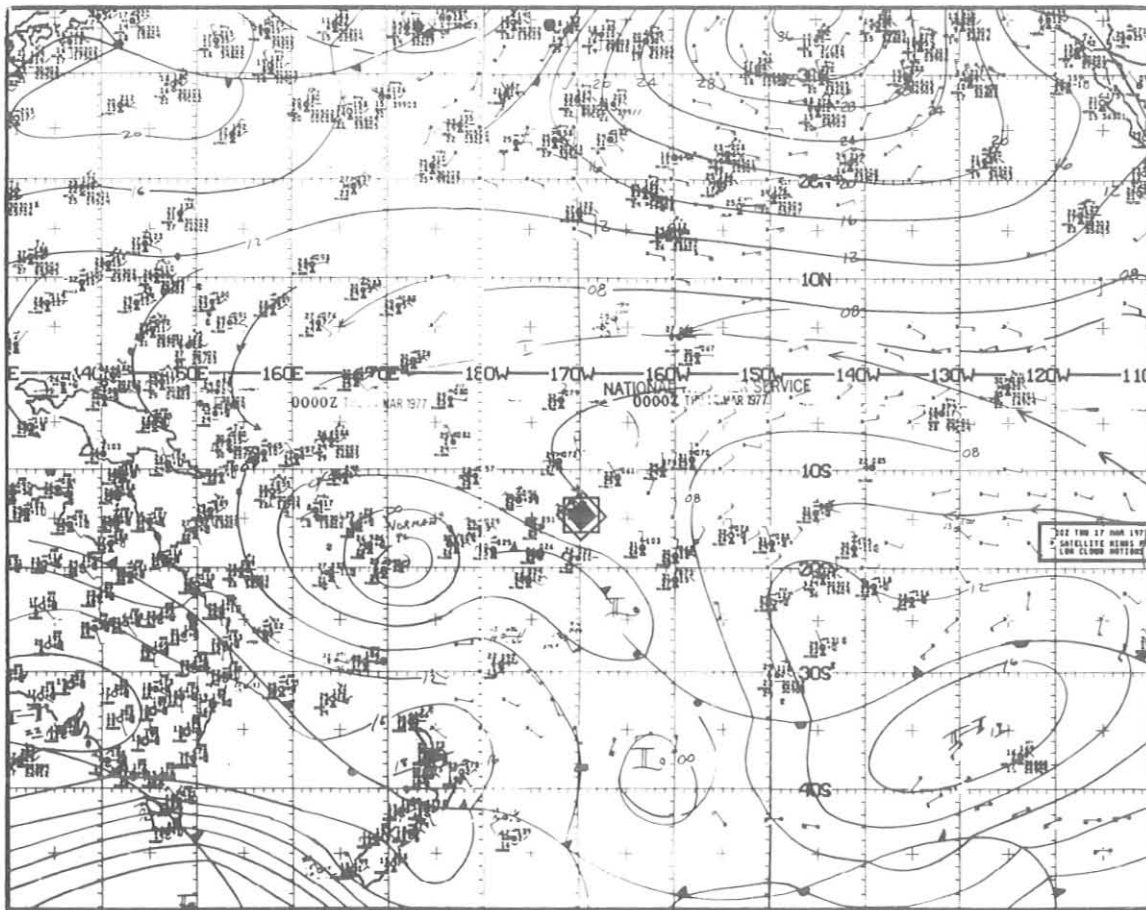
Figure 39.--NMC surface analysis for 17 March 1977. SMO is marked ◈.

of isentropic surfaces are used to determine the approximate heights of the surfaces at the destination. In this case the height of the surface at θ = 310 K (the 310-K surface) is about 3 km at MLO. If the θ value chosen is too low, these plots would show that the surface is not defined at MLO. In the latter case, the isentropic surface would intersect the earth before reaching MLO, indicating that air arriving there did not travel along that surface. To be examined is the possibility that there are day-to-day variations in θ large enough that would require frequent adjustments to the θ surface bringing air to the station. In the examples presented here θ = 310 K was close to the 700-mb level and θ = 325 K was close to the 500-mb level at MLO.
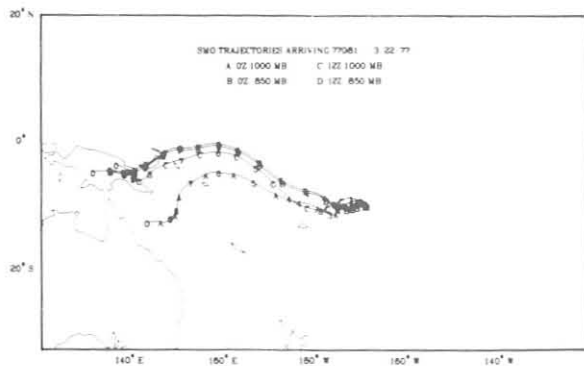
Figure 40.--SMO trajectories arriving on 22 March 1977 at the 1000- and 850-mb levels.

71
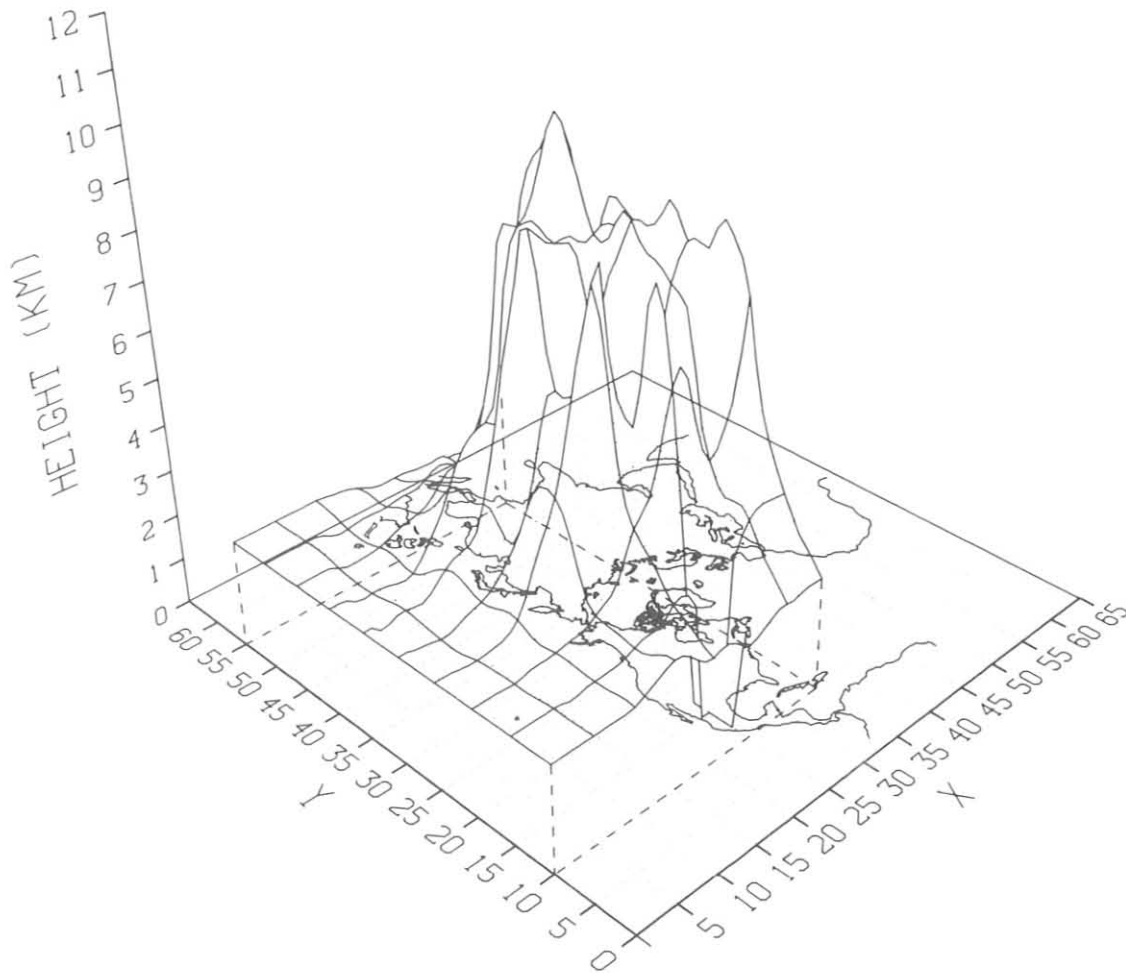
Figure 41.--The 310-K isentropic surface for 25 April 1979 at 0000 Z overlaying the MLO subgrid of the NMC Northern Hemisphere 65 × 65 grid.

Given the desired potential temperature θ_j, the program that computes the isentropic surface uses Duquet's (1964) method, described also in Haagenson and Shapiro (1979), to transform the data from NMC standard levels to the θ surface. Input data for this program are temperature, height, and u and v wind components reported at nine levels (850, 700, 500, 400, 300, 250, 200, 150, and 100 mb). On a gridpoint-by-gridpoint basis, the two pressure levels, i and i+1, that bracket θ_j are found. Assuming that temperature varies linearly as P^K, then

$$ T_j = \frac{\theta_j \, (T_i - B \, P_i^K)}{\theta_j - B \, 1000^K} \, , $$

where

$$ B = \frac{T_{i+1} - T_i}{P_{i+1}^K - P_i^K} \, ; \quad \kappa = \frac{R}{c_p} \simeq 0.286; $$

R is the gas constant; and c_p is the specific heat of air at constant pressure.

72

Knowing T_j and θ_j, and from the definition of θ,

$$P_j = \frac{1000}{\left(\dfrac{\theta_j}{T_j}\right)^{\frac{1}{\kappa}}}$$

Wind is assumed to vary linearly with height. Before interpolating to find u and v on the θ_j surface, z_j must be found by integrating the hydrostatic equation from the lower pressure level:

$$z_j = z_i + \frac{c_p}{g}\left[\frac{(T_i\Pi_j - T_j\Pi_i)}{\Pi_j - \Pi_i}\ln\frac{\Pi_i}{\Pi_j} + T_i - T_j\right], \tag{1}$$

where g is the acceleration of gravity, and $\Pi = \left(\dfrac{P}{1000}\right)^{\kappa}$.

Once T, P, z, u, and v are determined for each grid point on the chosen isentropic surface, the data are recorded on magnetic tape and the same computations are performed on data reported for 12 hours later. This process continues until a sufficient number of isentropic grids are available for the computation of trajectories. GAMBIT3 is similar to GAMBIT1 (Harris, 1982) except that the input wind data are on isentropic rather than isobaric surfaces. The other parameters, T, P, and z, are not used in determining the trajectories but are reported along with the trajectory segment endpoints as additional information characterizing the history of the air masses. Figure 42 shows how the isentropic trajectories are displayed on a map. A symbol (an identifying letter or numeral) marks every 12 hours along the trajectory. The numerals show days of travel to the destination. Table 27 is an example of the additional information that accompanies the plotted trajectories. The isentropic trajectories in fig. 42 are compared with the isobaric trajectories for the same day (fig. 43) when this case is discussed in detail later.

Additional study is needed to determine the validity of the GAMBIT3 procedure. The greatest weaknesses are probably those related to the input data. For example, as is true for the isobaric procedures, real data coverage over much of the ocean and polar regions is sparse. Both the isentropic and isobaric procedures are also limited by the coarse mesh of the NMC Northern Hemisphere grid, about 200 km per grid unit at the Equator to 400 km per grid unit at the pole. Further inaccuracies may be introduced into the isentropic trajectories by the fact that, although significant levels are used in the computation of heights by NMC, only the mandatory levels are provided. Thus, the hydrostatic equation may at times be inconsistent when used between mandatory levels as in (1).

A comparison between isentropic and isobaric trajectories for MLO during April and May 1979 yielded some interesting results. Figure 44 shows 310-K isentropic trajectories that are comparable with the 700-mb isobaric trajectories in fig. 45. Good agreement was also found between the 325-K isentropic trajectories in fig. 46 and the 500-mb isobaric trajectories in fig. 47. In cases like these, where good agreement is found, wind flow is approximately zonal so that height and pressure of the isentropic surface do not change significantly. The trajectories in fig. 42 arriving at MLO on the 310-K surface show better agreement with the 500- rather than the 700-mb trajectories in fig. 43, even though the 310-K trajectories arrive at MLO near the 700-mb
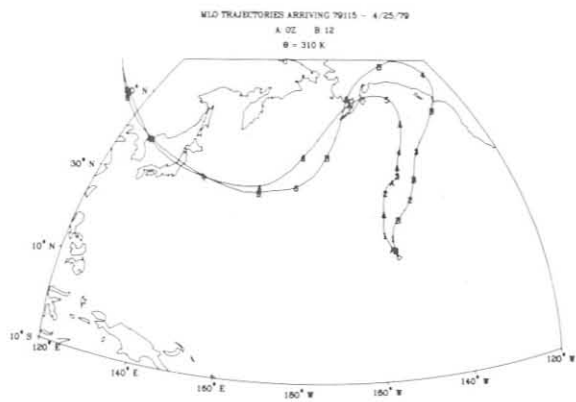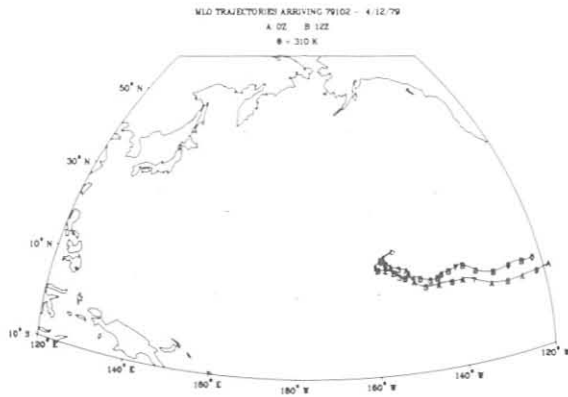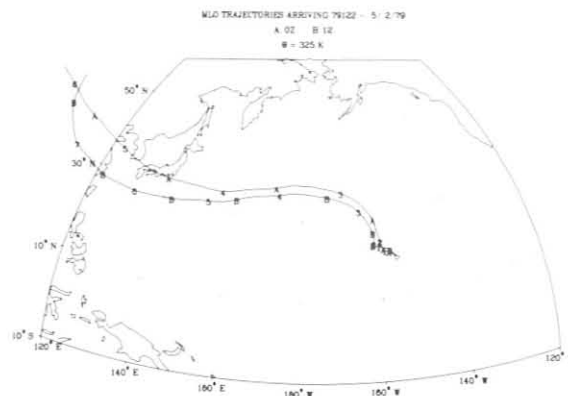
Figure 42.--MLO trajectories arriving on 25 April 1979 on the 310-K isentropic surface.
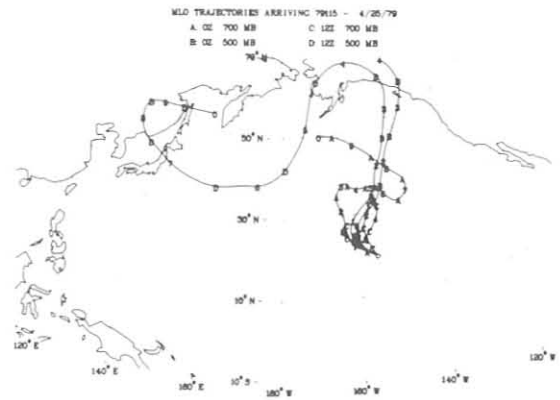
Figure 43.--MLO trajectories arriving on 25 April 1979 at the 700- and 500-mb levels.

Table 27.--Location, pressure, temperature, and height of the air mass at 12-h intervals along the isentropic trajectories shown in fig. 42

MLO 79 4 25 0 310.0					
NO. HRS BACK	LATITUDE	LONGITUDE	PRESSURE	TEMPERATURE	HEIGHT
0	19.53	-155.58	709.2	281.0	2996.
12	21.67	-156.81	664.5	275.8	3519.
24	25.30	-158.22	619.3	270.3	4062.
36	30.26	-157.46	577.5	264.9	4606.
48	35.13	-155.78	521.7	257.3	5407.
60	37.25	-152.91	496.4	253.7	5752.
72	38.40	-150.86	560.4	262.7	4856.
84	40.38	-150.05	571.4	264.1	4733.
96	43.74	-147.76	522.0	257.4	5417.
108	49.67	-143.50	473.0	250.2	6118.
120	56.04	-143.70	463.2	248.6	6214.
132	57.69	-159.33	457.0	247.7	6134.
144	45.97	179.97	505.4	255.0	5379.
156	38.12	166.48	546.3	260.8	4930.
168	37.49	149.22	485.8	252.0	5732.
180	41.02	127.94	429.0	243.1	6677.
192	46.41	112.86	367.9	232.5	7776.
204	50.61	97.94	361.0	231.1	7932.

MLO 79 4 25 12 310.0					
NO. HRS BACK	LATITUDE	LONGITUDE	PRESSURE	TEMPERATURE	HEIGHT
0	19.53	-155.58	679.2	277.5	3393.
12	21.28	-155.98	692.4	279.0	3201.
24	24.24	-156.18	640.2	272.9	3817.
36	28.26	-153.91	538.0	259.6	5101.
48	32.25	-149.17	518.1	256.9	5376.
60	36.51	-146.39	519.1	256.9	5433.
72	42.37	-142.36	410.0	240.0	7081.
84	48.92	-130.78	393.9	237.4	7348.
96	56.50	-124.47	360.4	231.4	7906.
108	63.53	-138.50	401.4	238.7	7142.
120	59.16	-159.94	404.9	239.3	6972.
132	45.77	-171.98	392.8	237.1	7284.
144	38.56	177.79	476.5	250.6	5968.
156	36.52	166.47	515.9	256.4	5374.
168	37.76	148.41	465.7	249.0	6097.
180	41.03	128.79	424.3	242.4	6767.
192	45.22	114.08	407.6	239.5	7077.
204	51.39	98.85	364.9	232.2	7788.

Figure 44.--MLO trajectories arriving on 12 April 1979 on the 310-K isentropic surface.
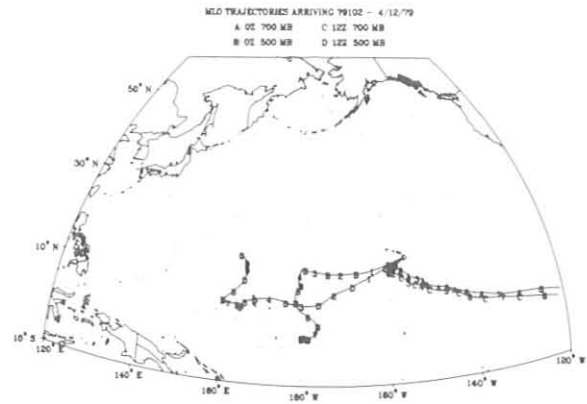
Figure 45.--MLO trajectories arriving on 12 April 1979 at the 700- and 500-mb levels.

pressure surface (see table 27). Within 2 days back along the trajectories shown in fig. 42, the northerly tracks locate the air masses higher up the isentropic "mountain" shown in fig. 41, approaching the 500-mb level. At its most northern location, track B (1200 Z) is close to 8 km in height (360 mb). Earlier in their journey to MLO (6-7 days back) both trajectories are farther south, hence at lower elevations. Poor agreement was found between isentropic and isobaric trajectories when, as in this case, wind flow was north and south, or when winds were light and variable.

In the future, case studies comparing isentropic with isobaric trajectories may reveal more conditions of agreement. Under favorable conditions isobaric trajectories may then be judged adequate, whereas the isentropic model could be used for case studies where isobaric results are uncertain. The benefits and practicality of a dynamic rather than kinematic isentropic model will be investigated next year. When opportunities arise, GMCC trajectories will be compared with those of other organizations. Verification with real wind observations will be attempted whenever possible.

Figure 46.--MLO trajectories arriving on 2 May 1979 on the 325-K isentropic surface.
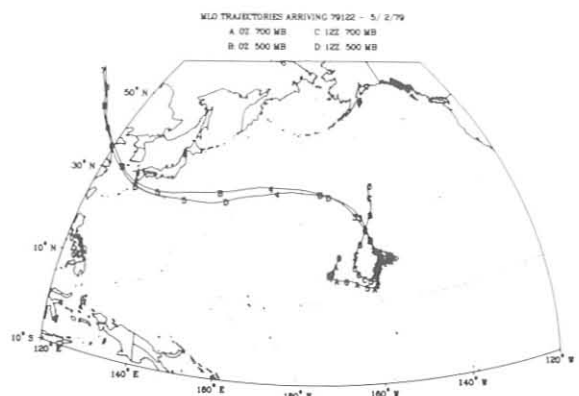
Figure 47.--MLO trajectories arriving on 2 May 1979 at the 700- and 500-mb levels.

75

4. SPECIAL PROJECTS

4.1 CO$_2$ Modeling

4.1.1 Introduction

This section is a progress report on the development of a CO$_2$ model designed to interact with data from the GMCC CO$_2$ flask and continuous sampling program. Large-scale features of the CO$_2$ data can imply physical mechanisms to be included in the global carbon cycle model. Discrepancies between model-calculated CO$_2$ values and the data may point to problems with flask sampling or the model.

The model is an adaptation of Machta's (1974) two-dimensional global diffusion model. It simulates transport of atmospheric CO$_2$ vertically and latitudinally; CO$_2$ flux into, out of, and within the ocean; and transport of CO$_2$ into and out of the biosphere. Output of the model is atmospheric CO$_2$ concentration as a function of latitude, altitude, and time. Rotty's (1982) values for anthropogenic CO$_2$ release are used and an ocean simulation having a mixed layer and a thermocline layer is included. Data for oceanic alkalinity, salinity, and total dissolved inorganic carbon were obtained from Takahashi et al. (1981). Partial pressure of CO$_2$ (pCO$_2$) was calculated by assuming that alkalinity remains constant and by solving the alkalinity and total absorbed inorganic carbon equations. Figure 48 shows pCO$_2$ vs. time and latitude.

A model by Kerman (1980) expressing CO$_2$ flux as a function of difference of pCO$_2$ in ocean water and volume mixing ratio of CO$_2$ in air, of wind friction velocity, and of temperature was used to simulate the air-sea exchange of CO$_2$. The flux of CO$_2$ can also be expressed as a speed or "piston velocity" times
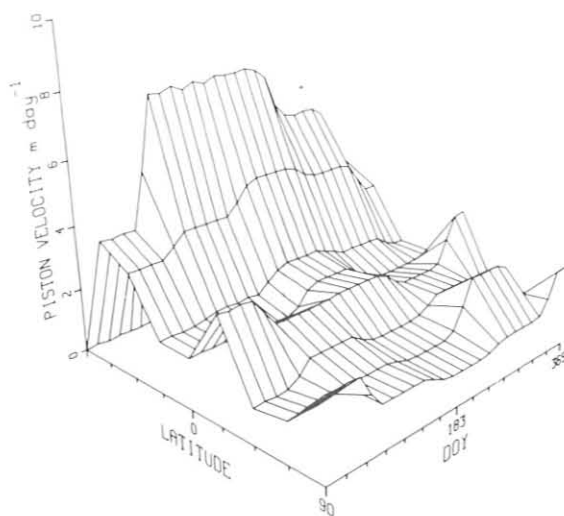
Figure 48.--Partial pressure of CO$_2$ dissolved in the mixed layer of the ocean as a function of latitude and DOY.
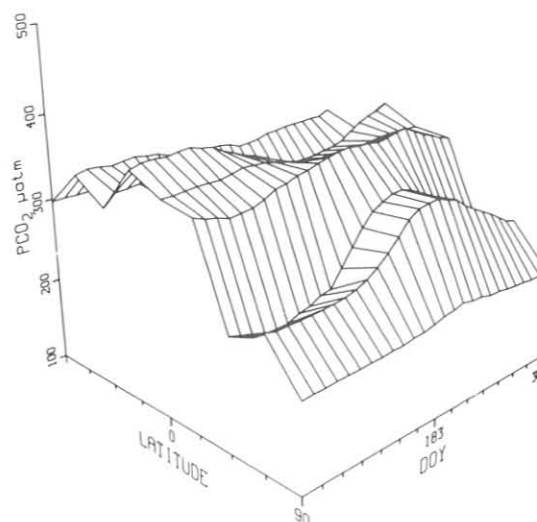
Figure 49.--Piston velocities for CO$_2$ air-sea exchange as a function of latitude and DOY.

76

the concentration difference; that expression is used here (fig. 49). These velocities are in reasonable agreement with the values of Peng et al. (1979).

Work is continuing with E. Box of the University of Georgia on a model of the biospheric fluxes of CO_2. The net flux (NEP) for a given latitude band (lat) and time (T) is expressed by

$$NEP(lat,T) = NPP(lat)[R(lat,T) - U(lat,T)],$$

where NPP is net primary productivity, and R (release) and U (uptake) are the fractions of the carbon liberated from and taken into the biosphere, respectively, as a function of time. The NPP values were taken from Box's data by R. Schnell (personal communication; NOAA/GMCC; 1982) along with the values for seasonal fractional uptake of CO_2 by photosynthesis. The release fractions were obtained by fitting the model to the data. Later, Box's decay values will be used to give these numbers. Fractional ice cover of the ocean was calculated by averaging sea-ice data for 5 years from the World Data Center. The average ice fraction vs. DOY and latitude is shown in fig. 50.

4.1.2 Results

A three-dimensional depiction of model results is shown in fig. 51. In general, the model accurately reproduces large-scale features of atmospheric CO_2 change with time and latitude. Figure 52 shows a map of mean and RMS differences between the model CO_2 concentrations and those of the flask sampling network. The mean differences reflect agreement in prediction of the annual mean CO_2 value, whereas the RMS differences reflect agreement in the
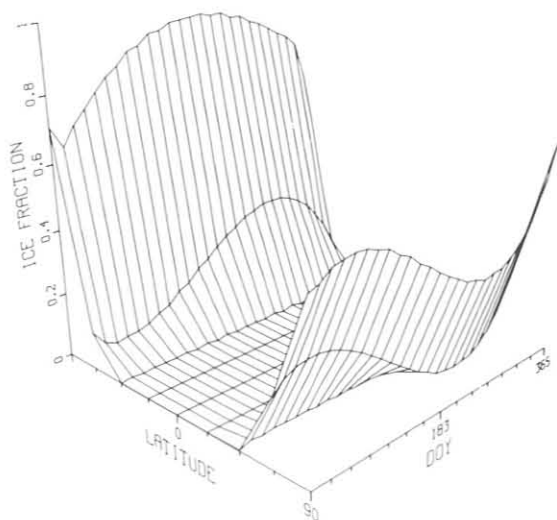
Figure 50.--Fraction of sea surface covered by ice as a function of latitude and DOY.
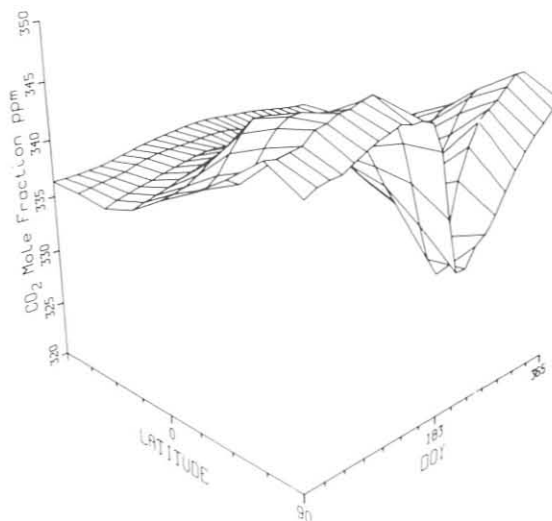
Figure 51. Model prediction of the concentration of atmospheric CO_2 at the Earth's surface as a function of latitude and DOY.
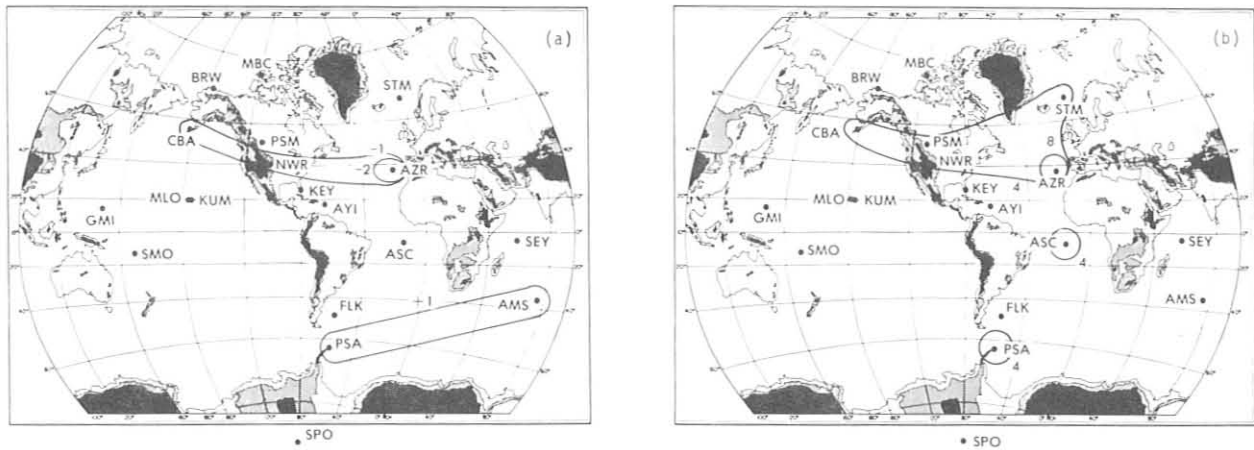
Figure 52.--(a) Mean difference and (b) RMS difference between model and observed CO_2 concentrations (ppm) at locations of sampling.

details of the annual cycle. In general, the annual mean agreement is good except at the Azores. The RMS differences of model and flask results are less than 4 ppm for 12 of the 18 locations. Southern Hemisphere flask CO_2 results are examined in sec. 4.2. Only at the Equator was there an obvious annual cycle phase difference in the time series of CO_2 concentrations for two locations having about the same latitude. Other cases of longitudinal differences were more subtle.

4.1.3 Conclusion

The above comparison of data vs. model CO_2 values shows that a two-dimensional (altitude-latitude) model of CO_2 exchange can explain a large proportion of the variability of CO_2 change in the course of 1 year. The model is intended for interactive use for evaluation of data and estimation of global carbon cycle fluxes. The prediction of global atmospheric CO_2 increase following an El Niño event is a possible future application.

4.2 A Preliminary Examination of CO_2 Data in the High Latitudes of the Southern Hemisphere

As part of the CO_2 flask sampling program, evaluation of the results of network sampling is important to see how the objectives of the program are being met. This brief report describes the beginning of such an effort in which several high-latitude Southern Hemispheric sampling locations are examined.

In an earlier examination of six sets of flask data for 3 years, Gillette and Hanson (1983) remarked that data from high-latitude southern locations seemed to have less year-to-year variability and possibly more spatial correlation than data from northern locations. Because in the Southern Hemisphere the annual CO_2 cycle is smaller, flask sampling errors tend to obscure

the annual cycle more there than they do at northern locations. Thus, an early examination of southern flask sampling locations was undertaken to gain experience for such analyses and to guide the strategy to obtain the best data possible for carbon cycle modeling. P. Fraser of CSIRO is cooperating in this examination of data and has provided data for Cape Grim, Australia. For this preliminary analysis, continuous data for 1980 from SPO and Cape Grim, and flask data for 1981 from Amsterdam Island, Falkland Island, Palmer Station, and SPO are used.

Equations were written that expressed concentration of CO_2 at one location as a linear function of CO_2 concentration at SPO (continuous) or Cape Grim or both, to test the data for independent information at the sampling sites. The equations expressing CO_2 flask concentrations at location i and day j are

$$X_{ij} = A_{1i} + A_{2i} X_{SPOj} + E_{ij} \qquad (2)$$

$$X_{SPOj} = D_1 + D_2 X_{CGj} + E_j \quad , \qquad (3)$$

where A_{1i}, A_{2i}, D_1, and D_2 are constants to be determined; E_{ij} and E_j are residuals; and CG refers to the Cape Grim data. Data for 1981 were used in (2) and data for 1980 were used in (3). Residuals E_{ij} and E_j were tested for independence by the Kolmogorov-Smirnov white-noise test as described by Box and Jenkins (1976).

Some results are shown in table 28. Amsterdam Island CO_2 values show independence from SPO data. Palmer Station concentrations can best be expressed as a linear function of SPO concentrations. The annual cycles are practically the same, but Palmer data are about 1.7 ppm higher than SPO data for 1981; this is possibly an oceanic effect. Falkland Island data show independence from SPO data, but show a decreasing trend near the end of the year that may indicate questionable data at that time. SPO and Cape Grim CO_2 data presented in fig. 53 were likewise shown to have some independence apparently over time periods of several months for 1980.

Table 28.--Results of CO_2 data tests

Location	Results
Amsterdam I.	Independent information
Falkland Is.	Questionable
Palmer Station--PSA	$X_{PSAj} = 1.005 \ X_{SPOj}$
	$E_{ij}^2 = 0.514$; white noise
SPO (flasks)	$X_{SPOj} = 0.9997 \ X_{SPOj}$
	$E_{ij}^2 = 0.444$; white noise
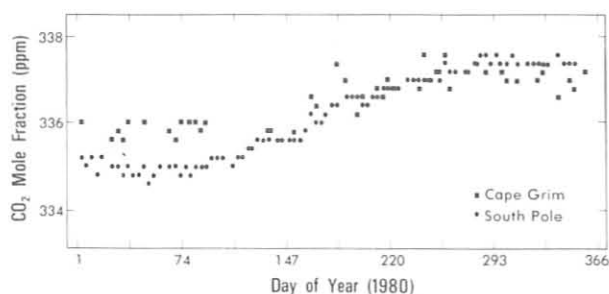
Figure 53.--CO_2 data for SPO and Cape Grim in 1980. Data are presented on the 1974 SIO scale.

Since only 1 year of data was available for analysis, a cross-spectrum analysis was done for the SPO and Cape Grim sites for periods of up to 4 months. Time series were linearly detrended and a sinusoid having a 1-yr period was removed from the data. For the 1980 data, no coherence was found for periods up to 4 months, possibly because of the month-long data gap in the Cape Grim data.

The following conclusions can be drawn from this study: (1) Amsterdam Island has a CO_2 concentration time series that cannot be written as a linear function of the SPO time series; (2) Palmer Station has an elevation of CO_2 concentrations but the same annual cycle as SPO; (3) Falkland Island has questionable CO_2 data; (4) the SPO and Cape Grim CO_2 records are significantly different for 1980 and there is no coherence for fluctuations of periods less than 3 months.

4.3 Dobson Spectrophotometer Automation and Establishment of the Global Umkehr Observation Network

Funding was received early in 1982 from EPA, CMA, and WMO for automation of six Dobson ozone spectrophotometers for Umkehr observations, which yield data on the vertical distribution of atmospheric ozone, at a select global network of stations. Data from the network are expected to provide information on possible long-term ozone destruction (e.g., by halocarbons) near 40 km, and to serve as comparisons for satellite ozone observations.

Stations tentatively selected for the Umkehr observations are MLO; Poker Flat, Alaska; Haute Provence, France; Pretoria, South Africa; Huancayo, Peru; and Perth, Australia. Boulder, Colo., will constitute the seventh station of the network, using Dobson instrument no. 61, which was automated in 1981.

With use of an automated Dobson instrument, the observer is replaced by an HP9915A computer and an HP2240A measurement and control processor. Stepper motors select wavelengths on which observations are made, and control the position of the instrument's optical wedge during observations. Temperature sensors located within the instrument automatically compensate for temperature effects. Voltage on the photomultiplier tube is controlled digitally. A battery-backed clock provides an accurate real-time base for computer operation.

Observatories housing the automated Dobson instruments will have automated shutters that allow Umkehr observations to be made, beginning at sunrise

and ending at sunset, without the presence of an observer. Precipitation detectors will keep the shutters closed during adverse weather conditions. Rotatable instrument chassis will track the Sun during observations, to minimize measurement-degrading polarization effects.

Although Umkehr observations will be fully automatic, measurements of total ozone will be semiautomatic. After positioning the Sun director on the instrument's light inlet window and orienting the instrument correctly with respect to the Sun, the operator will merely activate a switch to initiate the total ozone measurement. About 2 minutes later the computer will yield the total ozone amount.

The Umkehr observation network using automated Dobson spectrophotometers is expected to be fully operational by the summer of 1984.

4.4 Studies of Winter CO_2 Variability at BRW

4.4.1 Introduction

As part of a series of studies on variability of CO_2 concentration at BRW, the relation between anthropogenic aerosol and CO_2 in the Arctic was examined to gain a better understanding of the variations in CO_2 concentration of up to 3 ppm that occur over periods of 1-7 days during winter. Kelley and Gosink (1979) made measurements suggesting a CO_2 source in the Arctic Ocean during winter; Rahn (1981) discussed transport pathways of pollution aerosol from midlatitude industrial centers to the Arctic; Shaw (1981) suggested a synoptic-scale eddy diffusion of pollution aerosols into the Arctic; Shaw (1982) presented evidence of direct transport of pollutants into the Alaskan Arctic by atmospheric mean flow; and Barrie et al. (1981) discussed periodic injections of pollution aerosol into the Arctic from lower latitudes and the accumulation during winter of these pollutants in a horizontally mixed reservoir.

In the present study, continuous CO_2 analyzer data, meteorological data, and the results of aerosol chemistry filter samples, the last furnished by K. Rahn of URI, for December 1979-March 1980, were examined to determine whether these factors have some bearing on CO_2 measurements at BRW and, if so, to assess the relative contributions of these factors to CO_2 variability.

4.4.2 Analysis and Results

Daily averages of CO_2 and the pollution aerosol indicators, excess (non-crustal) sulfate (XSO_4) and vanadium (XV), are plotted in fig. 54. The cubic spline best-fit curve provided a reference for calculating departures of CO_2 concentration. Three approaches were used to study CO_2 variability.

The first approach involved weather map classification. Examination of 850-mb constant pressure charts identified three main atmospheric flow regimes affecting BRW for the study period: (1) northerly flow from the Arctic Ocean, (2) southerly flow from the Pacific region, and (3) easterly flow from the Canadian Arctic. These patterns accounted for 36%, 30%, and 11%, respectively, of all twice-daily 850-mb maps for the study period. CO_2 and aerosol
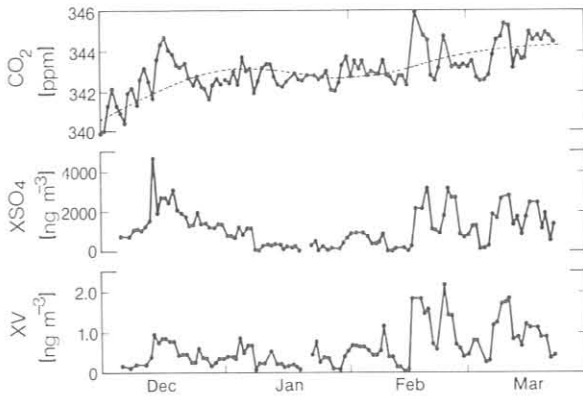
Figure 54.--Daily averages of CO_2 concentration and sample averages of noncrustal sulfate (XSO_4) and vanadium (XV) at BRW for December 1979-March 1980. The dashed line is a cubic spline best-fit curve to the CO_2 data based on hourly averages. CO_2 concentrations are given in the SIO 1959 Index scale.

chemistry data were partitioned according to the corresponding flow regime. The means for CO_2 departure, XV, and XSO_4 for the Arctic Ocean flow pattern were significantly greater (by the Student's t test) than those for the Pacific region flow pattern. Except for XSO_4, the means for the Arctic Ocean flow pattern were also significantly greater than those for the Canadian Arctic flow pattern. The standard deviations within map types were, however, quite large. For CO_2, this was a reflection of a few departures in both Arctic Ocean and Pacific region flow patterns that had an opposite sign from the mean.

The second approach was to consider the correlation of CO_2 concentration with meteorological variables and pollution aerosol. Correlation coefficients of CO_2 concentration with meteorological variables were low but of the sign expected from the results of previous studies (Peterson et al., 1980; Halter and Harris, 1981), suggesting higher CO_2 with northerly flow and colder, drier air masses than with warmer, moister southerly air. In contrast to the considerable variability of CO_2 departure within a particular atmospheric flow regime and the weak correlation with meteorological variables, the linear correlation of CO_2 with pollution aerosol indicators was considerably stronger, +0.7 for XV. This fairly high positive correlation reflects the correspondence of peaks and valleys in daily CO_2 and pollution aerosol indicator levels plotted in fig. 54.

In the third approach, CO_2 concentration as a function of air mass origin was determined. A division of the Arctic into sectors similar to those of Miller (1981b) was made. The origin sectors of all (twice-daily) 10-day, 850-mb back trajectories during the study period and the corresponding average daily CO_2 departures were noted. The significance of the difference between sector CO_2 means was tested by using t tests at the 0.05 confidence level. The results of this analysis, shown in fig. 55, indicate that average CO_2 departures associated with trajectory origins over much of the Arctic (sectors A and B) were slightly negative and were not significantly different from average CO_2 departures in the Pacific region. Another important result is that in moving from sector B to E and from E to H, average CO_2 departures become positive and increase significantly. In his study of low-level back trajectories to BRW, Miller (1981b) found a sharp April decline in the frequency of trajectory origins in the region corresponding to sectors E and H. Rahn (1982) demonstrated a corresponding decrease in XV levels. Although the level of CO_2
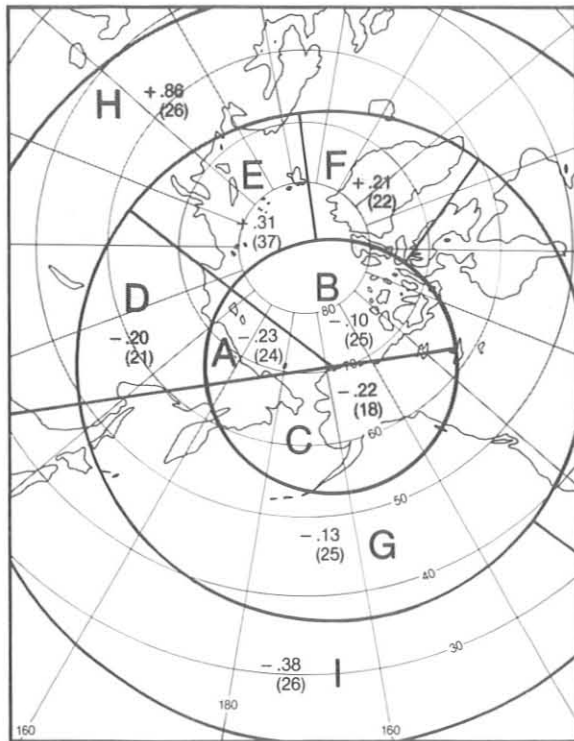
Figure 55.--Average CO_2 departure as a function of a 10-day, 850-mb trajectory origin. The signed numbers are average CO_2 departures (SIO 1959 Index). The tallies of daily averages used in calculating the sector averages are in parentheses.

during these events does not decrease correspondingly, variability in CO_2 does decrease markedly.

4.4.3 Discussion and Conclusions

The preceding evidence regarding winter CO_2 variability at BRW provides a basis for assessing the relative importance of the three possible causes: (1) a natural source in the Arctic Ocean, (2) a homogeneous Arctic air reservoir of midlatitude industrial CO_2 gradually accumulating during winter, and (3) transport of industrial CO_2 directly from source regions.

The first possibility is supported by the winter-spring supersaturation of CO_2 in Arctic Ocean water with respect to the atmosphere. The second possibility is supported by the positive average CO_2 departure for northerly Arctic flow, the negative average departure for Pacific region flow, and the oscillation between these two patterns being a major feature of the winter atmospheric circulation over the Alaskan Arctic. In contrast, the third possible cause is strongly evidenced by the greater predictive ability of pollution indicators (XV and XSO_4) than meteorological factors regarding CO_2 departure. The first and second possibilities seem less likely than the third for the following reasons. Some CO_2 departures with the Arctic Ocean flow pattern are negative. Also, the trajectory study suggests that much of the Arctic is not a CO_2 source. Furthermore, the spatial heterogeneity in the Arctic implied by that study does not seem in accord with a homogeneous, well-mixed Arctic air reservoir. A case in which a major positive CO_2 departure and pollution indicator peak occurred with a Pacific region flow pattern leads

83

to the suspicion that CO_2 variability is related to direct transport from specific industrial regions and that air mass or map type may be more coincidental than causal.

The trajectory study reinforces the third possibility as the most important factor contributing to short-term CO_2 variability. Additional evidence is furnished by the coincidence in April of a marked decline in the frequency of trajectory origins in sectors E and H, which are associated with the greatest positive departures in CO_2; the onset of a 2-mo period of relatively steady CO_2; and a rapid decline in XV. Therefore, based on the evidence presented here for the three possible causes, relatively direct transport of CO_2 from industrial regions makes the greatest contribution to short-term (periods of a few days) winter variability in CO_2 concentration at BRW. This variability appears as fluctuations of up to ±3 ppm superimposed on the annual trend.

A discussion of short-term CO_2 variability has implications concerning the representativeness of the data. Thus, CO_2 departures determined in this study are not necessarily departures from background; they are departures from a cubic spline best-fit curve to the data. The trajectory origin analysis shows that, for the winter of 1979-1980, average CO_2 departures associated with 10-day trajectory origins over a large area surrounding BRW were not statistically different.

The implied homogeneous distribution of CO_2 in the region centered at BRW is consistent with the concept of regional background. If this regional average CO_2 concentration is accepted as background, then the trajectory origin analysis is consistent with the idea that perturbations from regional background concentration are the result of rapid transport from areas outside of the region. For example, the 1- to 7-day episodes of large positive CO_2 departure are produced most often by transport of anthropogenic CO_2 from the vicinity of Europe and central Asia. Comparable periods of negative CO_2 departure reflect a return to cleaner conditions.

A contrasting idea is that these periods of negative CO_2 represent perturbations from characteristic Alaskan Arctic levels rather than a return to regional background. The latitudinal gradient in CO_2 concentration during winter (Bodhaine and Harris, 1982, pp. 21-22) suggests that arrival of air from the Pacific region south of 55°N should result in reduced CO_2 concentrations at BRW (Peterson et al., 1980). Our trajectory study agrees with this idea whereby the greatest negative CO_2 departures at BRW were associated with trajectory origins over the subtropical Pacific Ocean.

Thus, transport of air relatively low in CO_2 from the Pacific region may be involved in the short-term winter variability at BRW in addition to direct transport of industrially derived CO_2. Perhaps the application of the trajectory-origin vs. CO_2-departure analysis to a larger set of BRW data would clarify the role of long-range transport from the Pacific region. The resulting distribution of CO_2 departure as a function of trajectory origin might then provide the basis for using trajectories to identify background and nonbackground sampling conditions in the data selection process.

4.5 Measurements of Skylight Polarization at MLO

The well-known sensitivity of the polarization of light from the sunlit sky to the effects of dust, haze, and other particles in the atmosphere, in
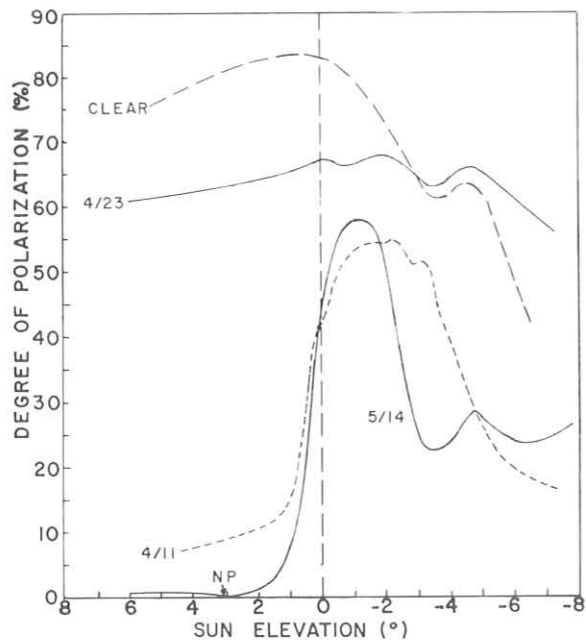
Figure 56.--Degree of polarization at 700 nm, as a function of Sun elevation, observed under the El Chichon stratospheric cloud at MLO. A curve typical of clear atmospheric conditions is given for comparison. (NP = neutral point.)

conjunction with the appearance of the volcanic cloud from El Chichon in the stratosphere over Hawaii in April 1982, provided strong motivations for continuing and expanding the measurements of skylight polarization at MLO. Of most interest are measurements in the red and near-IR spectral regions made during the morning twilight period at the 3.4-km altitude of the observatory. Measurements at these wavelengths are useful for detecting and characterizing atmospheric aerosols because the radiation is less subject to multiple scattering by ordinary oxygen and nitrogen molecules of the atmosphere than at shorter wavelengths. Measurements during morning twilight are preferable to those during evening twilight because of less interference from clouds in the morning.

The degree of polarization of light from the zenith sky, measured during twilight and in the immediate postsunrise period at MLO soon after the appearance of the volcanic cloud over Hawaii in April and May 1982, is shown as a function of Sun elevation in fig. 56. A curve for the average clear atmosphere, as observed under the clean stratospheric conditions of 1977, is given for comparison. Lidar observations at MLO showed the cloud to be markedly variable in density and height in its early stages. For instance, on 11 April the cloud was of sufficiently high density to cause a virtual reconfiguration of the polarization field, particularly in the immediate sunrise and postsunrise periods. The cloud top, however, was restricted at that time to an altitude of about 26 km so that the data during twilight were not transformed to the extent shown by later measurements. By 14 May, the cloud top had risen to at least 35 km, presumably by a process of gas-to-particle conversion in its upper levels. This increased cloud thickness caused not only a further decrease of polarization magnitude and the appearance of an anomalous neutral point after sunrise, but also the development of a definite presunrise polarization minimum that continued to exist through the remainder of the year. The cloud became very thin and tenuous on 23 April, as indicated by the tendency of the polarization field to return to normal.

85
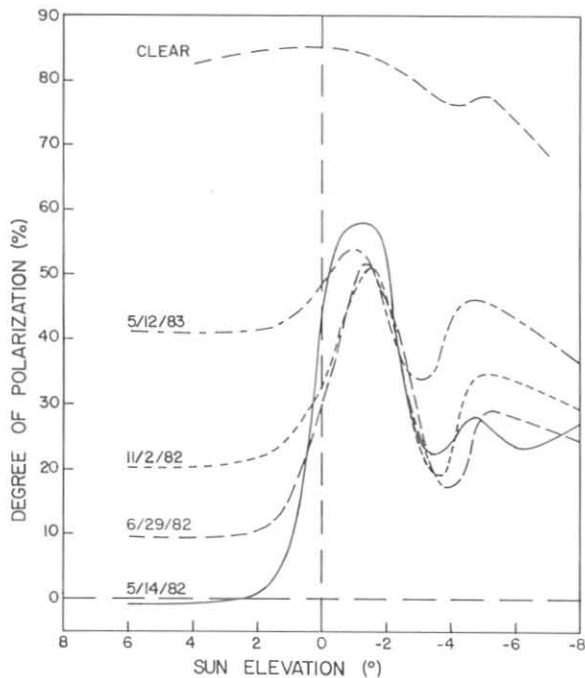
Figure 57.--Degree of polarization at 700 nm, as a function of Sun elevation, observed on various dates following the appearance of the El Chichon cloud over Hawaii. A curve typical of clear atmospheric conditions is given for comparison.

Measurements made later in 1982 and on 12 May 1983 (about 13 months after the cloud reached Hawaii) are shown in fig. 57. A tendency to return to normal is evident in the data, but the twilight configuration is surprisingly persistent in spite of decreasing cloud density and height as indicated by lidar measurements at MLO.

The polarization measurements will be continued to document as completely as possible the effects of volcanic material on the polarization field, as well as to develop the polarization method of detecting and characterizing stratospheric aerosols in the future.

4.6 Arctic Haze and AGASP

4.6.1 Introduction

Haze over the Arctic ice cap was first extensively documented by Mitchell (1957). He noted that the haze was generally observed during periods of otherwise clean air, extended over altitudes from near the ground to 300 mb, and extended over air routes up to 1,000 km long. On the basis of a range of optical and physical evidence, Mitchell suggested that the haze was composed of non-ice particles having diameters smaller than 2 μm. Two decades later his suggestions were confirmed. Beginning in the midseventies, research results from several groups confirmed the presence of much higher concentrations of aerosols in the Arctic atmosphere than one would expect in a remote and supposedly pristine environment.

A virtual explosion of information on Arctic haze followed the aerosol chemistry measurements of Rahn et al. (1977), and an entire issue of Atmospheric Environment (vol. 15, no. 8, 1981) was devoted to Arctic air chemistry. A consensus of these and other papers suggests that (1) Arctic haze is a widespread phenomenon having a major concentration peak in March-April;

(2) horizontal and slant visual ranges in Arctic haze may be restricted to 5-8 km by the haze; (3) wintertime Arctic haze has a large pollution-derived component of probable Eurasian origin; (4) the pollution component of the aerosol is dominated by sulfates (up to 2 μg m^{-3}), organics (1 μg m^{-3}), and black carbon (0.3-0.5 μg m^{-3}); (5) the haze is well aged, as evidenced by its high secondary/primary ratio and by peak concentrations in the low submicron range (accumulation mode).

4.6.2 Possible Climatic Effects of Arctic Haze

Elevated levels of aerosol concentrations in Arctic haze such as those measured at BRW have been shown to contain a large black carbon component. This component can attain a concentration of up to 40% of the total carbon content of the aerosol, which approaches that observed in urban atmospheres. Radiative-transfer modeling studies indicate that average local atmospheric heating by solar absorption from a thick layer of carbon aerosol in the Arctic haze may be comparable with that from doubling atmospheric CO_2 concentrations (Porch and MacCracken, 1982). These effects are most pronounced in the high Arctic latitudes, partly because of the high surface albedo of large and persistent areas of snow and ice.

4.6.3 The Arctic Gas and Aerosol Sampling Program

A multilaboratory NOAA group was formed in March 1982 to organize and direct an airborne study (AGASP) of the phenomenon of Arctic haze; flights were conducted from mid-March through mid-April 1983. The NOAA WP-3D Orion aircraft used in this study is a modern, highly versatile and efficient research platform. The aircraft has a range in excess of 3,000 nmi with a complement of up to 18 crew and scientists. An international cadre of government and university scientists joined the NOAA group in this unique undertaking. A list of the principal investigators and their programs is presented in table 29. A more detailed description of the AGASP project is given by Schnell (1983), and an up-to-date discussion of Arctic haze is given by Hileman (1983).

AGASP had these central measurement objectives: (1) to determine the distribution, trajectories, and chemical composition of Arctic haze aerosols; (2) to determine the concentration and distribution of trace gases, mainly anthropogenic, such as halocarbons; (3) to determine the concentration, flux, and gradients of atmospheric CO_2 in relation to important Arctic sources and sinks; (4) to measure the in situ radiative effects of the haze; and (5) to document the existence of, and conduct gas and aerosol measurements in, polar tropopause folds. AGASP allows the comparison of measurements, theory, and modeling of the climatic effects of Arctic haze.

The measurements were conducted during 120 research flight hours in the Arctic atmosphere, which included profiles above and upwind of surface stations (such as at BRW) in the international Arctic Air-Sampling Network. Coordinated aircraft operations were conducted from Spitzbergen by NIAR (one aircraft) and by the Max-Planck Institute for Chemistry, Mainz, Germany (two aircraft). In addition, the DOE WB-57 flew above the NOAA WP-3D during the Alaskan flights to conduct complementary stratospheric measurements. Approximate flight tracks for the NOAA WP-3D are shown in fig. 58. Dropwindsondes

Table 29.--AGASP management and scientists

Project leader	Institution	Responsibility
		Administration
R. Schnell	CIRES	Overall project management
S. Naegle	CIRES	Data manager
		Aerosols
B. Bodhaine	NOAA/GMCC	Integrating nephelometer, PIXE, CNC
K. Rahn	URI	Trace elements, organics
W. Zoller	Univ. of Md.	SO_x, HNO_3, H_2S, Hg, trace elements
H. Rosen	LBL	Carbon
K. Jayaweera	Univ. of Alaska	Spores, bacteria
W. Berg	NCAR	Cl, Br, I, Na, K, V, Mn
A. Lazrus	NCAR	$SO_4^=$
R. Borys	CSU	Aerosol size distributions
G. Grams	Georgia Inst. of Tech.	Polar nephelometer
G. Shaw	Univ. of Alaska	Aerosol size distributions
F. Parungo	NOAA/OWRM	Aerosol composition
A. Hogan	SUNYA	Aerosol size distributions and composition
		Gases
S. Oltmans	NOAA/GMCC	Ozone
R. Rasmussen	OGC	Trace gases
G. Bingham	LLL	CO_2 flux/concentration
R. Gammon	NOAA/GMCC	CO_2 concentration and source-sinks
L. Heidt	NCAR	Halogens
		Exchange Processes/Trajectories
G. Herbert	NOAA/GMCC	Energy-CO_2 fluxes
R. Gilmer	NOAA/GMCC	NOAA gust probe
J. Harris	NOAA/GMCC	Air mass trajectories
		Cooperating Aircraft/Satellite Measurements/Meteorological Analyses Programs
M. Shapiro	NOAA/WPL	Tropopause folding events
A. Kruger	NASA/Goddard	TOMS satellite ozone data
R. Liefer	DOE/New York	HASP WB-57 Flights
P. Guthals	Los Alamos Natl. Lab.	HASP aerosol chemistry analysis
W. Raatz	Univ. of Alaska	Arctic meteorological analyses
P. Crutzen	Max-Planck Inst., Mainz, FRG	German aircraft measurements
		Carbon/Radiation Measurements/Climate Modeling
T. Cahill	Univ. of Calif., Davis	Carbon optical properties
A. Clarke	Univ. of Wash.	Aerosol light absorption
J. DeLuisi	NOAA/GMCC	Surface radiation measurements
T. Ackerman	NASA/Ames	Arctic haze modeling
F. Vallero	NASA/Ames	Net radiation flux/airborne measurements
		Surface Measurements
B. Mendonca	NOAA/GMCC	BRW operations
H. Rodhe	Univ. of Stockholm	Swedish stations
B. Ottar	NIAR, Norway	Norwegian measurements
R. Hoff	AES, Canada	Canadian measurements
		NOAA WP-3D Research Aircraft
S. Rossby	NOAA/RFC	RFC Project Director
J. DuGranrut	NOAA/RFC	RFC Project Engineer
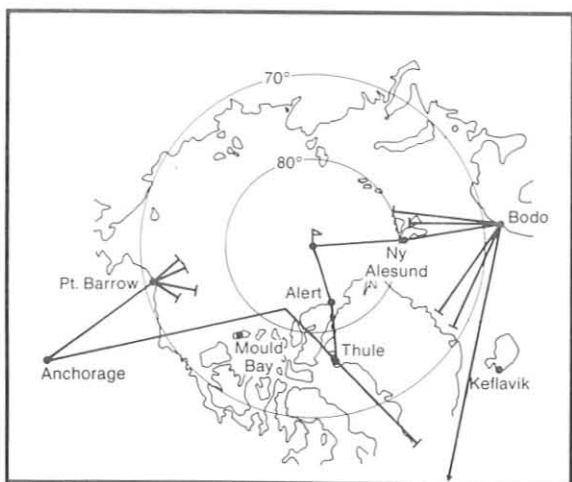
Figure 58.--Approximate NOAA WP-3D flight tracks during AGASP.

were released from the WP-3D in remote locations, including over the North Pole, to study the vertical structure of the atmosphere. Flight patterns were designed to transect all major pathways of Arctic haze precursors into the Arctic basin.

Initial data reduction and preliminary analysis indicated that AGASP was a very successful field experiment. Results will be summarized in next year's GMCC Summary Report.

4.7 Light Scattering, Condensation Nuclei, and Air Mass Trajectories at Whiteface Mountain

4.7.1 Introduction

A cloud chemistry and radiation experiment was jointly conducted by ASRC and GMCC at WFM during the summers of 1981 and 1982. WFM, operated by ASRC of SUNYA, is ideally located (44.39°N, 73.86°W) as a continental site, intermediate between an urban area and a background site such as a GMCC observatory.

The experiment was designed to investigate possible changes in the interaction between clouds and solar radiation caused by aerosol scavenging in the cloud. Since anthropogenic aerosols can alter cloud droplet sizes, it follows that the radiative scattering and absorption properties of clouds could be affected by the aerosols dispersed within the clouds. The objectives of the experiment were (1) to collect cloud water and analyze the residue for optical absorption, (2) to identify the residue chemically, (3) to measure the optical properties of the free aerosol, (4) to calculate the modified cloud optical properties, and (5) to estimate the enhanced absorption of the cloud caused by absorbing anthropogenic aerosols.

4.7.2 Instrumentation

The instruments supplied by GMCC for installation at WFM were a Gardner CNC, a G.E. automatic CNC, a four-wavelength nephelometer, a one-wavelength nephelometer, an HP data acquisition system, and a Leeds and Northrup multichannel chart recorder. All instruments were installed and operating on

WFM TRAJECTORIES ARRIVING 82150 - 5/30/82
A: 0Z 850 MB   C: 12Z 850 MB
B: 0Z 700 MB   D: 12Z 700 MB

WFM TRAJECTORIES ARRIVING 82157 - 6/6/82
A: 0Z 850 MB   C: 12Z 850 MB
B: 0Z 700 MB   D: 12Z 700 MB

WFM TRAJECTORIES ARRIVING 82182 - 7/1/82
A: 0Z 850 MB   C: 12Z 850 MB
B: 0Z 700 MB   D: 12Z 700 MB

WFM TRAJECTORIES ARRIVING 82198 - 7/17/82
A: 0Z 850 MB   C: 12Z 850 MB
B: 0Z 700 MB   D: 12Z 700 MB
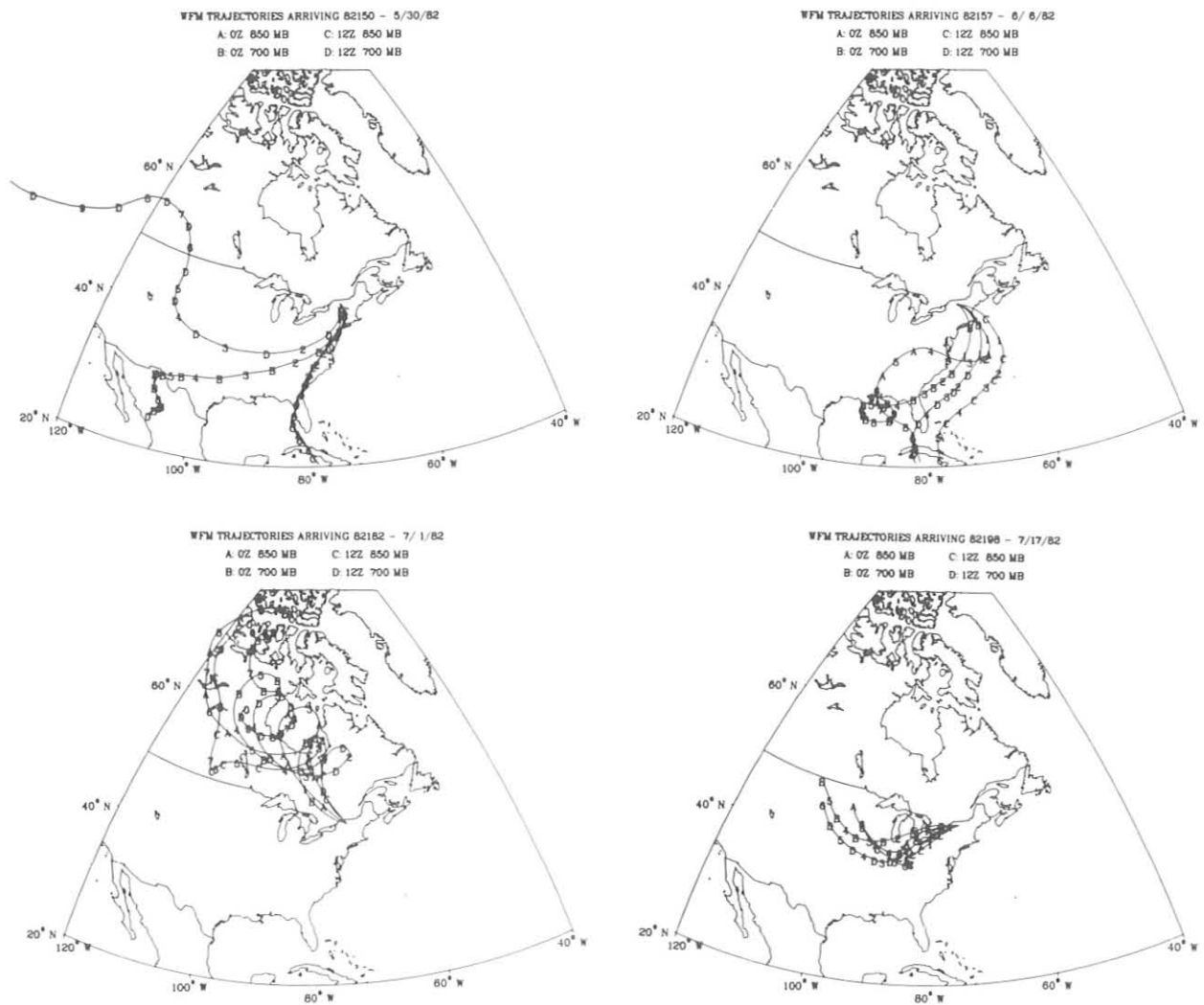
Figure 59.--Examples of air mass trajectories from the south (upper left), east (upper right), north (lower left), and west (lower right) at 850 and 700 mb on DOY 150, 157, 182, and 198 respectively.

22 May 1982 (DOY 142), and the experiment was terminated on 19 August 1982 (DOY 231).

4.7.3 Discussion of Selected Data

All data for the summer of 1982 at WFM were presented by Bodhaine et al. (1983). This report gives all light-scattering and CN data in graphic form with both 10-min and 1-h time resolution, and in tabular form with 1-h and 1-day geometric means. In addition, twice-daily (0000 and 1200 GMT) 10-day back trajectories, calculated at the 850- and 700-mb levels with WFM as the end point, are presented. These trajectories were calculated as described by Harris (1982).

Examination of the 1982 WFM data showed that a variety of meteorological conditions existed with air mass trajectories arriving from all directions. Four trajectory classes were examined: (1) those from the west with paths over

90
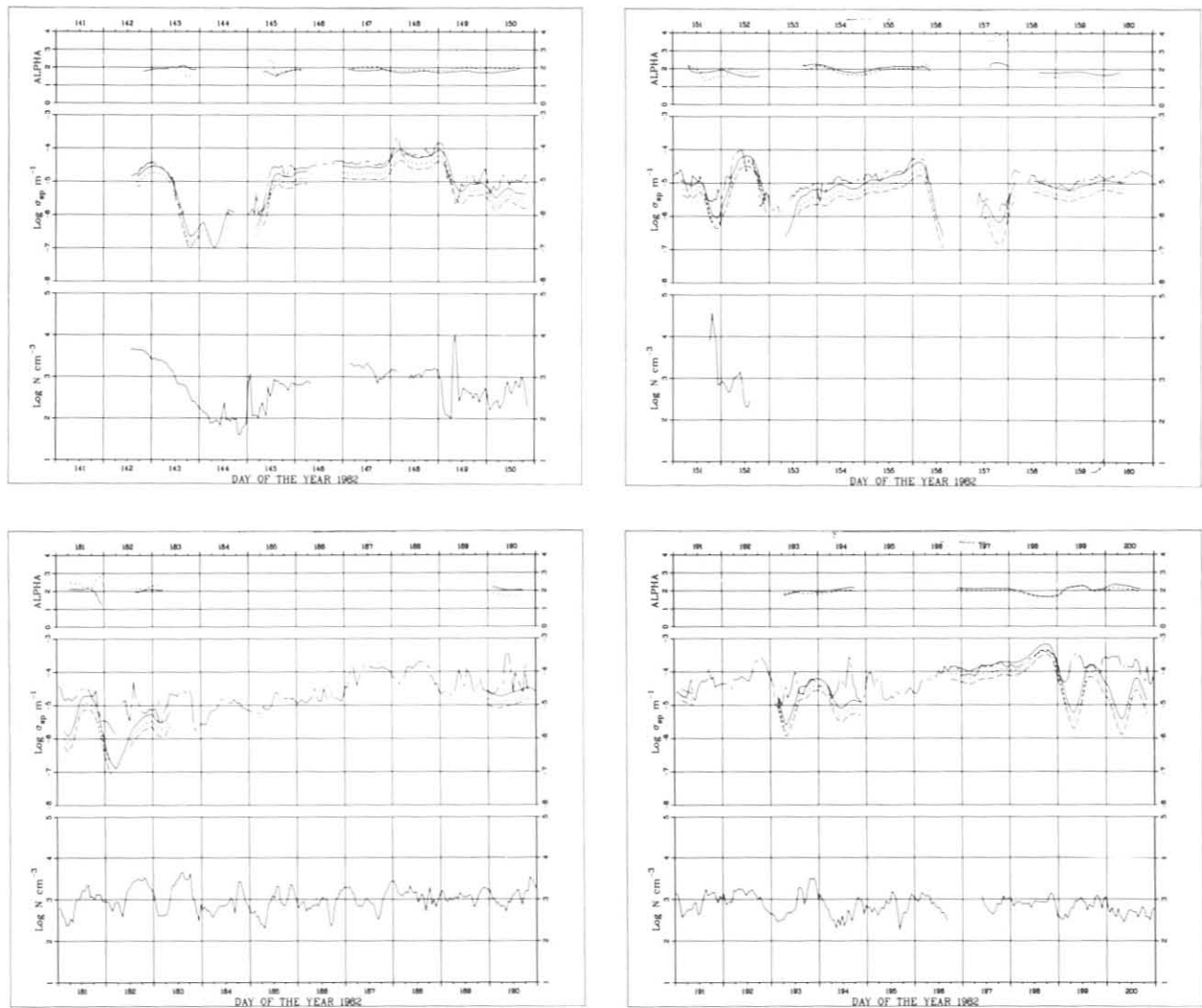
Figure 60.--Selected 10-day periods of aerosol data at WFM. Each frame shows Angstrom exponent (upper), light scattering (middle), and CN concentration (lower). Light-scattering data are for 450- (dotted), 550- (solid), 700- (dashed), 850- (long-dashed), and 525-nm (chain-dashed) wavelengths. Angstrom exponents were calculated from the 450- and 550-nm (dotted), 550- and 700-nm (solid), and 700- and 850-nm (dashed) light-scattering data.

the Great Lakes region, (2) those from the east with a maritime origin, (3) those from the south with a southern U.S. continental origin, and (4) those from the north with a Canadian continental origin. One example from each class is shown in fig. 59. Each of these days is included in the time series of CN, light-scattering, and Angstrom exponent data shown in fig. 60. Table 30 gives the daily geometric means of these data for the four examples given in fig. 59.

DOY 198 exhibited the highest light-scattering values of the entire summer. The weather pattern during the time period DOY 194-198 recurred throughout the summer, and consisted of increasing atmospheric pressure and hazy, polluted conditions that generally worsened until a front passed the station

91

Table 30.--Daily geometric means of light scattering,* Angstrom exponent, and CN concentration at WFM for days selected to illustrate trajectories arriving from the four different directions shown in fig. 59

	South DOY 150	East DOY 157	North DOY 182	West DOY 198
$\sigma_{sp}(450)$ m^{-1}	6.55-6	1.74-6	1.67-6	4.91-4
$\sigma_{sp}(550)$ m^{-1}	4.66-6	1.18-6	1.11-6	3.59-4
$\sigma_{sp}(770)$ m^{-1}	2.97-6	7.08-7	7.49-7	2.32-4
$\sigma_{sp}(850)$ m^{-1}	2.00-6	3.53-7	4.73-7	1.69-4
$\alpha(450,550)$	1.7	1.9	2.0	1.6
$\alpha(550,700)$	1.9	2.1	1.6	1.8
$\alpha(700,850)$	2.0	3.6	2.4	1.8
CN cm^{-3}	385	-	1413	841

*Values appear in a compact exponential format (6.55-6 = 6.55×10^{-6}).

early on DOY 199. Trajectories were from the west during that time period. The peak hourly mean light-scattering values were 9.4×10^{-4}, 7.2×10^{-4}, 4.8×10^{-4}, and 3.5×10^{-4} m^{-1}, in order of increasing wavelength at 1700 EST on DOY 198. The peak CN concentration of 1400 cm^{-3} occurred 3 hours later.

Table 30 shows that light scattering (or haziness) was about 2 orders of magnitude greater when trajectories were from the west than when trajectories were from other directions. Trajectories from the west were most common, followed by those from the north, south, and east.

4.7.4 Conclusions

When trajectories arrived from the west after having passed over the Great Lakes industrial region, generally hazy conditions were observed in the vicinity of WFM and light-scattering values of nearly 10^{-3} m^{-1} were recorded. Trajectories arriving from the north or the south were representative of continental background conditions and gave light-scattering values of about 10^{-6} m^{-1}. Trajectories from the east, having a maritime origin, were representative of the cleanest conditions and gave light-scattering values below 10^{-6} m^{-1}. During this study, the majority of trajectories arrived at WFM from the west, accompanied by polluted atmospheric conditions.

4.8 Lidar Observations of El Chichon Stratospheric Dust

More than 50 lidar observations of stratospheric dust were made at MLO during 1982. These observations captured the essence of the time changes of

vertical profile shape and optical depth of the Mystery Cloud and the El Chichon cloud described in detail in sec. 2.1.2.

Figure 61 shows monthly average profiles of El Chichon dust for 2.5-km intervals starting in April and ending in December. These profiles are scaled to unity at the profile maximum. The number above each profile is a scaler multiplier that gives the absolute optical depth of dust when multiplied by the integral of the respective profile. Some interesting features seen in this figure are the altitude rise in the profile maximum from 24 to 28 km that occurred between April and May, followed by a slow descent from 28 km in May to 21 km in December. Another feature of interest is that the altitudes of the half-maximum points on the profile seem to display a constant difference of about 5 km for the entire 9 months.
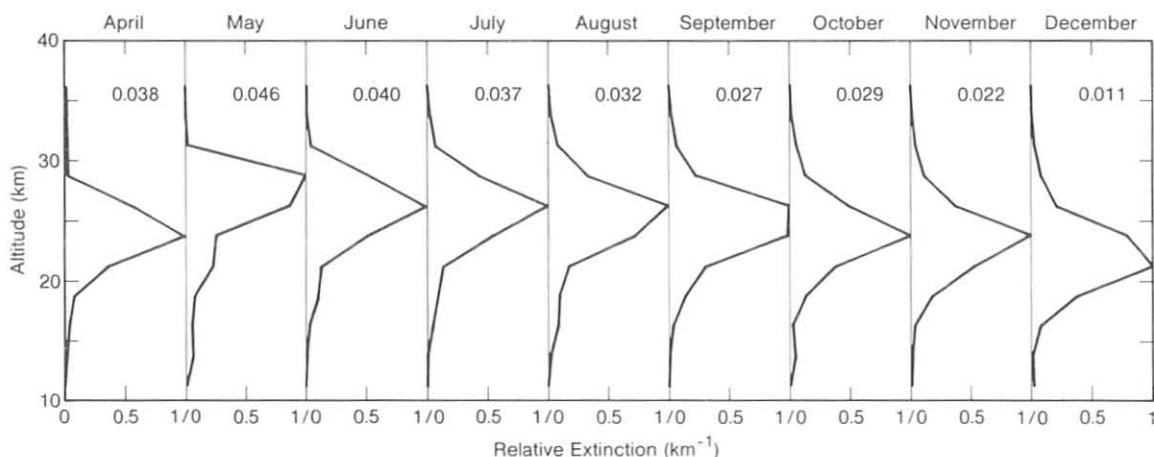
Figure 61.--Monthly averages of lidar observations at MLO in 1982, in terms of backscatter ratio (Rayleigh + Mie)/Rayleigh. Vertical resolution is 2.5 km. The profiles have been normalized so that the maximum has a value of 1. The scalar number given on each curve is in units of 4 km^{-1}, which when multiplied by the integral of the profile, gives the optical depth of the stratospheric cloud.

Figure 62 shows a comparison between lidar-derived optical depth and sunphotometer monthly average optical depth. The period January through March was marked by enhanced stratospheric dust from the Mystery Cloud. Note the horizontal line labeled "Average for 1980-81 Above 1958-62 Background." The historical MLO measurements show the cleanest stratosphere during this background period.

To compute scattering optical depth from the lidar measurements, a value of 50 was used for the total-scatter-to-backscatter ratio. A value of 56 was calculated from size distributions deduced from spectral optical depth inversions. If this value were used, the lidar-scattering optical depth would be lower by about 15%.
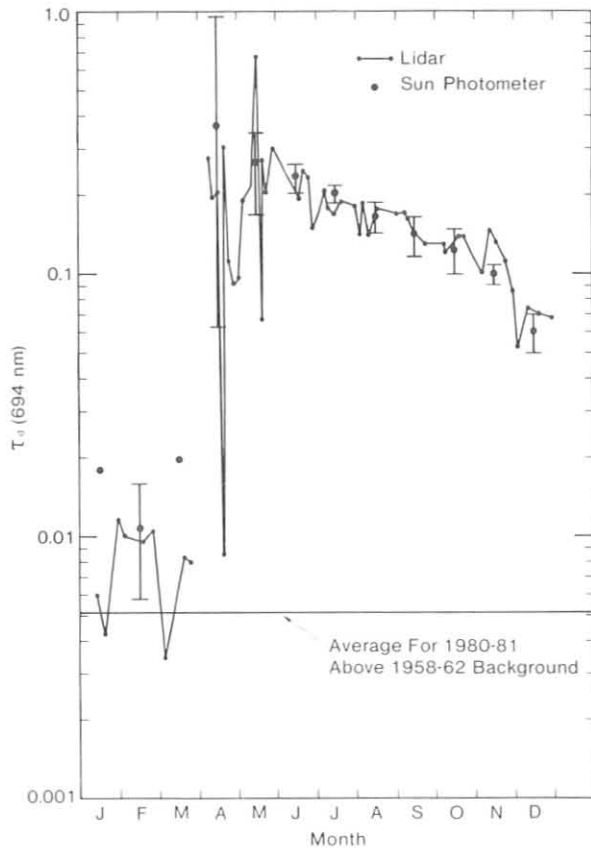
Figure 62.--Lidar-derived optical depth (small dots connected by lines) vs. sunphotometer (large dots) monthly average optical depth at the 694-nm wavelength, at MLO in 1982.

4.9   Umkehr Ozone Profile Error Caused by El Chichon Stratospheric Dust

Past theoretical investigations have indicated a linear relationship between stratospheric dust optical depth and amount of error in the Umkehr ozone profile. Umkehr and stratospheric dust optical depth measurements were routinely made at MLO shortly following the March-April 1982 eruption of El Chichon. A plot of ozone concentration in Umkehr layer 9 vs. optical depth at 380 nm is shown in fig. 63. The slope of this plot gives the linear error term for layer 9 as

$$E_9 = \frac{1}{P_3(\tau=0)} \frac{\partial P_3}{\partial \tau_d} \quad ,$$

where P_3 is ozone partial pressure and τ_d is the stratospheric dust optical depth at 380 nm.

The straight line through the points of fig. 63 was drawn without regard to the points beyond $\tau = 0.25$ because this may be a region of nonlinearity. However, this is not certain because of factors such as dust profile, seasonal variation in background dust optical depth, and ozone profile, which have not been accounted for and may be involved. Such factors must be investigated for a thorough understanding of the present set of measurements.

The most recent theoretically calculated stratospheric dust Umkehr errors indicated an error sensitivity of about 950% per unit optical depth of stratospheric dust (Herbert, 1980, pp. 65-68). The MLO empirical error indicates
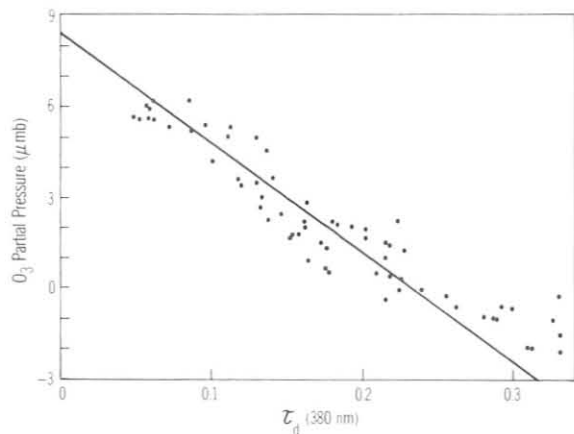
Figure 63.--Plot of Umkehr ozone partial pressure in layer 9 (~45 km) vs. El Chichon stratospheric dust optical depth τ_d at λ = 380 nm. Points beyond τ_d = 0.25 were disregarded in the straight-line fit.

that the error is more on the order of 400%-500% per unit optical depth of stratospheric dust. The difference may be due in part to errors in the difficult theoretical calculation for a solar zenith angle of 90°.

4.10 MLO Trajectory Ensembles, April and May 1979-1982

The transport of Asian dust to the central Pacific Ocean has received considerable attention since the dramatic duststorm of late April 1979 at MLO (Shaw, 1980; Darzi and Winchester, 1982a). In February 1979 filter sampling began at MLO to determine aerosol chemistry (Zoller et al., 1981). The relative importance of the spring dust events of 1979 can be seen in the accompanying plot (fig. 64) of aluminum (Al) concentrations measured during downslope winds (nighttime). In discussing the Al concentrations, Parrington et al. (1983b) computed the concentration for February-June 1979 to be a factor of 10 greater than that observed during the remainder of the year. They also showed the pronounced decrease in Al concentration from 115 ng m^{-3} in spring 1979 to 57 ng m^{-3} in spring 1980. The spring concentrations for 1981 and 1982 are approximately the same as for 1980. In an effort to understand the causes for the change in the dust loading from 1979 to 1980, air mass trajectory ensembles representing each spring were obtained by plotting the 0000 Z, 500-mb back trajectories from MLO for April and May. These 2 months represent the peak of the dust season, and one trajectory per day was found to be fairly representative; thus, relatively uncluttered plots containing 61 paths
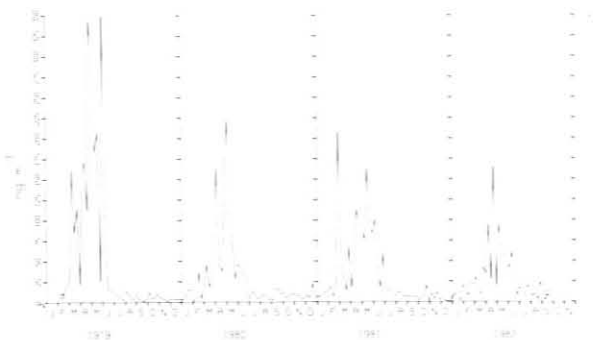
Figure 64.--Weekly filter samples of Al obtained during downslope winds at MLO using a high-volume aerosol sampler (from Parrington et al., 1983).

95
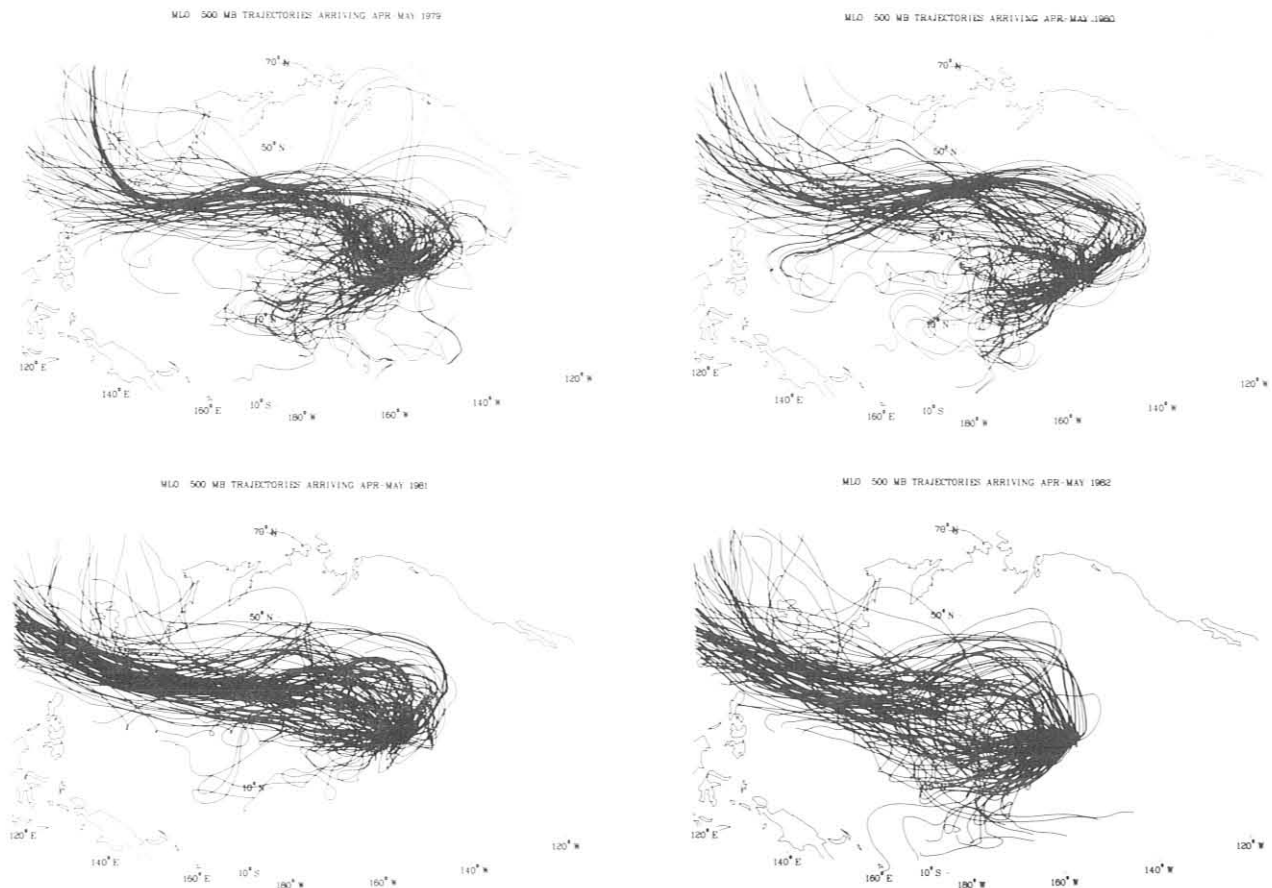
Figure 65.--Back trajectories arriving above MLO along the 500-mb surface for April and May 1979-1982.

are used for comparison. The 500-mb isobaric surface is considered representative of midtropospheric conditions for this period.

Ensembles of back trajectories from MLO for April and May 1979-1982 are plotted in fig. 65. The trajectories were computed according to the method described by Harris (1982). In 1979 the transport paths from the west show a relatively direct route from the Asian deserts, the eastern parts of which are at ~40°N, 100°E. These trajectories have cyclonic curvature for the first 2-3 days of transit off the Asian coast. During the last 2-3 days, as they approach Hawaii, the curvature is anticyclonic. The cyclonic curvature on the western part of the trajectories indicates associated storminess in the source region. One would also expect that the air parcels arriving in the region of Hawaii are descending from higher levels following an anticyclonically curved path from the northwest.

In 1980 and the subsequent 2 years, the westerly trajectories that track to Hawaii seem to originate in a region to the south of the deserts for a larger percentage of the time. The midtropospheric flow is often zonal, yet the transit times are longer in the latter 3 years than in 1979. The trajectory model indicates that the air parcels are moving relatively slowly while making the sharp anticyclonic curve just before reaching the islands. Overall the indicated paths from Asia are longer than the paths in 1979. The reduced

occurrence of curved trajectories off the Asian continent indicates a lower frequency of storms for this period. The trajectory ensembles for 1980-1982 clearly indicate fewer storms and longer transit paths to Hawaii originating to the south of the main Asian deserts. These three features are probably related and may explain the decrease in the dust concentration that occurred from 1979 to 1980.

Although samples of 7-day duration are very useful in evaluating monthly and seasonal variations, the form of presentation in fig. 64 does not show the intermittent nature of the dust episodes. Filter samples taken on a much shorter time scale (Darzi and Winchester, 1982a) and the analysis of wind, aerosol, and ozone measurements (Herbert el al., 1982) have shown the typical dust period to last 18-36 hours. In one particular case that was reported to have lasted a week, a wind change occurred midperiod causing dusty air to recirculate from the east. Generally the dust-free periods have concentrations of crustal material that are representative of typical summer or fall values. Parrington et al. (1983b) contend that if samples of shorter duration were taken, the peak concentrations would be much larger. Dust-free periods during the spring have been found to correspond to trajectories from the southwest. A relatively large number of the April and May trajectories originate well south of the east Asian deserts or in the equatorial western Pacific. The spring trajectory ensembles clearly show that air arriving over Hawaii is not influenced by the North American continent.

4.11   The Photovoltaic Power System at SMO

The majority of the work on the PV power system for SMO in 1982 involved the procurement, construction, and testing of the components of the system. This project is funded in part by the DOE Federal Photovoltaic Utilization Program. From the six respondees to the second issue of the Request for Proposal (NOAA RFP 54-81), the source evaluation board selected Solarex Corp., Rockville, Md., as the supplier for the entire system. After further cost evaluation, the government chose to purchase the batteries directly from the supplier recommended by Solarex and to provide installation. It was also determined to be less expensive for the government to procure the materials and construct the PV array stands directly, using local Polynesian hardwoods. Detailed plans and specifications were provided by Solarex. All outside wiring and internal installation were also done by government employees. By March 1982 the details of the agreement had been resolved and a contract was signed.

One of the main evaluation criteria concerned the method proposed for battery charge regulation and protection. A typical voltage regulator establishes a ceiling voltage when the battery approaches full charge. This method of charge control is relatively inefficient because a battery accepts energy only as the voltage is rising. A better method of charging, especially at state-of-charge levels between 85% and 100%, is one where the voltage oscillates between two setpoints. Solarex suggested just such a system calling it "pump-charging." The high setpoint is substantially above the ceiling voltage of a typical regulator. When this voltage is reached, a module is shed from each string in the PV array, thus reducing the voltage on the battery. When the voltage drops to the lower setpoint, the array output is restored to full voltage, causing the battery voltage to rise. Additional energy is pumped into the battery as the voltage rises. When the voltage rises to the high

Table 31.--Monthly average ratios of the daily insolation on a
tilted surface to that on a horizontal surface, for 1982

Month	14° tilt, this study	14° tilt, Jordan and Liu (1977)	Variable tilt, this study
Jan	0.87	0.93	0.94
Feb	0.91	0.97	0.94
Mar	0.95	1.06	0.95
Apr	0.96	1.15	0.97
May	M*	1.22	M*
Jun	1.10	1.26	1.23
Jul	1.08	1.24	1.22
Aug	1.01	1.17	1.03
Sep	0.97	1.08	0.93
Oct	0.92	1.00	0.92
Nov	0.98	0.96	1.04
Dec	0.94	0.91	1.04

*M = missing data.

setpoint, the module is shed again, initiating another pump cycle. This is
the preferred method of battery charging because in addition to being the most
efficient, it drives the battery briefly to a voltage high enough to cause the
electrolyte to emit gas slightly. This condition eliminates electrolyte strat-
ification, ensuring efficient charging and good battery life.

The system consists of six major components. (1) The PV array is made up
of 10 strings of 10 modules each; 1 or 3 modules can be shed from each string
to control the voltage. The modules are Solarex no. HE-80 with a peak power
current of 3.8 A at about 17.5 V DC. The modules are mounted in five subar-
rays of 20 modules each (2.4- × 6.1-m panels at a height of 3.7 m). The pan-
els cover a total area of about 75 m^2. (2) The battery bank consists of 10
C & D type 6ZP75-13 deep discharge batteries. The battery cells have a nomi-
nal 510-Ah capacity with a 16-h rating. The bank physically comprises 10
identical six-cell modules connected in series. Hydrogen recombiners will be
installed on each cell. (3) The inverter is a 2-kW, continuous (3 kW for
2 seconds) capacity unit manufactured by Abacus, no. 423-4M3-120. (4) A Sola-
rex model ACR-6 controller, with two-stage PV module shorting, controls the en-
ergy flow to the batteries. (5) A battery charger, Custom Power no. BC1-6020,
supplies 20 A at 120 V, nominal, when prolonged cloudy periods significantly
reduce insolation. (6) A transfer switch, to shift the load to island power
in case of inverter failure, is built into the system. By December 1982 all
major components had been purchased and tested. The entire system will be
tested and installed in April and May 1983.

Early in 1981 two pyranometers were installed on tiltable stands. One
stand was fixed at an angle equal to the latitude of the station, -14°. The
other was changed monthly between angles of -10° and 35°. The ratio of the
daily insolation on the tilted pyranometer to that on a horizontal pyranometer
was computed and averaged by month (table 31). Measurements for 1982 show the
greatest enhancement during the Southern Hemisphere winter months of June and

July. Except for the summer months, the theoretical estimates of Jordan and Liu (1977) overestimate the enhancement resulting from tilting. Improper treatment of cloudiness is probably the cause of this error. On a month-by-month comparison, the values measured in 1982 are within a percent or two of those measured in 1981 (Bodhaine and Harris, 1982, p. 103). Because changing the tilt of 100 photovoltaic panels requires much effort, a schedule requiring four changes per year will be used with the PV system.

4.12 Atmospheric CO_2 Measurements Aboard R/V DISCOVERER, May-June 1982

4.12.1 Introduction

In May and June of 1982 the MTG Group participated in a NOAA/PMEL project, Marine Sinks of Atmospheric CO_2, aboard the R/V DISCOVERER in the equatorial and northern Pacific Ocean. J. Cline used a portable sampling unit to collect 36 pairs of flask samples in 500-cm^3 glass flasks for CO_2 analysis. The cruise track and locations of sampling are shown in fig. 66.

The principal objective of the GMCC sampling program was to obtain atmospheric CO_2 data from remote marine regions for comparison with the GMCC CO_2 flask network data. Since land-based stations may be influenced by local anthropogenic or biospheric sources and/or sinks of CO_2, the shipboard data are useful in assessing the suitability of these stations for obtaining regional or background atmospheric CO_2 data. Also, the shipboard data are valuable for determining atmospheric CO_2 gradients over this region of the Pacific Ocean and identifying possible marine sources and sinks of CO_2.
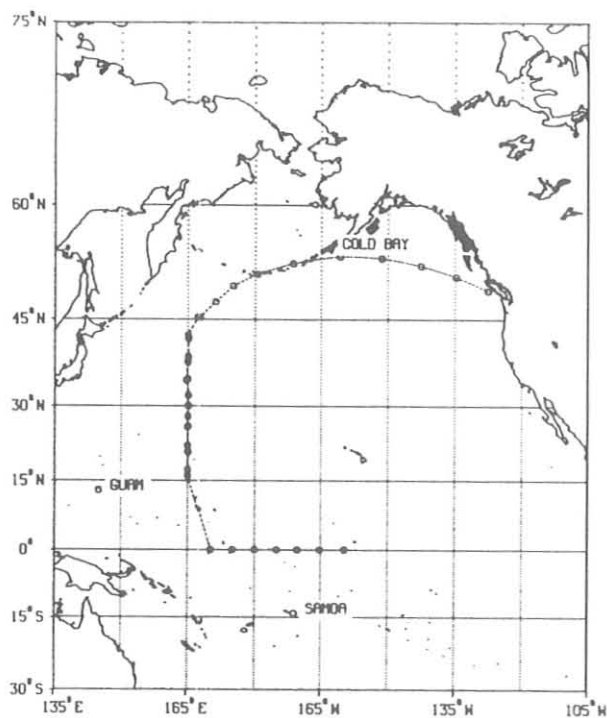
Figure 66.--The cruise track and sampling locations (circles) of the 1982 cruise flask sampling program aboard R/V DISCOVERER. Three GMCC CO_2 flask sampling sites are shown for reference.

4.12.2 Results

The results of the CO_2 analyses performed on the semiautomatic NDIR CO_2 flask analysis apparatus (Komhyr et al., 1983) in Boulder are presented in table 32. The CO_2 concentration given is the average for a pair of simultaneously filled flasks. In two cases (indicated by asterisks) the pair difference was greater than 0.5 ppm, and the higher value was rejected as being

Table 32.--Date, position and CO_2 concentration for
R/V DISCOVERER 1982 cruise samples

Date	DOY	Latitude (degrees)	Longitude (degrees)	CO_2 (ppm)
14 May	134	0.00N	159.75W	342.22
15 May	135	0.00N	165.17W	341.82
17 May	137	0.00N	170.28W	342.13
17 May	137	0.00N	175.00W	342.08
18 May	138	0.00N	180.00	342.11*
19 May	139	0.00N	175.00E	342.02
20 May	140	0.00N	170.00E	341.95
29 May	149	16.00N	165.03E	344.96
30 May	150	16.00N	165.03E	344.66
31 May	151	17.27N	165.03E	344.77
1 Jun	152	20.95N	165.10E	344.59
2 Jun	153	20.97N	165.03E	344.96
3 Jun	154	22.25N	165.02E	344.75
4 Jun	155	26.10N	165.08E	345.09
5 Jun	156	25.97N	164.92E	344.36
6 Jun	157	28.02N	165.03E	344.43
7 Jun	158	30.05N	165.12E	344.63
9 Jun	160	32.00N	165.05E	344.15
10 Jun	161	35.00N	165.00E	344.28
12 Jun	163	34.77N	164.65E	344.41
13 Jun	164	38.00N	165.00E	343.73
14 Jun	165	38.93N	165.08E	342.99
15 Jun	166	41.97N	165.05E	343.30
16 Jun	167	42.47N	165.03E	341.27
17 Jun	168	45.32N	167.25E	339.57
18 Jun	169	45.32N	167.37E	342.12
19 Jun	170	47.67N	171.02E	341.56
20 Jun	171	--	--	342.26
21 Jun	172	49.98N	175.00E	341.05*
22 Jun	173	51.58N	179.53W	343.25
23 Jun	174	53.02N	171.32W	342.79
24 Jun	175	53.93N	160.73W	341.12
25 Jun	176	53.70N	151.38W	342.29
26 Jun	177	52.72N	142.57W	340.66
27 Jun	178	51.23N	134.68W	342.69
28 Jun	179	49.28N	127.58W	341.75

*The pair difference for two flasks was greater than 0.5 ppm, and the higher value was rejected.
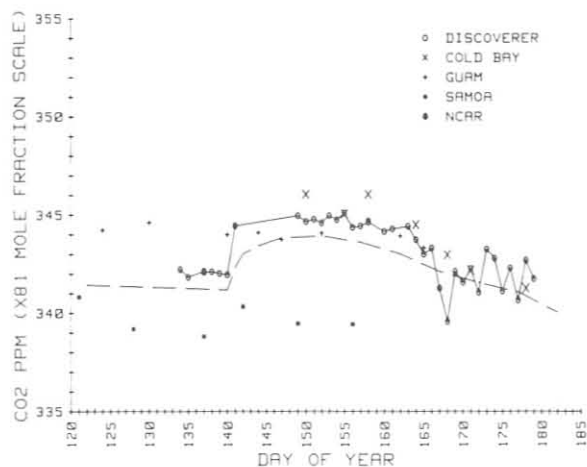
Figure 67.--CO_2 vs. DOY 1982 for the data in table 32 (o). Also shown for comparison are GMCC flask data from Cold Bay, Guam, and Samoa. The NCAR point is from a GMCC analysis of a stainless steel flask sample obtained by L. Heidt of NCAR. The dashed line consists of data extracted from fig. 8, sec. 3.1.

probably contaminated through a leaking flask stopcock. The quality of the samples appears to be quite good, which is largely attributable to the conscientious methods of the sample taker. The cruise data are plotted vs. DOY in fig. 67, along with GMCC flask network data for comparison.

Essentially no atmospheric CO_2 gradient exists along the Equator from 160°W to 170°E. Also, the equatorial concentration lies roughly midway between that at Samoa (14°S) and Guam (13°N) at this time of year. This gradient is unusual compared with previous years in which the northern tropics showed a higher CO_2 concentration because of the upwelling of CO_2-rich waters (sec. 3.1). The lower northern tropical concentrations during 1982 were probably caused by reduced upwelling associated with the unusually intense El Niño event.

Although no GMCC samples were collected between the Equator and 16°N because of following winds, several samples were collected along this track for L. Heidt of NCAR. One of these samples, collected at 5°N, was not contaminated and contained 344.43 ppm of CO_2. This point, plotted in fig. 67 as a filled-in circle, indicates the existence at this time of a gradient of ~3 ppm between the Equator and 5°N, the probable late spring location of the ITCZ (Bortniak, 1981). This suggests that the annual average interhemispheric gradient of 3 ppm is due to very slow mixing across the ITCZ barrier during most of the year.

The atmospheric CO_2 concentration measured aboard R/V DISCOVERER (DSC) along 165°E from 16°N to 42°N (DOY 149-166) is in good agreement with that measured at Guam (GMI) during the same period ($CO_{2_{DSC}}$ = 344.4 ppm, N = 16; $CO_{2_{GMI}}$ = 344.0, N = 4). That the agreement is good over such a range of latitude is partly due to the latitudinal gradient of CO_2 being at its minimum at this time of year in the Northern Hemisphere (see sec. 3.1).

A note on the sample data sheet indicates that the Subarctic Front, a boundary between warm midlatitude and cold northern water, was crossed on DOY 165. This crossing was followed by a sharp drop in atmospheric CO_2 concentration of ~3.5 ppm by DOY 168 (45°N). Comparisons with simultaneous pCO_2 measurements of the surface seawater made by C. Wong will be useful in interpreting this sudden drop in atmospheric CO_2 concentration.

101

From 165°E to 128°W (DOY 166-179) through the North Pacific, the atmospheric CO_2 concentration was quite variable, but it is still in good agreement with the few values available from Cold Bay, Alaska, during the same period ($CO_{2_{DSC}}$ = 341.8, N = 14; $CO_{2_{CBA}}$ = 342.1, N = 3). The variability is probably due to the proximity of the ship to the Aleutian Islands, where the CO_2 concentration may be influenced by the local terrestial biosphere and short-term atmosphere-ocean interaction.

The dashed line in fig. 67 represents data extracted from fig. 8 (sec. 3.1), a three-dimensional surface that is a smoothed interpolation of the zonally averaged CO_2 concentration vs. latitude and DOY, for the sea-level stations of the GMCC flask sampling network. The agreement of the cruise data with the surface is remarkable both in shape and actual concentration, supporting the representativeness of the flask sampling network. The systematic difference of <1 ppm is because the surface is zonally averaged, the Atlantic values being generally lower than the Pacific values.

From these results it is apparent that high-quality CO_2 data can be obtained by flask sampling aboard ships. It is also clear that stations such as Guam and Cold Bay are in fact suitable sites for measuring background CO_2 concentrations representative of large regions. However, a network of land-based stations is not able to locate the sharp CO_2 gradients that were found between the Equator and 5° (ITCZ) and in crossing the Subarctic Front. This information, which can only be obtained by shipboard sampling, is significant and will be useful in understanding the global distribution of CO_2 and the natural variability of the global carbon cycle.

Our interpretation of these data will be extended by considering various meteorological and oceanographic parameters, such as location of the ITCZ, sea surface temperature, pCO_2 in the sea water, and large-scale atmospheric circulation. Also, the results from this cruise have encouraged participation in several cruises to be made in 1983, including a circumnavigation of Antarctica by the USCG Icebreaker POLAR STAR.

4.13 Airborne Optical Measurements of the El Chichon Cloud

The potential climatic impact of the enormous El Chichon volcanic eruption in 1982 attracted considerable attention from climatic specialists, the general scientific community, and the general public. Consequently, much research effort has gone into attempts to quantify and describe the radiative effects of the long-lived stratospheric cloud. Previous theoretical work suggested that an eruption of this magnitude (stratospheric impact) would sufficiently impact the global radiation balance to cool the lower troposphere by a few tenths of a degree Celsius (e.g., Toon and Pollack, 1980).

Application of radiative transfer calculations to, and subsequent verification of, climatic effects relative to the major stratospheric aerosol event resulting from El Chichon, is complicated by the spatial distribution pattern of the debris material. Sustained uneven distribution of the material would invalidate one-dimensional models that assume uniformity for global effects. Additionally, two- or three-dimensional models that could properly account for the spatial distribution of the debris material also need to include atmospheric dynamics that could respond to the perturbed radiative forcing.

As an initial step toward identification of the climatic effect of the El Chichon stratospheric debris, the GMCC ARM group participated in three survey flight series sponsored by NASA. The flight series were designed to establish the latitudinal extent and variability of the cloud's optical properties as determined from remote measurement of its optical effects on sunlight. The flights were flown near the top of the troposphere so that the measured effects on the direct solar beam would only be influenced by the stratosphere and above. Spectral solar extinction was measured on all three flight programs, while 2π-sr diffuse-to-total flux ratios and total reflectance were measured on only one. The remainder of this report discusses the results and implications of the direct solar beam extinction measurements made on these flights.

Spectral aerosol optical depths for the three flight series were derived from the spectral solar extinction measurements obtained by hand-operated sunphotometers on the aircraft. The results for one spectral wavelength are shown in fig. 68 where the flights' dates are also indicated. The flights were in the general longitude range of the continental United States. Details of these observations and subsequent analysis and interpretation were given by Dutton and DeLuisi (1983b).

The main features shown in fig. 68 are the relative maximum in the Northern Hemisphere tropics, the local minimum indicated at 25°N in flights 2 and 3, and the increase in optical depth at the northern end of the flights. The tropical maximum corresponds to the original cloud, which was observed by satellite to remain confined to this latitude region for several months following the eruption. The satellites were not designed to quantify the shortwave optical properties of the cloud, however. The high values in the north were unexpected and raise some questions about the transport mechanisms. The spatial extent of the cloud and relatively high values of optical depth (stratospheric background is close to 0.005) 8-10 months after the eruption provide useful information about the extent of the effect of the cloud on the global shortwave radiation balance.

An important conclusion from these observations is that significant latitudinal variations existed at least up to 8 months after the eruption. If there are significant impacts by the cloud on climatic radiative forcing, the perturbations will have definite latitudinal variations.
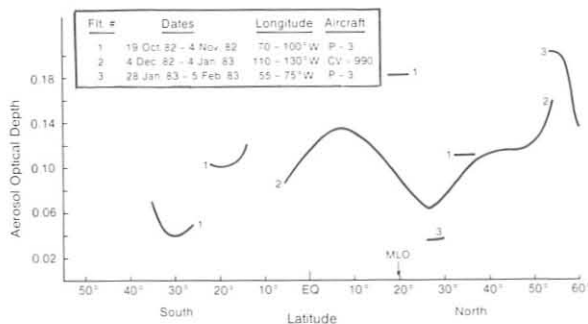
Figure 68.--Aerosol optical depth above the aircraft for three NASA flights at 500-nm wavelength.

4.14   MLO Normal Incidence Irradiance Record

Measurements of normal incidence solar irradiance have been made at MLO since 1958.   The instruments and methods used have been described in past GMCC Summary Reports, and by Ellis and Pueschel (1971), Mendonca et al. (1978), and Bodhaine et al. (1981).

In the solar irradiance record, several decreases in normal incidence flux have been observed after explosive volcanic eruptions.   By inference, the decreases in solar irradiance at MLO have been used as an indirect measure of the transport, intensity, and duration of stratospheric volcanic debris over MLO and the equatorial Pacific.   The validity of this assumption was confirmed after Hoyt (1979) and Bodhaine et al. (1981) documented that the magnitude and variability of the seasonal annual change in solar irradiance caused by tropospheric attentuation above MLO was too small to account for the long-term changes observed in the record.   Other contributions to secular changes in tropospheric attenuation at MLO have been shown by Bodhaine and Pueschel (1974), Mendonca et al. (1979), and Shaw (1980) to be very small and barely detectable, if at all.   Consequently, the major cause of secular change in the normal incidence solar irradiance at MLO has been attributed to explosive volcanic eruptions.

Figure 69 shows an updated plot of yearly means of normal incidence solar irradiance for 1958-June 1983.   Values are plotted for irradiances obtained at relative air masses of 2, 3, 4, and 5 during cloudless skies.   Only morning values are used because they are more representative of the undisturbed atmosphere above MLO.   Measurements in the afternoon are subject to a mountain upslope circulation that carries moisture and clouds to the observatory and makes the afternoon measurements responsive to local conditions.
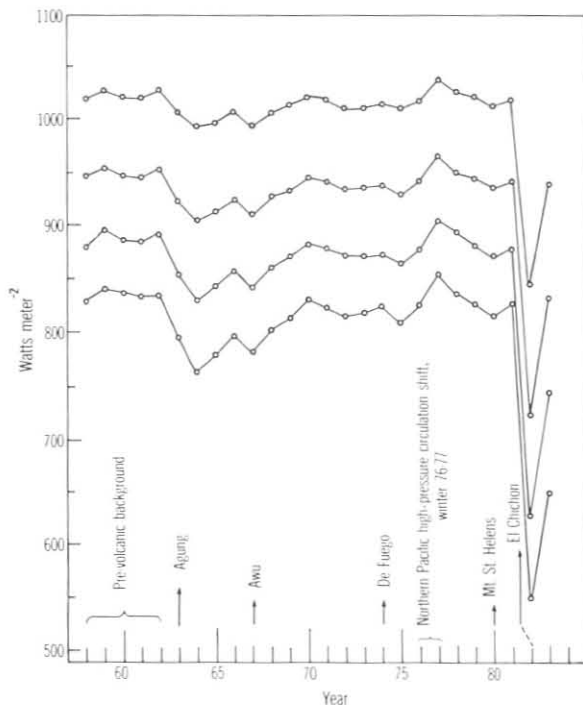
Figure 69.--Normal incidence irradiance values for relative air masses 2, 3, 4, and 5 (top to bottom) at MLO.   Irradiances are averaged for the year during cloudless sky conditions as the Sun rises in the morning.   Data for 1983 include only January to June.

The normal incidence irradiance values are also plotted after they have been corrected for instrument drift using the method described by Robinson (1982). Previously the data were presented as an apparent atmospheric transmission. Robinson's method allows for examination of decreases in actual solar irradiances after each volcanic episode and in relation to the apparent atmospheric transmission changes.

In fig. 69 the data from the different relative air masses (2-5 from top to bottom) track each other well. This is to be expected, but the fact that every rise and dip is mirrored at all air masses also attests to the uniformity of the atmosphere in the mornings at MLO.

When the pre-Agung years 1958-1962 are used as a base to determine the magnitude of the decreases in normal incidence flux, a comparison can be made between the decreases in apparent transmission described by Ellis and Pueschel (1971) and Mendonca et al. (1978) and the decreases in normal incidence flux. Table 33 shows the comparisons. In fig. 69 and table 33 several features are evident. The decrease observed after the eruption of El Chichon in April 1982 is by far the largest observed in the 26-yr record. Even up to 14 months later (the data for 1983 include only January to June) the normal incidence flux and apparent transmission are lower than after the Agung eruption. Although the Agung eruption as measured at MLO shows a smaller decrease in normal incidence flux compared with El Chichon, the recovery time is long, and near-background irradiance values are not observed until 1970. It should be stated that the long recovery time could have been influenced by other eruptions that may have occurred close in time to Agung and Awu. These could have added debris to the stratosphere during the period 1963-1967 (Mendonca et al., 1978) and prolonged the return to background. The decrease after De Fuego is the smallest observed that can be attributed to a particular volcanic eruption and is short lived.

A hemispheric circulation shift and corresponding high irradiance values at MLO in 1976 and 1977 should be noted. The irradiance values measured during the winter of 1976-1977 and 1977-1978 were the highest recorded at MLO for

Table 33.--Percent decrease in apparent transmission and normal incidence flux at MLO for five selected periods, using the pre-Agung 1958-1962 period as a base

Event	Apparent transmission* (%)	Normal incidence flux† (%)				
		2	3	4	5	Aver.
Agung 1963-1965	2	2	4	5	7	4.5
Awu 1967-1968	2	2	4	5	7	4.5
De Fuego 1974-1976	1	1	2	3	3	2.3
El Chichon 1982	9	17	20	30	34	25.3
Jan-Jun 1983	4	8	13	16	23	15.0

*Apparent transmission decreases are averages for relative air masses 2-5, obtained from Mendonca et al. (1978).
†Normal incidence flux decreases are given at relative air masses 2-5.

the entire record. The daily log sheets at MLO show unusually clear and dry periods over these winters. More than 82% of the mornings during these winters were clear, to the extent that a complete set of solar irradiance measurements was obtained.

When the apparent transmission decreases are compared with the irradiance decreases, a one-to-one agreement is observed at a relative air mass of 2 until the El Chichon eruption. For El Chichon, the percent decrease in actual irradiance is about twice that determined by the apparent transmission record at a relative air mass of 2. Normal incidence irradiance values at relative air mass 2 (zenith angle 60°) are used as an approximation for the daily total of irradiance received during a cloudless day near the Equator. The relationships between the apparent transmission decreases and normal incidence irradiance decreases for the different relative air masses are shown in table 33. Lower Sun angles (larger air masses) give larger decreases.

The apparent transmission record and the normal incidence irradiance record at MLO both indicate decreases after explosive volcanic eruptions, with recovery times lasting from a few months to several years. The eruption of El Chichon volcano has resulted in the largest decrease in normal incidence flux measured at MLO since observations began in 1958. As of June 1983 the atmosphere over MLO was still more turbid than at any time after the Agung eruption in 1963, even after debris from El Chichon had already spread around the world. Measurements will continue to be made to monitor the lifetime, evolution, and spread of the cloud over MLO.

5. COOPERATIVE PROGRAMS

5.1 Measurements, Sources, and Sinks of Atmospheric Benzene and Toluene

R. A. Rasmussen and M. A. K. Khalil
Oregon Graduate Center
Beaverton, OR 97006

5.1.1 Introduction

Benzene (C_6H_6) and toluene (C_7H_8) are short-lived trace gases in the atmosphere that arise from a number of natural and anthropogenic sources. Their common sources include automobiles, solvent uses, chemical manufacturing, diesel fuel, forest fires, refuse combustion, petroleum, lacquer and polymer manufacturing, gasoline vapor, sewage treatment, tobacco smoke, landfills, and possibly natural sources (Graedel, 1978). We recently found that burning wood, such as for heating homes, also produces benzene and toluene. The main atmospheric removal process for both compounds is believed to be reaction with tropospheric OH radicals, resulting in atmospheric lifetimes on the order of weeks for benzene and a few days for toluene. On a global scale the concentration of benzene and particularly of toluene is dependent on nearby sources.

During the past year and a half we developed a gas chromatographic system (GC/FID) with a capillary column to measure the concentration of benzene and toluene along with dozens of other hydrocarbons in the range of parts per trillion by volume. The system has a detection limit of about 5 pptv for benzene and toluene, and a precision of ±10%. The analytical system is described in more detail by Rasmussen and Khalil (1983).

Over the last year or so air samples were collected in stainless steel flasks at nine sites, including several supported by our cooperative agreement with GMCC. The sampling containers and collection procedures are designed to keep the samples free from contamination and to allow extended storage (Rasmussen and Khalil, 1980). Laboratory studies have verified that concentrations of benzene, toluene, and other hydrocarbons do not change over periods of storage much longer than usually encountered in this experiment. The measurements at Cape Meares, Oreg., were based on large-volume, high pressure, cryogenically collected air samples, using sampling containers that are even better in preserving air than the smaller flasks used at the other, more distant sites.

5.1.2 Data

Table 34 gives the benzene and toluene data obtained so far, showing daily average concentrations. Often two or three smaller air samples collected on the same day were combined before analysis. Sometimes several samples collected on the same day were analyzed separately, in which case the concentrations obtained were combined to form a daily average. The distinctive features are analyzed and discussed by Rasmussen and Khalil (1983). Samples obtained from SPO revealed no significant levels of benzene and toluene. Following are some conclusions on the sources, sinks, and distribution of benzene and toluene based on the collected data.

Table 34.--Benzene and toluene concentrations

BRW (71°N)

Date	C$_6$H$_6$ (pptv)	C$_7$C$_8$ (pptv)
1982		
22 Mar	294	73
26	213	BDL
29	245	96
30	263	49
8 Apr	220	51
12	256	49
14	250	27
20	216	31
24	230	BDL
26	212	17
7 May	145	BDL
13	123	BDL
15	97	BDL
18	80	BDL
24	89	BDL
1 June	67	36
10	42	31
14	53	75
26	38	28
1 Jul	44	BDL
5	29	29
12	BDL	33
22	BDL	BDL
29	34	BDL
7 Aug	41	44
9	24	BDL
21	142	151
31	BDL	BDL
6 Oct	90	27
14	305	393
23	101	24
29	182	BDL
1 Nov	171	94
22	197	68
3 Dec	164	68
14	195	BDL
20	182	84
27	194	95
1983		
14 Jan	245	117
21	313	184
24	280	235
31	252	136
8 Feb	270	200
15	232	138
22	269	102
11 Mar	251	71
13	276	120
6 Apr	235	48
7	282	44
9	229	31
14	209	56
15	165	BDL
19	179	BDL
20	132	BDL
21	191	22
27	143	BDL
4 May	85	BDL
10	164	BDL
17	76	BDL

Cape Meares, Oreg. (45°N)

Date	C$_6$H$_6$ (pptv)	C$_7$C$_8$ (pptv)
1980		
10 Dec	701	--
31	160	207
1981		
15 Jan	184	234
25 Feb	196	117
11 Mar	165	87
18	531	712
1 Apr	180	42
17	224	224
29	96	88
13 May	108	36
27	61	37
17 Jun	34	BDL
1 Jul	79	127
15	60	66
29	19	21
19 Aug	601	--
2 Sep	29	26
16	171	254
30	85	61
1 Oct	247	237
14	155	95
28	410	575
20 Nov	587	960
2 Dec	357	472
16	514	754
30	313	334
1982		
13 Jan	415	552
3 Feb	285	289
24	448	596
10 Mar	234	220
24	140	53
7 Apr	401	420
21	155	89
19 May	83	20
16 Jun	23	28
14 Jul	--	68
28	165	140
11 Aug	58	BDL
22 Sep	269	192
24 Nov	291	297
30	166	139
8 Dec	144	105
29	300	156
1983		
12 Jan	201	147
31	184	113
11 Feb	167	98
23	254	254
9 Mar	207	264

NWR (40°N)

Date	C$_6$H$_6$ (pptv)	C$_7$C$_8$ (pptv)
1982		
4 May	36	29
14	76	31
18	40	33
25	54	15
2 Jun	BDL	BDL
8	39	29
16	36	BDL
22	43	34
29	28	28
6 Jul	28	BDL
13	55	31
20	34	51
3 Aug	33	34
10	BDL	49
17	29	50
27	182	71
31	155	30
8 Sep	134	22
14	140	20
23	78	20
28	73	23
5 Oct	70	22
12	63	22
26	74	35
2 Nov	94	44
9	210	BDL
16	52	BDL
7 Dec	491	689
12	42	BDL
19	113	37
28	445	--
1983		
4 Jan	125	44
8	93	38
16	285	320
22	226	119
29	152	88
5 Feb	180	65
13	89	23
20	134	44
26	129	60
20 Mar	253	200
25	200	168
1 Apr	156	15
12	241	303
26	232	412

SMO (14°S)

Date	C$_6$H$_6$ (pptv)	C$_7$C$_8$ (pptv)
1982		
17 May	24	BDL
28	BDL	BDL
5 Jun	114	22
12	46	39
22	BDL	50
28	21	34
29	47	--
10 Jul	63	59
17	BDL	41
26	BDL	37
6 Aug	BDL	115
25	229	43
30	207	21
10 Sep	136	39
25	167	29
6 Oct	90	33
9	150	14
17	93	14
1 Nov	88	20
13	73	BDL
27	88	BDL
6 Dec	85	16
8	40	BDL
11	127	BDL
17	39	BDL
18	43	21
25	62	21
1983		
1 Jan	55	33
8	BDL	BDL
15	57	28
19 Feb	79	123
26 Mar	31	88
16 Apr	11	12
23	BDL	BDL
30	119	BDL

Table 34.--Benzene and toluene concentrations--Continued

MLO (20°N) Date	Concentrations (pptv) C_6H_6	C_7C_8	WFM (44°N) Date	Concentrations (pptv) C_6H_6	C_7C_8	Tasmania (42°S) Date	Concentrations (pptv) C_6H_6	C_7C_8	Cape Pt., S.Africa (35°S) Date	Concentrations (pptv) C_6H_6	C_7C_8
1982			1982			1982			1982		
28 Apr	66	BDL	8 Aug	160	253	15 May	41	28	24 May	30	59
6 May	22	22	9	90	105	27	179	167	2 Jul	30	43
15	73	BDL	10	73	198	2 Sep	56	16	3 Aug	33	52
19	339	21	11	41	97	7	53	BDL	1 Sep	304	BDL
26	33	13	12	121	834	9 Nov	BDL	BDL	2 Nov	115	BDL
2 Jun	22	5	13	84	92	16	BDL	BDL	8	64	110
9	108	36	19	170	152	25	BDL	BDL			
16	--	38	2 Sep	397	254	6 Dec	71	26	1983		
23	493	63	9	395	103				15 Feb	BDL	38
30	BDL	BDL	10	781	256	1983			18 Apr	102	243
7 Jul	17	BDL	13	278	79	24 Jan	BDL	BDL			
14	BDL	BDL	21	213	205	28 Mar	11	BDL			
29	317	116	1 Oct	290	173						
4 Aug	38	7	5	216	143						
12	BDL	BDL	22	162	43						
25	217	32	27	185	72						
1 Sep	151	20	14 Dec	343	160						
8	69	27									
6 Oct	118	28	1983								
15	173	BDL	25 Jan	543	628						
20	23	BDL	3 Feb	591	804						
27	84	BDL	4	311	228						
3 Nov	76	BDL	9	233	130						
10	140	19	10	195	116						
1 Dec	53	BDL	21	385	257						
8	BDL	BDL	1 Mar	183	81						
15	65	BDL	5	191	BDL						
23	BDL	39	7	138	85						
29	271	BDL	10	430	44						
			14	166	95						
1983			15	228	93						
7 Jan	91	BDL	16	273	76						
20 Apr	BDL	BDL	17	339	188						
27	38	27									

BDL = Below Detection Level

5.1.3 Discussion

The data show that benzene and toluene concentrations are variable in both space and time. Generally the concentrations observed reflect the effects of local sources. Transport over long distances is possible at high latitudes in wintertime when OH levels are extremely low. Transport of these gases from one hemisphere to the other is not likely to occur because of the high levels of OH that are believed to exist in the tropics and the slow latitudinal mixing at these latitudes. For benzene and toluene seasonal variations of OH can have enormous effects on the ambient concentrations. Such effects have been observed, as shown by Rasmussen and Khalil (1983).

The lifetimes of these gases depend primarily on the local and seasonal concentrations of OH. Measured reaction rate constants are about 1.2×10^{-12} molecule-s cm^{-3} for benzene and 6.4×10^{-12} molecule-s cm^{-3} for toluene (Graedel, 1978; Hampson, 1980; Perry et al., 1977). The local lifetime may be estimated by $\tau \simeq K[OH]$. If typical average atmospheric OH concentrations are

$(0.5-1.0) \times 10^6$, then the typical lifetimes of benzene and toluene will be 10-20 days and 2-4 days respectively. Since OH is believed to exist only during daytime, the OH levels would have to be $(1-2) \times 10^6$ molecules cm^{-3} during the day for the lifetimes calculated above to be effective. At high latitudes, the seasonal variation of solar radiation flux and water vapor may cause the OH levels to be an order of magnitude lower in winter, thus allowing benzene and toluene to survive for several months. Under these circumstances, benzene, toluene, and similar gases could be transported over long distances.

The global sources of benzene and toluene are extremely difficult to estimate accurately, since they are many and varied. A global mass balance may be constructed as $\bar{S} = \bar{C}/\bar{\tau}$, where $\bar{S}$ is the annual emissions (Tg yr^{-1}), $\bar{C}$ is the global burden (Tg), and $\bar{\tau}$ is the average global lifetime (yr). Since the concentrations vary with latitude and longitude, especially for toluene, the estimate of $\bar{C}$ based on present measurements is subject to sizable uncertainties. Similarly, the evaluation of an average lifetime leads to uncertain results. Within these constraints, the most likely values for the global emissions of benzene and toluene based on the present data were estimated. First the globally averaged ground-level mixing ratio C_0 was evaluated. The atmosphere was divided according to latitude ϕ at intervals of 0.1 for sin ϕ; thus, 20 equal-volume boxes were obtained. The estimate of ground-level concentration was then obtained from the available measurements in or near these boxes. BRW data were used for $0.8 < \sin \phi \leq 1.0$; Cape Meares, WFM, and NWR data for $0.5 < \sin \phi \leq 0.8$; MLO data for $0 < \sin \phi \leq 0.5$; SMO data for $-0.4 < \sin \phi \leq 0$; Tasmania and South Africa data for $-0.7 < \sin \phi \leq 0.4$; and SPO data for $-1 \leq \sin \phi \leq -0.7$. This weighted the sites latitudinally and provided an estimate of

$$C_0 = \int_{-\pi/2}^{\pi/2} C_0(\phi) \cos \phi \, d\phi.$$

The values of C_0 for benzene and toluene are 90 pptv and 62 pptv respectively. Next, a decrease of mixing ratio with height had to be accounted for (see Rasmussen et al., 1983). The height profile was estimated by a one-dimensional model as $C(z) = C_0 \exp(-z/\sqrt{K_* \tau})$, where z is height and K_* is the upward diffusion parameter (Khalil and Rasmussen, 1983). K_* is taken to be approximately 10^5 cm^2 s^{-1}. The global burden is estimated to be

$$\bar{C} = 10^{-24} \frac{N_T}{N_0} M \frac{1}{z_T} \int_0^{z_T} C(z) \, dz \, , \tag{4}$$

where $\bar{C}$ is in Tg, N_T is the number of molecules of air in the troposphere, N_0 is Avogadro's number, M is the molecular weight (g mol^{-1}), z_T is the average height of the tropopause, and $C(z)$ is in pptv (see Khalil, 1979). Because of the short lifetimes, (4) becomes

$$\bar{C} \simeq 10^{-24} \frac{M N_T}{N_0} \frac{C_0 \sqrt{K_* \tau}}{z_T} \, . \tag{5}$$

110

Thus, from (5) the global burdens $\bar{C}$ of benzene and toluene are estimated to be 0.3 Tg and 0.1 Tg respectively, assuming average OH levels of 0.7×10^6 molecules cm^{-3} to determine the lifetimes. $\bar{S}$ then turns out to be 8 Tg yr^{-1} for benzene and 14 Tg yr^{-1} for toluene. As stated earlier, these estimates are subject to uncertainties; still, they constitute a beginning for evaluating annual global emissions of these hydrocarbons.

Since benzene and toluene have different lifetimes and often come from the same sources, measurements of their concentration ratio can be used, along with other atmospheric data, to trace the origins and locations of the sources of pollution on regional scales. The use of benzene and toluene as tracers of air pollution is currently being investigated.

5.2   Aerosol Light Absorption at MLO

A. D. Clarke and R. J. Charlson
Environmental Engineering and Science Program
University of Washington, Seattle, WA 98195

A filter sampling program aimed at characterizing the optical and chemical features of the size-fractionated aerosol at MLO was initiated with measurements during 28 May-28 June 1981 (Clarke and Charlson, 1982) and continued during 25 April-29 May 1982. These studies involved separate day and night sampling of the aerosol along with measurements of the size distributions using a modified Royco 220 OPC. From June 1982 through June 1983, 3-h samples of the downslope (Mendonca, 1969) aerosol were taken nightly to eliminate local upslope contamination and to obtain aerosol samples representative of midtropospheric air subject to long-distance transport. Samples representative of both the annual and daily variability associated with the springtime aerosol transport from Asia (Uematsu et al., 1983) were collected along with those representative of summer "unperturbed" conditions.

The intent of these measurements was to examine the variability in both fine- and total-aerosol light-absorption properties, single-scatter albedo, and total/excess sulfate fractionation for the background midtropospheric aerosol. The measurement of the absorption coefficient b_{ap} (m^{-1}) is valuable as a direct measurement of radiative effects and, in conjunction with the scattering coefficient b_{sp} (m^{-1}), it allows specification of the single-scatter albedo $\omega = b_{sp}/(b_{ap} + b_{sp})$ for assessment of climatic effects. These measurements were compared and interpreted in conjunction with Asian-dust concentrations (Parrington et al., 1983b), light-scattering data, and meteorological data available at MLO over the same time period.

During sample collection, a 3-cm-diameter tube conveyed the aerosol from the top of the MLO sampling tower (10 m) to tapered, diffusing filter holders. Two Pallflex QAS 2500 quartz fiber filters were changed daily to obtain concurrent samples at 60 ℓ min^{-1}. Upstream of one filter a modified Bendix Model 18 Cyclone provided a 50% size cut at a particle diameter of about 0.7 μm, corresponding to the intermode minimum between fine and coarse OPC mass peaks observed at MLO (Clarke and Charlson, 1982), so that total- and fine-aerosol characteristics could be intercompared. The light-absorption coefficient was later measured at the laboratory using the nondestructive integrating sandwich technique (Clarke, 1982).

Some results for the limited springtime sampling in 1981-1982 are presented in fig. 70. Apart from the indicated day and night samples, the figure also reveals the effect of excluding sample periods when CN concentrations were above 300 cm^{-3}. This is a common criterion for background midtropospheric air and generally serves to eliminate periods of intruding boundary layer air at MLO. The range of the lower background values of b_{ap} was $(1-7) \times 10^{-8}$ m^{-1} for May-June 1981 and $(3-17) \times 10^{-8}$ m^{-1} for April-May 1982 in spite of apparent elevated Asian-dust transport for the 1981 period. The higher b_{ap} values for 1982 are also reflected in relatively low background values of ω (fig. 70) that averaged about 0.97 (1981) and 0.93 (1982). Most of the absorption (70% ± 10%) was confined to the fine-particle mode passed by the Cyclone. Crustal material in this mode appears to account for only a small fraction of this absorption, and EC is suggested as the primary light absorber.

Because of limited resources, sample collections have continued only on a nightly basis, and only a limited preliminary analysis of those data is available. At present, initial measurements indicate that the overall annual variability of b_{ap} parallels that of b_{sp} and that both coefficients increase together during the spring incursions of Asian-dust aerosol (Parrington et al., 1983b) and drop considerably by midsummer. Nightly high variability indicates that such aerosol incursions have considerable spatial and temporal variability. Light-absorbing particles appear concentrated in the fine-particle mode throughout the year although some variability in the proportions seems evident. Indications are that fine-mode crustal material cannot account for most of the measured light absorption, and the long-distance transport of continentally derived soot is implicated. When springtime b_{ap} values are divided by the specific absorption of EC (about 10 m^2 g^{-1}), the resulting estimates of MLO background EC concentrations are in the range of 1-20 ng m^{-3} and are in close agreement with recent minimum values measured for the Atlantic marine boundary layer (Andrea, 1983).

More than 800 filter samples have been accumulated to date. The optical and chemical data that could be obtained would be of particular value for comparison with the light-scattering and elemental-analysis data that are also available for this period. A selection of samples from various times of the year having simultaneous changes in the data should be examined to evaluate the significance of continental sources and long-distance transport for the maintenance of a background tropospheric aerosol. An annual record of the magnitude and variability of the single-scatter albedo for the remote midtroposphere would be a valuable parameter for current climate modeling and also for predicting future trends. It is relevant to note that such measurements are both necessary and central to the primary function of the GMCC program. Insofar as soot is implicated as a primary light absorber at MLO, b_{ap} could be an effective tracer for aerosol reaching MLO from continental combustion sources. The variability in b_{ap} could also be valuable in the interpretation of other background atmospheric studies at MLO.
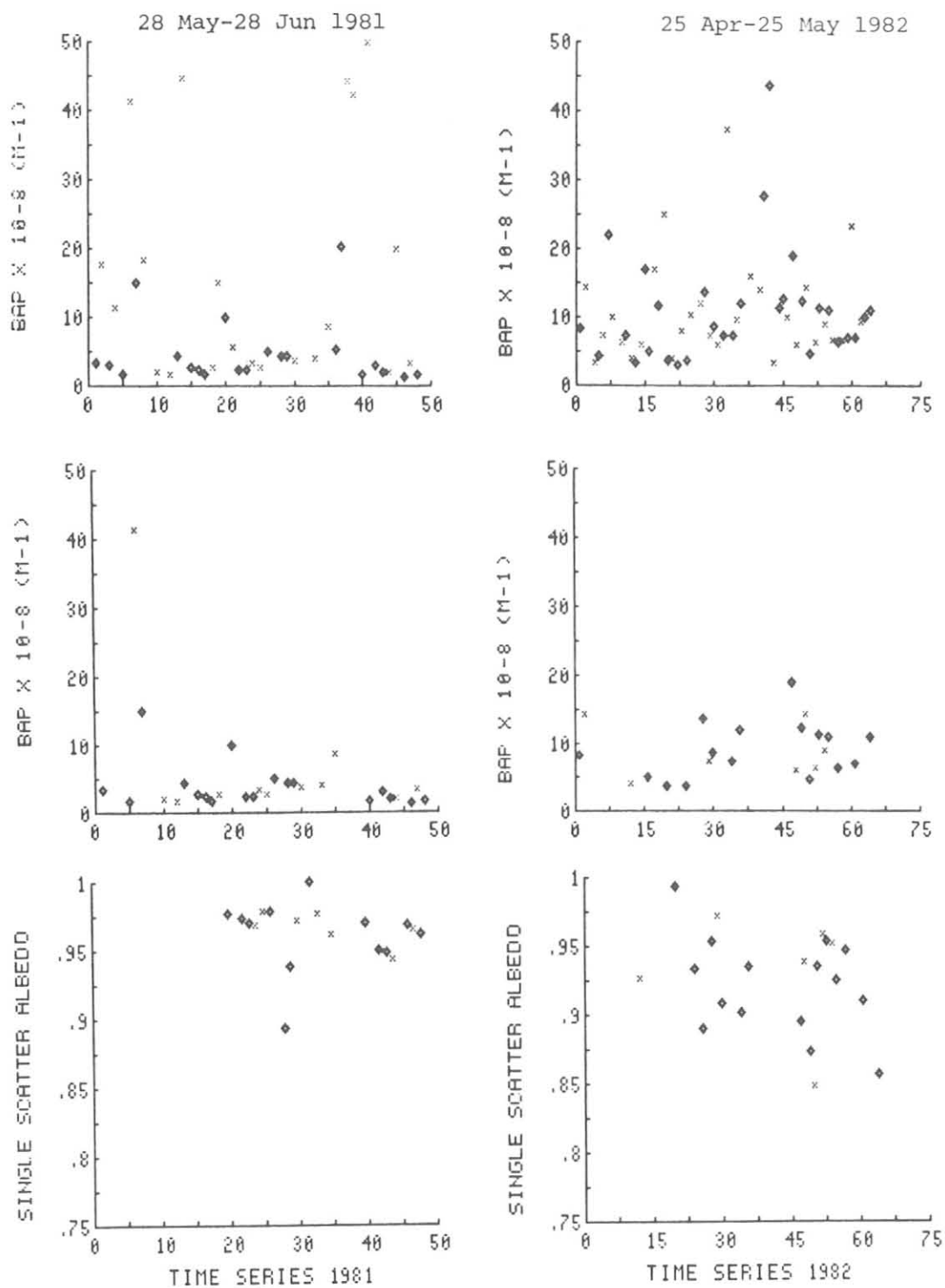
Figure 70.--Time series by sample number for indicated sampling periods at MLO for daytime upslope (✖) and nighttime downslopes (◆) conditions. From top to bottom: absorption coefficient (BAP) for all samples; BAP for background conditions (CN concentration < 300 cm^{-3}); and single-scatter albedo for background conditions (CN concentration < 300 cm^{-3}).

5.3 Solar Radiation Assessment for BRW

G. Wendler
Geophysical Institute, University of Alaska
Fairbanks, AK 99701

The four climatic regions in Alaska are the maritime region in the south, the intermediate zone, the interior continental region, and the Arctic region north of the Brooks Range. Solar radiation stations were established at Kodiak, Anchorage, Fairbanks, and BRW, respectively, to represent the four regions. These stations will give a basis for the amount of solar radiation available at different times of the year and on different exposed surfaces in these four regions.

The following measurements were added to those already being taken at BRW by GMCC and the Smithsonian Institution: (1) global solar radiation, (2) reflected solar radiation, (3) all-wave incoming radiation, (4) all-wave outgoing radiation, (5) sky radiation, (6) global radiation on a south slope inclined to latitude, and (7) global radiation on a south wall. The data are recorded on a Datel data logger.

The data are helpful in the design of systems such as PV arrays currently being used for such applications as thawing road culverts and operation of remote railroad-crossing lights. Design of buildings to maximize the passive use of solar energy is another application.

Besides these practical applications, some theoretical problems are of interest. Examples are snowmelt and the multiple reflection between snow cover and the stratus clouds, or the radiation phenomenon found in BRW in spring. This radiation phenomenon, which is being studied systematically, showed that even in late May at noon the net radiation (shortwave and thermal IR) is less positive under clear sky than under cloudy conditions and results in colder temperatures for a clear day. This is, of course, common knowledge for the Alaskan winter; however, that this is also experienced in May at noon is at first surprising. Cloudiness does not decrease the global radiation substantially, because multiple reflection between the lower extent of the clouds and the highly reflecting snow surface increases the sky radiation. On the other hand, the cloud cover is rather opaque in the thermal IR region, and protects the surface from larger IR losses.

5.4 Climatology of Aerosol Concentration at SPO
February 1974-December 1982

J. A. Samson and A. W. Hogan
Atmospheric Sciences Research Center
State University of New York, Albany, NY 12222

ASRC and GMCC began a joint aerosol research program at SPO in 1974. Total CN concentration is measured with a photoelectric CNC twice daily at 0000 Z, once coincident with radiosonde launch and once at another time, at least 8 hours apart. These observations have continued without interruption to the present. The measurements have been made by several GMCC and ASRC observers over the years. The observations are recorded in duplicate in notebooks archived both at ASRC and at GMCC, Boulder. Each observation consists

of date, time, relevant comments, and 20 individual parameters including the CN concentration. The Antarctic aerosol is unique in the study of climatological trends, because it represents a background aerosol appearing at the endpoint of nature's meteorological removal processes, unadulterated by contamination from vegetation, wind-blown spray, or fossil-fuel combustion.

The study of the Antarctic aerosol has been limited by instrument problems encountered with measuring low values of concentration and with the practical operation of instruments in such a harsh envrionent. Voskresenskii (1968) was the first to measure the total concentration of CN in Antarctica, along the coast near the Mirnii region in 1965. The CN measurements used in this paper were made with a Pollak photoelectric CNC with convergent light beam (Pollak and Metnieks, 1960), which is sufficiently sensitive to measure the low concentrations found in Antarctica with high accuracy (Hogan et al., 1981). The Pollak counter is attached to the Komhyr (1983) stainless steel sampling stack. The size and charge of ambient aerosol are determined using the Sinclair (1972), Rich (1966), and Spurney et al. (1969) techniques. A diffusion battery, filter, or denuder is inserted in the sample line, and the loss of particles of selected physical property is determined by repetitive measurement.

The photoelectric CNC operates on the principle that the percent of light transmitted through the chamber after a fog has been formed on the nuclei is a function of the aerosol concentration. The 2.5-cm-diameter chamber is about 58 cm long and is lined with porous ceramic that is kept moist. Air is allowed to flow through this chamber and is then contained by closing the upper and lower flush valves. An overpressure of approximately 105 torr is produced by compressing the air in the chamber. Quickly releasing the pressure causes an adiabatic expansion to produce water fog. The amount of fog formed is measured by the extinction of a light beam passing through the column using a light source and photocell.

Three separate readings are made at each observation. These readings are taken over a period of about 5 minutes, because 1-2 minutes are required per reading, to flush the chamber and to achieve saturation prior to expansion. Each reading is then converted to the number of particles per cubic centimeter, using the calibration of Pollak and Metnieks (1960). Three readings per observation, averaged to obtain a mean aerosol concentration for the observation, increases the reliability of the value obtained and determines the variability of the aerosol concentration.

Figure 71 and table 35 show the monthly mean aerosol concentration for 1974-1982; table 35 also gives the number of observations per month. A repeatable seasonal variation is evident, with the aerosol concentration highest during the austral summer and lowest during the austral winter. No apparent increase or decrease in mean aerosol concentration is detectable over the time span of the observations. The lowest monthly mean concentrations occur in June, July, or August of each year, whereas the highest monthly mean concentrations appear to be bimodal and are divided among the summer months. November consistently has a high monthly mean, with the average concentration in December always lower. With equal frequency, January, February, and March also experience a large monthly average. The wide range in concentrations that occur in November were noted by D. Nelson, station chief, during the initial year of observations in 1974.

115
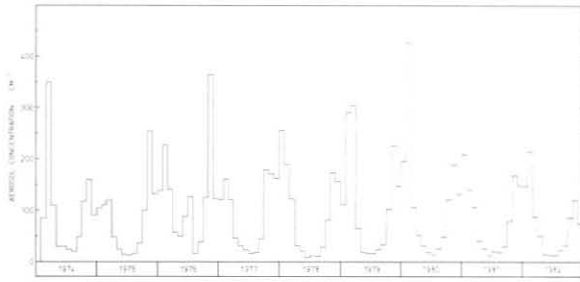
Figure 71.--SPO monthly mean aerosol concentration for 1974-1982.

Table 35.--SPO monthly mean aerosol concentration*

	1974	1975	1976	1977	1978	1979	1980	1981	1982
Jan	--†	103	138	119	254	109	193	208	146
	--†	(25)	(43)	(48)	(62)	(33)	(97)	(60)	(105)
Feb	85	109	226	159	188	289	426	139	214
	(6)	(56)	(42)	(48)	(56)	(55)	(56)	(53)	(63)
Mar	349	119	140	120	121	303	104	105	87
	(22)	(91)	(72)	(62)	(84)	(63)	(62)	(59)	(62)
Apr	109	47	57	44	30	63	51	39	50
	(22)	(85)	(56)	(54)	(102)	(61)	(60)	(58)	(58)
May	29	24	49	31	20	17	29	25	14
	(4)	(61)	(60)	(62)	(93)	(61)	(61)	(61)	(63)
Jun	29	13	87†	22	7	15	17	11	13
	(13)	(57)	(58)	(59)	(90)	(60)	(60)	(58)	(59)
Jul	23	12	126†	15	10	15	12	19	13
	(49)	(59)	(61)	(62)	(93)	(62)	(61)	(61)	(60)
Aug	19	16	15	16	9	22	25	18	22
	(19)	(63)	(62)	(62)	(91)	(62)	(62)	(60)	(62)
Sep	48	36	37	43	27	32	47	29	32
	(94)	(57)	(83)	(60)	(90)	(60)	(60)	(57)	(60)
Oct	117	99	124	178	79	101	119	78	85
	(56)	(40)	(61)	(62)	(93)	(62)	(63)	(62)	(62)
Nov	159	254	364	169	172	225	188	167	119
	(23)	(25)	(55)	(56)	(80)	(83)	(58)	(71)	(59)
Dec	89	131	121	161	154	146	129	147	74
	(1)	(41)	(32)	(57)	(53)	(101)	(73)	(68)	(59)
Annual mean (weighted)	82†	68	117†	88	76	116	114	84	77
	(309)	(660)	(685)	(692)	(987)	(763)	(773)	(728)	(772)
Annual mean (unweighted)	96†	80	124†	90	89	111	112	82	72
	(11)	(12)	(12)	(12)	(12)	(12)	(12)	(12)	(12)

*Values in parentheses indicate the number of observations per month.
†Missing or questionable data.

116

The standard deviations associated with these means are least in the winter months and greatest in the summer. These standard deviations vary from 3 to 19 cm^{-3} for the winter and from 40 to 95 cm^{-3} for the summer averages. The concentrations are more variable in spring and summer months. The wide range of observed concentration in November is due to frequent exchange in lower layers, accompanying the breakup of the polar vortex. Concentrations vary little throughout the winter because minimum low-layer exchange occurs. Measurements rarely exceed 50 cm^{-3} in winter and occasionally approach the threshold sensitivity of the instrument. A minimum deflection of the meter is equivalent to about 3 cm^{-3}. The lowest monthly mean concentrations vary from 7 to 19 cm^{-3} during these 9 years of data.

The data collected by this joint program have been stratified by season and wind direction to provide a preliminary climatology of aerosol concentration. Recent analysis of the 9-yr data set shows that rising barometric pressure most frequently occurs concurrent with northwest (grid) winds at the surface, and brings not only cloudiness and precipitation but increased surface aerosol concentration as well. The rising barometric pressure is evidence of actual transport of air from the coastal regions to the Polar plateau, which brings lower latitude influence along an upslope path.

The most recent GMCC-ASRC cooperative field program was conducted during January 1983. A cascade impactor was operated simultaneously with the GMCC aerosol, ozone, and meteorological instrumentation in the CAF. A slow-rising radiosonde was launched each day, in addition to regular radiosonde flights, to determine stability and mixing parameters near the surface. These observations showed manyfold increases in aerosol concentration and a slight decrease in ozone concentration to accompany near-surface mixing that results from destruction of the radiation inversion by cloudiness. These mixing events are brief, with few surviving long enough to be detected on successive radiosonde launches. This indicates that aerosol events detected at SPO result from brief downward mixing of more highly aerosol-laden air. The surface concentrations may be enhanced for several hours after the mixing occurs. The simultaneous decrease in ozone, observed with an increase in aerosol concentration during these events, is evidence that this exchange is confined to the lower layers of the troposphere.

5.5 Size Characteristics of Asian Dust Sampled at MLO

T. A. Cahill and D. A. Braaten
Air Quality Group, Crocker Nuclear Laboratory
University of California, Davis, CA 95616

5.5.1 Introduction

Long-range transport of soil dust from arid regions of central and eastern Asia, which include the Gobi, Takla Malan, and Ordos deserts, can significantly increase the particulate load of the portion of the troposphere above the marine layer at MLO during February-June. This results from both synoptic flow patterns that provide the necessary transport flow regime, and increased duststorm activity throughout central Asia resulting from low rainfall amounts,

increased occurrence of strong surface winds associated with cold fronts, and soil cultivation. This long-range transport of dust has been verified in terms of both meteorological trajectory analysis and particle sampling. Miller (1981a) established a 5-yr climatology of trajectories to MLO and showed a predominance of trajectories from the region of duststorms (northwest of MLO) during periods of greatest activity. Relationships between trajectories and sampled particles at MLO have been investigated by Parrington et al. (1983b) and Darzi and Winchester (1982a), and relationships between trajectories and light-scattering properties have been studied by Shaw (1980). To date, sampling and analysis of transported Asian dust have been limited to a total sample with no size differentiation. This discussion focuses on the properties of transported Asian dust segregated by size.

5.5.2 Procedures

Particles were sampled at MLO between January 1980 and February 1982 to obtain information on the size distribution and chemistry of background mid-tropospheric particles. Sampling was conducted using a modified multiday sampler (Flocchini et al., 1976) consisting of an inlet stack to exclude particles having diameters greater than 15 μm, two grease-coated Mylar impaction stages with cutpoints of 3.0 and 0.5 μm respectively, and a 3-μm Ghia Teflon final filter for the remaining particles having diameters less than 0.5 μm. Sampling was performed 7 hours per day, between 2200 and 0500 LST, for a duration of 8 days. Limiting sampling to only these hours, which correspond to downslope winds, should normally result in the sampled particles being of mid-tropospheric origin and not locally generated. Since the sampler was triggered by time rather than wind direction, the possibility does exist that particles of local origin were sampled during upslope flows. The 8-day sampling period was chosen to assure sufficient particle loadings for elemental analysis.

5.5.3 Results and Discussion

The period between 5 May and 25 August 1981 was analyzed and appears to include a dust transport episode at MLO followed by a period without significant concentrations of soil-related particles. The period between 12 May and 8 June was strongly influenced by Asian dust, 16 June-25 August was clean, and 5-11 May and 9-15 June were transition periods.

The characteristics of the dust transport episode were high concentrations of soil-related elements on the final filter stage (stage 3) and the second drum stage (stage 2). Also, low concentrations of Cl on the first drum stage (stage 1) were used to indicate whether the sampled aerosol was primarily of midtropospheric or local marine-layer origin. Both the relative concentrations and size distribution of the soil-related elements measured during the Asian-dust episode and the postdust period were significantly different on stages 2 and 3 for all soil-related elements.

Figure 72 shows the mean relative concentration and uncertainty for Si and S during the Asian-dust episode and the period following, which had little or no Asian-dust influence. During the dust episode the relative concentration of Si was increased significantly for stages 2 and 3, and the size distribution was shifted toward a greater mass in the smaller particle size ranges. Caution is advised, however, in interpreting fig. 72 in terms of size
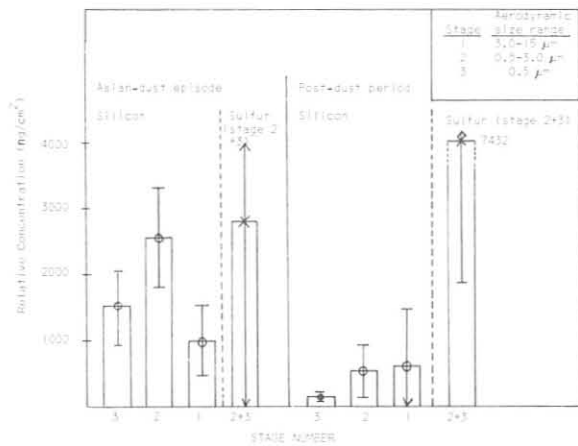
Figure 72.--Comparison of size-segregated Si and S during and after an Asian-dust episode.
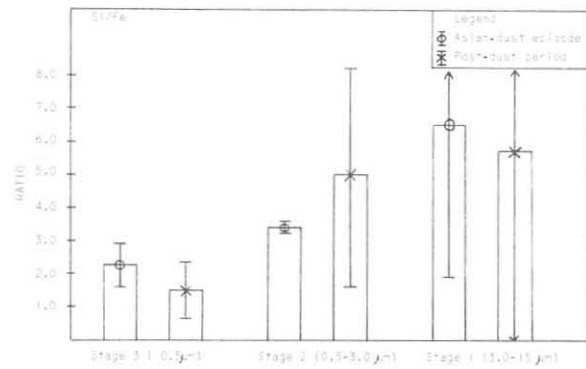
Figure 73.--Size-segregated ratio of Si to Fe during and after an Asian-dust episode.

distribution since some bounce-off between stages 2 and 3 did occur, as identified by scanning electron microscopy, because of the heavy particle loadings in duststorm periods. No statistically significant difference between the dust episode and the postdust period was found for concentrations of coarse soil particles (stage 1), nonsoil-related elements such as S, or the S size distribution. This is contrary to the findings of Darzi and Winchester (1982a) who found a direct relationship between increased concentration of soil-dust elements and increased S concentrations.

Various mean elemental ratios during the Asian-dust episode and the postdust period were calculated. Figure 73 shows the mean ratios and standard deviations of Si and Fe for both periods. During the Asian-dust episode, stage-2 ratios were very constant and were within the range of Si/Fe ratios of 3-4 for North China dust particles in the size range of 2-4 μm (Wang et al., 1982). During the postdust period the stage-2 Si/Fe ratio increased to a mean value of 5.0, which is the mean crustal Si/Fe ratio.

5.5.4 Conclusion

The measurement of size-segregated midtropospheric aerosols and subsequent elemental analysis by PIXE has permitted identification and characterization of soil dust transported from central and eastern Asia to MLO. The majority of the transported dust is in the size range of 0.5-3.0 μm aerodynamic diameter and is composed primarily of Si, Al, K, Ca, Ti, and Fe. Asian-dust episodes were identified by increased concentrations of soil-related elements on stages 2 and 3, and low concentrations of Cl (seasalt particles) on stage 1. Results indicated a shift toward higher concentrations of soil-related elements in the smaller size ranges and a nearly constant stage-2 Si/Fe ratio corresponding to that observed in North China for soil-dust particles of the same size range.

Acknowledgment

5.6 CO_2 and Other Air Chemistry Studies at Palmer Station

E. Robinson and W. L. Bamesberger
Laboratory for Atmospheric Research, College of Engineering
Washington State University, Pullman, WA 99164

The first year of operation of the air chemistry facility at Palmer Station, Anvers Island, Antarctica, was completed in February 1983, and some preliminary sampling results for CO_2 and other trace atmospheric constituents can be reported. A description of the station can be found in Robinson and Bamesberger (1982).

The air chemistry facility is used as a base for gathering CO_2 flask samples for analysis in the GMCC laboratories. In addition, gas-chromatographic instrumentation is operated to measure CO_2 and other trace constituents continuously. A Carle Model 211 automatic GC is used for CO_2 monitoring. The instrument is calibrated against standard CO_2-in-air mixtures that in turn have been given a preliminary standardization check by the GMCC CO_2 laboratory. Figure 74 shows weekly average CO_2 concentrations based on hourly samples from 6 February to 15 July 1982 and 15 December 1982 to 4 June 1983. The approximately 25-wk break in the continuous record was caused by a failure in the hydrogen generator for the automatic GC. During this period canister samples were collected at a frequency of about 2 mo^{-1} and subsequently analyzed at WSU. The CO_2 concentrations from the individual canisters are shown in fig. 74 and noted as "canisters."

The concentration trend in these data is clearly increasing by about 1.5 ppm yr^{-1}. The regression line for the ~16-mo period shown in fig. 74 is CO_2 (ppm) = 336.084 + 0.029X, where X is weeks since the week of 6 February 1982. In addition to the general upward trend, some shorter-period cycles also appear in the continuous data. In late March and early April 1982 there was a marked decrease in CO_2 concentrations, while late in the period covered there was a period of sharply increasing concentrations containing a clear cycle with about 1-1.5 months between maximum and minimum. Both the 1982 and 1983 shorter-term cycles occurred in about the same season, namely in late March and April. It should be emphasized that the calibrations used as a basis for these data are preliminary and will be rechecked against GMCC standards before final data are published.
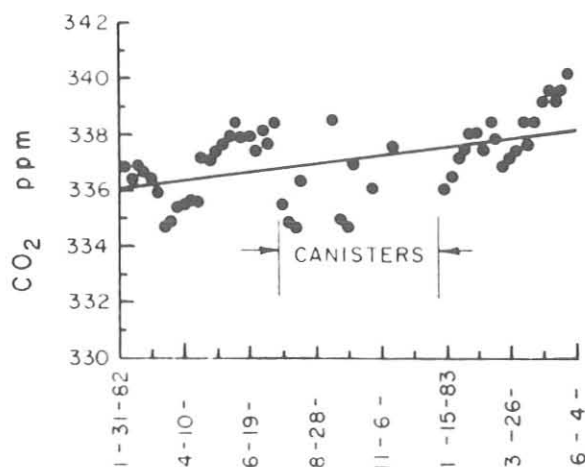
Figure 74.--Weekly average CO_2 concentrations at Palmer Station, based on automatic GC analyses except where individual canister samples are indicated.

Table 36.--Anvers Island, Palmer Station, trace atmospheric
constituent data, 1982 preliminary results

Constituent	Mean concentration December 1982	1982 annual trend
CFC-11	190.0 ppt	$+8.5$ ppt yr^{-1} (4.7%)
CFC-12	304.6 ppt	$+11.2$ ppt yr^{-1} (3.7%)
CH_3CCl_3	117.5 ppt	$+6.7$ ppt yr^{-1} (6.0%)
CCl_4	148.1 ppt	$+3.1$ ppt yr^{-1} (2.1%)
N_2O	300.9 ppb	$+4.37$ ppb yr^{-1} (1.5%)
CO_2	337.4 ppm	$+1.51$ ppm yr^{-1} (0.45%)
CH_4	1.50 ppm	Not available
CO	0.059 ppm	Not available

As mentioned above, other trace gas constituents in addition to CO_2 are
measured continuously at Palmer. Table 36 lists these compounds, the approxi-
mate average concentrations measured in December 1982, and the time trends ob-
served during the 1982 sampling period. It is important to note that all of
the constituents with anthropogenic sources, such as the halocarbons, show
upward annual trends. The trend for N_2O is also upward by about 1.5% yr^{-1}.
Even though this is primarily a biologically generated compound there is prob-
ably some perturbation of this constituent by agricultural operations and
large fuel combustion sources. However, an upward trend of this magnitude is
not typical of the data from other locations, and it will be given careful
study. The trends of the halocarbon concentrations, 3%-5% annually, are about
half the annual trends observed in Antarctic halocarbon samples taken in the
years 1975-1978 at McMurdo and SPO. Additional measurements showed the ap-
proximate annual range for O_3 concentration to be 10-30 ppb and for CN concen-
tration to be 20-1000 cm^{-3}.

5.7 Raman Study of Graphitic Carbon Concentrations in the Western Arctic

H. Rosen and T. Novakov
Lawrence Berkeley Laboratory
University of California, Berkeley, CA 94720

Recent studies at ground level in the Alaskan Arctic (Rahn and McCaffrey,
1980; Shaw, 1981; Rosen et al., 1981) show the presence of substantial concen-
trations of carbon- and sulfur-containing particles that seem to be character-
istic of the Arctic region as a whole (Barrie et al., 1981; Ottar, 1981;
Heintzenberg, 1980). These particles are effective scatterers and absorbers
of visible radiation (Rosen et al., 1981; Bodhaine et al., 1981) and appear to
be responsible for the phenomenon of Arctic haze first reported by Mitchell
(1957). On the basis of trace-element analysis, it has been suggested that
these particles originate from anthropogenic sources at midlatitudes (Rahn and
McCaffrey, 1980; Barrie et al., 1981). Direct substantiation of combustion-
generated particles in the Arctic atmosphere has been provided by the identi-
fication of large concentrations of graphitic carbon particles at BRW (Rosen
et al., 1981). These graphitic particles, which can only be produced from
high-temperature combustion processes, have been identified on a molecular
level using Raman spectroscopy. If one excludes natural burning processes

121

that are not expected to be a significant source during winter and spring when the Arctic haze is at a maximum, then one can attribute these graphitic particles directly to anthropogenic activities. These particles, which have large absorption cross sections (~ 10 m^2 g^{-1}) in the solar spectral region, can lead to significant heating effects (Shaw and Stamnes, 1980; Porch and MacCracken, 1982; Cess, 1983). The magnitude of these effects largely depends on the vertical and horizontal distributions of the graphitic particles as well as their concentrations as a function of time of year.

This paper reports on an extension of these studies of carbon particles in the Alaskan Arctic to the Canadian and the Norwegian Arctic. These studies, using the Raman scattering technique, identify substantial concentrations of graphitic-carbon particles at ground-level stations throughout the western Arctic. Results show that the large concentrations of graphitic particles found at BRW do not constitute a local phenomenon but are characteristic of ground-level stations throughout the western Arctic.

The Raman spectra are obtained directly from aerosol particles collected on various filter media without any pretreatment procedures. These spectra are superimposed on a large fluorescent background, which is due both to the filter media and the highly fluorescent material in the sample. Irradiation of the sample with an argon laser for 24 hours reduced this background by about an order of magnitude. The intensity of the Raman spectra was typically about 1% of the fluorescent background. Aerosol samples were obtained from six Arctic sites: BRW in the Alaskan Arctic; Mould Bay, Igloolik, and Alert in the Canadian Arctic; and Bear Island and Spitzbergen in the Norwegian Arctic. The samples from the Alaskan Arctic were collected on prefired quartz-fiber filters (Pallflex 2500 QAO) with a sampler installed at BRW in cooperation with B. Bodhaine of the GMCC program. The samples from the Canadian and Norwegian Arctic were collected on Whatman 41 filters and were provided respectively by L. Barrie of AES and B. Ottar of NIAR.

Raman scattering and IR absorption spectroscopy are complementary techniques that measure vibrational spectra of gases, liquids, and solids. Often vibrational modes that are IR inactive are Raman active and vice versa. Graphitic structures in which trivalent carbon atoms occupy lattice sites in a two-dimensional hexagonal honeycomb network have intense Raman modes but very weak IR vibrational spectra. These Raman modes, which were first observed by Tuinstra and Koenig (1970), enable the identification of graphitic structures even in the presence of a complex mixture of substances. Solvent extraction, heat treatment, optical absorption, and morphology studies (Wolff and Klimisch, 1982) can provide indirect evidence for a graphitic component, but Raman spectroscopy appears to be the only presently available method for making unambiguous identifications on a molecular level.

The Raman scattering technique has been applied to identify substantial concentrations of graphitic particles in combustion effluents, urban air (Rosen et al., 1978, 1980), and the Alaskan Arctic at BRW (Rosen et al., 1981). The spectra from these samples show the presence of two Raman modes located at ~ 1350 and 1600 cm^{-1} that are caused by phonons propagating within graphitic planes (Tuinstra and Koenig, 1970). In fig. 75 these measurements are extended to samples collected from three sites in the Canadian Arctic (Alert, Igloolik, and Mould Bay) and two sites in the Norwegian Arctic (Spitzbergen and Bear Island). All samples were collected at similar times of the year, but due to sample availability, some samples are from 1980 and
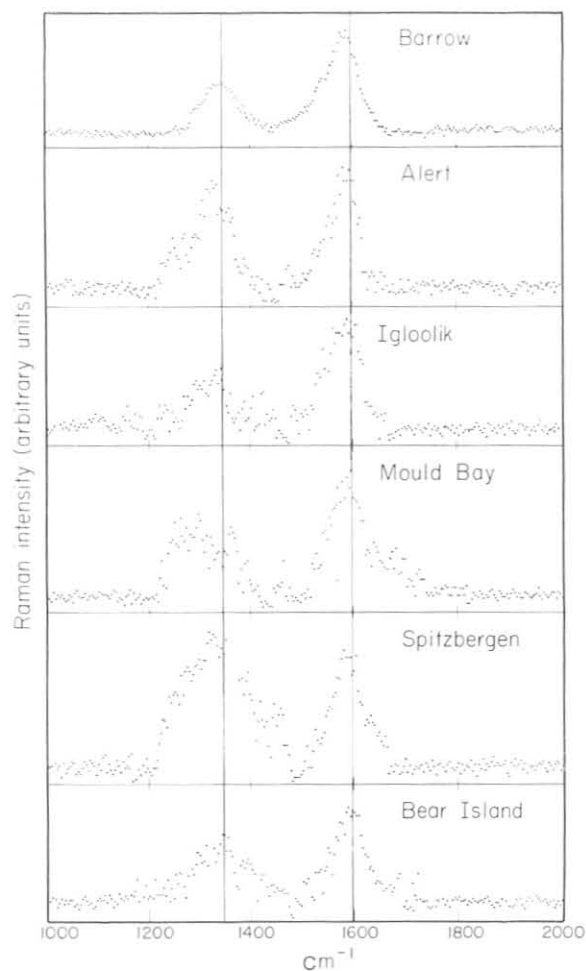
Figure 75.--Raman spectra of particles collected in the Alaskan Arctic (Barrow, 23-28 Jan 1980) compared with samples collected in the Canadian Arctic (Alert, 20-26 Jan 1981; Igloolik, 26 Jan-3 Feb 1981; Mould Bay, 26 Jan-2 Feb 1981) and the Norwegian Arctic (Spitzbergen, 21-23 Jan 1980; Bear Island 28-30 Jan 1980).

others from 1981. It is clear from the spectra that all sites show the presence of significant concentrations of graphitic particles. There are some differences in the relative intensities and line shapes of the two Raman modes, but these could be due to systematic errors in fluorescence subtraction for the 1350 cm^{-1} mode, which is located on a highly sloping background. If one assumes fixed optical constants (Raman cross sections, absorption cross sections), one can use the integrated intensity of the 1600 cm^{-1} Raman mode as a measure of the relative concentrations of graphitic particles at the sites. These analyses indicate that the concentrations at all the sites are quite comparable, with the largest and smallest within about a factor of 3 of each other. The relative ordering of these concentrations for Spitzbergen, Bear Island, BRW, Mould Bay, Alert, and Igloolik are 2.1, 1.7, 1.0, 0.8, 0.8, and 0.7. It should be emphasized that this analysis is for a particular time interval, and the relative contributions could vary considerably from one time period to the next.

Acknowledgments

5.8 Ultraviolet Erythema Global Measuring Network

D. Berger
Skin and Cancer Hospital, Temple University
Philadelphia, PA 19140

The global network of meters has been recording the half-hourly dose of sunburning (erythema) UV solar radiation since 1973. The number of stations has increased from 30 in the past years to 40 this year. Three of these meters are located at BRW, MLO, and SMO.

Meter response correlates not only with erythema but with DNA damage, vitamin D synthesis, nonmelanoma skin cancers, tobacco-leaf spotting, egg mortality of some fish species, sewage-water purification, and various plant stresses. In seven U.S. communities the meter is being used to educate the public about skin cancer risk by publicizing in the local media the daily erythema intensity. A report on the results from 14 of the longest running stations was published by Berger and Urbach (1982). The absolute radiant energy of the meter was measured by DeLuisi and Harris (1983). Data from this network are distributed by NOAA/ARL, 6010 Executive Blvd., Rockville, MD 20852.

5.9 Aerosol Concentration Periodicity and Optimum Sampling Strategy at MLO

M. Darzi and J. W. Winchester
Department of Oceanography, Florida State University
Tallahassee, FL 32306

5.9.1 Introduction

The location and high altitude of MLO, as well as of HVO and other sites on the island of Hawaii, are ideally suited for monitoring aerosol constituents in the midtroposphere. Since 1980 several reports have shown that dust transport from Asia to Hawaii is a regular spring occurrence, bringing soil mineral particles, and possibly sulfur (S) and other anthropogenic pollutants, not only to the 3.4-km MLO site but to the lower, 1.2-km HVO site as well. Most investigators have considered that the successful measurement or sampling of aerosol that has been transported from afar should guard against interference from aerosol particles that may be of local island origin, e.g., by simply avoiding upslope wind conditions that could carry locally derived aerosol from lower elevations to the sampling site. However, apparently it is not generally understood that such a discrimination may bias the sampling of the long-range-transported aerosol constituents, resulting in misleading information, for example concerning their mean maximum concentrations and important short-term periodicities (Darzi and Winchester, 1983).

A diurnal sampling strategy, based on local meteorological conditions, for example, daily upslope-downslope wind shifts, or on time of day, has often been employed to avoid local aerosol components (e.g., Simpson, 1972; Bigg, 1977; Dittenhoefer, 1982; Parrington et al., 1983b). For weekly average samples, nighttime downslope airflow sampling periods have been composited. However, such a strategy may lead to aliasing, an alteration of the apparent periodicities, within the time-series record of concentration for the long-range components if they should be periodic but not diurnal. Not only may it result

in an incorrect assessment of the mean maximum concentrations of these compo-
nents, for example, terrestrial dust and air pollution S of Asian origin, but
some potentially important linkages between them may be obscured if they
should exhibit similar short-term periodicities.

5.9.2 Nondiurnal Periodicity of Spring Aerosol Concentrations at MLO

Several investigators have now established, on the basis of physical and
chemical measurements of aerosol concentrations, that spring dust concentra-
tions at MLO are mainly of Asian origin. During this season, dust storms of-
ten occur over Japan. Over Hawaii, haze layers can be observed, aerosol light
scattering exceeds that of other seasons, and dust composition resembles that
of continental rather than island basaltic material. Air trajectory calcula-
tions suggest that arid lands of China are the most probable source. Darzi
and Winchester (1982a) have determined that this dust exhibits a regularity of
fluctuation in concentration that is shorter than diurnal, a periodicity that
cannot be caused by local meteorological effects, which on Hawaii are gener-
ally strongly diurnal. This pattern is distinct from what has been observed
(Darzi and Winchester, 1982c) at the lower elevation HVO where concentration
maxima average 24 hours apart during the same spring period of observation,
and can be attributed to daily changes in winds.

A comparison of these two simultaneous sets of measurements is shown in
fig. 76. In neither case are volcanic emissions important contributors to the
soil elements determined (Darzi and Winchester, 1982d), but instead surface
dust from weathered Hawaiian volcanic rock is the dominant component during
daily maxima at HVO, and surface dust from a continental source, apparently
Asia, is dominant during MLO concentration maxima, peaks that occur on the
average about every 21 hours. This periodicity, apparent by inspection of
fig. 76, is also determined to be statistically significant by time-series
analysis of the concentration measurements into Fourier components. A similar
nondiurnal periodicity is found in the NOAA record of hourly light-scattering
measurements made concurrently by a nephelometer (Darzi and Winchester, 1982b).
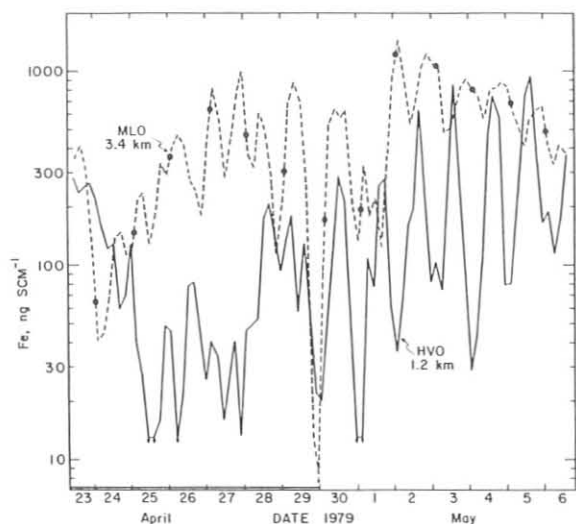
Figure 76.--Fe concentrations (ng
SCM^{-1}) for 3.7-h sampling time steps
for aerosols collected concurrently
at MLO and HVO. Days having ≥ 1.3 mm
of total rainfall at HVO are indi-
cated by the bar at the bottom.
Dots on the MLO curve are Fe concen-
trations at 0200 LST. The figure
illustrates the strongly diurnal
variation of Fe at HVO, especially
during nonrainy days, and the regu-
lar but less than 24-h variation of
Fe at MLO during an Asian dust epi-
sode (Darzi and Winchester, 1982c).

125

By time-series analysis, light scattering at 850 nm was found to be strongly coherent with iron (Fe) concentration, but less so with aerosol S concentration; however, at 450 nm the coherence is stronger with S than with Fe, suggesting that S occurs in smaller particle sizes (by oxidation of gaseous sulfur dioxide) than does dispersed soil aerosol containing Fe. Coherence of either element, however, is much weaker with CN concentration, implying that the CN measurement is not as useful an indicator of aerosol mass concentrations during spring at MLO as is light scattering. The observed concentration fluctuations of S are more complex than those of Fe, but time-series analysis shows a 21-h period to be present, and a 24-h period is not found, suggesting causes of the variations in S to be principally outside the influence of local meteorological processes on Hawaii.

At the 21-h period a strong coherency between Fe and S is found, suggesting that both vary in part because of similar meteorological processes remote from Hawaii, e.g. over the Asian mainland, where their principal source locations may not be far from each other, as well as during their transport over the Pacific. Possibly both dust, containing Fe and other soil elements, and air pollution, containing S and other constituents, are transferred from their sources to the midtroposphere and transported above the boundary layer to Hawaii. If initially diurnal pulses of aerosol are transferred upward over the source areas into horizontally moving air with wind speed convergence, a shortening on the order of 1% per day of travel from Asia would be required to account for the observed average times between arrival of the pulses at Hawaii. Thus, the periodicities in the time-series records of concentration, as well as the concentrations themselves, are of value in inferring the sources and long-range transport of these aerosol constituents.

5.9.3 Considerations for Aerosol Sampling Strategy

It should be clear from the above discussion that the sampling strategy is of great importance when sampling the long-range transported components at MLO since the strategy chosen will have a bearing on the interpretation of results. In particular, a diurnal sampling strategy can lead to a serious loss of information when only the nighttime samples are examined in the belief that they are more representative of the free troposphere and that aerosol concentration variations during the spring are similar to other seasons. Important information on the maximum concentration of Asian dust, for example, would be lost since our results show that Asian-dust maxima may be as likely to occur during the day in the spring when this component dominates at all times. During spring, therefore, both day and night samples may be of equal interest.

The imposition of a diurnal sampling strategy on an aerosol whose major variations occur with a period of less than 24 hours (or, more generally, twice the sampling interval) gives rise to the problem of aliasing, causing a distortion of the apparent periodicities of the concentration time series. For example, during the MLO dust event of 23 April-6 May 1979 shown in fig. 76, an examination of samples taken only at night causes a false 7-day periodicity, $1/(1/21 - 1/24) = 168$ cycle^{-1}, from the dominant 21-h period of the actual record. We plotted points on the MLO curve at 0200 LST of each day to illustrate how this transformation to a longer periodicity occurs. A curve drawn through those points would convey the impression that synoptic events, which also act in periods of approximately 7 days, were mainly responsible for

the variation in the concentration of the Asian dust. Moreover, a diurnal sampling rate would not have allowed the strong coherency of S and crustal elements at 21 hours to have been observed. It was this coherency that suggested to us that S sampled at MLO during this period had probably originated in Asia and had been transported to Hawaii together with the desert dust. A real periodicity of about 7 days may be present in springtime aerosol concentration variations at MLO, as suggested by fig. 76. However, aliasing would introduce an additional apparent 7-day period if 24-h sampling strategy is used with 21-h periodic concentrations.

As a result of these considerations, detection limits permitting, investigators are strongly urged to use a sampling period as small as possible and not more than 8 hours when studying Asian dust during the spring at MLO. If a longer period is used, not only does loss of information on the variations of the sampled species occur, but also erroneous longer-term variations may be induced. Consequently, the sampling time interval should be carefully considered by anyone collecting data on atmospheric species as a time trend.

5.10   Chemical Analyses of Atmospheric Particulates at MLO and SPO

J. R. Parrington, G. Tuncel, C. M. Thompson, and W. H. Zoller
Department of Chemistry, University of Maryland
College Park, MD 20742

5.10.1   Introduction

In February 1979, the first version of a selective sampling system was installed at MLO. Two 24-h timers controlled the sampling pumps for upslope samples during 0800-1800 LST and for downslope samples during 2100-0500 LST. To facilitate the collection of atmospheric particles at MLO, an improved and more versatile sector controller was designed and constructed as a joint project between the University of Maryland and NBS (Parrington et al., 1983a). The decision to sample is based on wind direction, wind speed, time of day, and CN concentration. To differentiate between upslope and downslope winds, the parameter controls were duplicated to provide two independent sampling sectors, downslope and upslope. A third case exists when neither sector is being sampled. In this case, an additional circuit is activated, allowing collection of samples that could contain valuable information about aerosols at MLO during storms or contamination episodes. The new system began operation at MLO in April 1980, and by the end of August 1980, the system appeared to operate reliably. Samples were collected every 10 days on three high-volume filters for subsequent chemical analysis.

5.10.2   Results

Concentrations observed for particulate samples are given in table 37 for four classes: downslope clean season, downslope dust season, upslope clean season, and upslope dust season. The clean and dust seasons are identified by a ten-fold increase in crustal material that is transported throughout the Pacific from Asian deserts between mid-February and July (a 19-wk period) for 1979-1982. Geometric means are used in table 37 because the distribution of Al (and nearly all other elements) is apparently log normal during both the clean and dust seasons at MLO.

Table 37.--Geometric mean concentrations of elements measured on downslope and upslope particle filters during clean (July to mid-February) and dust (mid-February to July) seasons at MLO from February 1979-June 1982*

Element (units)	Downslope Clean		Downslope Dust		Upslope Clean		Upslope Dust	
Na (ng)	6.6	(2.7)	22	(2.0)	86	(2.2)	140	(1.9)
Mg (ng)	2.6	(2.1)	26	(2.5)	14.2	(2.1)	45	(2.0)
Al (ng)	4.9	(2.1)	56	(2.5)	16.0	(2.2)	73	(2.5)
S (ng)	80	(2.0)	160	(1.7)	150	(1.8)	230	(1.7)
Cl (ng)	2.4	(4.0)	3.4	(3.0)	19	(4.2)	30	(5.0)
K (ng)	2.8	(1.8)	27	(2.3)	10	(1.9)	41	(1.9)
Ca (ng)	3.7	(2.5)	64	(3.0)	13	(2.2)	83	(2.7)
Sc (pg)	1.2	(2.2)	12.9	(2.6)	3.9	(2.1)	15.3	(2.1)
Ti (ng)	0.53	(2.6)	4.3	(2.4)	2.4	(2.5)	7.3	(2.2)
V (pg)	10.5	(2.5)	104	(2.4)	48	(2.2)	157	(2.2)
Mn (pg)	62	(2.3)	810	(2.5)	280	(2.2)	1300	(2.4)
Fe (ng)	4.0	(2.3)	42	(2.6)	15.5	(2.2)	52	(2.3)
Co (pg)	3.2	(2.6)	20	(2.4)	9.0	(2.7)	30	(2.2)
Cu (ng)	0.22	(5.0)	0.85	(3.0)	0.33	(4.0)	0.6	(3.0)
Zn (pg)	90	(4.0)	320	(2.2)	250	(3.0)	700	(3.0)
Ga (pg)	8.4	(4.0)	20	(2.5)	22	(2.7)	42	(2.0)
As (pg)	12.6	(2.9)	70	(4.0)	39	(2.5)	111	(3.0)
Se (pg)	11.2	(2.0)	21	(1.7)	22	(1.7)	36	(1.7)
Br (ng)†	1.45 ± 0.60		1.60 ± 0.45		1.63 ± 0.50		1.92 ± 0.90	
Rb (pg)	15.5	(0.19)	130	(2.5)	21	(2.5)	150	(2.0)
Sr (ng)	0.24	(3.0)	0.62	(2.6)	0.28	(1.8)	0.72	(2.1)
Ag (pg)	1.36	(3.1)	1.8	(2.7)	2.8	(3.5)	2.8	(4.0)
Sb (pg)	1.85	(0.26)	7.7	(2.4)	4.6	(2.4)	9.7	(1.9)
I (ng)†	2.1 ± 1.3		1.45 ± 0.60		2.2 ± 0.80		2.3 ± 0.60	
Cs (pg)	0.95	(2.6)	9.9	(2.8)	1.05	(3.0)	11.1	(2.5)
Ba (ng)	0.51	(4.0)	1.05	(2.1)	0.42	(2.7)	1.14	(3.0)
La (pg)	3.0	(2.3)	53	(3.3)	11.8	(2.2)	66	(2.5)
Ce (pg)	7.8	(2.3)	71	(2.5)	31	(2.5)	107	(2.6)
Sm (pg)	0.52	(2.8)	7.0	(2.7)	2.0	(2.6)	10.1	(3.0)
Eu (pg)	0.19	(2.5)	1.19	(2.4)	0.65	(2.2)	1.54	(2.4)
Tb (pg)	0.20	(2.5)	0.96	(2.6)	0.41	(2.1)	1.12	(2.0)
Yb (pg)	1.10	(2.1)	3.2	(2.2)	1.55	(2.0)	4.0	(2.0)
Lu (pg)	0.36	(3.1)	0.51	(3.0)	0.48	(3.0)	0.85	(2.0)
Hf (pg)	0.44	(2.1)	3.3	(2.5)	1.7	(2.5)	5.4	(2.2)
Ta (pg)	0.23	(2.3)	0.86	(3.0)	0.58	(2.5)	1.54	(1.7)
W (pg)	2.7	(3.3)	6.0	(4.0)	12.7	(4.0)	17	(1.7)
Au (pg)	0.15	(3.0)	0.24	(4.5)	0.28	(3.5)	0.37	(2.5)
Th (pg)	0.80	(2.6)	11.4	(3.0)	1.8	(2.8)	12.7	(2.6)

*Geometric standard deviations for elemental concentrations are shown in parentheses.
†Normal means and standard deviations expressed for Br and I.

Another method of presenting the data is by comparison of the relative elemental abundances in the sample to those of an average crustal source such as Taylor's crustal average (Taylor, 1964). In this way it is possible to note which elements have abundances similar to crustal material and, thus, probably originate from crustal sources. The crustal enrichment factor EF_c can be calculated from

$$EF_c = \frac{(X/Al)_{sample}}{(X/Al)_{crust}} \quad ,$$

where X is the element of interest and Al is the reference element. Al is used because it is easily analyzed, has known abundances in several crustal materials with few other sources, and is commonly used in this type of calculation. Figure 77 presents downslope and upslope EF_c during the clean season. An element having an EF_c of unity occurs in the same relative abundance in the sample as in the reference soil. However, deviations are typical because of variations in soil composition and elemental fractionation during mobilization and transport. Thus, an EF_c range of about 0.7-5 may be considered to be typical for an element that originates primarily from crustal sources.

As can be seen in fig. 77, most elements, Se through Lu, appear to be primarily crustal in origin. Variations in the upslope and downslope EF_c values may be due to crustal source variations or contributions from additional sources. For example, marine sea salt is known to be about a factor of 18 higher in upslope samples than in downslope samples. This source contains significant concentrations of Na, Mg, K, and Ca, which are reflected by the higher upslope EF_c for these elements. Another example is Hawaiian basalt, which averages a factor of 5.4 higher in concentration in upslope samples. This material exhibits slight enrichments of Sc, Ti, V, Mn, and Fe, and depletions of Cs, Rb, and Th, all of which appear to affect the relative EF_c's of
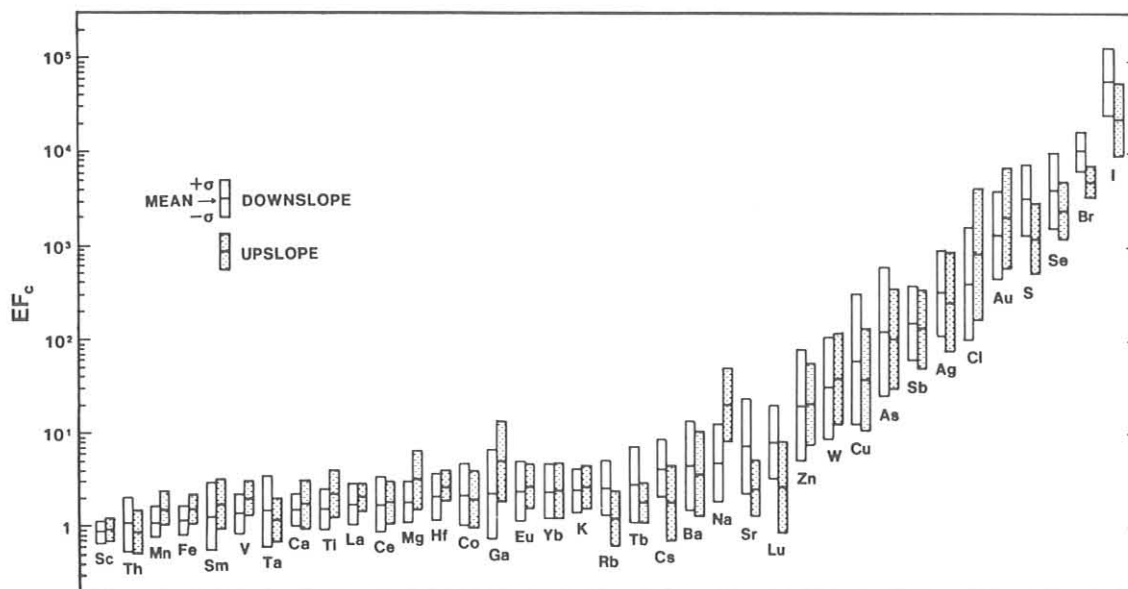
Figure 77.--Downslope and upslope crustal enrichment factors calculated for elements in clean-season atmospheric particulate samples at MLO.

upslope elements in fig. 77. The anomalously enriched elements apparent in this figure are S, Cl, Cu, Zn, As, Se, Br, Ag, Sb, I, W, and Au. Sea salt can directly account for only a small amount of the S, Br, and I, so there remain additional sources for these elements related to natural enrichment from the ocean.

The effectiveness of the separation of upslope and downslope aerosols can be assessed by comparison of marine components in the samples. The marine component can be calculated based upon excess sodium from

$$Na_s = Na_T - 0.0158 \; C,$$

where Na_s is marine Na, Na_T is the measured total concentration of Na on a sample, C is the mass of crustal material in the sample, and 0.0158 is the estimated fraction of Na in average Asian dust (Parrington and Zoller, 1983a). The mass of crustal material in a sample is estimated based on the airborne concentrations of eight typical crustal elements (Al, Sc, Ti, V, Mn, Fe, Sm, and Th) and their concentrations in average Asian dust. Figure 78 is a plot of upslope and downslope marine Na determined in this manner. Upslope sampling was stopped after March 1982 to reduce the number of samples to be analyzed.

The most striking feature of fig. 78 is the large amount of marine Na in upslope winds compared with downslope conditions. If this difference is expressed as a ratio of the upslope-to-downslope marine Na concentrations, the ratio should reflect the efficiency with which the mountain winds have been separated by the sampling conditions. The geometric mean of the ratio of upslope to downslope data for samples collected under the time-of-day controller (prior to May 1980) is 14 (σ_g = 4.1, where σ_g is the geometric standard deviation). The mean ratio increases to 21 (σ_g = 4.1) with addition of the digital sector controller, indicating that the newer system indeed provides a better separation of upslope and downslope particles than the time-of-day method above does. In general, peaks in upslope marine Na correlate with storm activity; however, the influence of storm activity on downslope marine Na is much weaker, with only strong storms of long duration (~5 days) appearing to be capable of sufficient tropospheric mixing to add much marine Na to the midtroposphere and hence to the downslope samples.
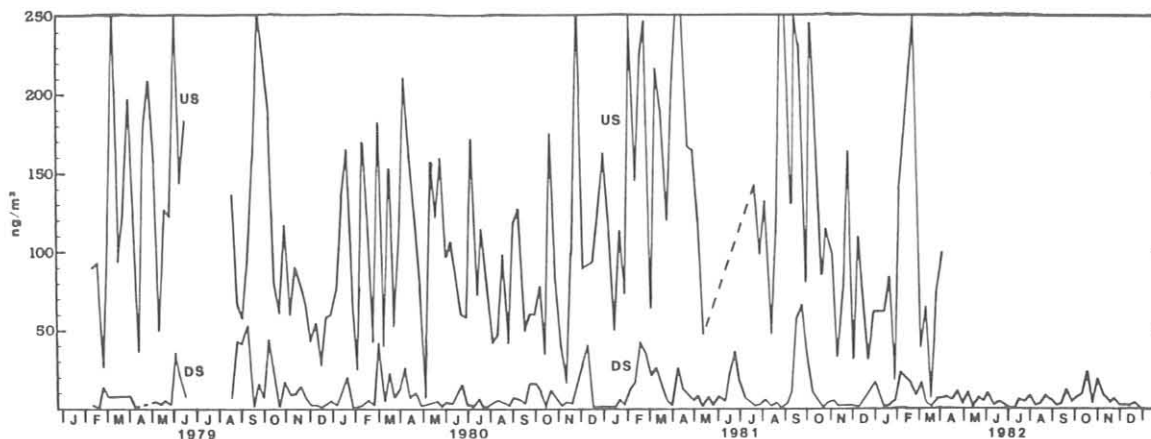
Figure 78.--Upslope (US) and downslope (DS) marine Na at MLO.

Figure 79 is a plot of the upslope and downslope estimated crustal masses from February 1979 through 1982. The influxes of Asian dust from mid-February to July of each year are clearly evident in both the upslope and downslope traces of this figure. In general, upslope concentrations are larger than downslope concentrations, especially during the clean periods (July to mid-February). During dust occurrences, downslope and upslope concentrations usually peak at similar times, as clearly shown in May 1979, February-June 1980, and March 1981. The average of all the upslope-to-downslope concentration ratios for crustal material again appears to be log-normally distributed with a geometric mean of 2.4 (σ_g = 2.8).

To determine if the higher mass of crustal material found in upslope particles originates from local Hawaiian material, a chemical element balance of the samples was made (Gordon, 1980). Accounted for in this balance were the compositions of various groups of airborne particles as a linear combination of the compositions of four source materials: Hawaiian basalt (Gladney and Goode, 1981), average crustal material (Taylor, 1964), average Asian-dust composition (Parrington and Zoller, 1983a), and a marine component. Results of these balances are summarized in table 38. Quantities of Hawaiian basalt were nearly the same for the clean and dust data sets in both downslope and upslope winds; however, the upslope concentrations exhibited about 5 times as much local basalt as the downslope concentrations.

During periods of high dust loading, downslope crustal particles consist of 93% Asian dust, and upslope crustal particles are 83% Asian dust-type material. From the results of similar balances on individual filters, the geometric mean mass of local basalt is 15 ng m^{-3} (σ_g = 3.3) in downslope winds vs. 87 ng m^{-3} (σ_g = 2.7) in upslope winds (Parrington and Zoller, 1983b). After removal of the local crustal component, the average upslope-downslope crustal ratio drops from the previous value of 2.4 to 2.2 (σ_g = 2.5). This ratio should be representative of crustal material transported from large continental sources, i.e., Asia or North America, to Hawaii. During the dust period, the upslope-downslope ratio of continental material drops to 1.2 (σ_g = 1.7), suggesting that this material is distributed with about an equal probability in the troposphere at the altitudes from which downslope and upslope winds originate (~4 and 2 km, respectively). Similar observations were
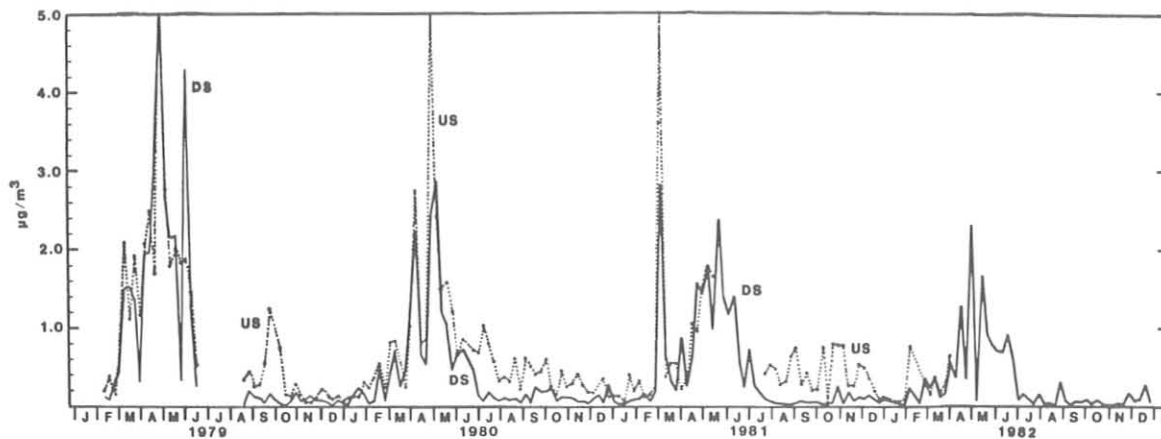
Figure 79.--Upslope (US) and downslope (DS) total estimated crustal masses at MLO.

Table 38.--Downslope and upslope components in MLO samples and
geometric mean concentrations of all individual samples*

Component	Downslope Mass (ng m^{-3})		Upslope Mass (ng m^{-3})	
	Clean†	Dust§	Clean†	Dust§
Sulfate**	240 (2.1)	480 (1.7)	450 (1.8)	640 (1.8)
Marine	16 (3.0)	22 (3.5)	250 (2.5)	320 (2.2)
Continental Crust	50 (2.2)	730 (2.4)	160 (2.2)	870 (2.4)
Hawaiian Basalt	13 (3.1)	25 (3.3)	82 (2.6)	115 (2.7)

*Geometric standard deviations are in parentheses.
†Samples collected July to mid-February.
§Samples collected mid-February through June.
**Total sulfate concentrations shown.

noted by Prospero et al. (1981) in reference to long-range transport of Saharan dust across the Atlantic, where they found that Saharan dust became well-mixed throughout the troposphere, above the marine boundary layer, with some more stratified layers in existence after transport over several thousand kilometers.

A detailed examination of the chemistry of Asian dust episodes by Parrington and Zoller (1983a) between 1979 and 1982 reveals that, with the exception noted below, the composition is very uniform from year to year, suggestive of a single major source of this dust. Results of other studies of dust episodes in Alaska and Enewetak exhibit elemental compositions nearly identical to the MLO dust composition (Parrington and Zoller, 1983a). Thus, widespread dust throughout the Pacific basin each spring apparently comes from the same Asian source area (or areas).

During an 8-wk period, 20 March-13 May 1980, in the peak 1980 dust episodes, the composition of the dust changed. Several elements were enriched in this period, especially Sm, La, and As, and the distribution of several rare-earth elements, Ce, Eu, Tb, Yb, and Lu, was different from that of other crustal material observed at MLO. Thus, a different area could have been a significant source of dust over this period. Because no information is available on compositions of various desert sands or soils of China, this source area cannot be identified; however, air mass trajectories indicate the dust originated in China (Parrington and Zoller, 1983a). Further research on Asian dust episodes may include studies of the compositions and dust generation in the desert areas of China.

Parrington and Zoller (1983a) examined the possibility that dust from the source areas normally responsible for spring Asian dust episodes continued to dominate crustal material of cleaner periods at MLO. Significant differences were noted for several heavy elements, Rb, Hf, and Ta, and large differences for the enrichments of alkaline-earth elements. These data, together with major changes in the rare-earth distribution pattern, indicated a different source area for the clean-period crustal aerosol.

132

During May 1982, air was sampled with cascade impactors at MLO. The goal was to determine the size distribution of the Asian dust and atmospheric particles in the upper troposphere. Unfortunately, particle concentrations were unusually low during this period, about 1 μg m^{-3} (see fig. 79). Figure 80 is a plot of the percent Al per impactor stage vs. particle size. The vertical bars represent the standard deviations among five impactor sets collected during this period. Although the deviations are large, all of the impactors show a similar size distribution. Most of the mass is in the small-particle range, with the mass median diameter being 2.6 μm (for particles of unit density). The mass on the first stage of the impactor (16 μm) is probably due to local production of large particles.

The samples that were collected at SPO have also been analyzed by neutron activation analysis and some of the results are shown in figs. 81-83. Because many samples from Antarctica were contaminated, the quality of the data and the samples that were collected there are not as good as those from Hawaii. When obviously contaminated samples are removed from the data set, certain trends are easily observed. A plot of the average S concentration over the last few years is shown in fig. 81. From this plot it is obvious that the austral winter S values are lower than the summer values, and are usually about 20-30 ng m^{-3}. The summer values show more variability from year to year as well as within a year so that long-term trends are difficult to observe.

Concentrations of two volatile elements that are highly enriched in the Antarctic, As and Se, are plotted in figs. 82 and 83. Both elements are highly enriched in anthropogenic emissions, but the data from SPO suggest that they are of natural origin and their concentrations are not increasing. The very large increase in As during the winters of 1975 and 1976 was due to the injection of volcanic debris into the Antarctic stratosphere by a volcanic eruption. Since that time, the concentration has decreased and is remaining relatively constant. For Se, the volcanic impact is not as noticeable. An enhancement of both elements appears during the summer months when transport from continental areas causes an increase of crustal dust. No trends are evident at this time, but the data base is not of sufficient length to show long-term trends.
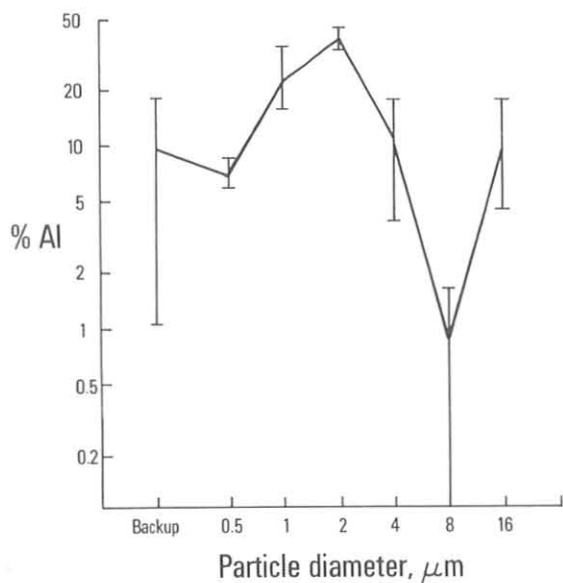
Figure 80.--Percent Al per impactor stage vs. particle size at MLO during the Asian-dust episodes (downslope conditions) on 7, 9, 15, 22, and 25 May 1982. The mass median diameter is 2.6 μm.

133
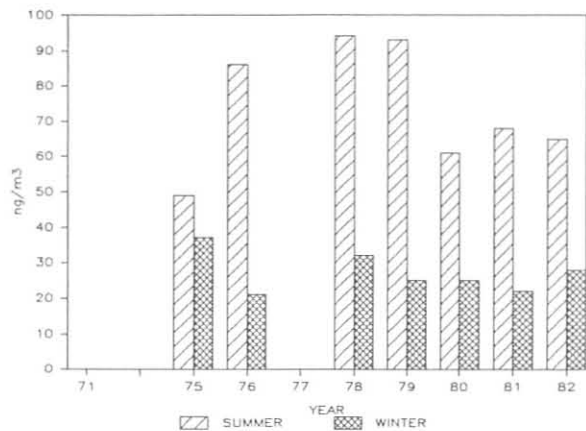
Figure 81.--Average S concentration observed at SPO.
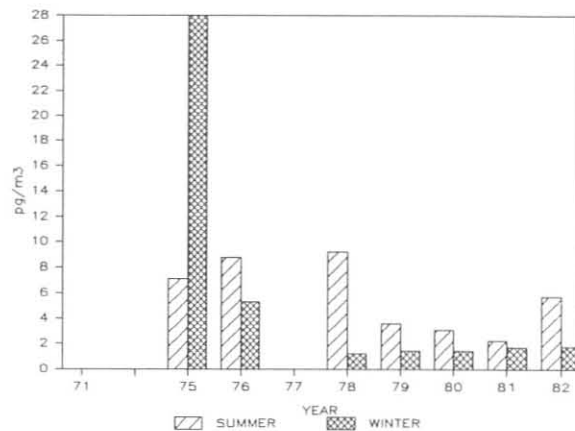
Figure 82.--Average As concentration observed at SPO.
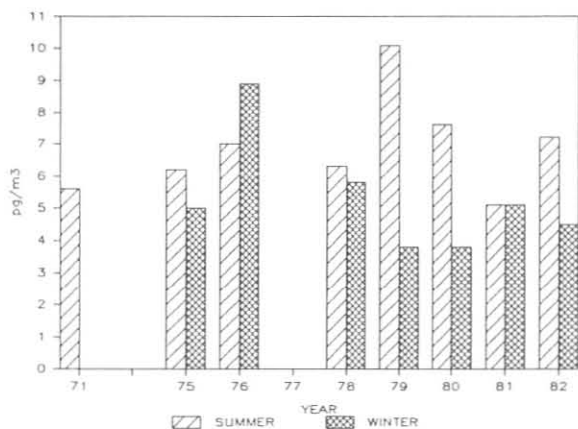
Figure 83.--Average Se concentration observed at SPO.

5.11 Electric Fields and Currents in the Vicinity of a Mountain

I. Tzur and R. G. Roble
National Center for Atmospheric Research, P.O. Box 3000
Boulder, CO 80307

Because the electric conductivity of the atmosphere increases almost exponentially with altitude, the Earth's orography can play an important role in the global electric circuit. In addition, the orography and its environment interact and produce local electric effects that are an integral part of the atmospheric electricity. The basic electrical parameters, namely the electric field, current, and ion conductivities, should be measured near mountain tops to avoid noise from air pollution, trees, buildings, and other local boundary layer disturbances. These electrical parameters depend on the altitude and geometry of the mountain and on atmospheric conditions like winds, clouds, aerosols, day-night variations, and solar events. To understand the atmospheric electric phenomena, the interaction between the electrical parameters and these environmental conditions should be studied. At MLO, electric field, current, and conductivity data are collected along with valuable data on weather and atmospheric conditions.

ELECTRIC POTENTIAL, LOG Φ (V)
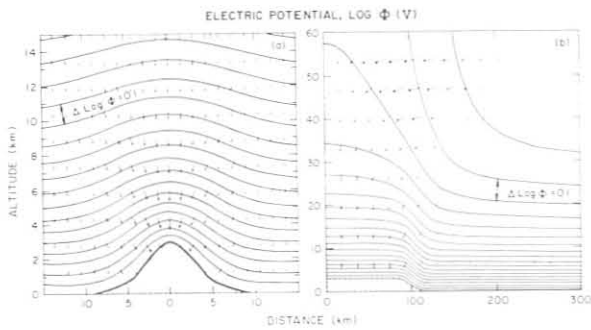
Figure 84.--Distribution of electric
potential and of current density
over (a) a mountain peak and (b) a
mountain plateau. The arrows indi-
cate direction and intensity of the
electric currents.

In this research, a numerical model was developed that calculates the
electric field and currents around various orographic features. The results
show that a mountain of a few kilometers in altitude, which extends in the
horizontal to about 40 km or less, can amplify significantly the electric
field and current near its top; however, on a global scale the mountain has
small effect. When the horizontal extent of the mountain is larger than about
50 km (Mauna Loa falls into this category), the current is increased at the
top of the mountain while relatively large vertical and horizontal currents
develop in the large scale. These results are demonstrated in fig. 84, which
shows the electric-potential contours and current distribution around a moun-
tain extending to about 20 km in the horizontal (fig. 84a) and a plateau ex-
tending to 100 km from its center (fig. 84b). The arrows represent the direc-
tion and intensity of the electric currents.

Figures 85a and 85b show the contours of the electric potential and cur-
rent for fair weather conditions, respectively, and figs. 85c and 85d show the
same parameters when a cloud is situated above the mountain top. The surface
electric field and currents for both cases are shown in figs. 86a and 86b.
The calculated increase in the current is in agreement with the data collected

ELECTRIC POTENTIAL, LOG Φ (V)   CONDUCTION CURRENT (10⁻¹²A/m²)
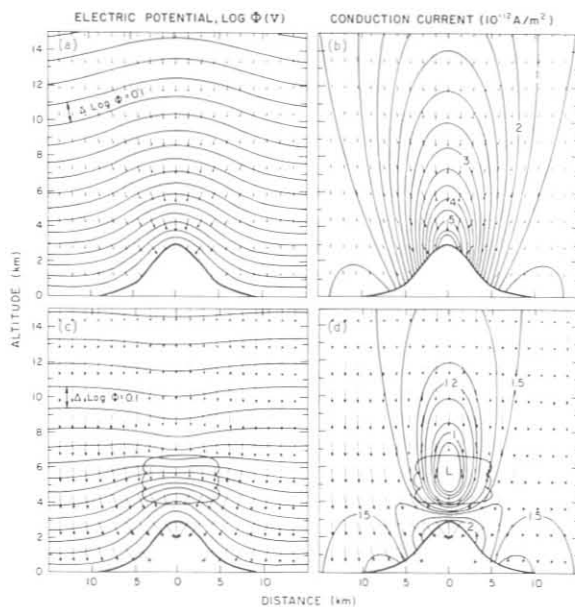
Figure 85.--Distribution of electric
potential and of current density
flow around a mountain peak for (a)
and (b) fair weather conditions, and
(c) and (d) when a cloud is situated
above the mountain peak.
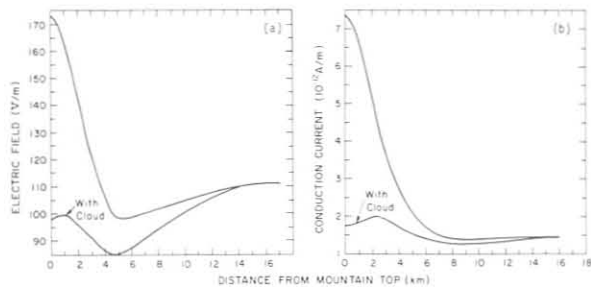
Figure 86.--(a) Surface electric field and (b) surface conduction current over a mountain peak for fair weather conditions and for when a cloud is situated above the mountain peak.

at MLO (Cobb, 1968). However, this research is in its beginning, and more detailed calculations of the Mauna Loa orography and atmospheric conditions must be done before further comparisons can be made.

Acknowledgment

5.12   Atmospheric Bromine in the Arctic

W. W. Berg and P. D. Sperry
National Center for Atmospheric Research
Boulder, CO 80307

K. A. Rahn
Graduate School of Oceanography
University of Rhode Island
Kingston, RI 02881

E. S. Gladney
Los Alamos National Laboratory
Los Alamos, NM 87545

5.12.1   Introduction

Because of the potential role that Br compounds may play in the stratospheric photochemistry of ozone (Wofsy et al., 1975; Yung et al., 1980), increased attention has been focused on this halogen and its movement through the troposphere. The geochemical pathways of Br-containing species from oceanic, biospheric, and anthropogenic sources have not been delineated. Mounting evidence suggests that a substantial fraction of the gaseous and particulate Br species found in the atmosphere has an oceanic source either directly from seawater or indirectly from organisms in seawater (Duce et al., 1965; Moyers and Duce, 1972; Lovelock, 1975; Rahn et al., 1976; Singh et al., 1977, 1983). Smaller anthropogenic sources have been identified and include the production of CH_3Br, used as a soil fumigant; tetrabromobisphenol-A, used as a flame retardant in printed-circuit boards; CF_3Br, used as a fire retardant and refrigerant; and $C_2H_4Br_2$, together with assorted brominated additives, used in automotive and other fossil fuels. The relative intensities of the various global sources of atmospheric Br compounds, however, remain largely unknown. In addition, recent stratospheric measurements (e.g., Sedlacek et al., 1979; Berg et al., 1980) have raised the possibility that one or more additional sources for atmospheric Br near the Earth's surface remain to be identified.

136
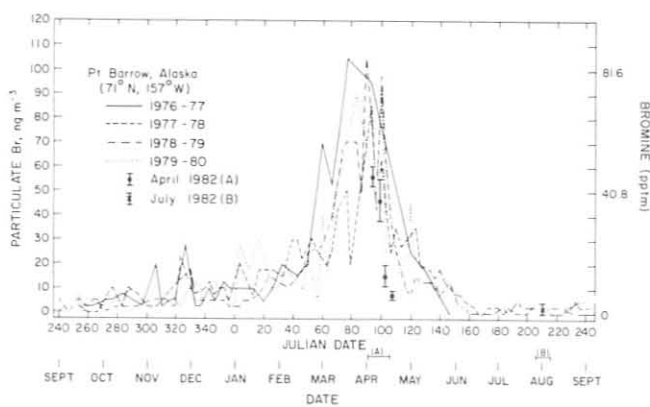
Figure 87.--Particulate Br content of the Arctic aerosol for 1976-1980 at BRW. This 4-yr data record represents a compilation of over 200 analyses. The points shown with the error bars (above A and B) correspond to the data presented in fig. 91. The conversion 1 ng SCM^{-1} = 0.816 pptm was used for the aerosol data.

5.12.2 Results

The results of our particulate Br measurements at BRW during 1976-1980 are shown in fig. 87. The inflection points in each curve represent a single measurement of the Br content in the Arctic aerosol. Over 200 data points were used to develop the Br aerosol plots shown in this figure. It is clear that during this 4-yr period the Br content in the Arctic aerosol increased an order of magnitude over the background aerosol values beginning every mid-February and continuing for a period of 3 months. The particulate Br content in the Arctic aerosol (Br$_p$) during the summer, fall, and winter months typically ranged at about 6 ± 4 ng SCM^{-1}. During the 3-mo Arctic spring period, however, the Br content of the aerosol reached over 100 ng SCM^{-1}, with typical values ranging near 65 ng SCM^{-1}.

Similar plots over the same 4-yr period are presented in figs. 88 and 89 for particulate Cl and I, respectively. Both of these halogens exhibit a distinctly different annual behavior compared with that of Br. During the 3-mo Br maximum, the Cl and I content in the Arctic aerosol show no significant change from typical background values measured throughout the year.

Since the BRW aerosol is strongly influenced by the Arctic Ocean and its adjacent seas, the Na content of the aerosol was also determined over the 1976-1980 period. Na is an especially valuable elemental index since it is
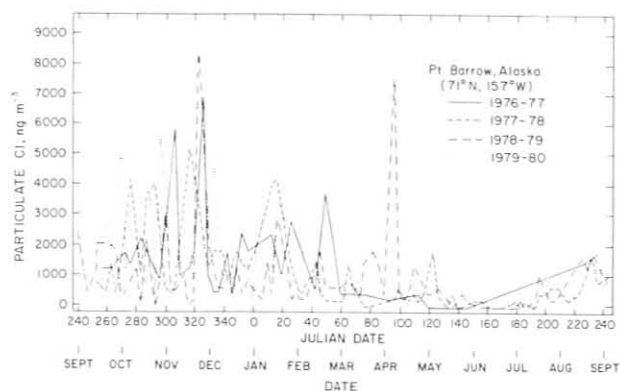
Figure 88.--Particulate Cl content of the Arctic aerosol for 1976-1980 at BRW.
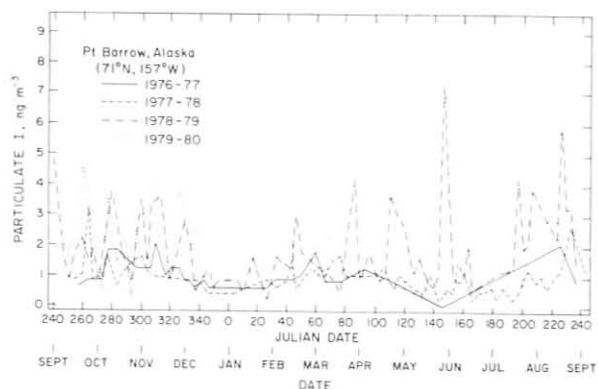

Figure 89.--Particulate I content of the Arctic aerosol from 1976-1980 at BRW.
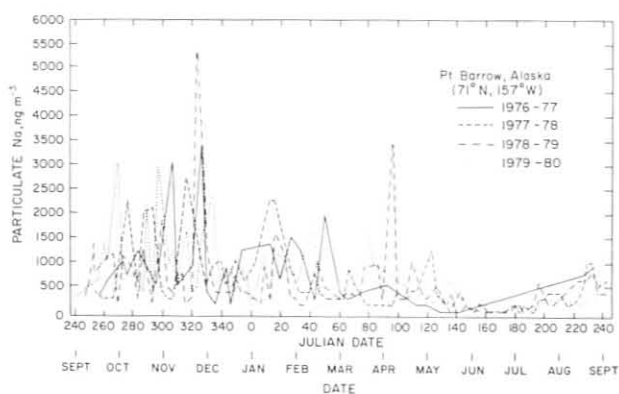
137

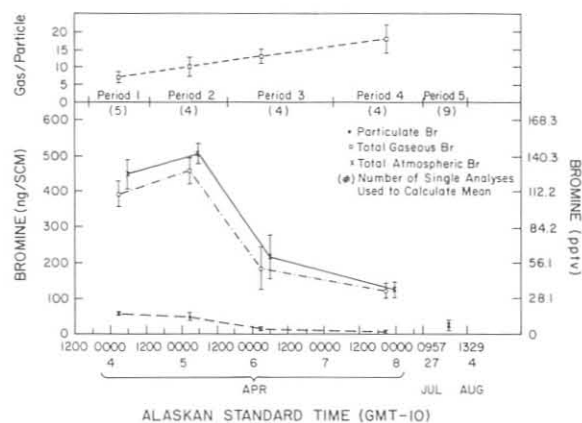Figure 90.--Particulate Na content of the Arctic aerosol from 1976-1980 at BRW.

Figure 91.--Gaseous and particulate Br data taken at BRW during April and July-August 1982. The error bars represent one standard deviation of the mean. The number of values included in the mean is shown in parentheses. The conversion 1 pptv Br = 3.565 ng SCM^{-1} was used.

known to cross the air-sea interface with no significant enrichment in the aerosol relative to seawater (Duce et al., 1972; Duce and Hoffman, 1976; Berg and Winchester, 1978). The annual variation of Na in the Arctic aerosol over this 4-yr period is shown in fig. 90. The dominant source for both Na and Cl in the Arctic aerosol at BRW most probably is the ocean. A detailed comparison, peak by peak, of the data in figs. 88 and 90 shows that these two elements are closely coupled.

The gaseous and particulate Br measurements made during April and July-August 1982 at BRW are shown in fig. 91. During periods 1 and 2 in April, total gas-phase Br levels (Br_g) averaged 422 ± 48 ng SCM^{-1} (118 ± 14 pptv) with a minimum value of 373 ng SCM^{-1} and a maximum value of 498 ng SCM^{-1}. Br_p averaged 52 ± 8 ng SCM^{-1} (42 ± 7 pptm) with total atmospheric Br levels (Br_{tot}) averaging 474 ± 49 ng SCM^{-1}. During periods 3 and 4, however, all Br values showed a marked decrease, with Br_p at 11 ± 5 ng SCM^{-1}, Br_g at 154 ± 54 ng SCM^{-1}, and Br_{tot} at 165 ± 54 ng SCM^{-1}. The samples taken in July-August 1982 (period 5) showed very little Br present, with the Br_{tot} level averaging 27 ± 14 ng SCM^{-1}.

For comparison, the Br_p data in fig. 91 have been plotted on the 4-yr particulate Br record shown in fig. 87. The mean values of each of the four sampling periods in April 1982 (above time line A in fig. 87) show clearly that the 1982 particulate Br data were not atypical for that time frame. The 15 February-15 May Br aerosol peak that was observed in the 4-yr data record of fig. 87 was also present in 1982 at approximately the same strength. The gaseous Br levels measured during April 1982 are also probably typical for this period. This conclusion is supported by the fact that the gas-to-particle ratios plotted in fig. 91, running from 7 to 18, are in the characteristic range for atmospheric Br.

138

To ensure that the unusual gas phase Br levels did not occur at other times during the year, data were also taken during July-August 1982 (period 5). As seen in fig. 87, this time frame represents a period in which the Arctic aerosol Br content is at a 3-mo sustained minimum. Figure 91 shows that the total atmospheric Br levels were, in fact, very low during this period. The corresponding Br_p levels, as expected, were also typically low for this period as shown in fig. 87 (above time line B). The possibility still remains, however, that other periods may exist during a normal Arctic year in which high levels of gaseous Br products are present in the Arctic troposphere. In view of the above data, however, this possibility seems remote.

5.12.3 Discussion

A significant source (or group of sources) must exist that is capable of supporting exceptionally high levels of Br in the Arctic troposphere for periods of approximately 3 months. The source term must exhibit a strong seasonal dependence. It is unlikely that the Br comes directly from bulk seawater. Other potential sources include (1) local contamination from power plant, oil well, or automotive emissions; (2) long-range transport, involving Br-containing gases and/or aerosols from anthropogenic sources possibly in eastern North America or from the Eurasian continent; (3) extraterrestrial input, entailing meteoric and other cosmic debris folding down from the low Arctic stratosphere; (4) natural terrestrial input, from the blooming of Arctic tundra or other flora; and (5) natural marine input, involving the production of brominated compounds in the water column, sea surface microlayer, or sea ice by various life forms including diatoms, dinoflagellates, and green, bluegreen, and red algae.

The 4-yr Br data record was clearly subject to potential local contamination since no control was exercised over the wind direction during sampling. However, only the 3-mo aerosol peak period is of concern here since it has been shown that during the rest of the year most of the Br appeared to be of marine origin. The data shown in fig. 91 were all taken during this 3-mo aerosol peak under rigorous clean-air sector-controlled conditions. During this peak Br episode (period 2), sampling was conducted entirely in the clean-air sector with winds from 60° to 100°. Hence, period 2 was most likely not subject to local contamination.

A comparison of data taken in the Arctic with published values from other areas of the world reveals that the Br content of the Arctic aerosol during the 3-mo peak period exceeds all other measurements made in the unperturbed troposphere by factors ranging from 5 to 10. Gas phase Br levels also exhibit this same behavior. When particulate and gaseous Br levels are considered together, the levels of total Br in the Arctic atmosphere during the 3-mo maximum exceed all measurements made in the natural troposphere by up to a factor of 10. A more comprehensive description and evaluation of this field study was given by Berg et al. (1983).

Acknowledgments

measurements there. NCAR is sponsored by the National Science Foundation. Los Alamos National Laboratory is operated by the University of California for DOE.

5.13 Spectrum and Cross-Spectrum Analysis of Daily Meteorological and Chemical Data at BRW

W. E. Raatz
Geophysical Institute, University of Alaska
Fairbanks, AK 99701

Time series of data can be analyzed by spectrum analysis in order to estimate which oscillations of a specific frequency (period) contribute significant portions to the total variance of the time series. In this way, a time-series spectrum is analogous to an optical spectrum, indicating the contribution of different wavelengths or frequencies to the total energy of radiation.

When two time series appear to be correlated, the correlation could be due to a correlation between high-frequency components (short periods) or low-frequency components (long periods) of the data. Two time series may appear to be uncorrelated because the low-frequency components are negatively correlated and the high-frequency components are positively correlated. A cross-spectrum analysis determines the coherence, which varies from 0 to 1 and is analogous to the square of a correlation coefficient. The coherence represents a frequency-dependent correlation coefficient.

Daily data of noncrustal vanadium (XV), noncrustal manganese (XMn), surface temperature, and pressure during 5 December 1979-30 April 1980 were subjected to a spectrum and cross-spectrum analysis program (SAS 79, SAS Institute, Cary, N.C.). Gaps in the chemical data series were closed by filling in the data of the previous day. Sometimes samples were collected over 2 days instead of over 1 day. However, 2-day samples did not coincide with weekends, which would produce an artificial period in the spectrum. The seasonal trend was removed by calculating mean values for each element for each month and subtracting them from the actual data. Thus, our data set of temperature, pressure, XMn, and XV concentrations represents daily deviations from the monthly means. Inspection of the time series of the deviations showed that removing the monthly trend did not cause a distortion of the original time series.

In fig. 92 the power spectra for XV and XMn are presented. In each case the 80% confidence limit is indicated. Both spectra have a similar appearance with several peaks. The XV spectrum reveals significant periods at 24.6-18.5 days, 7.7-7.0 days, and 4.1-3.8 days. The XMn spectrum reveals significant periods at 8.7-7.7 days, 49.3-29.6 days, 4.7-4.4 days, and 2.5 days. It appears that the spectrum of XMn compared with that of XV is slightly shifted toward longer periods. The cross-spectrum analysis revealed that high coherency values of 0.93 and 0.78 were present in the periods of 7.0-6.5 days and 21.1-16.4 days, respectively. It should be noted that highest coherency was found at the shoulders of the peaks in the spectra and not at the peaks themselves. This high coherency, however, seems to support the overall high correlation coefficient between XV and XMn.

The power spectra for temperature and pressure are presented in fig. 93. It is obvious that these spectra are similar to each other but different from
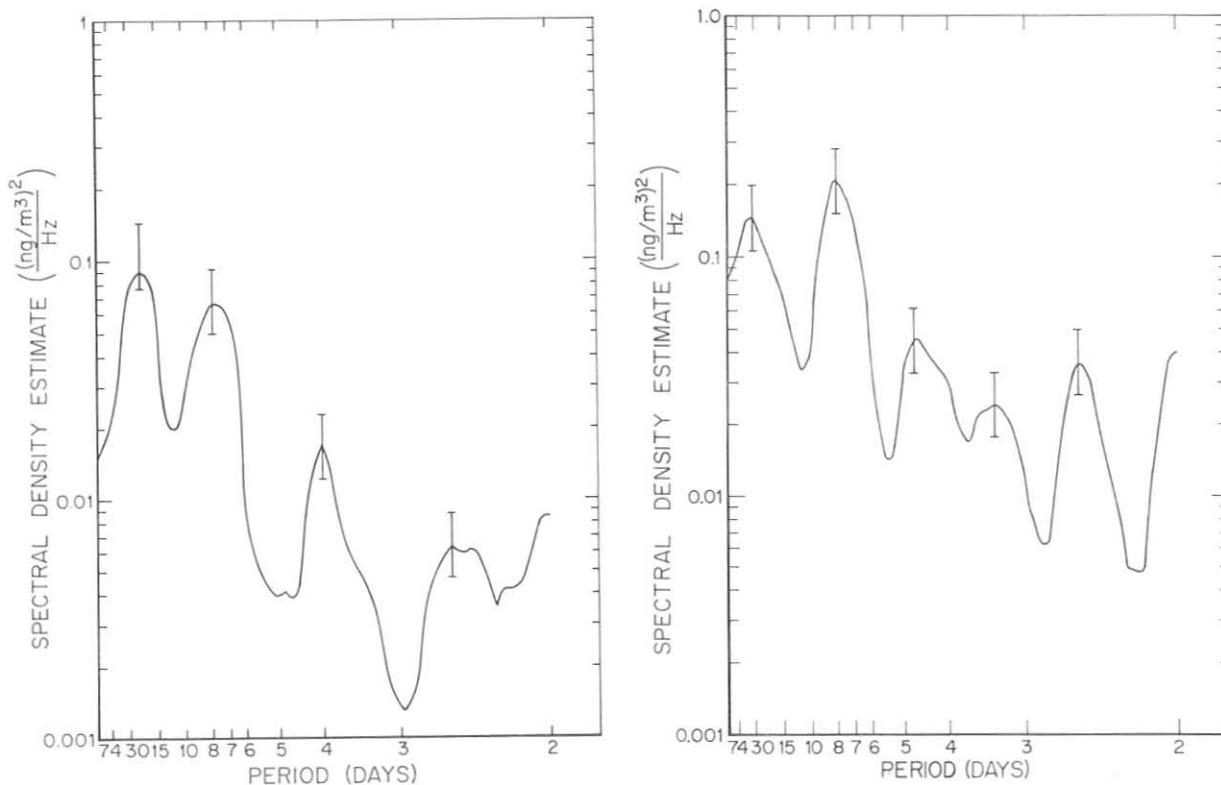
Figure 92.--Power spectra for (left) excess vanadium and (right) excess manganese, for 5 December 1979-30 April 1980 at BRW. The 80% confidence limit is indicated.

the power spectra of XV and XMn. The spectra of temperature and pressure fall off rapidly with smaller periods and do not show as much detail as the spectra of XV and XMn. The pressure spectrum reveals significant periods at 29.6-21.1 days and 6.4-5.9 days. The temperature spectrum reveals significant periods at 21.1-16.4 days and 4.9-3.8 days. In this case, the spectrum of pressure seems to be slightly shifted to longer periods than the spectrum of temperature, analogous to XMn and XV. Applying a cross-spectrum analysis on temperature and pressure resulted in a coherency of 0.86 in the period of 4.3-4.0 days. Again strong coherency was not present between the centers of the peaks but was displaced to the shoulders of the peaks. Cross-spectrum analysis between the meteorological elements and the chemical elements resulted in overall weak coherences. Some stronger coherences were suggested but never occurred within the significant periods. Therefore, the significance of these coherences appears doubtful.

The following hypothesis is presented to explain the signficant periods found in the spectra. By inspecting daily weather maps it can be estimated that about every 6-7 days polluted air masses were injected over source regions in midlatitudes. On the average, such injections lasted for about 4-5 days. These two periods seem to be reflected in the spectra of XV and XMn. Investigation of height-time cross sections of potential temperature and mixing ratio at BRW for December-March showed that the presence of Arctic and
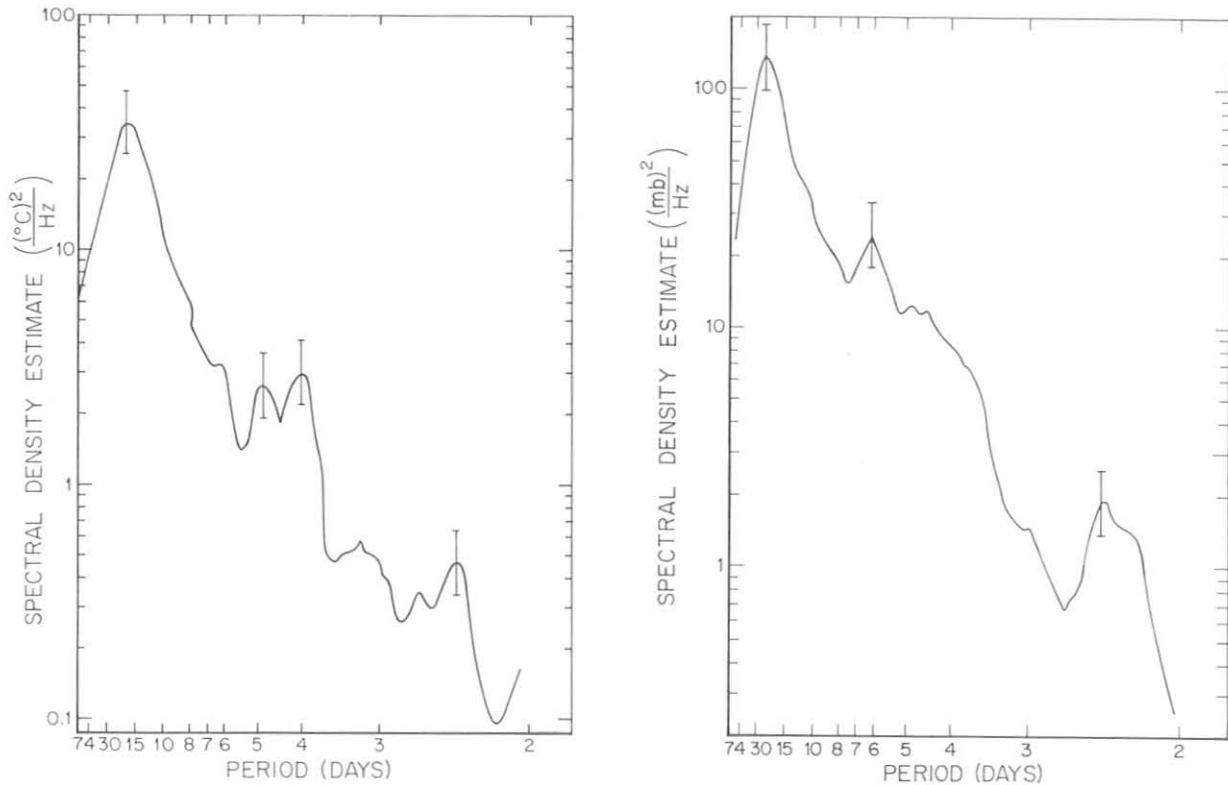
141

Figure 93.--Power spectrum for (left) temperature and (right) pressure, for 5 December 1979-30 April 1980 at BRW. The 80% confidence limit is indicated.

Pacific air masses seems to alternate with a period of about 18 days. The presence of Pacific air at BRW lasted for about 4-5 days; Arctic air was usually present over a longer time. Therefore, it appears that the large-period peaks in all four spectra can be associated with the varying influence of Pacific and Polar air, or in other words, the large-scale synoptic situation. Pacific air is clean; Arctic air is polluted. The peak at small periods in the pressure and temperature spectra might reflect the duration of Pacific air present.

In summary, spectrum and cross spectrum analyses suggest that the large-scale variations of the atmosphere are represented in the long periods of the spectra of all four parameters investigated. The peaks in the smaller periods, however, are due to different physical processes and therefore are not correlated with each other. In the case of XV and XMn, the peaks can be explained based on the frequency and duration of pollution surges in midlatitudes. Peaks in the spectra of temperature and pressure can be explained by the local synoptic conditions.

Acknowledgments

5.14   Changes in the Seasonal Amplitude of CO_2 at MLO

L. P. Steele
National Research Council Resident Research Associate
Geophysical Monitoring for Climatic Change, Boulder, CO 80303

The GMCC continuous CO_2 data from MLO for 1975-1982 inclusive have been analyzed for evidence of changes in the amplitude of the seasonal cycle. The primary data used were daily mean values after a preliminary selection procedure had been carried out by W. Komhyr. The method used for the analysis was essentially identical to that described by Bacastow et al. (1981a), in which a long-term trend was first removed from the data. It was removed in this work by fitting a cubic spline to the monthly means. Knots were located every 12 months (January of each year), and the spurious end effects of the spline-fitting procedure were overcome by appending 2 years of monthly data (suitably adjusted for an estimated long-term trend) to each end of the time series.

The next step was to generate 5-day mean values from the daily data (including one 6-day value in February of each leap year), and then to subtract the long-term trend from these data by evaluating the fitted cubic spline at each 5-day point. A function of the form $S = a \sin 2\pi t + b \cos 2\pi t + c \sin 4\pi t + d \cos 4\pi t$ (where t is in years) was fitted by methods of linear least squares to the resultant 5-day values to determine the parameters of an average annual cycle. Finally, each year of the detrended 5-day data was taken in turn and a function $g_0 + g_1 S$ was fitted. The resultant values of g_1 are thought to provide an estimate of how the amplitude of the seasonal cycle in any year compares to an average value taken over all available years. As expected, the values of g_0 are close to zero in each case. The values of g_1 as percentages (relative to the average seasonal amplitude) are 91.9, 103.8, 103.5, 98.0, 98.2, 100.0, 99.0, and 109.9, for 1975-1982 respectively.

If these values of g_1 are regressed linearly with time, a slope of $1.1 \pm 0.8\%$ yr^{-1} is obtained. This result compares closely with that reported by Bacastow et al. (1981b) for 11 years of CO_2 flask data (1970-1980) collected at Station P in the north Pacific. Nevertheless, some caution is urged in the interpretation of the results from the present analysis. First, the selection of the MLO data is not yet completed. Second, the largest value of g_1 occurred for 1982, a year of a very strong El Niño event. Further, when the 5-day data for 1982 were plotted together with the fitted function $g_0 + g_1 S$ for that year, it was obvious that the function did not provide a good description of the minimum in the data, with the difference between the two being approximately 1 ppm. This feature was also evident in the data for 1976, another year with an El Niño event.

It would seem to be necessary to make some explicit allowance for the perturbations in the amplitude of the CO_2 seasonal cycle that are caused by these El Niño events prior to searching for evidence of changes in the amplitude that may be due to other causes such as a global increase in the level of photosynthetic activity. Such a scheme has been described recently by Bacastow et al. (1983), where the variation in atmospheric CO_2 was modeled as the sum of three independent components: (1) growth in use of fossil fuel, (2) the seasonal cycle (with allowance made for changes in amplitude), and (3) a measure of the Southern Oscillation. They reported a growth in amplitude of the cycle at MLO of $0.75 \pm 0.06\%$ yr^{-1} over the period 1958-1983. A particularly noteworthy feature of this result is the small error term, which differs markedly from the error found in this work and the errors quoted previously by Bacastow et al. (1981a, 1981b).

6. INTERNATIONAL ACTIVITIES

The monograph on the status of U.S. aerosol research and climatic implications, which is being written in parallel with a U.S.S.R. effort under the sponsorship of the U.S.-U.S.S.R. Working Group VIII Committee on the Environment, has progressed beyond the planning stage. Several contributions were submitted to the U.S. Chief Editor, G. Robinson, for review. See GMCC Summary Report No. 10 (Bodhaine and Harris, 1982, sec. 6), for additional details on the U.S.-U.S.S.R. joint monograph.

A workshop was hosted by GMCC in Boulder on 8-9 February 1982 to write chapter 2, "Soil Aerosols," of the U.S. contribution for the Aerosols-Climate Assessment Monograph being prepared under the U.S.-U.S.S.R. Working Group VIII scientific exchange program. Participants were J. Prospero of University of Miami, C. Patterson of Georgia Institute of Technology, M. Jackson of University of Wisconsin, J. Rosinski of NCAR, and D. Gillette, convener, of GMCC. A first draft report was largely completed reviewing U.S. research over the last 5 years. The Soviet side will be preparing a similar report reviewing their literature.

Funding was received in 1982 from EPA, CMA, and WMO for automation of six Dobson ozone spectrophotometers for Umkehr observations at a select global network. The stations within this network have been tentatively identified as MLO; Poker Flat, Alaska; Haute Provence, France; Pretoria, South Africa; Huancayo, Peru; Perth, Australia; and Boulder, Colo. For more details, see sec. 4.3.

GMCC continued the program to upgrade foreign Dobson spectrophotometers under the auspices of WMO (see sec. 3.2.2). The calibration checks of Dobson spectrophotometers in the global network continued; details can be found in sec. 3.2.3.

CIRES Research Assistant, A. Chopra of the Indian Meteorological Service, New Delhi, India, who began temporary employment with GMCC in December 1980, continued work during 1982 in assisting with development and testing of ECC ozonesondes for high altitude use (up to 40 km). Emphasis in the research was accurate measurement of sonde pump efficiencies in the range 50-2 mb. Chopra also helped with routine ozone soundings and sonde data processing in Boulder, as well as with logistics of the MLO ozone sounding program, including data· processing. Furthermore he participated in a program at Hilo, Hawaii, in September 1982 to measure ozone and SO_2 in the presence of the El Chichon volcanic cloud, and assisted with Dobson instrument optical adjustments and calibrations from key stations of the world.

W. Komhyr traveled to the Main Geophysical Observatory in Leningrad, U.S.S.R, 23-29 May 1982, under the auspices of the U.S.-U.S.S.R. Working Group VIII Committee on the Environment, to check on progress of the Soviet scientists in establishing a facility for collecting air samples from ocean Station C in the North Atlantic, and in analyzing the samples for atmospheric CO_2 content. During a visit to Boulder earlier, A. Shashkov of the Main Geophysical Observatory studied GMCC methodologies for CO_2 monitoring and obtained specifications for building a semiautomatic CO_2 analyzer apparatus (Komhyr et al., 1983). Tests conducted on the apparatus built in Leningrad by Shashkov and colleagues indicated highly satisfactory performance.

P. Obtinario, a meteorologist from Pagaso Weather Bureau, Philippine Meteorological Service, visited GMCC in Boulder during 11 August-30 September

1982 under a WMO fellowship to obtain training in operation and calibration of Dobson ozone spectrophotometers and to obtain information on all facets of the GMCC ozone program. During his visit, Manila Dobson instrument no. 52 was shipped to Boulder, repaired, and recalibrated. The majority of Obtinario's training goals were achieved, even though his planned duration of stay in Boulder was curtailed for health reasons.

P. Steele from Australia began a 1-yr term as an NRC-NOAA Research Associate on 15 September 1982. His objective is to continue work on carbon cycle modeling begun during the previous year while visiting GMCC as a CSIRO Postdoctoral Student.

P. Fraser of the CSIRO Division of Atmospheric Physics (now Atmospheric Research) arrived at GMCC during November 1982 to assume a 1-yr position as a CIRES Research Associate sponsored by GMCC. This appointment continues an informal, reciprocal arrangement for cooperative overseas study by research staff of NOAA and CSIRO. The major purpose of the visit is to make detailed comparisons of gas chromatographic and IR absorption techniques for the measurement of CO_2 concentrations in the atmosphere, and to evaluate the feasibility of measuring methane and carbon monoxide through the GMCC global flask sampling network.

During 12-18 December 1982, E. Dutton participated in a NASA-sponsored flight program based in Acapulco, Mexico, to measure optical properties of the stratospheric cloud caused by the eruption of El Chichon. In cooperation with the Mexican and Canadian meteorological services, this program involved measurements along 120°W longitude between 6°S and 20°N latitude.

Flask sampling for CO_2 at Stanley, Falkland Islands, ceased on or about 1 April as a result of local hostilities. The last shipment of samples was received in Boulder on 7 April and included those collected through 4 February. Word was received in November that the 64 flasks and P^3 sampling apparatus then on hand had been lost.

Arrangements were made in June 1982 with the British Antarctic Survey to begin weekly collections of CO_2 flask samples at Halley Bay, Antarctica, commencing in 1983. The initial supply of flasks was sent to England to be transported to the station by the supply ship RRS BRANSFIELD. The first year's samples are expected in Boulder by June 1984.

Arrangements were made through L. Heidt, NCAR, for a cooperative sampling program to be carried out by M. Verstraete, NCAR GHOST Flight Station, Christchurch, New Zealand, at Kaitorete Spit, South Island, New Zealand, a coastal site about 50 mi from the city. Samples are collected in stainless steel evacuated containers once per week. L. Heidt provides one container each week for the exclusive use of GMCC for CO_2 analysis. The first samples were collected on 25 October 1982; regular weekly sampling began on 14 December 1982.

B. Mendonca visited Brazil, Chile, and Peru from 26 November to 20 December at the request of WMO as a consultant to the BAPMoN program in these countries. In Brazil, siting criteria and identification of potential locations for the establishment of stations were discussed. Instruments were installed and the measurement program commenced on Easter Island. A review of 1 year of BAPMoN operation, data collection, and instrument maintenance at the Huancayo and Cosmos sites in Peru was made.

7. PUBLICATIONS AND PRESENTATIONS BY GMCC STAFF, 1982

Bodhaine, B. A. Background aerosol measurements at four remote sites. Pre-prints, Second Symposium, Composition of the Nonurban Troposphere, Williamsburg, Va., 25-28 May 1982, American Meteorological Society, Boston, Mass., 154-158.

Bodhaine, B. A. The GMCC four-wavelength nephelometer. In Light Absorption by Aerosol Particles, H. E. Gerber and E. E. Hindman (eds.), Spectrum Press, Hampton, Va., 149-168.

Bodhaine, B. A., and J. M. Harris. Calibration formulas for the Pollak condensation nucleus counter. J. Aerosol Sci. 13(2):121-126.

Bodhaine, B. A., and J. M. Harris (eds.). Geophysical Monitoring for Climatic Change, No. 10: Summary Report 1981. NOAA Environmental Research Laboratories, Boulder, Colo., 158 pp.

Charlson, R. J., T. Silver, A. D. Clarke, and B. A. Bodhaine. Comments on "Transport of Asian Desert Aerosol to the Hawaiian Islands." J. Appl. Meteorol. 21(11):1775-1776.

Cline, J. D., R. H. Gammon, and D. Wisegarver. Meridional distribution of dissolved Freon-11 in the eastern North Pacific Ocean. Paper 41A-4 presented at Ocean Sciences: AGU/ASLO Joint Meeting, San Antonio, Tex., 16-19 February 1982.

Dutton, E. G., and J. J. DeLuisi. Results of a sunphotometer intercomparison held at Boulder, 19 October to 16 December 1981. NOAA Tech. Memo. ERL ARL-114, NOAA Environmental Research Laboratories, Boulder, Colo., 47 pp.

Gammon, R. H., and J. Bullister. Age-dating the North Atlantic deep water with chlorofluoromethane transient tracers. Paper presented at the AGU Fall Meeting, San Francisco, Calif., 7-15 December 1982.

Gammon, R. H., and J. Bullister. Freon penetration into the North Atlantic deep water. Paper 41A-3 presented at Ocean Sciences: AGU/ASLO Joint Meeting, San Antonio, Tex., 16-19 February 1982.

Gammon, R. H., and W. D. Komhyr. The global atmospheric CO_2 monitoring net-work of GMCC/NOAA. Paper presented at the Carbon Dioxide Research Conference: Carbon Dioxide, Science and Consensus, Berkeley Springs, W. Va., 19-23 September 1982, sponsored by DOE.

Gammon, R. H., J. Cline, and D. Wisegarver. Chlorofluoromethanes in the Northeast Pacific Ocean: Measured vertical distributions and application as transient tracers of upper ocean mixing. J. Geophys. Res. 87(C12):9441-9454.

Gillette, D. A. Decomposition of annual patterns of atmospheric carbon dioxide concentrations: A preliminary interpretation of one year of data at 13 globally distributed locations. Atmos. Environ. 16(11):2537-2542.

Gillette, D. A. Future research in resuspension. Paper presented at the Fourth International Conference on Precipitation Scavenging, Dry Deposition, and Resuspension, Santa Monica, Calif., 28 November-3 December 1982.

Gillette, D. A. Threshold velocities for wind erosion on natural terrestrial arid surfaces (a summary). Paper presented at the Fourth International Conference on Precipitation Scavenging, Dry Deposition, and Resuspension, Santa Monica, Calif., 28 November-3 December 1982.

Gillette, D. A., and C. Cowherd. The concept of resuspension rates applied to problems of fugitive dust emissions and wind erosion. Paper presented at the Fourth International Conference on Precipitation Scavenging, Dry Deposition, and Resuspension, Santa Monica, Calif., 28 November-3 December 1982.

Gillette, D. A., J. Adams, D. Muhs, and R. Kihl. Threshold friction velocities and rupture moduli for crusted desert soils for the input of soil particles into the air. J. Geophys. Res. 87(C11):9003-9015.

Harris, J. M. The GMCC Atmospheric Trajectory Program. NOAA Tech. Memo. ERL ARL-116, NOAA Environmental Research Laboratories, Boulder, Colo., 30 pp.

Herbert, G. A., J. M. Harris, B. A. Bodhaine, and S. J. Oltmans. Variations of atmospheric trace constituents measured during periods representative of the background troposphere at Mauna Loa Observatory. Preprints, Second Symposium, Composition of the Nonurban Troposphere, Williamsburg, Va., 25-28 May 1982, American Meteorological Society, Boston, Mass., 209-213.

Mendonca, B. G., J. J. DeLuisi, and J. A. Schroeder. Arctic haze and solar irradiance measurements at Barrow, Alaska. Preprints, Second Symposium, Composition of the Nonurban Troposphere, Williamsburg, Va., 25-28 May 1982, American Meteorological Society, Boston, Mass., 176-178.

Miller, S. W., and B. A. Bodhaine. Calibration of Pollak condensation nuclei counters using charged, monodisperse aerosols. J. Aerosol Sci. 13(5): 419-428.

Miller, S. W., and B. A. Bodhaine. Supersaturation and expansion ratios in condensation nuclei counters: An historical perspective. J. Aerosol Sci. 13(6):481-490.

Oltmans, S. J., and J. London. The quasi-biennial oscillation in atmospheric ozone. J. Geophys. Res. 87(11):8981-8989.

Osborn, J., J. DeLuisi, and R. Fegley. Stratospheric lidar investigations of the Mt. St. Helens volcanic cloud over Boulder, CO. NOAA Tech. Memo. ERL ARL-110, 45 pp.

Patterson, E. M., B. A. Bodhaine, A. Coletti, G. W. Grams. Volume scattering ratios determined by the polar and the integrating nephelometer: A comparison. Appl. Opt. 21(3):394-397.

Peterson, J. T., W. D. Komhyr, T. B. Harris, and L. S. Waterman. Atmospheric carbon dioxide measurements at Barrow, Alaska, 1973-1979. Tellus 34(2): 166-175.

Radke, L. F., B. A. Bodhaine, G. A. Herbert, and J. M. Harris. Aerosol light scattering and condensation nuclei measurements at Barrow, Alaska (discussion). Atmos. Environ. 16(5):1274-1275.

Schnell, R. C. Airborne ice nucleus measurements around the Hawaiian Islands. J. Geophys. Res. 87(C11):8886-8890.

Schnell, R. C. Increased production and reduced energy costs in snowmaking: Some recent research results. Ski Area Manage. 21:78-80.

Schnell, R. C. (ed.). Report on the Mount Kenya Baseline Station Feasibility Study. Environmental Pollution Monitoring Programme, No. 12, World Meteorological Organization, Geneva, Switzerland, 171 pp.

Schnell, R. C., and S. N. Tan. Kenyan tea litter: A source of ice nuclei. Tellus 34:92-95.

Schnell, R. C., S. W. Miller, P. A. Allee, and B. Wrobel. Ice nucleus measurement intercomparisons using three systems and three natural ice nucleants. Preprints, Conference on Cloud Physics, Chicago, Ill., 15-18 November 1982, American Meteorological Society, Boston, Mass., 119-122.

Schnell, R. C., R. F. Pueschel, and D. L. Wellman. Ice nucleus characteristics of Mount St. Helens effluents. J. Geophys. Res. 87(C13): 11109-11112.

Thompson, T. M., and S. K. Cox. Subtropical climatology of direct beam solar radiation. J. Appl. Meteorol. 21(3):334-338.

8. REFERENCES

Andrea, M. O., 1983. Soot carbon and excess fine potassium: Long-range transport of combustion derived aerosols. Science 220:1148-1151.

Bacastow, R. B., and C. D. Keeling, 1981. Atmospheric carbon dioxide concentration and the observed airborne fraction. In Carbon Cycle Modelling, SCOPE 16, B. Bolin (ed.), John Wiley and Sons, New York, 390 pp.

Bacastow, R. B., J. A. Adams, C. D. Keeling, D. J. Moss, and T. P. Whorf, 1980. Atmospheric carbon dioxide, the Southern Oscillation, and the weak 1975 El Nino. Science 210:66-86.

Bacastow, R. B., C. D. Keeling, and T. P. Whorf, 1981a. Seasonal amplitude in atmospheric CO_2 concentration at Mauna Loa, Hawaii, 1959-1980. Papers presented at the WMO/ICSU/UNEP Scientific Conference on Analysis and Interpretation of Atmospheric CO_2 Data, Bern, Switzerland, 14-18 September 1981, World Meteorological Organization, Geneva, Switzerland, 169-176.

Bacastow, R. B., C. D. Keeling, T. P. Whorf, and C. S. Wong, 1981b. Seasonal amplitude in atmospheric CO_2 concentration at Canadian Weather Station P, 1970-1980. Papers presented at the WMO/ICSU/UNEP Scientific Conference on Analysis and Interpretation of Atmospheric CO_2 Data, Bern, Switzerland, 14-18 September 1981, World Meteorological Organization, Geneva, Switzerland, 163-168.

Bacastow, R. B., C. D. Keeling, and T. P. Whorf, 1983. Review of some observations relevant to the interaction between atmospheric CO_2, the oceans, and the climate. Paper presented at the XVIII General Assembly, IUGG Inter-Disciplinary Symposia, Symposium 19, The Ocean and the CO_2 Climate Response, Hamburg, F.R.G., 18-19 August 1983.

Barrie, L. A., R. M. Hoff, and S. M. Daggupaty, 1981. The influence of mid-latitudinal pollution sources on haze in the Canadian Arctic. Atmos. Environ. 15(8):1407-1419.

Berg, W. W., and J. W. Winchester, 1978. Aerosol chemistry of the marine atmosphere. In Chemical Oceanography, vol. 7, 2nd ed., J. P. Riley and R. Chester (eds.), Academic, New York, 173-231.

Berg, W. W., P. J. Crutzen, F. E. Grahek, S. N. Gitlin, and W. A. Sedlacek, 1980. First measurements of total chlorine and bromine in the lower stratosphere. Geophys. Res. Lett. 7(11):937-940.

Berg, W. W., P. D. Sperry, K. A. Rahn, and E. S. Gladney, 1983. Atmospheric bromine in the Arctic. J. Geophys. Res. 88(C11):6719-6736.

Berger, D., and F. Urbach, 1982. A climatology of sunburning ultraviolet radiation. Photochem. Photobiol. 35:187-192.

Bigg, E. K., 1977. Some properties of the aerosol at Mauna Loa Observatory. J. Appl. Meteorol. 16:262-267.

Bodhaine, B. A., and R. F. Pueschel, 1974. Source of seasonal variations in solar radiation at Mauna Loa. J. Atmos. Sci. 31(3):840-845.

Bodhaine, B. A., and J. M. Harris (eds.), 1982. Geophysical Monitoring for Climatic Change, No. 10: Summary Report 1981. NOAA Environmental Research Laboratories, Boulder, Colo., 158 pp.

Bodhaine, B. A., J. M. Harris, and G. A. Herbert, 1981. Aerosol light scattering and condensation nuclei measurements at Barrow, Alaska. Atmos. Environ. 15(8):1375-1389.

Bodhaine, B. A., J. J. DeLuisi, J. M. Harris, and R. C. Castillo, 1983. Light scattering, condensation nuclei, and air mass trajectories at Whiteface Mountain: Summer 1982. NOAA Data Rep. (in press).

Bortniak, J. C., 1981. The wind climatology of American Samoa. NOAA Tech. Memo. ERL ARL-98, NOAA Environmental Research Laboratories, Boulder, Colo., 67 pp.

Box, G., and G. M. Jenkins, 1976. Time Series Analysis Forecasting and Control. Holden-Day Press, San Francisco, Calif., 575 pp.

Cess, R. D., 1983. Arctic aerosols: Model estimates of interactive influences upon the surface-troposphere radiation budget. Atmos. Environ. (in press).

Clarke, A. D., 1982. The integrating sandwich: A new method of measurement of the light absorption coefficient for atmospheric particles. Appl. Opt. 21:3011-3020.

Clarke, A. D., and R. J. Charlson, 1982. Light absorption studies at MLO. Geophysical Monitoring for Climatic Change, No. 10: Summary Report 1981, B. A. Bodhaine and J. M. Harris (eds.), NOAA Environmental Research Laboratories, Boulder, Colo., 125-130.

Cleveland, W. S., A. E. Freeny, and T. E. Graedel, 1983. The seasonal component of atmospheric CO_2: Information from new approaches to the decomposition of seasonal time series. J. Geophys. Res. 88 (in press).

Cobb, W. E., 1968. The atmospheric electric climate at Mauna Loa Observatory, Hawaii. J. Atmos. Sci. 25(3):470-480.

Coulson, K. L., 1983a. Effects of the El Chichon volcanic cloud in the stratosphere on the intensity of light from the sky. Appl Opt. (in press).

Coulson, K. L., 1983b. Effects of the El Chichon volcanic cloud in the stratosphere on the polarization of light from the sky. Appl. Opt. 21:1036-1050.

Darzi, M., and J. W. Winchester, 1982a. Aerosol characteristics at Mauna Loa Observatory, Hawaii, after east Asian dust storm episodes. J. Geophys. Res. 87:1251-1258.

Darzi, M., and J. W. Winchester, 1982b. Dynamic properties of continental aerosol over Hawaii determined by time series analysis. Preprints, Second Symposium on the Composition of the Nonurban Troposphere, Williamsburg, Va., 25-28 May 1982, American Meteorological Society, Boston, Mass., 150-153.

Darzi, M., and J. W. Winchester, 1982c. Resolution of basaltic and continental aerosol components during spring and summer within the boundary layer of Hawaii. J. Geophys. Res. 87:7262-7272.

Darzi, M., and J. W. Winchester, 1982d. Volcanic aerosol phosphorus, chlorine, and sulfur at Kilauea, Hawaii. J. Geophys. Res. 87:11095-11101.

Darzi, M., and J. W. Winchester, 1983. The problem of aliasing in inferring long-range air pollution transport to Mauna Loa, Hawaii. Water Air Soil Pollut. 19:407-409.

DeLuisi, J. J. (ed.), 1981. Geophysical Monitoring for Climatic Change, No. 9: Summary Report 1980. NOAA Environmental Research Laboratories, Boulder, Colo., 163 pp.

DeLuisi, J. J., 1982. Comments on stratospheric dust. EOS 63(23):529.

DeLuisi, J. J., and J. M. Harris, 1983. A determination of the absolute radiant energy of a Robertson-Berger meter sunburn unit. Atmos. Environ. 17(4):751-758.

DeLuisi, J. J., E. G. Dutton, K. L. Coulson, T. E. DeFoor, and B. G. Mendonca, 1983. On some radiative features of the El Chichon volcanic stratospheric dust cloud and a cloud of unknown origin observed at Mauna Loa. J. Geophys. Res. (in press).

Dittenhoefer, A. C., 1982. The effects of sulfate and non-sulfate particles on light scattering at the Mauna Loa Observatory. Water Air Soil Pollut. 18:105-121.

Duce, R. A., and E. J. Hoffman, 1976. Chemical fractionation at the air/sea interface. Ann. Rev. Earth Planet. Sci. 4:187-228.

Duce, R. A., J. W. Winchester, and T. W. Van Nahl, 1965. Iodine, bromine, and chlorine in the Hawaiian atmosphere. J. Geophys. Res. 70:1775-1799.

Duce, R. A., W. Stumm, and J. M. Prospero, 1972. Working symposium on sea-air chemistry: Summary and recommendations. J. Geophys. Res. 77(27):5059-5061.

Duquet, R. T., 1964. Data processing for isentropic analysis. Tech. Rep. No. 1, Contract AT (30-1)-3317, Air Force Cambridge Research Laboratories, Cambridge, Mass., 36 pp.

Dutton, E. G., and J. J. DeLuisi, 1983a. Optical thickness features of the El Chichon stratospheric debris cloud. Preprints, Fifth Conference on Atmospheric Radiation, Baltimore, Md., 31 October-4 November 1983, American Meteorological Society, Boston, Mass. (in press).

Dutton, E. G., and J. J. DeLuisi, 1983b. Spectral extinction of direct solar radiation by the El Chichon cloud during December 1982. Geophys. Res. Lett. 10(11):1013-1016.

Ellis, H. T., and R. F. Pueschel, 1971. Solar radiation: Absence of air pollution trends at Mauna Loa. Science 172:845-846.

Flocchini, R. G., T. A. Cahill, D. J. Shadoan, S. J. Lange, R. A. Eldred, P. J. Feeney, G. W. Wolfe, D. C. Simmeroth, and J. K. Suder, 1976. Monitoring California's aerosols by size and elemental composition. Environ. Sci. Technol. 10:76-82.

Gammon, R. H., and W. D. Komhyr, 1983. Response of the global atmospheric CO_2 distribution to the atmospheric/oceanic circulation perturbation in 1982. Paper presented at the XVIII General Assembly, IUGG Inter-Disciplinary Symposia, Symposium 19, The Ocean and the CO_2 Climate Response, Hamburg, F.R.G., 18-19 August 1983.

Gillette, D., and K. Hanson, 1983. Sampling strategy to obtain data used in models of global annual CO_2 increase and global carbon cycle. J. Geophys. Res. 88:1345-1348.

Gladney, E. S., and W. E. Goode, 1981. Elemental concentrations in eight new United States Geological Survey rock standards. Geostandards Newsl. 5(1):31-64.

Gordon, G. E., 1980. Receptor models. Environ. Sci. Technol. 14:792-800.

Graedel, T. E., 1978. Chemical Compounds in the Atmosphere. Academic Press, New York, 440 pp.

Haagenson, P., and M. A. Shapiro, 1979. Isentropic trajectories for derivation of objectively analyzed meteorological parameters. NCAR Tech. Note NCAR/TN-149+STR, National Center for Atmospheric Research, Boulder, Colo., 30 pp.

Halter, B. C., and J. M. Harris, 1981. On the variability of atmospheric carbon dioxide concentration at Barrow, Alaska, during winter. Papers presented at the WMO/ICSU/UNEP Scientific Conference on Analysis and Interpretation of Atmospheric CO_2 Data, Bern, Switzerland, 14-18 September 1981, World Meteorological Organization, Geneva, Switzerland, 13-18.

Hampson, R. F., 1980. Chemical kinetic and photochemical data sheets for atmospheric reactions. Rep. No. FAA-EE-80-17, U.S. Dept. of Transportation, Washington, D.C., 488 pp.

Harris, J. M., 1982. The GMCC atmospheric trajectory program. NOAA Tech. Memo. ERL ARL-116, NOAA Environmental Research Laboratories, Boulder, Colo., 30 pp.

Harris, J. M., and G. A. Herbert, 1980. Carbon dioxide, condensation nuclei, and wind climatology of the Barrow GMCC Observatory (1973-1979). NOAA Data Rep. ERL ARL-2, NOAA Environmental Research Laboratories, Boulder, Colo., 112 pp.

Heffter, J. L., and A. D. Taylor, 1975. Trajectory model: Part I, A regional-continental scale transport, diffusion, and deposition model. NOAA Tech. Memo. ERL ARL-50, NOAA Environmental Research Laboratories, Boulder, Colo., 28 pp.

Heintzenberg, J., 1980. Particle size distribution and optical properties of Arctic haze. Tellus 32:251-260.

Herbert, G. A. (ed.), 1980. Geophysical Monitoring for Climatic Change, No. 8: Summary Report 1979. NOAA Environmental Research Laboratories, Boulder, Colo., 120 pp.

Herbert, G. A., J. M. Harris, B. A. Bodhaine, and S. J. Oltmans, 1982. Variations of atmospheric trace constituents measured during periods representative of the background troposphere at Mauna Loa Observatory. Preprints, Second Symposium on the Composition of the Nonurban Troposphere, Williamsburg, Va., 25-28 May 1982, American Meteorological Society, Boston, Mass., 209-213.

Hileman, B., 1983. Arctic haze. Environ. Sci. Technol. 17(6):232-236.

Hogan, A. W., W. Winters, and S. C. Barnard, 1981. Photoelectric nucleus counters for aerosol climatology. J. Aerosol Sci. 12:477-489.

Hoyt, D. V., 1979. Apparent atmospheric transmission using the pyrheliometric ratioing technique. Appl. Opt. 18:2530-2531.

Jordan, R. C., and B. Y. H. Liu, 1977. Availability of solar energy for flat-plate solar heat collectors. Applications of solar energy for heating and cooling of buildings, R. C. Jordan and B. Y. H. Liu (eds.), ASRAE GRP 170, American Society of Heating, Refrigerating, and Air Conditioning Engineers, Inc., New York, V1-V16.

Keeling, C. D., 1983. The global carbon cycle: What we know and could know from atmospheric, biospheric, and oceanic observations. Proceedings, Carbon Dioxide Research Conference: Carbon Dioxide, Science and Consensus, Berkeley Springs, W. Va., 19-23 September 1982, prepared for DOE by Inst. for Energy Analysis, Oak Ridge Associated Universities, Washington, D.C., II.3-II.62 (available NTIS, Rep. No. CONF-820970).

Kelley, J. J., and T. A. Gosink, 1979. Gases in sea ice: 1975-1979. Final Rep. to Office of Naval Research, Contract No. N000 14-76C-0331, Institute of Marine Science, University of Alaska, Fairbanks, Alaska, 104 pp.

Kerman, B., 1980. Gas transfer at the air-sea interface by breaking waves. Rep. AQRB-81-018-L, Atmospheric Environment Service, Downsview, Ontario, Canada, 21 pp.

Khalil, M. A. K., 1979. Topics in the behavior of atmospheric trace gases. Ph.D. Dissertation, Oregon Graduate Center, Beaverton, Oreg., 369 pp.

Khalil, M. A. K., and R. A. Rasmussen, 1983. Modeling chemical transport and mass balances in the atmosphere. In Environmental Exposure from Chemicals, ch. 12, W. B. Neely and G. E. Blau (eds.), CRC Press, Boca Raton, Fla. (in press).

Komhyr, W. D., 1983. An aerosol and gas sampling apparatus for remote observatory use. J. Geophys. Res. 88:3913-3918.

Komhyr, W. D., L. S. Waterman, and W. R. Taylor, 1983. Semiautomatic non-dispersive infrared analyzer apparatus for CO_2 air sample analyses. J. Geophys. Res. 88(C2):1315-1322.

Komhyr, W. D., R. H. Gammon, T. B. Harris, L. S. Waterman, T. J. Conway, W. R. Taylor, and K. W. Thoning, 1984. Global CO_2 distribution and variations from 1968-1982 NOAA/GMCC CO_2 flask sample data. J. Geophys. Res. (submitted).

Lovelock, J. E., 1975. Natural halocarbons in the air and in the sea. Nature 256:193-194.

Machta, L., 1974. Global scale atmospheric mixing. In Turbulent Diffusion in Environmental Pollution, F. Frenkiel and R. E. Munn (eds.), Academic Press, New York, 392 pp.

Mastenbrook, H. J., and S. J. Oltmans, 1983. Stratospheric water vapor variability for Washington, D.C./Boulder, Colo.: 1964-1982. J. Atmos. Sci. (in press).

Mendonca, B. G., 1969. Local wind circulation on the slopes of Mauna Loa. J. Appl. Meteorol. 8(4):533-541.

Mendonca, B. G. (ed.), 1979. Geophysical Monitoring for Climatic Change, No. 7: Summary Report 1978. NOAA Environmental Research Laboratories, Boulder, Colo., 131 pp.

Mendonca, B. G., K. J. Hanson, and J. J. DeLuisi, 1978. Volcanically related secular trends in atmospheric transmission at Mauna Loa Observatory, Hawaii. Science 202:513-515.

Mendonca, B. G., J. J. DeLuisi, K. J. Hanson, and J. T. Peterson, 1979. Signatures in atmospheric transmission variations at Mauna Loa Observatory, Hawaii. Papers presented at the WMO Technical Conference on Regional and Global Observations of Atmospheric Pollution Relative to Climate, Boulder, Colo., 20-24 August 1979, WMO No. 549, Spec. Environ. Rep. No. 14, World Meteorological Organization, Geneva, Switzerland, 159-163.

Miller, J. M., 1981a. A five-year climatology of back trajectories from the Mauna Loa Observatory, Hawaii. Atmos. Environ. 15(9):1553-1558.

Miller, J. M., 1981b. A five-year climatology of five-day back trajectories from Barrow, Alaska. Atmos. Environ. 15(8):1401-1405.

Mitchell, J. M., Jr., 1957. Visual range in the polar regions with particular reference to the Alaskan Arctic. J. Atmos. Terr. Phys., Special Supplement:195-211.

Moyers, J. L., and R. A. Duce, 1972. Gaseous and particulate bromine in the marine atmosphere. J. Geophys. Res. 77(27):5330-5338.

NESDIS (National Environmental Satellite, Data, and Information Service), 1983. Global ionospheric background monitoring for selected environmental parameters: BAPMoN data for 1979. NESDIS/National Climatic Center, Asheville, N.C.

Ottar, R., 1981. The transfer of airborne pollutants to the Arctic region. Atmos. Environ. 15:1439-1446.

Parrington, J. R., and W. H. Zoller, 1983a. The chemistry of Asian dust. J. Geophys. Res. (submitted).

Parrington, J. R., and W. H. Zoller, 1983b. Selective sampling of diurnal winds at Mauna Loa, Hawaii. J. Geophys. Res. (submitted).

Parrington, J. R., J. K. Whittaker, and W. H. Zoller, 1983a. Automatic instrumentation for selective sampling of diurnal mountain winds at Mauna Loa, Hawaii. J. Appl. Meteorol. (submitted).

Parrington, J. R., W. H. Zoller, and N. K. Aras, 1983b. Asian dust: Seasonal transport to the Hawaiian Islands. Science 220:195-197.

Pearman, G. I., and P. Hyson, 1980. Activities of the global biosphere as reflected in atmospheric CO_2 records. J. Geophys. Res. 85:4457-4467.

Pearman, G. I., and P. Hyson, 1981. The annual variation of atmospheric CO_2 concentration observed in the Northern Hemisphere. J. Geophys. Res. 86:9839-9843.

Peng, T.-H., W. S. Broecker, G. G. Mathieu, Y. H. Li, and A. E. Bainbridge, 1979. Radon evasion rates in the Atlantic and Pacific Oceans as determined during the Geosecs Program. J. Geophys. Res. 84:2471-2486.

Perry, R. A., R. Atkinson, and J. N. Pitts, Jr., 1977. Kinetics and mechanism of gas phase reaction of OH radicals with aromatic hydrocarbons over the temperature range 296-473 K. J. Phys. Chem. 81:296-304.

Peterson, J. T. (ed), 1978. Geophysical Monitoring for Climatic Change, No. 6: Summary Report 1977. NOAA Environmental Research Laboratories, Boulder, Colo., 145 pp.

Peterson, J. T., K. J. Hanson, B. A. Bodhaine, and S. J. Oltmans, 1980. Dependence of CO_2, aerosol, and ozone concentrations on wind direction at Barrow, Alaska during winter. Geophys. Res. Lett. 7(5):349-352.

Pollak, L. W., and A. L. Metnieks, 1960. Intrinsic calibration of the photoelectric condensation nucleus counter model 1957 with convergent light beam. Tech. Note No. 9, School of Cosmic Physics, Dublin Institute for Advanced Studies, Dublin, Ireland, 53 pp.

Porch, W. M, and M. C. MacCracken, 1982. Parametric study of the effects of Arctic soot on solar radiation. Atmos. Environ. 16(6):1365-1371.

Prospero, J. M., R. A. Glaccum, and R. T. Nees, 1981. Atmospheric transport of soil dust from Africa to South America. Nature 289:570-572.

Rahn, K. A., 1981. Relative importances of North America and Eurasia as sources of Arctic aerosol. Atmos. Environ. 15(8):1447-1455.

Rahn, K. A., 1982. Trace-element sampling at BRW. Geophysical Monitoring for Climatic Change, No. 10: Summary Report 1981, B. A. Bodhaine and J. M. Harris (eds.), NOAA Environmental Research Laboratories, Boulder, Colo., 132-134.

Rahn, K. A., and R. J. McCaffrey, 1980. On the origin and transport of the winter Arctic aerosol. Ann. N.Y. Acad. Sci. 388:486-503.

Rahn, K. A., R. D. Borys, and R. A. Duce, 1976. Tropospheric halogen gases: Inorganic and organic components. Science 192:549-550.

Rahn, K. A., R. D. Borys, and G. E. Shaw, 1977. The Asian source of Arctic haze bands. Nature 268:713-715.

Rasmussen, R. A., and M. A. K. Khalil, 1980. Atmospheric halocarbons: Measurements and analysis of selected trace gases. Proceedings of the NATO Advanced Study Institute on Atmospheric Ozone: Its Variations and Human Influences, Algarve, Portugal, 1-13 October 1979, A. C. Aikin (ed.), Rep. No. FAA-EE-80-20, U.S. Dept. of Transportation, Washington, D.C., 209-231.

Rasmussen, R. A., and M. A. K. Khalil, 1983. Atmospheric benzene and toluene. Geophys. Res. Lett. (in press).

Rasmussen, R. A., M. A. K. Khalil, and R. J. Fox, 1983. Altitudinal and temporal variation of hydrocarbons and other gaseous tracers of Arctic haze. Geophys. Res. Lett. 10:144-147.

Rich, T. A., 1966. Apparatus and method for measuring size of aerosols. J. Rech. Atmos. 2:79-86.

Robinson, G. D., 1982. Attenuation of the solar beam at Mauna Loa Observatory by particles and water vapor. CEM Rep. No. 7005-68-750, The Center for the Environment and Man, Inc., Hartford, Conn., 25 pp.

Robinson, E., and W. L. Bamesberger, 1982. Air chemistry monitoring at Palmer Station. Geophysical Monitoring for Climatic Change, No. 10: Summary Report 1981, B. A. Bodhaine and J. M. Harris (eds.), NOAA Environmental Research Laboratories, Boulder, Colo., 108-109.

Rosen, H., A. D. A. Hansen, L. Gundel, and T. Novakov, 1978. Identification of the optically absorbing component in urban aerosols. Appl. Opt. 17:3859-3861.

Rosen, H., A. D. A. Hansen, R. L. Dod, and T. Novakov, 1980. Soot in urban atmospheres: Determination by an optical absorption technique. Science 208:741-743.

Rosen, H., T. Novakov, and B. A. Bodhaine, 1981. Soot in the Arctic. Atmos. Environ. 15(8):1371-1374.

Rotty, R. M., 1982. Distribution of and changes in industrial carbon dioxide production. Rep. ORAU/IEA-82-2 CM, Institute for Energy Analysis, Oak Ridge Associated Universities, Oak Ridge, Tenn., 23 pp.

Rotty, R. M., 1983. Distribution of and changes in industrial carbon dioxide production. J. Geophys. Res. 88(C2):1301-1308.

Schnell, R. C., 1983. Arctic haze and the Arctic Gas and Aerosol Sampling Program (AGASP). Preprints, AIAA 21st Aerospace Sciences Meeting, Reno, Nev., 10-13 January 1983, American Inst. of Aeronautics and Astronautics, New York, 6 pp.

Sedlacek, W. A., A. L. Lazrus, and B. W. Gandrud, 1979. Measurements of stratospheric bromine. Proceedings, NATO Advanced Study Institute on Atmospheric Ozone: Its Variation and Human Influences, Algarve, Portugal, 1-13 October 1979, A. C. Aikin (ed.), Rep. No. FAA-EE-80-20, U.S. Dept. of Transportation, Washington, D.C., 273-280.

Shaw, G. E., 1980. Transport of Asian desert aerosol to the Hawaiian Islands. J. Appl. Meteorol. 19:1254-1259.

Shaw, G. E., 1981. Eddy diffusion transport of Arctic pollution from the mid-latitudes: A preliminary model. Atmos. Environ. 15(8):1483-1490.

Shaw, G. E., 1982. Evidence for a central Eurasian source area of Arctic haze in Alaska. Nature 299:815-818.

Shaw, G. E., and K. Stamnes, 1980. Arctic haze: Perturbation of the polar radiation budget. Ann. N.Y. Acad. Sci. 338:533-539.

Simpson, H. J., 1972. Aerosol cations at Mauna Loa Observatory. J. Geophys. Res. 77:5266-5277.

Sinclair, D., 1972. A portable diffusion battery. J. Am. Ind. Hyg. Assoc. 33:729-735.

Singh, H. B., L. J. Salas, H. Shigeishi, and A. Crawford, 1977. Urban-nonurban relationships of halocarbons, SF_6, N_2O, and other atmospheric trace constituents. Atmos. Environ. 11:819-828.

Singh, H. B., L. J. Salas, and R. E. Stiles, 1983. Methyl halides in and over the eastern Pacific (40°N-32°S). J. Geophys. Res. 88(C6):3684-3690.

Spurny, K., J. P. Lodge, Jr., D. C. Sheesly, and E. R. Frank, 1969. Aerosol filtration by means of Nuclepore filters. Environ. Sci. Technol. 3:464-468.

Takahashi, T., W. S. Broecker, and A. Bainbridge, 1981. Supplement to the alkalinity and total carbon dioxide concentration in the world oceans. In Carbon Cycle Modelling, SCOPE 16, B. Bolin (ed.), John Wiley and Sons, New York, 390 pp.

Taylor, S. R., 1964. Abundance of chemical elements in the continental crust: A new table. Geochim. Cosmochim. Acta 28:1280-1281.

Toon, O. B., and J. B. Pollack, 1980. Atmospheric aerosols and climate. Am. Sci. 68(3):268-278.

Tuinstra, F., and J. L. Koenig, 1970. Raman spectrum of graphite. J. Chem. Phys. 53:1126-1130.

Uematsu, M., R. A. Duce, J. M. Prospero, L. Chen, J. T. Merrill, and R. L. McDonald, 1983. Transport of mineral aerosol from Asia over the North Pacific Ocean. J. Geophys. Res. 88:5343-5352.

Voskresenskii, A. I., 1968. Condensation nuclei in the Mirnii Region. Tr. Sov. Antarktcheskia Eksped. 38:194-198.

Wang, M., J. W. Winchester, T. A. Cahill, and L. Ren, 1982. Chemical elemental composition of wind-blown dust, April 19, 1980, Beijing. Kexue Tongbao 27(11):1193-1198.

Wofsy, S. C., M. B. McElroy, and Y. L. Yung, 1975. The chemistry of atmospheric bromine. Geophys. Res. Lett. 2(6):215-218.

Wolff, G. T., and R. L. Klimisch (eds.), 1982. Particulate Carbon: Atmospheric Life Cycle. Plenum Press, New York, 411 pp.

Yung, Y. L., J. P. Pinto, R. T. Watson, and S. P. Sander, 1980. Atmospheric bromine and ozone perturbations in the lower stratosphere. J. Atmos. Sci. 37(2):339-353.

Zoller, W. H., J. R. Parrington, and N. K. Aras, 1981. Atmospheric particulate chemistry at the South Pole and Mauna Loa. Geophysical Monitoring for Climatic Change, No. 9: Summary Report 1980, J. J. DeLuisi (ed.), NOAA Environmental Research Laboratories, Boulder, Colo., 141-147.

9. GMCC STAFF, 1982

Director's Office
>   James Peterson, Director
>   Bernard Mendonca, Deputy Director
>   Jeanne Kelsey, Secretary
>   Carol Fee, CO-OP
>   Paul Fraser, Guest Scientist, CIRES
>   Dale Gillette, Physical Scientist
>   Chandra Shastri, CIRES
>   Gregory Siedelberg, Electronic Technician
>   Paul Steele, Guest Scientist

Acquisition and Data Management Group
>   Gary Herbert, Chief
>   Jo-Ann Garner, Secretary
>   Richard Clark, Computer Programmer
>   Edward Green, CIRES
>   Joyce Harris, Computer Specialist
>   Troy Higgins, Jr. Fellow
>   Gloria Koenig, Computer Programmer
>   Kenneth Thaut, Electronic Technician

Monitoring Trace Gases Group
>   Walter Komhyr, Chief
>   Jo-Ann Garner, Secretary
>   Ruth Alvirez, CO-OP
>   Amar Chopra, CIRES
>   Thomas Conway, CIRES
>   Robert Evans, CIRES
>   Richard Gammon, Chemist
>   Robert Grass, Physicist
>   Thomas Harris, Contract
>   Kent Leonard, CIRES
>   Samuel Oltmans, Physicist
>   Frank Polacek, III, Meteorological Technician
>   Steven Rush, CIRES
>   Thayne Thompson, Physicist
>   Kirk Thoning, CIRES
>   Alberta Vieira, CO-OP
>   Lee Waterman, Chemist

Aerosols and Radiation Monitoring Group
>   John DeLuisi, Chief
>   Bonnie Hill, Secretary
>   Barry Bodhaine, Meteorologist
>   Kenneth Cameron, CIRES
>   Forrest Cook, Electronic Technician
>   Ellsworth Dutton, Meteorologist
>   Daniel Endres, CIRES
>   Stuart Naegele, CIRES
>   John Osborn, NOAA Corps
>   Kenneth Thorne, CIRES

Analysis and Interpretation Group
John DeLuisi, Acting Chief
Bonnie Hill, Secretary
Joanne Edwards, CIRES
Bradley Halter, CIRES
Russell Schnell, CIRES

Mauna Loa Observatory
Kinsell Coulson, Director
Judith Pereira, Secretary
Arnold Austring, Physical Scientist
John Chin, Physicist
Thomas DeFoor, Electrical Engineer
Steven Garcia, Contract
Darryl Kuniyuki, Jr. Fellow
Cynthia McFee, NOAA Corps
Mamoru Shibata, Electronic Technician
Alan Yoshinaga, Analytical Chemist

Barrow Observatory
Randy Fox, Station Chief
Daniel Beard, Station Chief
Kenneth Bauer, Electronic Technician
Timothy Wolfe, Electronic Technician

Samoa Observatory
Donald Nelson, Station Chief
Roger Williams, Electronic Technician
Efaraima Peau, W. G. Laborer

South Pole Observatory
Rusty Brainard, NOAA Corps, Station Chief
Steven Fahnenstiel, Physicist
Robert Williscroft, NOAA Corps, Station Chief
Mark VandeRiet, Electronic Technician